CARBOHYDRATE DERIVED NANOPLATFORMS AS TOOLS FOR LECTIN ISOLATION, AND DELIVERY OF CYTOTOXIC T-CELL PEPTIDE EPITOPES FOR CYTOTOXIC T-CELL MEDIATED TUMOR IMMUNOTHERAPY

By

Herbert Wanjala Kavunja

A DISSERTATION

Submitted to
Michigan State University
in partial fulfillment of the requirements
for the degree of

Chemistry – Doctor of Philosophy

2015

ABSTRACT

CARBOHYDRATE DERIVED NANOPLATFORMS AS TOOLS FOR LECTIN ISOLATION, AND DELIVERY OF CYTOTOXIC T-CELL PEPTIDE EPITOPES FOR CYTOTOXIC T-CELL MEDIATED TUMOR IMMUNOTHERAPY

By

Herbert Wanjala Kavunja

Cancer cells can have characteristic carbohydrate binding properties. Previously, it was shown that a highly metastatic melanoma cell line B16F10 bound to galactoside functionalized nanoparticles much stronger than the corresponding less metastatic B16F1 cells. The results presented in the second chapter of this dissertation documents the isolation and characterization of endogenous galactose binding proteins from B16F10 cells using magnetic glyconanoparticles. The galactose coated magnetic glyconanoparticles could bind with lectins present in the cells and be isolated through magnet mediated separation. Through Western blot and mass spectrometry, arginine/serine rich splicing factor Sfrs1 was identified as a galactose selective endogenous lectin overexpressed in B16F10 cells compared to B16F1 cells. In addition, Sfrs1 was found in higher amounts in B16F10 cells. Finally, the glyconanoparticles exhibited a superior efficiency in lectin isolation, from both protein mixtures as well as live cells, than the more traditional microparticles functionalized with carbohydrates. The magnetic glyconanoparticles present a useful tool for discovery of endogenous lectins as well as binding partners of lectins without prior knowledge of protein identities.

On the other hand, cytotoxic T lymphocyte (CTL) mediated cancer immunotherapy has clinically shown the potential to treat cancer patients. For CTL therapy to be successful, cancer cells must express antigens that are targets for specific CTLs. However, it has been established that due to genetic instability of cancer cells, sub-population of cancer cells may fail to express

the target antigen, possibly leading to escape from CTL destruction, hence tumors grow progressively. These antigen-loss variant (ALV) cancer cells can be eliminated as bystanders by targeting tumor associated stromal cells, but only if the cancer cells generate sufficient antigens to be effectively cross-presented by the stromal cells. In the third chapter of this dissertation, we present results that investigated whether acid responsive nanoparticles can be used to deliver CTL-specific antigen to the cancer microenvironment to enhance tumor eradication by activated antigen-specific CTLs in a mouse model. Our results show that model CTL antigen (OVA peptide, SIINFEKL) encapsulated in pH sensitive acetalated dextran nanoparticles (OVA_(P)-Ac-Dx-NPs) could be successfully delivered to tumor cells in vitro and tumor microenvironment in vivo. The uptake and presentation of the peptide antigen by major histocompatibility molecules class I (MHC-I) in vitro and in vivo was confirmed by flow cytometry and confocal laser scanning microscopy through antibody staining. In addition, solid tumor bearing mice treated with OVA_(P)-Ac-Dx-NPs showed much slower tumor growth compared to mice treated with free OVA(P), empty Ac-Dx-NPs, or PBS. Taken together, these findings offer a promising new direction for treating established solid tumors using CTL therapy.

To my beloved family for their love and support and Nakurun Lapsetry for supporting my education throughout

ACKNOWLEDGEMENTS

I would like to thank everyone who has been part of my academic journey. It has been a team effort to get me to this level. First and foremost, I would like to express my thanks to my advisor Professor Xuefei Huang, for his patience, dedication, and guidance. He has been a role model to me, and to all my labmates with his thoroughness, excellence, persistence, his constant advice and valuable insights, which has led to my development as a scientist. I appreciate his mentorship and leadership.

I thank all my doctoral committee, Prof. John Wang, Prof. Dan Jones, and Prof. Jetze Tepe. They were always available and ready to answer my questions. Their feedback helped me to solve many challenges related to my research more efficiently.

I want to give a special thank you to Patricia Voss from Prof. John Wang's lab for her role and tireless efforts, sometimes taking time off her normal schedule to ensure that I become a successful researcher. I was able to learn research skills that can never be found in any published manuscripts.

I thank Michigan State University graduate school, especially the department of chemistry for giving me an offer to pursue my doctoral degree, supporting my studies through teaching assistantship, and providing me with a supportive and conducive learning atmosphere. I also want to thank past and present members of the Huang group; Moe, Medha, Gopinath, Hongguang, Jingguang, Abishek, Dino, Vivian, Bo, Hovig, Gilbert, Philip, Zhaojun, Weizhun, Sherif, Steve, Qian, Berm, Peng, Zereng, Mehdi, Jicheng, Shuyao, Hui, Jia, Claire and Anthony. In addition, I would like to thank undergraduate students, Sam, Matt, Andy, and Aaron, and high school students, Raven, Maria and Yuoa, whom I had an opportunity to work with. They gave me a chance to teach and learn from them. I also want to acknowledge the help and support of

the chemistry department staff. Their input has ensured the smooth running of our research work. As far as coming to graduate school is concerned, I express my sincere gratitude to Prof. John Onyari, advisor for my masters studies. If it were not for his persistence, I would not have applied to graduate school, and especially to Michigan State University.

I would like to thank my parents, brothers and sisters for always being there and providing that source of inspiration. Despite the fact that my parents have struggled with alcoholism, their parental love was always present, and especially the need for their children to get an education. I am indebted to my wife Victoria Kavunja and our children Lydia and Naomi for accepting my role as an absentee father. Their everlasting love, dedication and prayers have provided me with the required anchorage whenever the going was tough. I also give special thanks to my friends, Dr. Joel Lwande, Dr. Jane Okwako, Dr. Betty Okwako, and Ruth Muchiri, and the Kenyan community in Lansing, for their support. I extend my gratitude to cousins, Sam Balongo and Caro Nekesa for encouraging me to pursue my graduate studies.

Lastly I want to thank the most special people in my academic life, Mzee Heikki Jarkko, Mama Anna-Liisa Jarkko, and Mama Justine Oduya. Through Nakurun Lapsetry they are responsible for financially supporting and nurturing my academic life since I was seven years until I finished my masters studies. In addition they paid for my air ticket to come to graduate school. I am very blessed to have them in my life, and they will forever remain special to me. Thank you.

Herbert Wanjala Kavunja

TABLE OF CONTENTS

LIST OF TABLES	x
LIST OF FIGURES	xi
LIST OF SCHEMES	xx
KEY TO ABBREVIATIONS	xxi
CHAPTER 1: Review of magnetic nanoparticles functionalized with biomolecules and their	
application in bioseparation and enrichment	1
1.1: Introduction	
1.2: Synthesis of magnetic nanoparticles	3
1.2.1: The co-precipitation method	
1.2.2: Thermal decomposition method	5
1.3: The chemistry of immobilization of biomolecules	
1.3.1: Ideal criteria and general considerations for immobilization	
1.3.2: Non-covalent attachment	15
1.3.3: Covalent approach	
1.4: MNPs functionalized with biomolecules for bioseparation and enrichment	
1.4.1: Carbohydrate functionalized MNPs	
1.4.2: Lectin functionalized MNPs	
1.4.3: Antibody functionalized MNPs	58
1.4.4: Aptamers/oligonucleotides functionalized MNPs	65
1.4.5: Enzyme, protein and peptide functionalized MNPs	73
1.4.5.1: Enzymes	
1.4.5.2: Peptides	75
1.4.5.3: Other proteins	84
1.5: Summary	86
REFERENCES	88
CHAPTER 2: Identification of lectins from metastatic cancer cells through magnetic glyco-	
nanoparticles	115
2.1: Abstract	
2.2: Introduction	
2.3: Results	
2.3.1: Synthesis and lectin binding specificity of MGNPs	
2.3.2: Isolation of exogenous lectin added to cell lysate	
2.3.3: Isolation of endogenous lectin added to cell lysate	
2.3.4: Proteomic analysis of proteins bound to Gal-NP	
2.3.5: Confirmation of Sfrs1 in the galactose-eluted fraction of Gal-NP by Western blot	
2.3.6: Binding properties of Sfrs1 expressed as a fusion protein with GST	
2.3.7: Comparison of the amount of Sfrs1 isolated on Gal-NP from B16F10 versus B16F1	, 15 1
cells.	. 139

2.4: Discussion	141
2.5: Conclusions	143
2.6: Future directions	145
2.6: Experimental Section	149
2.6.1: Materials and instrumentation	149
2.6.2: Synthesis and characterization of iron oxide magnetic glyconanoparticles	151
2.6.3: Lysate preparation	
2.6.4: Silver staining, Coomassie blue staining, and Western blot	153
2.6.4.1: Silver staining	153
2.6.4.2: Coomassie blue staining	153
2.6.4.3: Western blot	
2.6.5: Isolation of endogenous and exogenous lectins	155
2.6.6: Isolation of lectins after binding Gal-NP to intact cells	156
2.6.7: LC/MS/MS	156
2.6.8: Binding of GST and GST fused proteins to Gal-NP	
2.6.9: Comparison of Sfrs1 from F10 and F1 using Gal-NP	
2.6.10: Quantification of Western blot protein gel band using ImageJ software	
REFERENCES	162
CHAPTER 3: Acid responsive nanoparticle mediated antigen delivery for tumor immun	
3.1: Abstract	
3.2: Introduction	
3.3: Result	
3.3.1: Synthesis and characterization of nanoparticles containing $OVA_{(P)}$ encapsulated by	
acetalated dextran nanoparticles	
3.3.2: Assessing the presentation of OVA _(P) peptide by MHC I molecules	
3.3.3: B3Z assay	
3.3.4: OVA _(P) antigen delivery to tumor environment by the assistance of acetalated d	
nanoparticles	
3.3.5: <i>In vivo</i> tumor protection	
3.4: Discussion	
3.5: Conclusion	
3.6: Future directions	
3.6: Experimental Section	
3.6.1: Materials and instrumentation.	
3.6.2: Animals and cell lines	
3.6.3: OVA peptide synthesis	201
3.6.4: Preparation of acetalated dextran nanoparticles containing OVA peptide (OVA	
Dx-NPs)	
3.6.5: OVA peptide presentation on MHC-I by flow cytometry (FACS)	
3.6.6: B3Z T cell activation assay	204
3.6.7: Assessing the delivery of OVA to tumor environment by FACS and confocal	<u> </u>
microscopy	
3.6.7.1: FACS	
3.6.7.2: Histopathology staining	205

3.6.8: Tumor immunotherapy	206
APPENDIX	207
REFERENCES	214

LIST OF TABLES

Table 1: Quantification of SBA in fraction after incubation with Gal-NP	126
Table 2: Quantification of Gal3 in fraction after incubation with Gal-NP	126
Table 3: Quantification of Gal3 fraction using ImageJ after incubation of cell lysate with particles from Figure 38	128
Table 4: Quantification of Gal3 in fraction using ImageJ after incubation of cells with partifrom Figure 42	
Table 5: Amount of iron in cells after Gal-NPs and commercial micro-particles were incub with B16F10 cells	

LIST OF FIGURES

Figure 1: Synthesis of IONPs using the co-precipitation method (A) General scheme for synthesis of IONPs using the co-precipitation method, (B) Synthesis of silica-coated IONPs and subsequent amine functionalization with APTES, TEM images of (C) Bare IONPs (the scale bar 20 nm), (D) IONPs coated with APTES (the scale bar is 5 nm). Reproduced with permission from reference ¹⁷ Copyright 2014, John Wiley and Sons
Figure 2: Synthesis of monodispersed IONPs via thermal decomposition (A) An example of a synthetic scheme. TEM images of (B), 6 nm and (C), 12 nm IONPs. Adapted with permission from reference ²⁰ Copyright 2004 American Chemical Society
Figure 3: Synthesis of water soluble IONPs via thermal decomposition (A) Synthesis of water soluble HA functionalized IONPs (HA-IONPs) via thermal decomposition. (B) Picture of OA-IONPs and HA-IONPs in a toluene-water two phase system, (C) TEM images of HA-IONPs (scale be is 10 nm). Adapted with permission from reference ²⁷ Copyright 2011, Royal Society of Chemistry.
Figure 4: Selected methods for covalent immobilization of substrates to solid supports. Partly adapted with permission from references ^{6,35} Copyright 2013 and 2011, American Chemical Society
Figure 5: Representative of non-covalent immobilization of biomolecules on NPs. (A) Immobilization of carbohydrate (B) immobilization of oligonucleotide through Au-thiol dative bond formation. (C) Immobilization of antibody (D) Immobilization of biotin labeled protein through secondary interaction
Figure 6: Representative of the main methods for carbohydrate immobilization on NPs. (A) Amide bond formation, (B) Amine bond formation through reductive amination (C) Imidine formation (D) $[2+3]$ Huisgen cycloaddition (E) Amine bond formation through photochemical reactions. Adapted with permission from reference ¹⁷ Copyright 2014, John Wiley and Sons 22
Figure 7: Protein engineering through expressed protein ligation (EPL) to introduce α -thioester at the C-terminus. The protein can be covalently conjugated to NPs by (A) [2 + 3], Huisgen cycloaddtion (B) Staudinger ligation (C) Native chemical ligation (NCL)
Figure 8: Incorporation of unnatural amino acid into a recombinant protein. Incorporation of azidohomoalanine into a recombinant protein followed by immobilization on to NPs through (A) Staudinger ligation, (B) [2 + 3] Huisgen cycloaddition reaction
Figure 9: Schematic picture of a protein immobilized to NP via the chelation assisted photoimmobilization (CAP) principle. The ligand has a hexahistidine tag, located distantly from the analyte binding site, which first coordinates to Ni ²⁺ –NTA. Photoimmobilization then tethers the protein permanently to the NP
Figure 10: Immobilization of proteins by using Sortase A and through O6 -alkylguanine-DNA alkyltransferase (SNAP). (A) Immobilization of proteins by using Sortase A. (B) Mechanism of

O ₆ -alkylguanine-DNA alkyltransferase (SNAP)-mediated immobilization of protein on NP Adapted with permission from references. 92,94 Copyright 2010, American Chemical Society and copyright 2003, Nature publishing group. 25
Figure 11: Profiling and differentiation of cancer cells using magnetic glyco-nanoparticles through MRI. (A) Synthesis of magnetic glyconanoparticles (MGNPs) (B) Percentage changes of $T2$ relaxation time (% $\Delta T2$) obtained upon incubating MGNPs 2-6 or the control NP 1 (20 μ g/mL) with 10 cell lines (105 cells/mL). The $\Delta T2$ was calculated by dividing the $T2$ differences between MGNP and MGNP/cancer cell by the corresponding highest $\Delta T2$ from each MGNP category. (C) LDA plots for the first three LDs of $\Delta T2$ patterns obtained with the MGNP array upon binding with the 10 cell lines (105 cells/mL). Reproduced with permission from reference Copyright 2010, American Chemical Society.
Figure 12: Fabrication of Le ^X -coated MNPs and selective capture of DCs. Capture of DCs from a mixed cell population using Le ^X -coated MNPs. Adapted with permission from reference ¹⁵⁴ Copyright 2012, American Chemical Society
Figure 13: Enrichment of moDCs using Le ^X -functionalized MNPs. PBMCs were incubated in the presence of GM-CSF and IL-4 for 6 days and differentiated into moDCs. (a) Contour plot shows the total cell population prior to capture. moDCs were defined as CD1a ⁺ /DC-SIGN ⁺ (gated in the box). (b) Cell flow-through following incubation with alkyne-functionalized MNPs. (c) Cell flow-through following incubation with Le ^X -functionalized MNPs. moDCs were absent from this population. (d) Histogram shows that the population of cells bound to Le ^X -functionalized MNPs are CD1a ⁺ /DC-SIGN ⁺ /HLA-DR ⁺ when stained with FITC-conjugated anti-DC-SIGN, PE/Cy5-conjugated Anti-CD1a, and PE-conjugated anti-HLA-DR. Shown is one representative experiment out of three replicates. Reproduced with permission from reference ¹⁵⁴ Copyright 2012, American Chemical Society.
Figure 14: Application of maltose functionalized MNPs in protein purification. Synthesis of maltose functionalized MNPs and their application in the separation/purification, and immobilization of maltose binding protein-Heparinase I fusion enzyme (MBP-HepA). Adapted with permission from reference ⁶¹ Copyright 2012, Royal Society of Chemistry
Figure 15: Protein isolation and analysis using maltose functionalized magnetic nanoparticles through MALDI-TOFMS. MALDI-TOFMS spectra of (A) Direct analysis of 5 pmol tryptic digest of human IgG, after enrichment with (B Fe ₃ O ₄ @SiO ₂ @PEGMaltose MNPs, (C) Fe ₃ O ₄ @SiO ₂ @PEG MNPs and (D) Fe ₃ O ₄ @SiO ₂ -Maltose MNPs, (E) After enrichment by Fe ₃ O ₄ @SiO ₂ @PEG-Maltose MNPs and then deglycosylation by PNGase F. Adapted with permission from reference ⁶⁹ Copyright 2012, Royal Society of Chemistry
Figure 16: Protein capture from cell lysate using MNPs. Magnetic bead-based capture for the identification of SSEA-4-binding proteins. Different amounts (20, 40, 80, 120, 180 μ g) of MCF-7 total cell lysate were mixed with SSEA-4-MBs or MEG-MBs (100 μ g each), and the bound proteins were eluted, separated by SDS-PAGE, and visualized after silver staining. Lane 1, marker; lane 2, MCF-7 total cell lysate (0.5 μ g); lanes 3, 5, 7, 9, and 11, protein eluted from SSEA-4-MBs; lanes 4, 6, 8, 10, and 12, protein eluted from MEG-MBs for comparison. Reproduced with permission from reference ¹⁵⁵ Copyright 2013, American Chemical Society 42

Figure 17: Analysis of FBBP4, SSEA binding protein. (A) Binding analysis of FKBP4 in a printed glycan array with 63 glycans. (B) Competitive inhibition of SSEA-4/FKBP4 interaction by FK-506. (C) Surface expression of the glycan markers of MCF-7 cells analyzed by flow cytometry after FK-506 treatment. "Cell only" means no staining performed, indicating the fluorescence background of the cells. Reproduced with permission from reference Copyright 2013, American Chemical Society
Figure 18: Protein capture and analysis using bifunctional MNP@matrix-Con A. (A) Workflow of functionalized MNP-assisted MALDI-TOF MS. The bifunctional MNP@matrix-Con A serves as an affinity matrix-free additive. Mannose extraction from human plasma by MNP@DHBCon A (B) The background signal of MNP@DHB-Con A; (C) The human serum profile; the black arrow indicates the spiked mannose (D) The mass spectrum of mannose [mannose + Na] ⁺ extracted by MNP@DHB-Con A. Adapted and reproduced with permission from reference Copyright 2007, American Chemical Society
Figure 19: Protein analysis using Con A functionalized MNP through boronic-acid-sugar sandwich. (A) Con A functionalized MNP through boronic-acid-sugar sandwich (B) One-dimensional SDS-PAGE of selective glycoproteins capture by Con A-immobilized MNPs. Lane 1, supernatant of standard protein mixture after enrichment; Lane 2, eluent of nanoparticales after enrichment. (C) Comparison of the three materials for glycoprotein enrichment from cell lysate, indicating the number of glycoproteins identified and the selectivity for glycosylated proteins. Bar 1, proteins identified with commercial Con A magnetic beads; Bar 2, proteins identified with homemade Con A MNPs; Bar 3, proteins identified with aminophenylboronic acid-functionalized MNPs Adapted and reproduced with permission from reference ¹⁷¹ Copyright 2010, John Wiley and Sons
Figure 20: Protein analysis using lectin functionalized MNPs. (A) Fetuin recovery by synthesized MNP@lectins: comparison between unprotected and sugar-protected MNP@lectins. Data are presented as mean standard deviation (SD) of micrograms of fetuin recovered per milligram of MNP@lectin (triplicates of n = 3). **p < 0.01. (B) Percentage of glycoprotein recovery of nanobeads MNP@ConA vs Sepharose@ConA. \pm Data are presented as mean SD (triplicates of n = 3) upon incubation with 10 μ g of fetuin or ovalbumin. **p < 0.01; ***p < 0.001 vs preceding concentration. Reproduced with permission from reference 177 Copyright 2011, American Chemical Society
Figure 21: Schematic illustration of the dual binding of a BAD-lectin to a glycoprotein. Schematic illustration of the dual binding of a BAD-lectin to a glycoprotein. (i) A BAD-lectin. (ii) A glycoprotein captured by the lectin by noncovalent glycan-specific recognition. (iii) A glycoprotein captured by both lectin and BA; the latter mediates boronate ester to form a stable covalent lectin-glycoprotein complex. (iv) A glycoprotein captured by a BA ligand alone. Reproduced with permission from reference ¹⁷⁰ Copyright 2013, American Chemical Society 55
Figure 22: SPR sensing of the affinity of the BAD-lectin probe for a carbohydrate-functionalized self-assembled monolayer (SAM). (A) Mannose functionalized molecules and the corresponding matrices for immobilization on sensor chips. SPR sensorgrams for the binding of (B) ConA and (C) BAD-ConA at a series of concentrations (from 10 to 1000 nM; bottom to top)

to a mannose-functionalized SAM chip. Reproduced with permission from reference ¹⁷⁰ Copyright 2013, American Chemical Society
Figure 23: Protein separation using MEG-protected antibody conjugated MNPs. (i) Immunoassay by MEG-protected antibody-conjugated MNPs. ii) MALDI-TOF mass spectra of human plasma (1 mL) from immunoaffinity extraction with anti-SAP MNPs: A) 25-fold dilution of human plasma; B) Extraction with anti-SAP MNPs (without blocking); C) Extraction with anti-SAP MNPs (BSA blocking); D) Extraction with anti-SAP MNPs (40 mm MEG blocking) after 1000-fold dilution. Adapted and reproduced with permission from reference Copyright 2006, John Wiley and Sons
Figure 24: Comparison of the antigen extraction performances of anti-SAP-R@MNP (R), anti-SAP-G@MNP (G), and anti-SAP-BA@MNP (BA) using mass spectrometry. MALDI-TOF MS spectra of the extracted antigen from (A) 16 and (B) 0.4 nM solutions of SAP. (C) Five consecutive measurements of the extracted antigen from a 12 nM SAP solution. Spectrum signal intensities were normalized to that of myoglobin, which was used as a mass spectrum internal standard. (D) MALDI-TOF MS analysis to examine the SAP extraction efficiency of anti-SAP-R@MNP (R), anti-SAP-G@MNP (G), anti-SAPBA-dex@MNP (BA), and anti-SAP-BA-dex@MNP (BA1) from human serum pretreated with 5 mM of <i>m</i> -aBA. Spectrum signal intensities (× 102 ion counts) were normalized to that of myoglobin (Myo), which was used as a mass spectrum internal standard. Adapted and reproduced with permission from reference ¹⁰² Copyright 2009, American Chemical Society
Figure 25: Light-induced covalent and oriented immobilization of Abs on BA-presenting surfaces. Upon UV irradiation (λ max = 365 nm), the (trifluoromethyl)phenyldiazirine functional groups in 1 generate highly reactive carbenes that spontaneously undergo insertion reactions to permanently tether the antibody on the surface. Adapted and reproduced with permission from reference ²¹³ Copyright 2014, American Chemical Society
Figure 26: Cancer cell isolation and analysis using two NP systems. (A) cell isolation using two NP systems. (B) Flow cytometric determination of MNP collection and separation efficiencies between target and control cells Images of extracted samples from (C) Target cells and (D) Control cells and (E) Flow cytometric comparison of target and control signal after 5-min incubation with magnetic and fluorescent NPs, followed by three washes by magnetic separation Confocal images of extractions from whole blood. (F) Extracted sample from target cell spiked whole blood, (G) Extraction from unspiked whole blood. Adapted and reproduced with permission from reference ²⁵² Copyright 2006, American Chemical Society
Figure 27: Using UCNP–Apt–Biotin and MNP–Av nanoprobes for CTCs detection and isolation (a) Schematic illustration of using UCNP–Apt–Biotin and MNP–Av nanoprobes for CTCs detection. Positive tumor cells are recognized by UCNP–Apt–Biotin nanoprobes, which are then specifically attached by MNP–Av NPs for magnetic separation. The UCL signals from UCNPs could be utilized for tumor cell detection. (b) A TEM image of as-made UCNPs (NaYF4:78% Y 20% Yb, 2% Er). (c) Upconversion luminescence spectrum of PEGylated UCNPs in an aqueous solution. Inset: a photograph of a UCNP aqueous solution excited by a 980-nm laser. (d) A TEM image of as-made MNPs. Reproduced with permission from reference ²⁵⁸ Copyright 2014, Springer.

Figure 28: Capture and SDS/PAGE analyses of GST-Ub using SC-GSH-NP. (A) From a protein mixture of GST-Ub and yeast proteome. Molecular weight marker (lane M), yeast proteome and GST-Ub mixture (lane 1), supernatants after mixing with glutathione sepharose 4B beads (lane 2), and capturing and eluting from glutathione sepharose 4B beads (lane 3), supernatants after mixing with SC-GSH-NP (lane 4), and after capturing and eluting from SC-GSH-NP (lane 5) (B) From a mixture of GST-Ub and the human serum proteome. Molecular weight marker (lane M), serum proteome with GST-Ub (lane 1), supernatant after mixing with glutathione sepharose 4B beads (lane 2), and after capturing and eluting from glutathione sepharose 4B beads (lane 3), supernatant after mixing with SC-GSH-NP (lane 4) and after capturing and eluting from SC-GSH-NP (lane 5). Adapted and reproduced with permission from reference ²⁸⁶ Copyright 2010, Korean Chemical Society
Figure 29: Glutathione functionalized MNPs for isolation of GST-fused proteins. (A) The synthetic route of the glutathione-decorated MNPs. (B) Glutathione-decorated MNPs selectively binds to GST-fused proteins of interest (POI) from a cell lysate and their own downstream applications. Adapted and reproduced with permission from reference ²⁸⁵ Copyright 2011, Royal Society of Chemistry
Figure 1.30: Circulating tumor cell isolation with MNPs modified with the EpCAM targeting peptide. (A) Screening of EpCAM targeting peptides from de novo designed peptide pool. (B) Isolation of CTCs in a magnetic field. (C) The binding capacity of IgG, anti-EpCAM and Pep10 on MCF-7, SK-BR-3, PC3 and Hep G2 cell lines was determined by flow cytometry. Percentage refers to the percentage of the cells fluorescence by FITC binding to the total cells. Experiments were done in triplicate and the reported error is the standard deviations. Reproduced with permission from reference ²⁷⁶ Copyright 2014, Royal Society of Chemistry
Figure 31: In vivo extraction and analysis of tumor cells with the help of YSA conjugated NPs. (i) <i>In vivo</i> incubation of cells with YSA conjugated NPs. (ii) Extraction efficiencies of the Hey and BG-1 cells. Compositions of Hey and BG-1 cells in the cell populations extracted from the peritoneum of three Balb/C female mice. The ratios were averaged from five counts performed on each of three mice. Error bars show the standard deviations. (iii) Confocal microscopic images of <i>in vitro</i> targeting of Hey cells. (a) Hey cells incubated with rhodamine-tagged MNPs (200X). (b) Hey cells incubated with rhodamine-tagged NP-YSA peptide conjugates (200×). (c) Higher magnification of Hey cells labeled with rhodamine-tagged NP-YSA peptide conjugates (400×). Adapted and reproduced with permission from reference ²⁸⁸ Copyright 2008, American Chemical Society.
Figure 32: TEM image of Gal-NPs, scale bar is 100 nm
Figure 33: curves for NP-NH2 2(dark blue), Gal-NPs (red) and Man-NPs (green)
Figure 34: Fluorescent emission spectra of the supernatant of TRITC labeled BS-I solutions after incubation with Gal-NP and magnetic mediated separation
Figure 35: Fluorescent emission spectra of the supernatant of FITC labeled Con A solutions after incubation with Man-NP and magnetic mediated separation

Figure 36: SDS-PAGE of lectins before addition of NP and after elution with 1 M sugar solutions. Lane 1: Molecular marker, lane 2: Con A before addition of Man-NP, lane 3: Con A eluted by 1 M mannose solution, lane 4: BS-I before addition of Gal-NP, lane 5: BS-I eluted by 1 M galactose solution.
Figure 37: Binding of galactose specific lectins to Gal-NP, Man-NP and TEOS-NP 1 as detected by Western blot using anti-SBA or anti-Gal3 antibodies respectively. Panel A: Isolation of exogenous lectin (SBA) spiked in B16F10 lysate using Gal-NP. Lane 1: before addition of glyco-NPs, Lane 2: unbound fraction (supernatant); Lane 3: PBS wash; Lane 4: galactose elution. Panel B: Blotting for Gal3 isolated from B16F10 cell lysate using Gal-NP. Lane 1: B16F10 lysate, Lane 2: unbound fraction (supernatant); Lane 3: PBS wash; Lane 4: mannose elution; Lane 5: galactose eluted fraction. Panel C: Isolation of Gal3 using TEOS-NP 1. Lane 1: B16F10 lysate; Lane 2: unbound fraction (supernatant); Lane 3: PBS wash; Lane 4: mannose elution; Lane 5: galactose elution. Panel D: Isolation of Gal3 using Man-NPs. Lane 1: B16F10 lysate; Lane 2: unbound fraction (supernatant); Lane 3: PBS wash; Lane 4: galactose elution; Lane 5: mannose elution. The numbers on left side of each panel indicate the positions of the corresponding molecular weight markers
Figure 38: Comparing commercial galactose micro-nanoparticles with Gal-NPs in Gal-3 isolation from B16F10 cell lysate. Lane 1-4 commercial gal-microparticles, lane 5-8 gal-NPs. Lane 1 and 5: lyaste, lane 2 and 6: unbound fraction, lane 3 and 7: mannose eluted fraction, lane 4 and 8: galactose eluted fraction
Figure 39: Binding of FITC labeled Gal-NPs to B16F10 cells incubated for 1 h or 12 hr. Incubation for 1 h (a, b, c) or 12 hr (d, e, f). Green channel showing FITC-labeled Gal-NPs, red channel for lysosome tracker and blue channel for DAPI showing nuclear staining
Figure 40: Identification of endogenous proteins bound to Gal-NPs. Identification of endogenous proteins bound to Gal-NPs. Panel A: B16F10 cells were incubated with Gal-NPs overnight, lysed, subjected to magnetic separation followed by elution of bound proteins. Lane 1: Supernatant after magnetic separation; Lane 2: PBS wash fraction; Lane 3: mannose eluted fraction; Lane 4: galactose eluted fraction. Panel B: Galactose eluted fraction passed through a desalting column to remove free galactose and subjected to fresh Gal-NP binding followed by sequential elutions. Lane 1: before addition of Gal-NPs, Lane 2: PBS wash; Lane 3: mannose eluted fraction; Lane 4: galactose eluted fraction. The bands around 37 kD and 15 kD were subjected to trypsinic digestion followed by LC/MS/MS analysis. The numbers on left side of each panel indicate the positions of the corresponding molecular weight markers
Figure 41: Blotting for endogenous lectins from whole cells bound to Gal-NP. B16F10 cells were incubated with Gal-NPs overnight. Blotting for endogenous lectins from whole cells bound to Gal-NP. B16F10 cells were incubated with Gal-NPs overnight. After incubation, cells were lysed through homogenization, followed by the elution protocols described above. Panel A: Blotting for Sfrs1. Lane 1: Residual lysis buffer after magnetic separation (supernatant); Lanes 2 and 3: PBS wash fraction, Lane 4: mannose eluted fraction; Lane 5: galactose eluted fraction. Panel B: Blotting for Gal3. Lane 1: Residual lysis buffer after magnetic separation (supernatant); Lanes 2 and 3: PBS wash fraction; Lane 4: mannose eluted fraction; Lane 5: galactose eluted

molecular weight markers
Figure 42: Comparing commercial gal-microparticles with Gal-NPs in Gal-3 isolation from whole cell. Lane 1-4 commercial gal-microparticles, Lane 5-8 gal-NPs. Lane 1 and 5: Residual lysis buffer after magnetic separation (supernatant), lane 2 and 6: wash fraction, lane 3 and 7: mannose eluted fraction, lane 4 and 8: galactose eluted fraction. The numbers on left side indicate the positions
Figure 43: Binding of GST, GST-Gal3, and GST-SFRS1 to Gal-NPs. Panel A: Binding of GST to Gal-NPs. Lane 1: Unbound fraction (supernatant), Lane 2: Wash fraction, Lane 3: Bound fraction. Panel B: Binding of GST-Gal3 to Gal-NPs. Lane 1: Unbound fraction (supernatant), Lane 2: Wash fraction, Lane 3: Bound fraction. Panel C: Binding of GST-Sfrs1 to Gal-NPs. Lane 1: Unbound fraction (supernatant), Lane 2: Wash fraction, Lane 3: Bound fraction. All of the blotting were carried out with the same anti-GST antibodies. The numbers on left side of each panel indicate the positions of the corresponding molecular weight markers
Figure 44: Further confirmation for the binding specificity of GST-Sfrs1 to Gal-NPs. Western blot results with anti-Sfrs1, and histogram representation of band intensities as determined by ImageJ. Lane 1: Before addition of Gal-NP; Lane 2: unbound fraction (supernatant); Lanes 3 and 4: PBS wash fraction; Lane 5: mannose eluted fraction; Lane 6: galactose eluted fractions. The numbers on left side of Western blot results indicate the positions of the corresponding molecular weight markers.
Figure 45: Further confirmation for the binding specificity of Sfrs1 to Gal-NPs. Binding of GST-Sfrs1 to TEOS-NPs as determined by Western blot using anti-GST. Lane 1: Before addition of TEOS-NP 1; Lane 2: Unbound fraction (supernatant); Lane 3: Wash fraction; Lane 4: mannose eluted fraction; Lane 5: galactose eluted fractions; Lanes 5 and 6: galactose eluted fractions. The numbers on left side of indicate the positions of the corresponding molecular weight markers 138
Figure 46: Comparison of Sfrs1 in B16F10 and B16F1 cells. Western blot results and histogram representation of the band intensities as analyzed by ImageJ software is shown. Lane 1: B16F10, Lane 2: B16F1. Panel B: Equal volume of the lysate prepared from equal number of B16F10 and B16F1 cells was resolved on SDS-PAGE and blotted for Sfrs1 and GAPDH. Western blot results and histogram representation of the band intensities as analyzed by ImageJ is shown. Lane 1: B16F10. Lane 2: B16F1. Blotting for glyceraldehyde 3-phosphate dehydrogenase (GAPDH) was used as loading control. The numbers on left side of Western blot results indicate the positions of the corresponding molecular weight markers
Figure 47: The probe carrying both the carbohydrate ligand that will provide the required affinity and specificity for the recognition of the lectins, and the photoactive group for covalent tethering of the captured lectin upon UV irradation
Figure 48: Lectin isolation from cell lysate using a carbohydrate affinity probe combinined with photoactivatable moiety
Figure 49: Lectin isolation from live cells using a carbohydrate affinity probe combinined with photoactivatable moiety

Figure 60: Conjugation of cathepsin B linkers-OVA(p) antigen construct by taking advantag the reducing end equilibrium between hemiacetal and straight chain forms of carbohydrate	e of
present at the surface of the Ac-Dx-NPs through reductive amination	. 199
Figure 61: Glycan microarrays by FITC labeled annexn-V	. 208
Figure 62: Glycan microarrays by FITC labeled histone protein.	. 209
Figure 63: HPLC chromatogram of purified OVA peptide	. 210
Figure 64: ESI spectrum of purified OVA peptide, OVA(P).	. 211
Figure 65: ESI spectrum of the supernatant after OVA(P)-Ac-Dx-NPs were resuspended in Fovernight	
Figure 66: ESI spectrum of the supernatant after OVA(P)-Ac-Dx-NPs were resuspended in 0 TFA overnight.	

LIST OF SCHEMES

Scheme 1: Synthesis of glyco-NP	118
Scheme 2: Synthesis of OVA(P) through solid phase peptide synthesis (SPPS)	176
Scheme 3: Synthesis of OVA(P)-Ac-Dx-NPs	177

KEY TO ABBREVIATIONS

AAL Aleuria aurantia lectin

Ac-Dx-NPs Acetalated dextran nanoparticles

AGP alpha-acid glycoprotein

ALVs Antigen loss variants

APTES Aminopropyltriethoxysilane

ATCC American Type Culture Collection

BA Boronic acid

BOP Benotriazole-1-yl-oxy-tris-(dimethlyamino)-phosphonium

hexafluorophosphate

BSA Bovine serum albumin

BSI Bandeiraea simplicifolia lectin

CAP Chelation assisted photoimmobilization

CBT 2-cyanobenzothiazole

CFG Consortium of functional glycomics

CFA Complete Freund's adjuvant

CID Collision induced dissociation

cm Centimeter

CoA Coenzyme A

Con A Concanavalin A

CPRG Chlorophenol red-β-D-galactopyranoside

CTC Circulating tumor cells

CTL Cytotoxic T lymphocyte

Cy5 Cyanine 5

DAPI 4',6-diamidino-2-phenylindole

DMSO Dimethyl sulfoxide

DC Dendritic cells

DCM Dichloromethane

DC-SIGN Dendritic cell specific intracellular adhesion molecule-3 grabbing

nonintegrin

DHA Dihydrobenzoic acid

DIPEA Diisopropylethylamine

DLS Dynamic light scattering

DMF Dimethyformamide

DMEM Dulbecco's modified Eagle medium

DNA Deoxyribonucleic acid

DTT Dithiothreitol

EDTA Ethylenediaminetetracetic acid

ELISA Enzyme linked immunosorbent assays

EpCM Epithelial cell adhesion molecule

EPL Expressed protein ligation

ESI-MS Electrospray ionization mass spectrometry

FACS Fluorescence activated cell sorting

FBS Fetal bovine albumin

FITC Fluorescein isothiocyanate

FKBP4 FK-506 binding protein 4

FTIR Fourier transform infrared spectroscopy

Gal Galactose

Gal3 Galectin-3

Gal-NPs Galactose functionalized nanoparticles

GAPDH Glyceraldehyde-3-phosphate dehydrogenase

GSH Reduced glutathione

GST Glutathione-S-transferase

HA Hyaluronic acid

Hb Hemoglobin

HBTU 2-(1H-benzotriazol-1-yl)-1,1,3,3-tetramethyluronium hexafluorophosphate

HCC Human hepatocellular carcinoma

HER2 Human endothelial receptor-2

HPLC High pressure liquid chromatography

HRP horseradish peroxidase

HOBt Hydroxybenzotriazole

hr Hour

HSA Human serum albumin

IACUC Institutional animal care and use committee

ICP-OES Inductively coupled plasma optical emission spectrometry

IFA Incomplete Freund's adjuvant

IgG immunoglobulin G

IOMNP iron oxide magnetic nanoparticle

IONPs Iron oxide nanoparticles

IP Immunoprecipitation

IPTG Isopropyl-β-D-thiogalactopyranoside

kDa Kilodalton

LC Long chain

LC/MS/MS Liquid chromatography tandem mass spectrometry

LDA linear discriminant analysis

LMWH low molecular weight heparin

M Molar

MA Maackia amurensis

MALDI-TOF MS Matrix assisted laser desorption time of flight mass spectrometry

Man Mannose

Man-NPs Mannose functionalized nanoparticles

MBs Magnetic beads

MBP-HepA maltose binding protein-heparinase-I

mDHFR Murine dihydrofolate reductase

MEAA 2-[2-(2-methoxyethoxy)ethoxy]acetic acid

MFI Mean fluorescence intensity

MGNPs Magnetic glyconanoparticles

MHC-I Major histocompatibility molecule class I

min Minutes

mM Millimolar

MNPs Magnetic nanoparticles

moDCs Monocyte derived dendritic cells

MPEG Methoxypolyethylene glycol

MRI magnetic resonance imaging

MYO Myoglobin

NCL Native chemical ligation

NIR Near infrared

nm Nanometer

NPs Nanoparticles

PEG Polyethylene glycol

^oC Degrees centigrade

OA Oleic acid

ODE Octadecene

OVA Ovalbumin

PBMCs Peripheral blood mononuclear cells

PBS Phosphate buffered saline

PMSF Phenylmethanesulfonyl fluoride

PNIPAA p(*N*-isopropylacrylamide)

POI Protein of interest

PVDF Polyvinylidene fluoride

PVP polyvinylpyrrolidone

RMS Reverse micelles system

RNA Ribonucleic acid

RNB Ribonuclease B

RT Room temperature

RuBpy Tris(bipyridine)ruthenium(II) chloride

SAP Serum amyloid P

SBA Soybean agglutinin

sc Subcutaneous

SC Short chain

SDS sodium dodecyl sulfate

SDS-PAGE sodium dodecyl sulfate polyacrylamide gel electrophoresis

SELEX Systematic evolution of ligands by exponential enrichment

SEM Scanning electron microscopy

SNA Sambucus nigra

SPR Surface plasmon resonance

SPPS Solid phase peptide synthesis

SSEA-4 Stage-specific embryonic antigen 4

TBS Tris buffered saline

TBST TBS-Tween 20

TCR T-cell receptor

TEOS Tetraethoxysilane

TEM Transmission electron microscope

TEMED N,N,N',N'-tetramethylethylenediamine

TEVp Tobacco etch virus protease

TFA Trifluoroacetic acid

TGA Thermogravimetric analysis

TIL Tumor infiltrating lymphocytes

TIPS Triisopropylsilane

TMR Tetramethylrhodamine

TRITC Tetramethylrhodamine

Ub Ubiquitin

UCL Upconversion luminescence

UCNPs Upconverion nanoparticles

μg Microgram

μL Microliter

μm Micrometer

UPLC Ultra performance liquid chromatography

UV Ultraviolet

VSSA Volume specific surface area

WGA Wheat germ agglutinin

XOD Xanthine oxidase

ZDS Zwitterionic dopamine sulfate

CHAPTER 1: Review of magnetic nanoparticles functionalized with biomolecules and their application in bioseparation and enrichment

1.1: Introduction

Nanoparticles/nanomaterials are the main products of nanotechnology. Nanotechnology involves the design, production and use of structures through control of the size and shape of the materials at the nanometer scale.¹ A number of definitions of nanoparticles/nanomaterials are currently available and all use size limits.²⁻⁴ The most typical definition of nanomaterials is any intentionally produced particles (engineered nanomaterials) with sizes between 1 and 100 nm in at least one of its dimensions that show properties not found in bulk samples of the same material.⁵ While the reference to a size range between 1 nm and 100 nm is useful and universally applicable, scientific evidence does not pinpoint any specific size associated with properties linked to the nanoscale. Defining nanoparticles (NPs) based on size parameters may exclude aggregates and agglomerates of primary particles or, more complex multi-component nanomaterials used in medical applications. Similarly restricting the definition on size may exclude materials which have acquired a coating as their external dimension may likely be larger than the specified upper size limit of 100 nm. A useful additional parameter to define NPs is the volume specific surface area (VSSA). This parameter includes internal surfaces if they exist with the same specified range as the external dimensions. The inclusion of a reference to internal structure will include materials that consist of aggregates, agglomerates and multi-component assemblies within the scope of the definition. A commonly used threshold for a nanoparticle is a VSSA greater than or equal to 60 m²/cm^{3/2} More recently, a new definition of NPs has been proposed to mean any material at the sub-micrometer level, be it biotic or abiotic that can be interfaced with a "biological" in pursuit of creating a novel

"value-added" entity. Further, this material must be intentionally produced on this scale, have discrete functional or structural parts arrayed on its surface or internally, and display a unique property. This definition allows the inclusion of all types of NPs as synthesized from metals, noble metals, oxides, and semiconductors, along with a variety of nontraditional and nonmetal NPs. The latter include carbon allotropes, polymeric, dendrimer, and chemical NPs, proteins, and virus-derived NPs, along with lipids, carbohydrates, liquid crystals, and other assorted materials. Since NPs form a basis for many engineered nanomaterials, this discussion will focus on NPs.

Biological molecules or biomolecules can be classified into four major categories: carbohydrates, proteins, lipids and nucleic acids. This classification encompasses all monomeric building blocks (i.e. amino acids, fatty acids, nucleotides, monosaccharides) or the fully formed functional polymers such as peptides, plasmids, and polysaccharides.⁶ From biotechnology perspective, biologicals may refer to functionally active molecules, offering binding, catalytic, or therapeutic activity (e.g. antibodies, enzymes, cytokines, antigens, hormones). Biologicals have been further expanded to include enzymatic active cofactors, all forms of drugs and other biologically active small molecules such as reporters and contrast agents, and biocompatible molecules such as poly(ethylene glycol) and metal complexes.^{6,8,9} In the course of our discussion, more emphasis will be given to magnetic nanomaterials immobilized with the major biomolecules; carbohydrates, lectins, antibodies, enzymes, nucleotides, oligopeptides and proteins other than lectins, enzymes and antibodies.

1.2: Synthesis of magnetic nanoparticles

This section will present major synthetic pathways utilized in preparation of magnetic iron oxide nanoparticles. Iron oxide nanoparticles (IONPs), mainly magnetite (Fe₃O₄) or its oxidized form maghemite (γ-Fe₂O₃), are tiny iron oxide particles with diameters ranging between 1-200 nm, and they can be easily synthesized from inexpensive iron salts. These two representatives of IONPs have received considerable attention due to their biocompatibility and their biodegradability. Usually, methods for IONP synthesis are given great importance as they can significantly affect the size, shape, structure, dimensions, properties and hence the applications of NPs. Biological applications especially require these NPs to have high magnetization values, narrow particle size distribution and a special surface coating for both avoiding toxicity and allowing the coupling of biomolecules. Most commonly, IONPs are prepared by co-precipitation of iron salts in basic media, high temperature thermal decomposition and to a lesser extent microemulsion and hydrothermal approaches. Co-precipitation and thermal decomposition are the two most used methods in IONPs preparations and will be briefly reviewed in this section.

1.2.1: The co-precipitation method

The co-precipitation method of preparing IONPs is probably the simplest and the most efficient chemical pathway to obtain magnetic nanoparticles (MNPs).¹¹ Iron oxide (Fe₃O₄) or its oxidized form (γ -Fe₂O₃) are prepared by co-precipitation of aqueous salts solutions of ferrous (Fe²⁺) and ferric (Fe³⁺) in an aqueous basic media, **Figure 1.1**, **panel A, and B**. The first controlled preparation of IONPs using alkaline precipitation of iron salts was performed by Massart.¹² Conventionally, magnetite preparation consists of mixing a solution of (Fe²⁺) and

(Fe³⁺) chloride at 1:2 molar ratio with mechanic agitation under an inert atmosphere by bubbling nitrogen or argon gas through the solution to protect against its oxidation to maghemite or hematite (γ-Fe₂O₃). Oxidation affects the physical and chemical properties of the NPs.¹³⁻¹⁵ The resulting solution is heated to 80 °C with elevated stirring speed while a solution of NH₄OH (10% by volume) is quickly added.¹⁶ According to the thermodynamics of the reaction, a complete precipitate of Fe₃O₄ magnetite NPs is expected to form between pH 9 and 14.¹³ Although a large amount of NPs can be synthesized using this process, the control of particle size distribution in aqueous media is limited due to particle agglomerations, since only kinetic factors are controlling the growth of the crystal. To reduce agglomeration, the surface of IONPs is usually modified with stabilizers such as surfactants or polymers at the time of preparation.

Surface modification of the NPs prepared through the co-precipitation method can be achieved by coating with non-polymeric organic stabilizers (chelating organic anions) such as oleic or citric acid, with polymeric stabilizers such as poly(vinyl alcohol) (PVA) or poly(ethylene glycol) (PEG). Also used are inorganic molecules such as gold, silica (especially tetraethoxysilane, TEOS and aminopropyltriethoxysilane, APTES), and gadolinium, and with target ligands some of which will be discussed in depth in the ensuing sections. Besides reducing agglomeration, surface modification during formation can help control the size of the NPs. 14

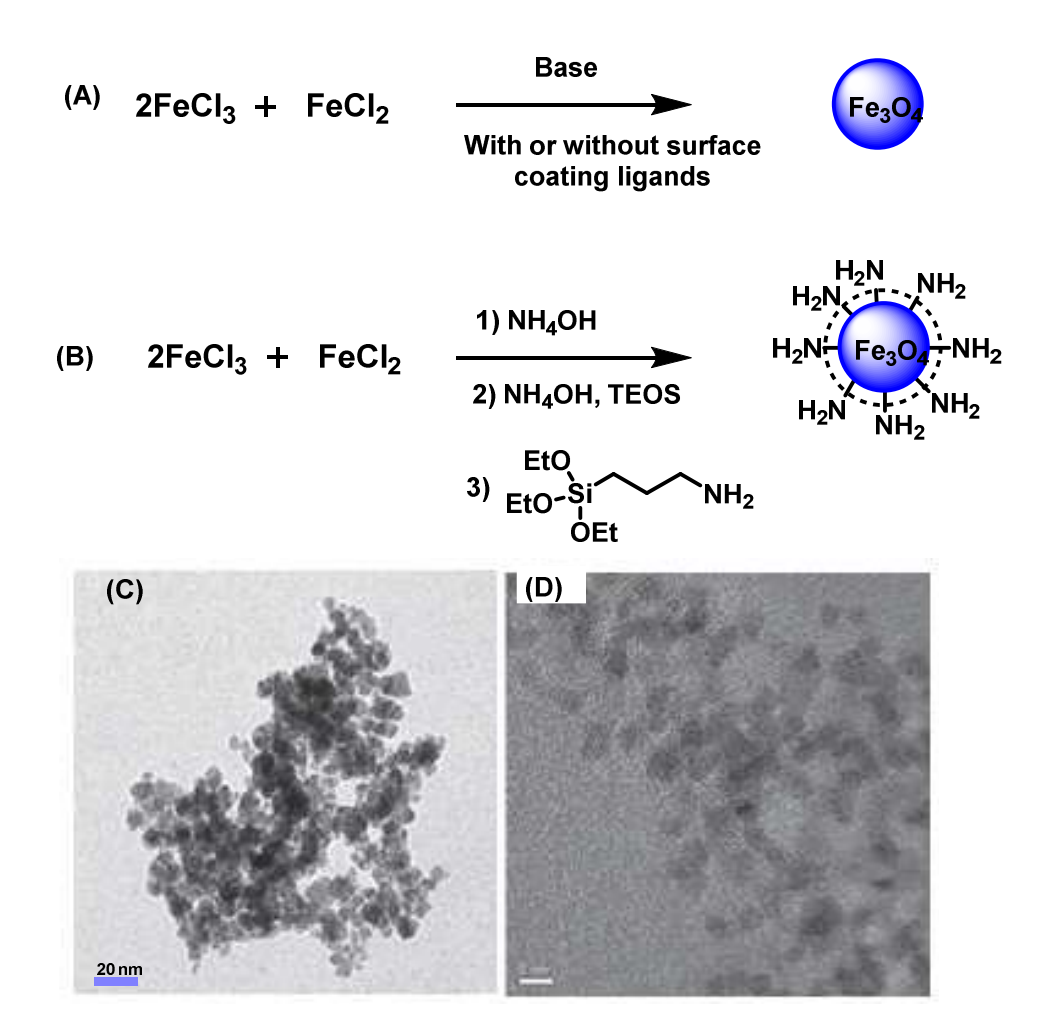


Figure 1: Synthesis of IONPs using the co-precipitation method (A) General scheme for synthesis of IONPs using the co-precipitation method, (B) Synthesis of silica-coated IONPs and subsequent amine functionalization with APTES, TEM images of (C) Bare IONPs (the scale bar 20 nm), (D) IONPs coated with APTES (the scale bar is 5 nm). Reproduced with permission from reference¹⁷ Copyright 2014, John Wiley and Sons

1.2.2: Thermal decomposition method

With the co-precipitation method, it is difficult to precisely control particle size uniformity and crystallinity. To improve monodispersity, size and magnetic susceptibility of the IONPs, high temperature thermal decomposition methods were developed. IONPs can be obtained by high temperature decomposition of iron organic precursors such as Fe(acac)₂,

Fe(CO)₅, or Fe(acac)₃.¹⁸ In this process, the reaction conditions such as solvent, temperature, and time, concentration and ratio of reactants, nature of precursors, usually have important effects on the size and morphology of the NPs. A representation of IONPs synthesis by thermal decomposition method is summarised in **Figure 2 and 3**.

Na and coworkers prepared highly crystalline and monodispersed maghemite nanocrystallites by high temperature aging of iron-oleic acid metal complex via thermal decomposition of iron pentacarbonyl in the presence of oleic acid at 100 °C.¹⁹ The synthetic procedures developed had several important advantages. First, they allowed highly crystalline and monodispersed NPs to be obtained directly without a further size-selection process; second, particle size could be easily and reproducibly altered by changing reacting ratios of iron precursor and oleic acid; and lastly, the nanocrystallites could be easily dispersed in many hydrocarbons without particle aggregation.

The research group of Shouheng Sun has done the pioneering work in the synthesis of monodisperse IONPs through high temperature thermal decomposition. In their earlier work, they demonstrate that high-temperature (265 °C) reaction of Fe(acac)₃ in diphenyl ether in the presence of alcohol, oleic acid, and oleylamine could be used to make monodispersed magnetite NPs. The as-synthesized Fe₃O₄ nanoparticle assemblies could be transformed easily into γ -Fe₂O₃ by oxidation under O₂. They later envisioned that this reaction could be readily extended to the synthesis of MFe₂O₄ NPs (with M = Co, Ni, Mn, Mg, etc.) by simply adding a different metal acetylacetonate precursor to the mixture of Fe(acac)₃ and 1,2-hexadecanediol. They were successful in the synthesis and characterization of Fe₃O₄ and related MFe₂O₄ NPs (with M = Co and Mn as two examples) with sizes tunable from 3 to 20 nm in diameter. The process involves high-temperature (up to 300 °C) reaction of metal acetylacetonate with 1,2-hexadecanediol, oleic

acid, and oleylamine. The size of the oxide NPs could be controlled by varying the reaction temperature or changing metal precursors. Alternatively, with the smaller NPs as seeds, larger monodispersed NPs up to 20 nm in diameter could be synthesized by seed mediated growth.²⁰ Ahniyaz et al. reported non-hydrolytic, alkoxide-based route to synthesize iron oxide nanocrystals. Their method was through the surfactant-free thermal decomposition of iron 2-methoxy-ethoxide precursor that resulted in the formation of uniform iron oxide nanocrystals with an average size of 5.6 nm.²²

The direct products of the above-mentioned thermal decomposition approaches are organic-soluble, which to some extent limits their use in the biological and biomedical fields, especially for *in vivo* applications. Therefore, it is very important to further develop the thermal decomposition method to make the nanoparticle products fully dispersible in aqueous media. Several approaches have been reported to make them dispersible in aqueous media: by directly synthesizing water-soluble magnetic NPs, or by using strong polar molecules to modify the MNPs and through ligand exchange among others.

Gao and coworkers report a one-pot reaction to achieve water-soluble iron oxide nanocrystals by thermal decomposition of Fe(acac)₃ or FeCl₃·6H₂O in 2-pyrrolidone yielding IONPs with 5 nm diameter.²³ In this one-pot reaction, 2-pyrrolidone was chosen as the solvent and stabilizer because it has strong polarity, a high boiling point, and coordination capacity with transition metal ions. Thus 2-pyrrolidone serves as a media for high-temperature reactions and surface coordination rendering the magnetite nanocrystal water soluble and colloidal stable in solution.^{23,24} Peng et al. showed that thermal decomposition of Fe(CO)₅ in octadecene (ODE) at 180 °C in the presence dopamine-based surfactant instead of oleylamine, resulted in the surface modification of monodispersed Fe₃O₄ NPs rendering them water soluble.²⁵ Water-soluble

superparamagnetic Fe₃O₄ NPs with an average diameter of 9.5±1.7 nm have also been synthesized by thermal decomposition of Fe(acac)₃ in methoxy polyethylene glycol (MPEG). Similarly in this reaction, MPEG was used as both a solvent and modifying agent.²⁶

Ligand exchange involves replacing the hydrophobic ligands on the particle surface by molecules containing polar groups. Because of the multiple carboxylic acid groups possessed by hyaluronic acid (HA), it has been used to displace oleic acid off the surface of the NPs rendering them water soluble.²⁷ Figure 1.3 highlights the transformation of IONPs to water soluble using HA. Using a two-step ligand exchange process, Bawendi and coworkers reported the displacement of oleic acid of the surface of the NPs with zwitterionic dopamine sulfate (ZDS). hydrophobic First the native oleic acid ligand was exchanged by 2-[2-(2methoxyethoxy)ethoxy]acetic acid (MEAA) ligand in methanol. The purpose of this first exchange was to increase the solubility of the NPs in the solvent mixture used in the second step. Next, in a dimethylformamide/water mixed solvent the MEAA ligand was replaced by ZDS moiety.²⁸ Polymer ligand exchange has also been used as an efficient method to prepare water soluble nanocrystals.²⁹ Narain et al. reported the thermal decomposition synthesis of water soluble 10 nm IONPs through the exchange of oleic acid by p(N-isopropylacrylamide)(PNIPAAm).³⁰

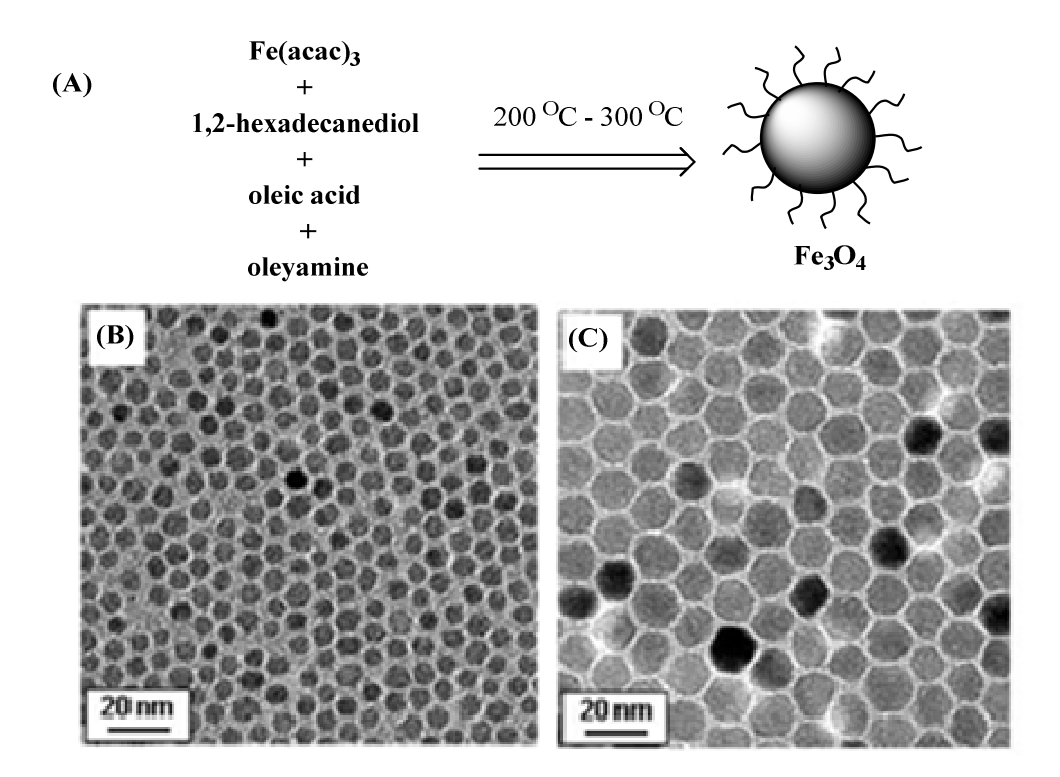


Figure 2: Synthesis of monodispersed IONPs via thermal decomposition (A) An example of a synthetic scheme. TEM images of (B) 6 nm and (C) 12 nm IONPs. Adapted with permission from reference²⁰ Copyright 2004 American Chemical Society

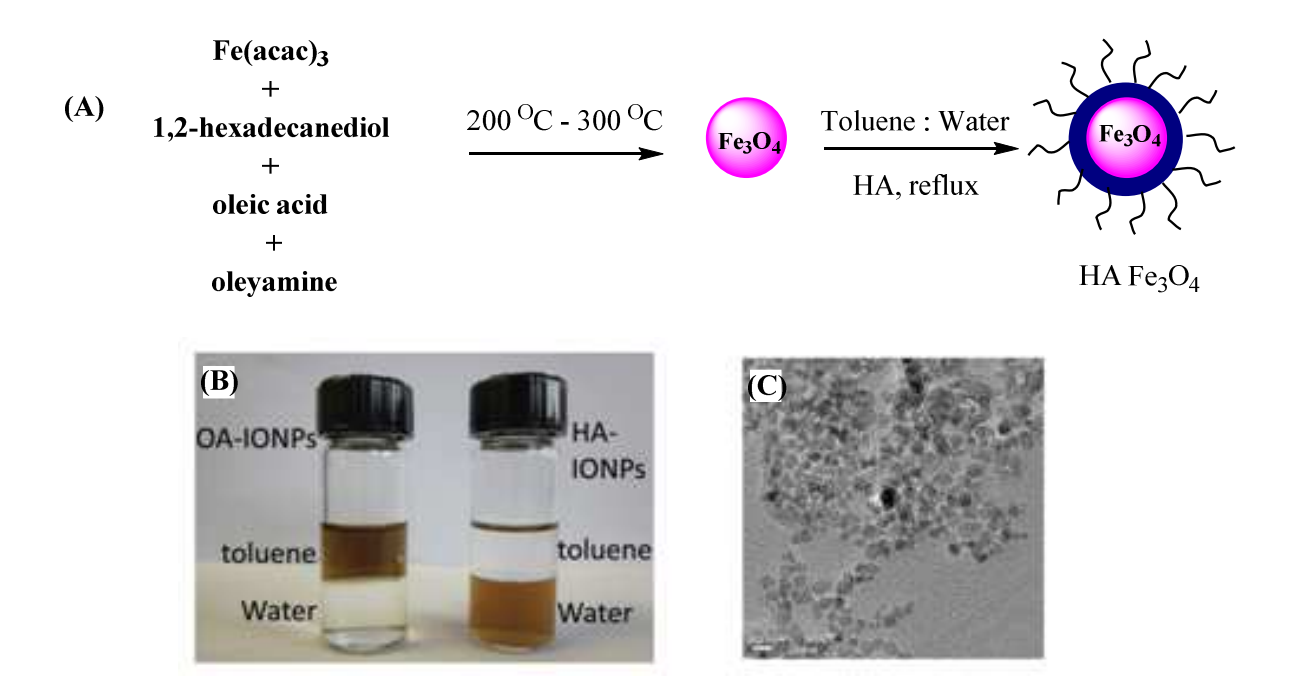


Figure 3: Synthesis of water soluble IONPs via thermal decomposition (A) Synthesis of water soluble HA functionalized IONPs (HA-IONPs) via thermal decomposition. (B) Picture of OA-IONPs and HA-IONPs in a toluene-water two phase system, (C) TEM images of HA-IONPs (scale bar is 10 nm). Adapted with permission from reference²⁷ Copyright 2011, Royal Society of Chemistry.

1.3: The chemistry for immobilization of biomolecules

1.3.1: Ideal criteria and general considerations for immobilization

The most common methods used to immobilize biomolecules on NPs have been partly adapted from those used in immobilization of biomolecules on other solid support systems. Therefore in this review, solid support systems, solid surfaces and NPs may be used interchangeably. Immobilization of biomolecules on solid support systems can be attained either by covalent or non-covalent linkages. The choice for a particular immobilization chemistry is dictated in part by a combination of factors including: surface chemistry, the nature of the NP

surface ligands and their available functional groups, the type of biological molecule and its chemical composition, and the utility desired in the final application of the NP.⁶

Several criteria that define ideal chemistries of choice for the controlled display of biomolecules on NPs making them suitable in bioseparation applications have been proposed. However, they may be hard to achieve in real practice. Firstly, the conjugation chemistry should have control over the valence or ratio of biomolecule per NP. 9 Usually, monovalency can be used to identify and correlate single binding events, while higher valency (multivalency) can improve binding interactions. Multivalency is a key principle in nature for achieving strong, yet reversible interactions and has been applied in many applications for a targeted strengthening of an interaction between different interfaces or molecules.³¹ Conversely, aiming for high valency may result in overconjugation, which can potentially impair binding interactions due to steric effect of the surface molecules.⁶ For effective bioseparation applications, the linkage between the NP and biomolecule should be permanent (i.e. covalently linked). A representative list of covalent immobilization of substrates to solid supports is summarised in **Figure 4**. Non-covalent linkages may not be stable under some conditions such as pH, and temperature changes. This could potentially impair the performance of the final conjugates. More importantly, the chemistry of choice should maintain the optimal function and activity of the biomolecules. It should not lead to loss of the biological recognition abilities of the biomolecule, or loss of NP stability. The conjugation chemistry of choice should be able to control the orientation of the biomolecule on the NP. For example, protein, enzyme, and antibody activities are dependent upon their binding sites having access to the environments. Similarly, the functionality of the NP should not be compromised. Finally the conjugation chemistry should be reproducible between experiments, between different types or batches of NP carrying the same biomolecule. ^{6,9}

Since maintaining the orientation and the biological activity of the biomolecule are the core requirements for bioseparation application of NP-biomolecule bioconjugates, several strategies of biomolecule immobilization have been proposed. The use of flexible spacer linkages between NP and biomolecules allows the biomolecules in NP-conjugates to adopt conformations that interact with their target and at the same time controls the attachment of the biomolecule to the NP. As reported by Yan and coworkers, spacer length and type play a significant role in influencing the binding ability of the immobilized biomolecules.³² The activity of the biomolecules can also be preserved by using bioorthogonal conjugation chemistries. These chemistries do not have reactivity towards the functional groups that are intrinsic to biomolecules because the functional groups providing the high reaction specificity are generally not naturally occurring. ⁶ Bioorthogonal chemistry is very useful for protein conjugation because the reactivity of many different amino acid residues can potentially result in undesirable sidereactions due to comparable number of carboxyl (e.g., glutamic acid, aspartic acid) and amino groups (e.g. lysine). Thus, protein-protein cross-linking efficiently competes with NP-protein coupling when using coupling chemistries such as carbodiimide chemistry.³³ Bioorthogonal reactions can enable clean and efficient labeling in biological matrices such as live cells, and as complex as serum.³⁴ Some of the best approaches to achieve bioorthogonal immobilization of biomolecules will be discussed in the next section.

NP	Substrate	Cunjugate product	Reaction
F6304—NH ₂	но	Fe ₃ O ₄ —N	Amide bond formation
Fe ₃ O ₄ —NH ₂	N-O	Fe ₃ O ₄ —N	Amidation
Fe ₃ O ₄ —NH ₂	S=C=N-	Fe ₃ O ₄ — N H	Thiourea
Fe ₃ O ₄ —NH ₂	н	Fe ₃ O ₄ —N—N	Reductive amination
Fe ₃ O ₄ —NHNH ₂	н	Fe ₃ O ₄ —NHN=	Hydrazone formation
Fe ₃ O ₄ —O-NH ₂	н	Fe ₃ O ₄ —O-N	Oxime formation
Fe ₃ O ₄ OH	H ₂ N—	Fe ₃ O ₄	Amide bond formation
OH B OH	HO	Fe ₃ O ₄ —B	Boronic ester formation

Figure 4: Selected methods for covalent immobilization of substrates to solid supports. Partly adapted with permission from references^{6,35} Copyright 2013 and 2011, American Chemical Society

Figure 4 (cont'd)

NP	Substrate	Conjugate produc	Reaction
Fe ₃ O ₄ —SH		Fe ₃ O ₄ —S	Thioether
O ₂ N S-S N	HS-	Fe ₃ O ₄ —S——S—	Disulfide bond formation
Fe ₃ O ₄ —N ₃	H ₃ C-	Fe ₃ O ₄ —N	Amine insertion r eaction
Fe ₃ O ₄ —N ₃	Ph ₂ P MeO	Ph ₂ P H ₂ P	Staudinger ligation
Fe ₃ O ₄ —N ₃	=-	Fe ₅ O ₄ —N-N-N-N-N-N-N-N-N-N-N-N-N-N-N-N-N-N-N-	Huisgen-2,3- cycloaddition
Fe ₃ O ₄ ——	N-O	Fe ₉ O ₄	Diel-Alders reaction
O SH N NH ₂	RS	Pe ₃ O ₄ NH	Native chemical ligation
NH ₂ N N N N N=NH	HS-	Fe ₃ O ₄ S	SNAP-mediated immobilization
Fe ₃ O ₄	N ₃	Fe ₃ O ₄ N	Copper free click chemistry

1.3.2: Non-covalent attachment

The non-covalent approach relies on electrostatic interactions, chelation, hydrogen bonding, or hydrophobic interactions to immobilize the biomolecules onto NP surface either directly or indirectly. Immobilization of biomolecules by direct adsorption onto NP surfaces has been successfully used to prepare functionalized magnetic NP and especially carbohydrate functionalized NP.³⁶⁻³⁸ Since these chemistries often require only stoichiometric mixing of the two components, they are typically referred to as self-assembly. These approaches can be advantageous in that they generally offer rapid and facile bioconjugation without the need for additional reagents and can often provide better control as a result.⁶ Although the direct absorption approach is operationally simple, biological recognition of the immobilized biomolecule may be impaired since the biomolecules are directly involved in NP chelation.³⁹

The indirect immobilization approach can address this problem. Besides, it can also help control the ligand orientation on NP surface. Indirect immobilization is achieved through secondary interactions between functional groups covalently attached to the NP surface and biomolecules. The main examples of such interactions include is biotin-avidin or biotin-streptavidin, 40-42 His tag-Ni²⁺, 43-47 and anti-GST-GST, 48 GST-glutathione, 49 an antibody-protein G, 50 interactions where the solid surface and biomolecular partner are functionalized to display one of the cognate pair, **Figure 5**. 28 Although these approaches have been successfully employed in several applications, the presence of avidin/streptavidin or antibodies on the surface could interfere with assay, while His tag-Ni interactions are unstable to some experimental conditions such as low pH. 51 Indirect non-covalent attachment of biomolecules can also be achieved through dative bond formation. Well known examples of dative bonding include Au-thiol, 52-57

Fe-dopamine,³⁸ and Fe-Phosphate^{58,59} chemisorption. The drawbacks of dative bonds are that they can be broken by changes in pH, oxidation, and displacement by other similar molecules.

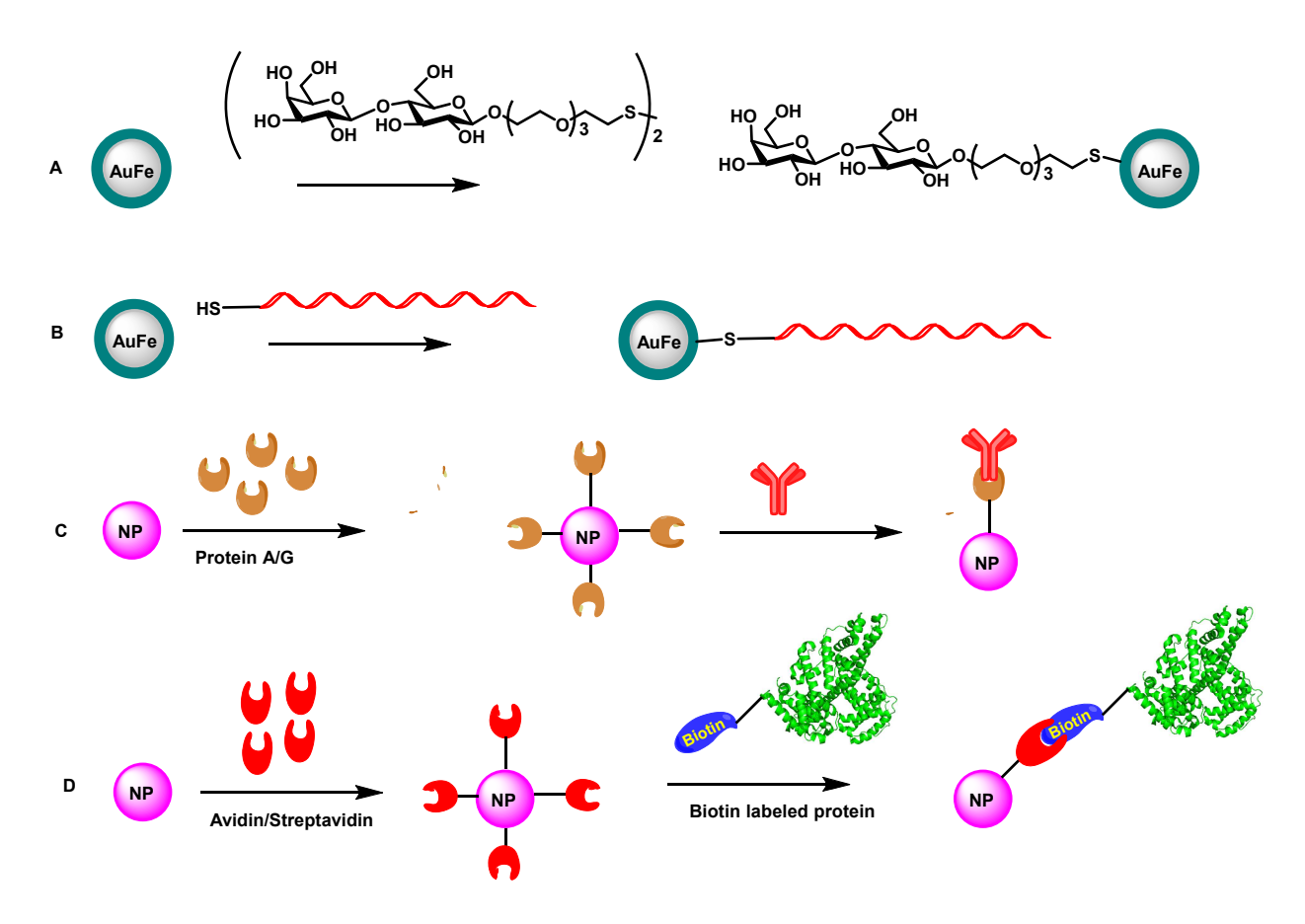


Figure 5: Representative of non-covalent immobilization of biomolecules on NPs. (A) Immobilization of carbohydrate (B) immobilization of oligonucleotide through Au-thiol dative bond formation. (C) Immobilization of antibody (D) Immobilization of biotin labeled protein through secondary interaction

1.3.3: Covalent approach

Conjugation of biomolecules to magnetic NPs through covalent bond formation is the most common approach, because it leads to strong bonds between the biomolecule and the NP. Most commonly, covalent functionalization of NPs starts from aminated NPs. Amines can be introduced onto the magnetic NPs through several approaches: functionalization of iron oxide

NPs with amine containing siloxanes through the Stöber process, 60-62 through the derivatization of dextran coated IONPs by treatment of epichlorohydrin followed by ammonia, 63-65 through coating with free amine containing proteins such as apoferritin. 66 Besides amine, other reactive groups that have been introduced onto the NPs surface and other solid surfaces to facilitate functionalization of biomolecules is summarized in Figure 3. Among the biomolecules, functionalization of NPs with carbohydrates is relatively easy compared to that of more complex biomolecules such as proteins and nucleic acids. The main reason is because the methods for chemical modification of the carbohydrate molecules prior to their conjugation to the NPs have been widely developed. In addition, most of these methods involve derivatization of carbohydrates at the reducing end leading to introduction of linkers that carry the reactive group used for immobilization on to the NP. This ensures that the biological recognition ability of the carbohydrate is preserved. To covalently conjugate carbohydrates to the NPs, a variety of strategies have been developed, which include the Huisgen [2+3] alkyne-azide cycloaddition reaction, 67-69 amide and amine bond formation, 70-73 thiol-ene reaction, 74 imidine linkage, and photochemistry. 75,76 A representative of carbohydrate conjugation to NPs is summarised in Figure 6, while a detailed discussion of these methodologies have been reported elsewhere.¹⁷

Immobilization of proteins, including lectins, enzymes and antibodies has traditionally relied on the reactions between the intrinsic reactive groups with their reacting partners immobilized on the solid support. As mentioned earlier this leads to random orientation of the proteins. In addition, since the reaction is not site-specific, the conjugation may occur at or in close proximity to the active binding site, which could damage their native biological functions, a factor very important for bioseparation application. To achieve uniform orientation and site-specific immobilization, bioorthogonal conjugation chemistries have been used. These

chemistries do not have reactivity towards the functional groups that are intrinsic to biomolecules because the functional groups providing the high reaction specificity are generally not naturally occurring. Subsequently, the participating functional groups are usually inert to biological moieties and selectively react with each other under biocompatible conditions. Additionally, it is considered helpful if one reactive group is small and therefore minimally perturbing a biomolecule into which it has been introduced.⁷⁷ Example of these chemistry from **Figure 5** includes; Huisgen cycloaddition (click chemistry), Staudinger ligation, native chemical ligation (NCL), enzymatic catalyzed ligation, and SNAP-mediated immobilization.

It is however important to note that the reactive groups can be introduced either chemically or biosynthetically. Chemical introduction can be disadvantageous as most proteins do not withstand the harsh conditions employed in the chemical modification, making biosynthetic pathway to be the best alternative. In biosynthetic pathway, proteins are expressed to display one of the requisite bioorthogonal functional groups followed by conjugating to its reacting partner displayed on the solid surface. Conjugation can be accomplished either chemically or enzymatically. As a requirement, bioorthogonal chemistry must be aqueous, resist nucleophilic attack, should not require extensive heating (usually $\leq 37^{\circ}$ C) or a high molar excess of a reagent while still having relatively short reaction times.

Biosynthetic reactive group introduction into proteins by expressed protein ligation (EPL) has been widely used because of its versatility in accommodating further modification. It has been established to be a simple but powerful method in protein engineering to introduce sequences of unnatural amino acids, posttranslational modification, and biophysical probes into proteins of any size. ^{78,79} In EPL, the C-terminus of a protein is engineered to express α -thioester ⁷⁸ and the protein thioester can be covalently attached to solid surfaces by native

chemical ligation⁸⁰ or modified to introduce reacting groups that can facilitate Staudinger ligation⁸¹ or Huisgen cycloaddition reaction⁸²; **Figure 7**. However, all the above approaches are restricted to immobilization at the C-terminus. Orientation of the immobilized protein on the surface (at either N or C-terminus) is crucial, because the activity of a protein depends on its three dimensional structure and on the location of the active or binding site. Recently, Lin and coworkers described a method for site-selective protein immobilization on solid surfaces (glass slides and MNPs), at either the N or C-terminus by a 2-cyanobenzothiazole (CBT)-cysteine (Cys) condensation reaction.⁸³ In their work, terminal cysteine was generated at either terminus of the target protein. EPL followed by NCL with di-cysteine was used to introduce the cysteine at the C-terminus. On the other hand, tobacco etch virus protease (TEVp) target peptide sequence (ENLYFQ\u2212C), was used to install the cysteine at the N-terminus. Addition of TEVp cleaves the substrate at the N-terminus between glutamine and cysteine, and releases the cysteine-protein, that can be immobilized on surfaces containing CBT.

The chemically reactive groups can also be introduced into protein by means of nonnatural amino acids through the utilization of a non-natural amino acid by the cell's native
translational apparatus, **Figure 8**. 84-89 Bertozzi and coworkers reported the incorporation of a
methionine surrogate, azidohomoalanine in a target protein (murine dihydrofolate reductase,
mDHFR) expressed in methionine-depleted bacterial cultures. The azidohomoalanine proteins
were selectively modified in the presence of other cellular proteins by means of Staudinger
ligation. 90 Similarly, Schultz and coworkers reported the incorporation of azide and acetylene
containing unnatural amino acids into proteins which were then modified by a Huisgen [2 + 3]
cycloaddition reaction with acetylene or azide derivatives. 88 Site-specific immobilization of
recombinant proteins has also been achieved through enzymatic ligation. Using enzymes as

catalysts rather than substrates of the immobilization reaction permits the easy optimization of reaction rates and extents by changing enzyme concentrations.

Shin et al. described a method that can be used to covalently immobilize proteins of interest site-specifically in a single, efficient enzymatic ligation step. This method utilizes phosphopantetheinyl transferase, Sfp enzyme, to catalyze a reaction between coenzyme A (CoA) covalently immobilized on a solid surface and proteins containing a natural or engineered phosphopantetheinylation site.⁵¹ Besides, bacterial transpeptidase Sortase A enzyme, which is extensively studied with known substrate specificity, has been used to catalyze the ligation of proteins onto solid supports. 91,92 The enzyme cleaves the LPXT \G sequence at the amide bond between the threonine and the glycine to form an acyl-enzyme complex. Nucleophilic attack by the amino group of the tris-glycine on the intermediate results in the formation of an LPXT-GGG bond and the liberation of the free enzyme, Figure 10, panel A. Because of the low tolerance of Sortase A for the deviation in the LPXTG recognition motif, this enzymatic ligation is highly selective. 92 Another elegant ligation strategy involves the use of fusion protein containing a small (typically 20-30 kDa) enzyme such as O₆-alkylguanini-DNA alkyltransferase (SNAP), capable of irreversibly cross-reacting with a suicide inhibitor anchored to the solid surface. 93,94 SNAP irreversibly transfers the alkyl group from its substrate, O₆-alkylguanini-DNA, to one of its cysteine residues, Figure 10, panel B. Colombo et. al, reported the conjugation of SNAP fused single-chain variable fragment (SNAP-scFv) selective for HER2 receptor in breast cancer cells was to MNPs displaying O₆-alkylguanini-DNA on the surface to generate HER2 imaging probe. 93 Site-specific immobilization has also evolved by improving on the traditional noncovalent immobilization with the introduction of extra functionalities for value addition. Ericsson et. al reported the site-specific covalent attachment of His-tagged proteins by chelation assisted

photoimmobilization (CAP).⁹⁵ The solid surface is functionalized with both nitrotriacetic acid-Ni complex and a photoactivatable moiety. Upon chelation with His-tagged protein in an oriented assembly, UV light activation leads to formation of covalent bonds, **Figure 9**.⁹⁵

The main advantage of the approaches highlighted above is that all the reacting groups or binding systems involve monovalent recognition partners, which overcomes the crosslinking effects associated with other conventional methods. Taken together, these advances in conjugation of proteins suggests a rich future for site-specific and oriented immobilization of proteins on NPs with a view of improving their performance as bioseparation probes.

For antibodies, covalent approach for site-specific and oriented immobilization can make use of a unique carbohydrate moiety at the Fc part of antibody. Specific oxidation on the carbohydrate vicinal hydroxyl group via the use of sodium periodate generates aldehydes. These aldehydes are reactive towards aminated ⁹⁶ or hydrazine-functionalized surfaces, ^{97,98} resulting in oriented covalent antibody. However, the resulting aldehyde groups can potentially react with other amine groups on the antibody itself. Furthermore, the harsh oxidation conditions might decrease the activity of the antibody through denaturation or conformational changes. ^{99,100} Another approach uses a boronic acid presenting surface to orient antibody via the carbohydrate moiety. ^{101,102} Boronic acids form cyclic boronate esters with 1,2- and 1,3-diols present in carbohydrates of antibody and thus provide an additional anchoring point with chemistry that is largely orthogonal.

Figure 6: Representative of the main methods for carbohydrate immobilization on NPs. (A) Amide bond formation, (B) Amine bond formation through reductive amination (C) Imidine formation (D) [2 + 3] Huisgen cycloaddition (E) Amine bond formation through photochemical reactions. Adapted with permission from reference¹⁷ Copyright 2014, John Wiley and Sons

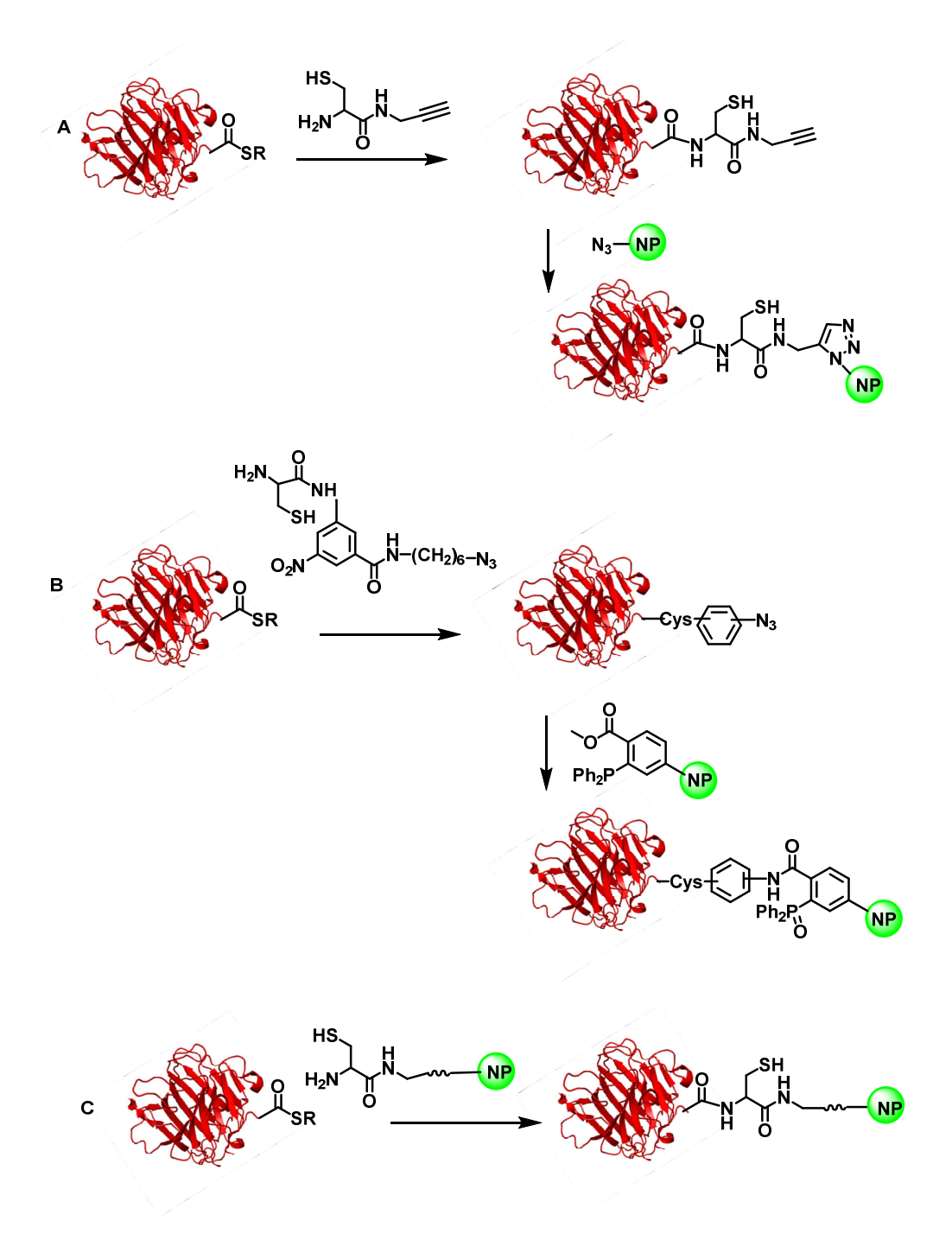


Figure 7: Protein engineering through expressed protein ligation (EPL) to introduce α -thioester at the C-terminus. The protein can be covalently conjugated to NPs by (A) [2 + 3], Huisgen cycloaddtion (B) Staudinger ligation (C) Native chemical ligation (NCL)

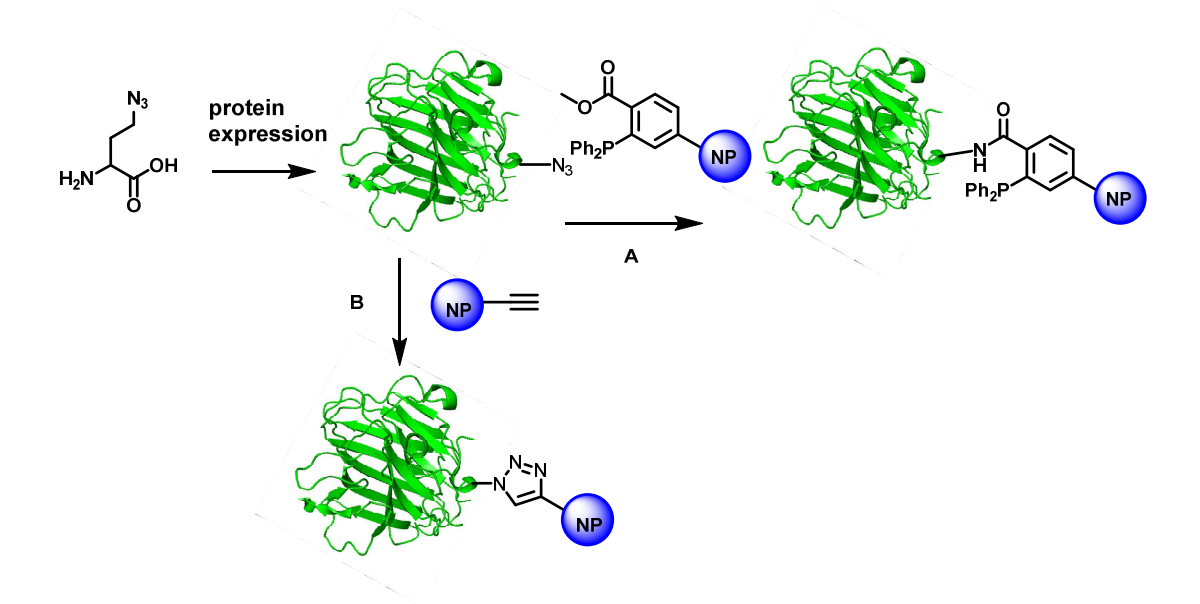


Figure 8: Incorporation of unnatural amino acid into a recombinant protein. Incorporation of azidohomoalanine into a recombinant protein followed by immobilization on to NPs through (A) Staudinger ligation, (B) [2+3] Huisgen cycloaddition reaction

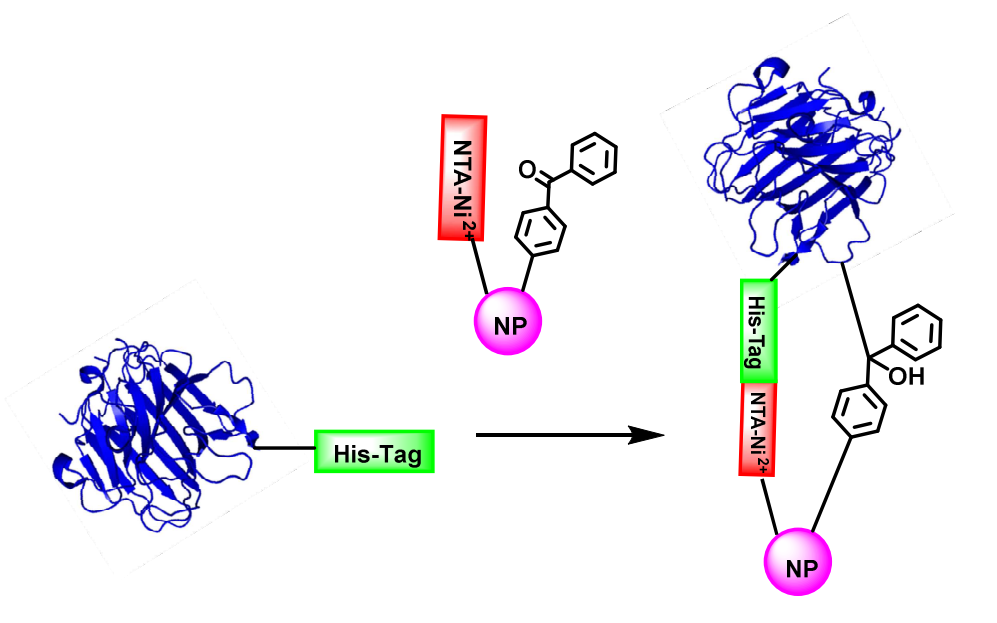


Figure 9: Schematic picture of a protein immobilized to NP via the chelation assisted photoimmobilization (CAP) principle. The ligand has a hexahistidine tag, located distantly from the analyte binding site, which first coordinates to Ni²⁺–NTA. Photoimmobilization then tethers the protein permanently to the NP

.

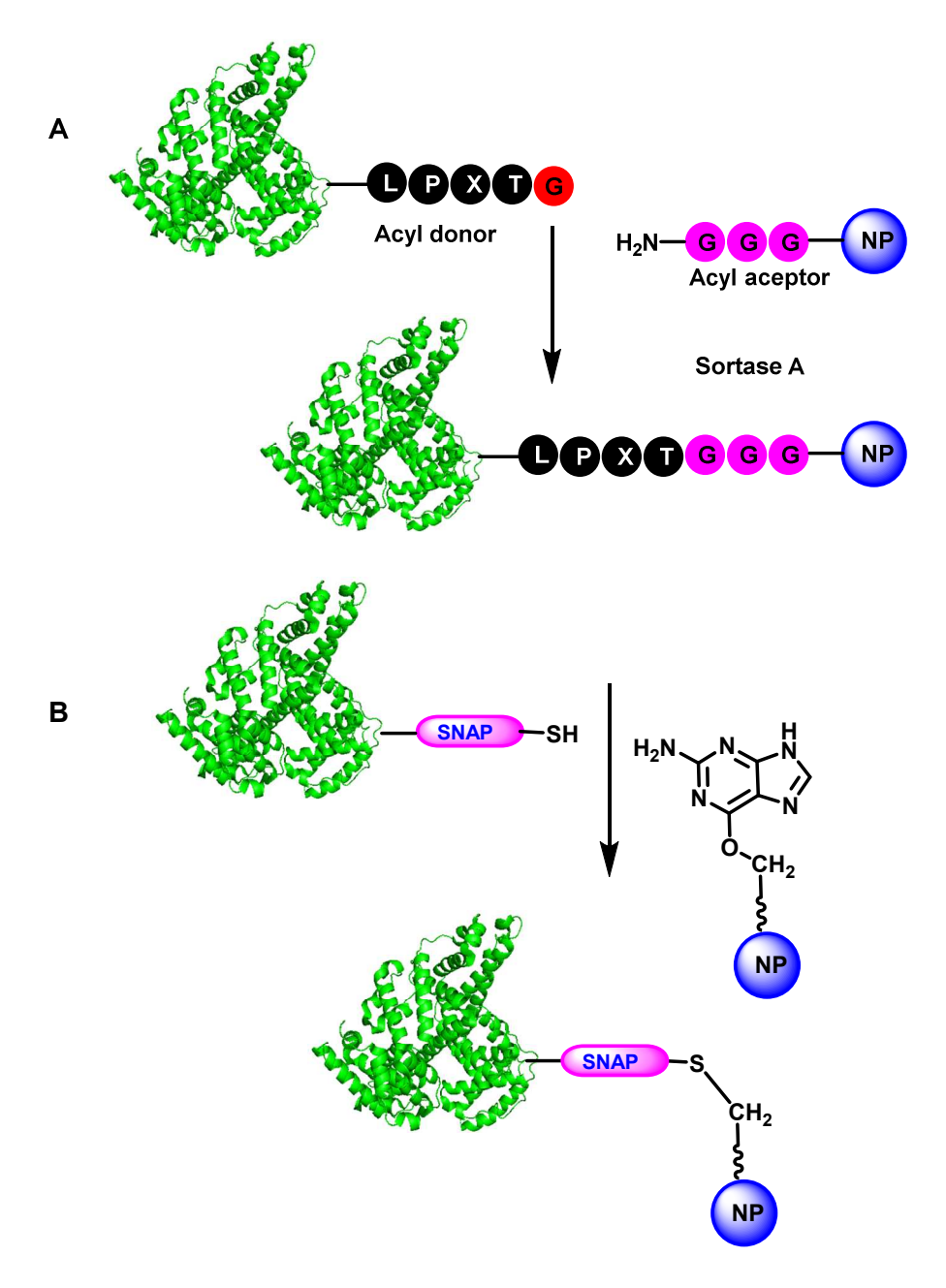


Figure 10: Immobilization of proteins by using Sortase A and through O6 -alkylguanine-DNA alkyltransferase (SNAP). (A) Immobilization of proteins by using Sortase A. (B) Mechanism of O_6 -alkylguanine-DNA alkyltransferase (SNAP)-mediated immobilization of protein on NP Adapted with permission from references. 92,94 Copyright 2010, American Chemical Society and copyright 2003, Nature publishing group

1.4: MNPs functionalized with biomolecules for bioseparation and enrichment

NPs functionalized with biological molecules have gained a lot of research interest because of their potential applications in a variety of areas, such as biosensors 103-106, imaging^{63,65,107-116}, biocatalysis and proteolysis, ¹¹⁷⁻¹²¹ targeted delivery of therapeutics, ^{64,122-124} and cancer diagnostics and therapy. 125-129 Another area where biomolecule functionalized NPs and particularly MNPs is gaining much interest is in bioseparation. The main reason is because detection, isolation, separation, and purification of specific biologically active compounds, cells, and pathogens is used in almost all areas of biosciences and biotechnology. Diverse procedures can be used to achieve this goal but recently, increased attention has been paid to the development and application of functionalized magnetic adsorbent particles in combination with magnetic based separation techniques. 130-133 Traditionally, isolation and purification of biomolecules has been performed using a variety of chromatographic techniques; electrophoretic, ultrafiltration, precipitation and other procedures with affinity chromatography being one of the most important approaches. The advantages of column affinity chromatography has been shown in a lot of successful applications. 134-136 However, the disadvantage of all standard column liquid chromatography procedures is the difficulty of the standard column systems to cope with the samples containing particulate material. Therefore they are not suitable for work in early stages of the isolation/purification process where suspended solid and fouling components are present in the sample. 131,133

Magnetic separation techniques have several advantages in comparison with standard separation procedures. They are fast, simple, inexpensive, with only a few handling steps. All the steps of the purification procedure can take place in one single test tube just by the application of an external magnetic field. It eliminates the need for expensive liquid chromatography systems,

centrifuges, filters or other equipment normally necessary to condition an extract before its application on packed affinity chromatography columns. The separation process makes it possible to separate selected target species directly out of crude biological extracts and samples containing suspended solid material. Magnetic separation is usually very gentle to the target species since the shear forces associated with the separation are minimal compared with centrifugation or filtration. Even large protein complexes that tend to be broken up by traditional column chromatography techniques due to induced stress during centrifugation may remain intact viable and unaltered. Furthermore, separation of target proteins using standard chromatography techniques often leads to the large volume of diluted protein solution which is not the case with magnetic separation techniques. Magnetic separation techniques.

Of the functionalized magnetic adsorbent particles, MNPs containing iron oxide core and functionalized with different active moieties including biological molecules, metal ions, short hydrophobic carbon chains, polymers have been widely applied in bioseparation (magnetic affinity capture). Affinity capture has found its usefulness in sample purification, analyte preconcentration, toxin decontamination, and in various sample preparation procedures in proteomics and peptidomics analysis. 137-140 In depth discussion of MNPs functionalized with the major biomolecules (proteins, carbohydrates, lectins, antibodies, proteins, peptides, and nucleotides) and their application in bioseparation will be given in later sections of this review. MNPs has promised high performance compared to micrometer-sized magnetic resins or beads used in affinity chromatography because (1) their high surface/volume ratio and good solubility result in a higher binding rate, (2) their nanometer sizes lead to faster movement and easy entry into cells, and (3) their magnetically controllable aggregation behavior allows them to be anchored onto a solid support for further usage. Specific multiple ligand-receptor interactions

(i.e., polyvalent interactions) offer high avidity between MNPs and target molecules or receptors when the ligands functionalized on to the MNPs. 141-143

1.4.1: Carbohydrate functionalized MNPs

The surfaces of mammalian cells are covered by a dense coating of carbohydrates termed as glycocalyx. In the glycocalyx, carbohydrates appear mainly conjugated to proteins and lipids (glycoproteins, glycolipids and proteoglycans) and the glycoconjugates exert their biological functions. 10,144,145 Due to their rich structural variations, carbohydrates are uniquely suited for biological information transfer. Carbohydrate can direct the initiation of many medicinally important physiological processes where they are involved in a wide variety of events, including inflammatory and immunological responses, tumor metastasis, cell-cell signaling, apoptosis, adhesion, bacterial and viral reognination, and anticoagulation. ¹⁵ As a result, solid support systems conjugated with physiologically relevant carbohydrates have been developed. The (glycopolymers). 146 polymers support systems largely used include, dentrimers (glycodentrimers), 147 and NPs (glyconanoparticles). 10,148

Carbohydrate functionalized NPs (glyconanoparticles) have wide applications ranging from studying of carbohydrate-protein interaction, *in vivo* cell imaging, glycan biosensors, vaccine development, to drug delivery. Since carbohydrate functionalized NPs comprise of a very large group of different NPs, this review section will only focus on carbohydrate functionalized MNPs.

To realize the full potential of magnetic glyco-nanoparticles in bio-separation, several hurdles need to be overcome. A characteristic feature of the biological interactions where carbohydrates are involved is their low affinity that has to be compensated by multivalent presentation of the ligands. ¹⁰ Thus NPs offer a suitable platform to display carbohydrates in a

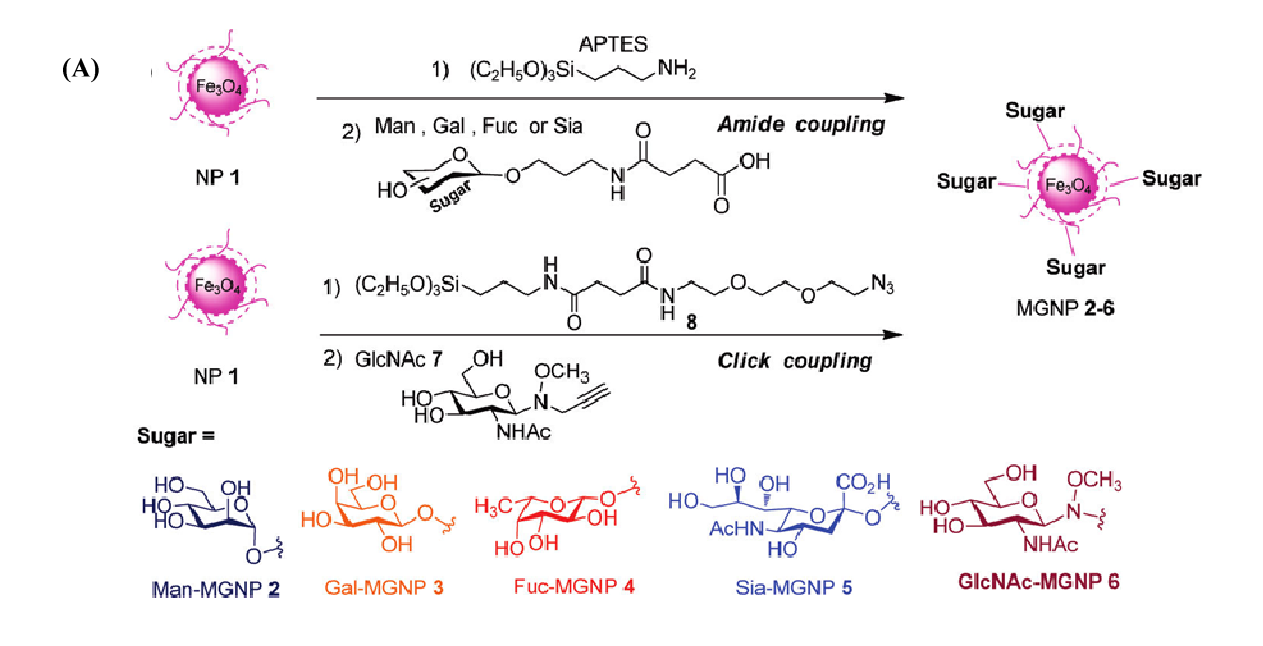
polyvalent format in order to improve the binding strength and selectivity. The second challenge is there can be several types of receptors recognizing the same carbohydrate ligand. The third obstacle relate to the biological recognition ability of the carbohydrate ligand functionalized on the NPs. To be able to mimic the biological system, the carbohydrate ligand conjugated onto the NPs should not lose its biological recognition ability. The fourth challenge is the lack of pure carbohydrate for biological studies. It is difficult to purify large quantities of complex oligosaccharides from natural sources due to the heterogeneity of carbohydrate on the cell surface. Scientists are trying to solve this problem through chemical and enzymatic synthesis of biologically relevant oligosaccharides. The surface of the surface o

It has been established that biological interactions involving carbohydrates can be mediated through cell surface carbohydrate binding proteins (lectins) as well as other carbohydrates (carbohydrate-carbohydrate interactions). L44 Carbohydrate-lectin interaction has been a subject of investigation during the past few decades because of the relevance of these interaction in disease processes like cancer growth and development. In order to achieve optimal performance of carbohydrate functionalized MNPs in bio-separation, it is important to carry out a series of characterization to confirm that the desired carbohydrate is immobilized on the NP surface. Thermogravimetric analysis (TGA), zeta potential, Fourier transform infrared spectroscopy (FTIR), X-ray diffraction, water solubility are among some of the techniques mostly used. To test that the immobilized carbohydrate maintains its biological binding ability, researchers have used plant lectins and *E. coli* as model systems because their carbohydrate binding specificities are well characterized. Sci. This particular step is critical because it provides initial clue that the carbohydrate on the NP surface is well-oriented, well-spaced, with little steric hindrance among the many copies of immobilized carbohydrates. Besides, good

control experiments to substantiate the binding specificity of the NP system to the target substrate is required. When studying lectins or *E. coli*, a good control will be to use MNPs functionalized with an irrelevant carbohydrate. In addition, lectin or *E. coli* strain that lacks the carbohydrate binding specificity of the immobilized sugar is often used.¹⁵²

Using mannose functionalized MNPs, El-Boubbou et al. 152 reported the capture and separation of E.coli strain ORN178, which possess mannose binding specificity from the supernatant. Up to 65% capture and separation efficiency was achieved in a time of 5 minutes which was reported to be much higher than the 10~30% range typically observed with antibody or lectin functionalized MNPs. In addition, bacterium differentiation was explored. *E.coli* strains: ORN178, ORN208 a mutant strain with greatly reduced mannose binding affinity, and environmental strain (ES) with unknown carbohydrate binding specificity were differentiated using mannose MNPs and galactose MNPs. The ES strain was found to have affinity for both mannose and galactose. Using galactose MNP as a control in isolating ORN178 and ORN208 was particularly attractive because it adds confidence on the ability of the carbohydrate functionalized MNPs to detect and separate bacteria from the medium. 152 Similar work of using mannose functionalized MNPs to evaluate the binding of the E. coli strains ORN178 and ORN208 E was reported by Liu et al. 76 In their work, the covalent coupling of mannose onto iron oxide magnetic nanoparticle (IOMNP) surface was achieved by the CH insertion reaction of photochemically activated phosphate-functionalized perfluorophenylazides (PFPA). Advantages associated with photochemical assisted CH insertion reaction is that the carbohydrate does not need to be derivatized hence this reduces synthetic steps. However, the CH insertion reaction is non-specific and it may occur at or next to the carbohydrate site need for binding recognition.

El-Boubbou et al. expanded this carbohydrate functionalized MNP technology to cancer cell detection. 16 They were not only able to detect and differentiate cancer cells but also to quantitatively profile their carbohydrate binding abilities by magnetic resonance imaging (MRI). Using an array of five carbohydrate functionalized MNPs (galactose, mannose, fucose, sialic acid and N-acetyl glucosamine), a range of cells including closely related isogenic cancer cells, cells with different metastatic potential and malignant vs normal cells were readily distinguished. As shown in Figure 11, panel B, breast cancer MCF-7/Adr-res caused a significantly larger MRI signal changes ($\Delta T2$) upon binding with galactose MNPs as compared with that of the normal breast cells 184B5. These enabled easy detection and differentiation of the two cell lines. Isogenic cancer cells on the other hand are cells that are derived from the same parent cell line, hence they have similar genetic composition. Due to this property, they present a significant challenge for identification and subsequent separation. This was however possible by using carbohydrate functionalized MNPs where two sets of isogenic cell lines, mouse mammary carcinoma cell lines TA3HA and TA3ST and melanoma cancer cell lines B16F10 and B16F1 were differentiated, Figure 11, panel B. Although multiple cell lines were found to bind to the same carbohydrate, the full differentiation of the ten cell lines was achieved through a statistic method, linear discriminant analysis (LDA), Figure 11, panel C.



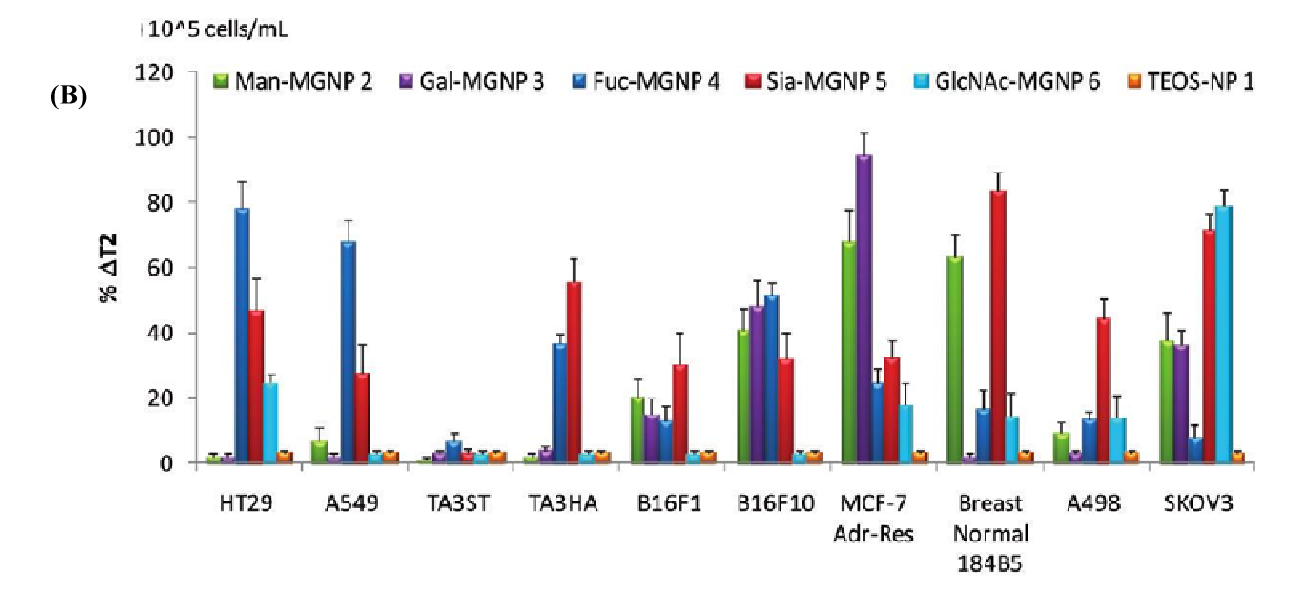
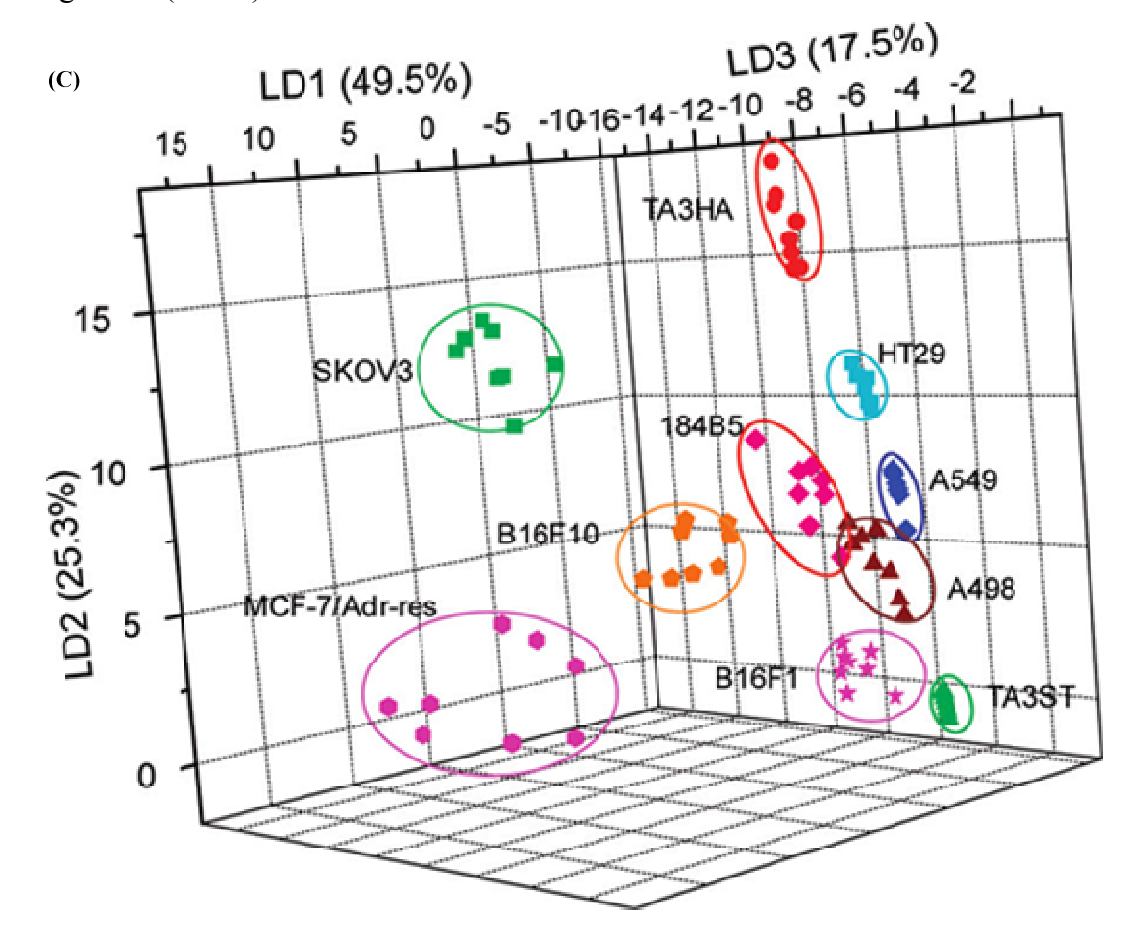


Figure 11: Profiling and differentiation of cancer cells using magnetic glyco-nanoparticles through MRI. (A) Synthesis of magnetic glyconanoparticles (MGNPs) (B) Percentage changes of T2 relaxation time (% $\Delta T2$) obtained upon incubating MGNPs 2-6 or the control NP 1 (20 μ g/mL) with 10 cell lines (10⁵ cells/mL). The $\Delta T2$ was calculated by dividing the T2 differences between MGNP and MGNP/cancer cell by the corresponding highest $\Delta T2$ from each MGNP category. (C) LDA plots for the first three LDs of $\Delta T2$ patterns obtained with the MGNP array upon binding with the 10 cell lines (10⁵ cells/mL). Reproduced with permission from reference¹⁶ Copyright 2010, American Chemical Society

Figure 11 (cont'd)



Following a similar strategy to purify cells, Wu and coworkers reported the functionalization of Lewis X (Le^X) on MNPs (Le^X-MNPs) as an efficient tool for dendritic cell detection and isolation in a mixed cell population. The success of isolating dendritic cells using Le^X functionalized MNPs is based on the fact that dendritic cells (DC)-specific intracellular adhesion molelcule-3 grabbing nonintegrin (DC-SIGN) is a receptor found on DCs that recognizes antigens bearing mannose-rich or fucosylated glycans including Le^X, **Figure 12**. To ensure that the NP system passed the stringent requirements as a tool for bioseparation and enrichment, it was tested for its ability to recognize anti-Le^X antibody and a FITC-labeled

Erythrina cristagalli (ECA, a lectin that recognizes lactosamine, LacNAc and lactose epitopes). This also served as a confirmation that the immobilized carbohydrate retained its biological binding capability. Dendritic cell isolation ability was proven through the isolation of fluorescent labeled DC-SIGN positive THP-1 cells from a mixed cell population with its parental cell line THP-1. They observed that a 15 min incubation of the cell mixture with MNPs was sufficient to achieve between 70-86% capture efficiency, which was much higher than the capture capacities (10-30%) of antibody functionalized commercially available MNPs. Following this success, the Le^X-MNP system was applied in the isolation of differentiated, immature monocyte derived dendritic cells (moDCs) from human peripheral blood mononuclear cells (PBMCs) derived from a mixed population of primary human cells. Successful isolation was confirmed through staining of the bound cells with fluorescently labeled antibodies for moDC markers DCSIGN, CD1a and HLA-DR. As shown in Figure 13, DC-SIGN⁺ and CD1a⁺ and HLA-DR⁺ moDCs were specifically isolated by the Le^X-MNPs with the concomitant disappearance of this cell population in the corresponding flow-through cells. On the other hand, the binding and capture specificity of Le^X-MNPs was determined by comparing their performance to unmodified alkyne MNPs, lactose-MNPs, LacNAc-MNPs, and sLe^X-MNPs. Le^X-MNPs showed superior performance. ¹⁵⁴ Taken together, these results suggest that glycan functionalized MNPs can be used as an alternative, cost effective method for isolating cells (including cancer cells) expressing glycan binding proteins.

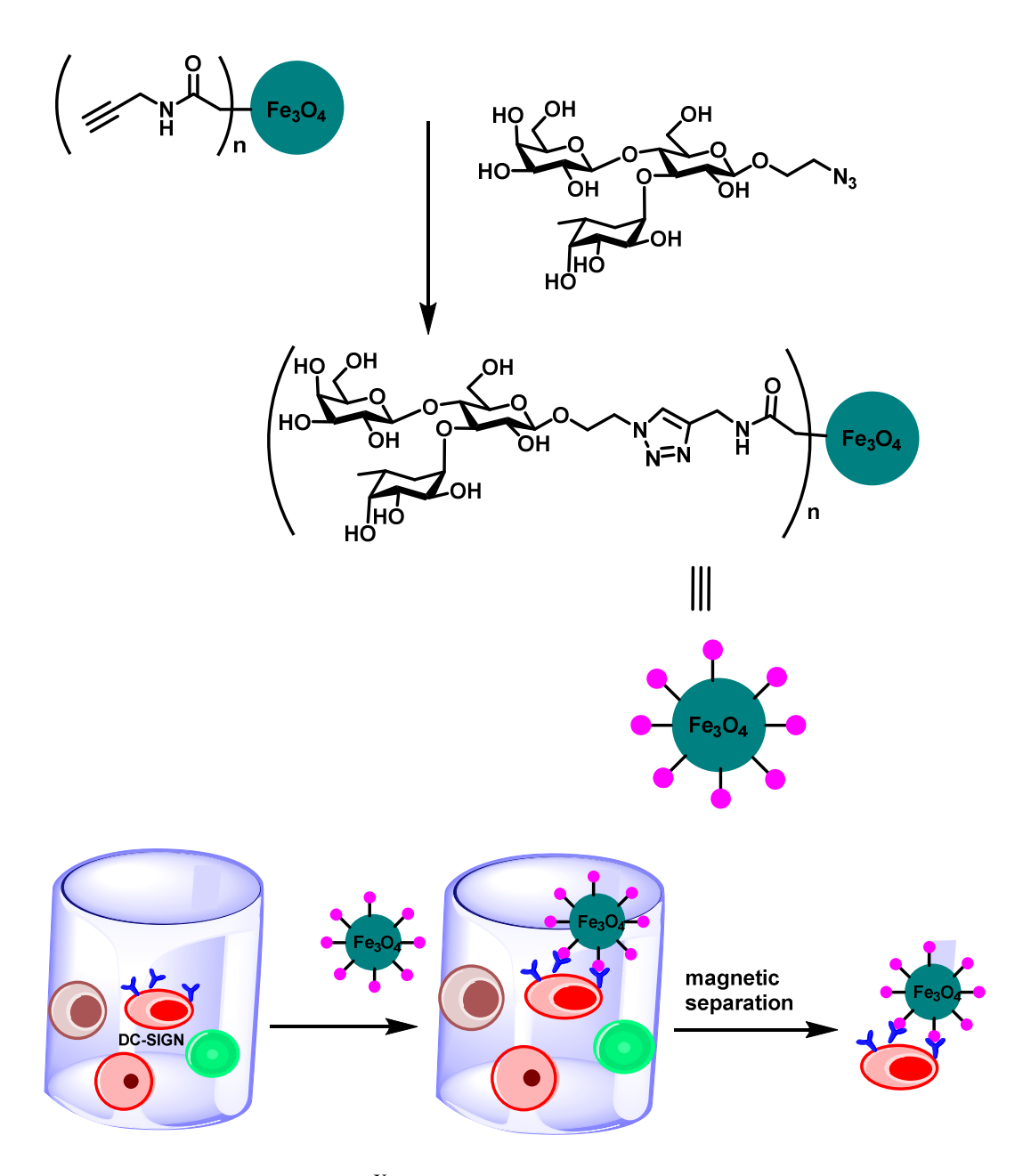


Figure 12: Fabrication of Le^X-coated MNPs and selective capture of DCs. Capture of DCs from a mixed cell population using Le^X-coated MNPs. Adapted with permission from reference¹⁵⁴ Copyright 2012, American Chemical Society

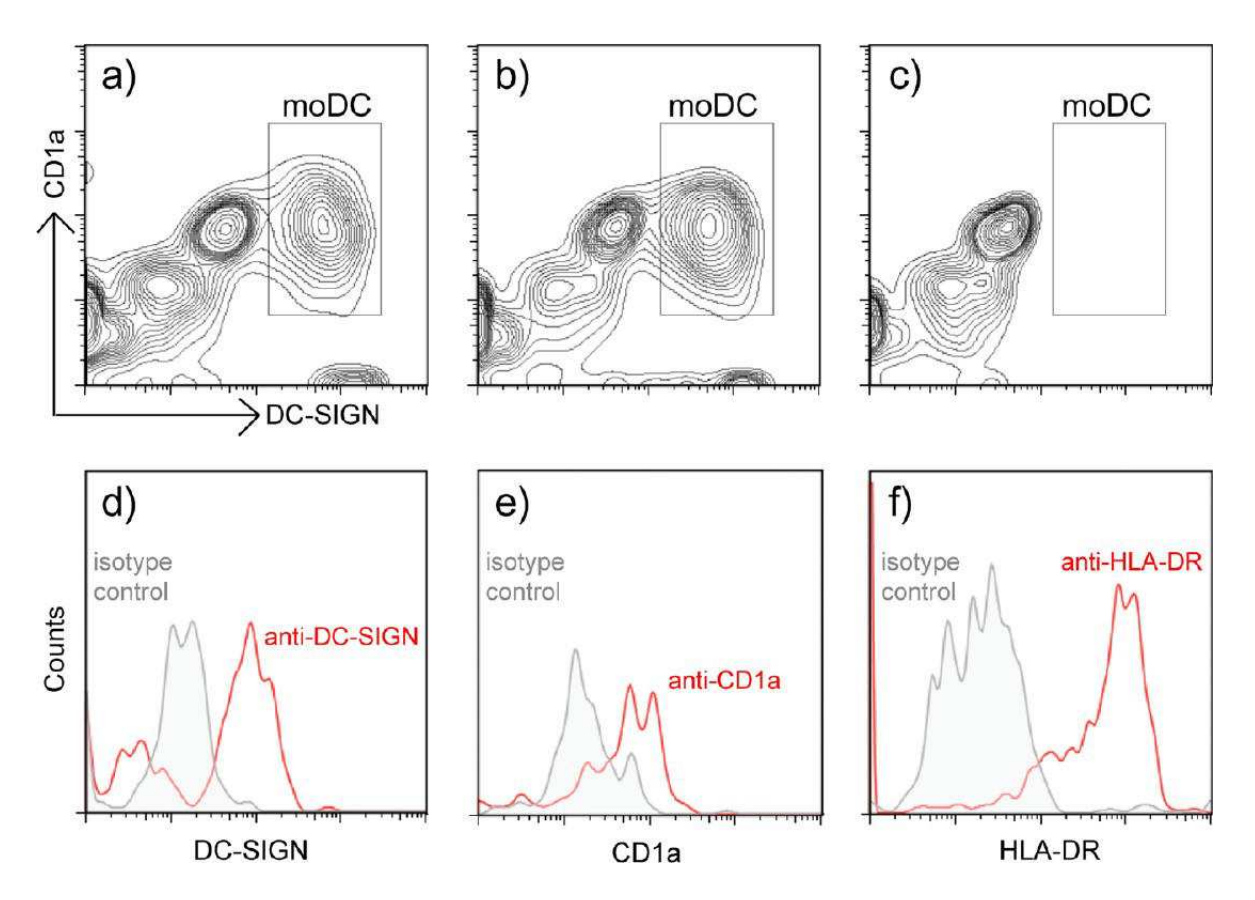


Figure 13: Enrichment of moDCs using Le^X-functionalized MNPs. PBMCs were incubated in the presence of GM-CSF and IL-4 for 6 days and differentiated into moDCs. (a) Contour plot shows the total cell population prior to capture. moDCs were defined as CD1a⁺/DC-SIGN⁺ (gated in the box). (b) Cell flow-through following incubation with alkyne-functionalized MNPs. (c) Cell flow-through following incubation with Le^X-functionalized MNPs. moDCs were absent from this population. (d) Histogram shows that the population of cells bound to Le^X-functionalized MNPs are CD1a⁺/DC-SIGN⁺/HLA-DR⁺ when stained with FITC-conjugated anti-DC-SIGN, PE/Cy5-conjugated Anti-CD1a, and PE-conjugated anti-HLA-DR. Shown is one representative experiment out of three replicates. Reproduced with permission from reference¹⁵⁴ Copyright 2012, American Chemical Society.

Besides cell isolation and purification, carbohydrate functionalized MNPs have also been proposed as a suitable alternative to commercially available carbohydrate immobilized microbeads for protein or peptide purification and enrichment. Zhou et al. synthesized a maltose functionalized silica coated IOMNP support for the integration technology of

separation/purification, and immobilization of maltose binding protein-heparinase I fusion enzyme (MBP-HepA).⁶¹ The novelty of this system was its integral applicability. After affinity capture, the NPs with the adsorbed MBP-HepA were used for enzymatic depolymerization of heparin to low molecular weight heparin (LMWH), Figure 14. This application also served as a confirmation that the protein-enzyme fused construct on the NP surface retained its biological activity. The immobilized enzyme had an advantage over free enzyme as it exhibited higher thermal stability (had halflife of 190 min at 30 °C compared to 10 min of free enzyme). Immobilization of the enzyme also offers reusability capability.⁶¹ To establish the specificity of MBP-HepA binding to maltose functionalized MNPs, the bound fraction was eluted with an elution buffer that contained trimaltose. The eluted fraction was analyzed by sodiumdodecyl sulfate polyacrylamide gel electrophoresis (SDS-PAGE) and compared to the eluted fraction where the elution buffer lacked triomaltose. The results of these analysis are shown in **Figure 14**. Based on these results however, it is clear that the capture efficiency of these NP system is low as indicated by protein band intensity of MBP-HepA in lane 2 (the amount of MBP-HepA remaining in the supernatant,) compared to the crude lysate, lane 1. Similarly the amount of MBP-HepA eluted by trimaltose seemed to be very low as indicated by the protein band intensity in lane 3, which further suggests low capture efficiency of the NP system. For practical application, it is always important to analyze all eluted protein to confirm if they are specific proteins. The protein band of the protein running below MBP-HepA in the crude lysate on the SDS-PAGE seemed to diminish in the supernatant (lane 2) but reappeared in the eluted fraction (lane 3). This is a clear evidence that it was captured by the NPs and released in the presence of maltose buffer. If its maltose binding properties had been investigated, it would have been a way to qualify the capacity of this NP system.

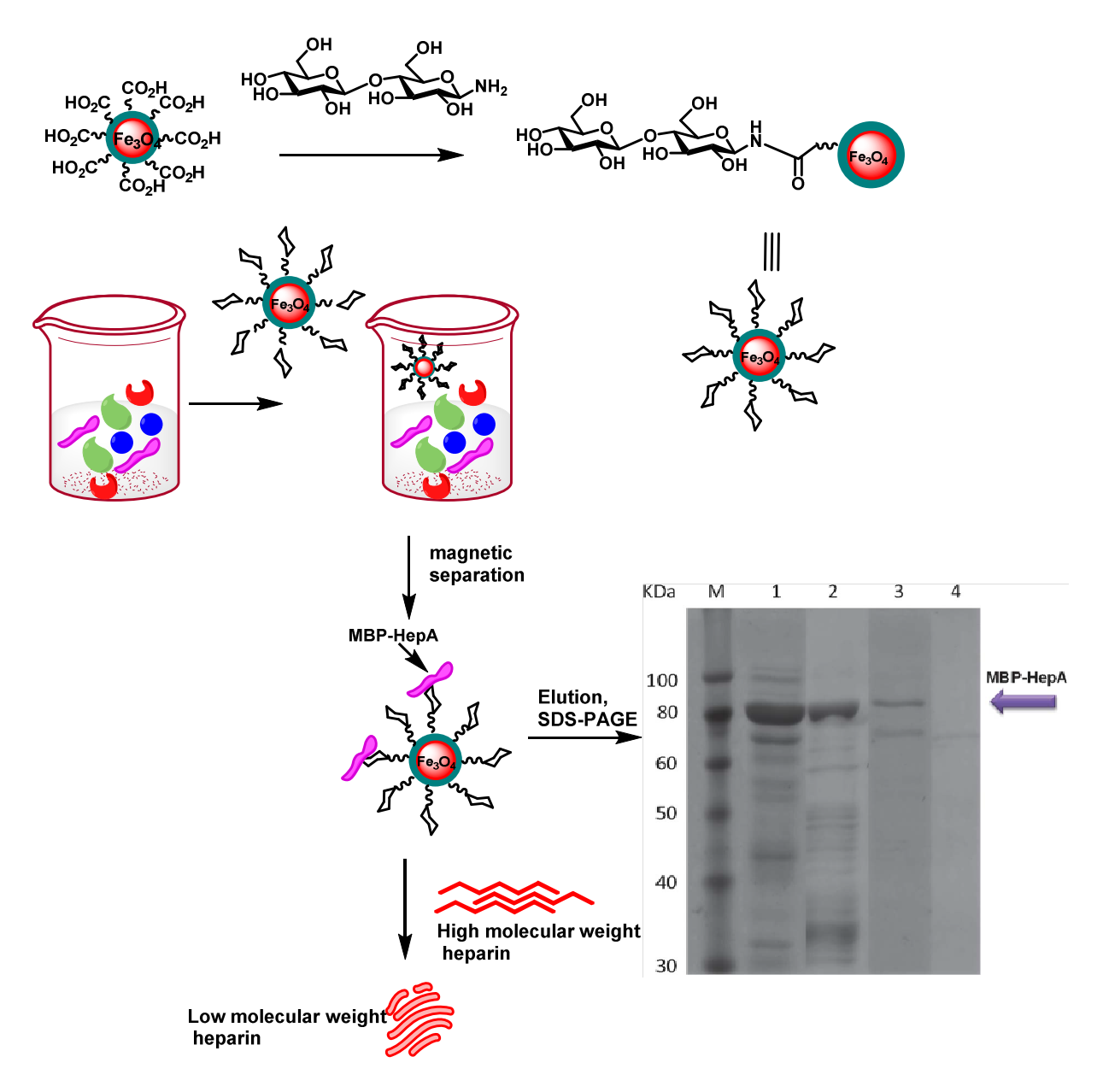


Figure 14: Application of maltose functionalized MNPs in protein purification. Synthesis of maltose functionalized MNPs and their application in the separation/purification, and immobilization of maltose binding protein-Heparinase I fusion enzyme (MBP-HepA). Adapted with permission from reference⁶¹ Copyright 2012, Royal Society of Chemistry

In a similar approach, Xiong et al. prepared maltose functionalized MNPs for enrichment of N-linked glycoproteins.⁶⁹ Their system was fabricated through growth of branched PEG polymer brushes on the surface of the NPs and subsequent functionalization with maltose (Fe₃O₄@SiO₂@PEGMaltose MNPs). To evaluate the efficiency of Fe₃O₄@SiO₂@PEGMaltose MNPs for selective enrichment of glycopeptides, tryptic digest of human immunoglobulin G (IgG), horseradish peroxidase (HRP), and human alpha-acid glycoprotein (AGP) were first employed as model samples. Protein concentration as low as 3 pmol was detected and enriched as analyzed by MALDI-TOF MS, **Figure 15**. The high sensitivity could be attributed to the high density of both linear and branched PEG polymer brushes modified with azido groups. This would subsequently lead to functionalization of large numbers of maltose that enhance binding avidity.

To validate the relevance of PEG and maltose on the NPs, the specificity of Fe₃O₄@SiO₂@PEGMaltose MNPs was evaluated by comparing with NPs without sugar (Fe₃O₄@SiO₂@PEG MNPs) and without PEG (Fe₃O₄@SiO₂-Maltose MNPs) in IgG enrichment. As shown in **Figure 15**, the intensities and signal to noise (S/N) values of enriched glycopeptides using Fe₃O₄@SiO₂@PEGMaltose MNPs are all much higher than those by the other two types of NPs. Besides known proteins, Fe₃O₄@SiO₂@PEGMaltose MNPs were successfully utilized to enrich and analyze low abundant glycoproteins in human plasma samples by LC/MS/MS where a total of 106 glycoproteins were identified.⁶⁹

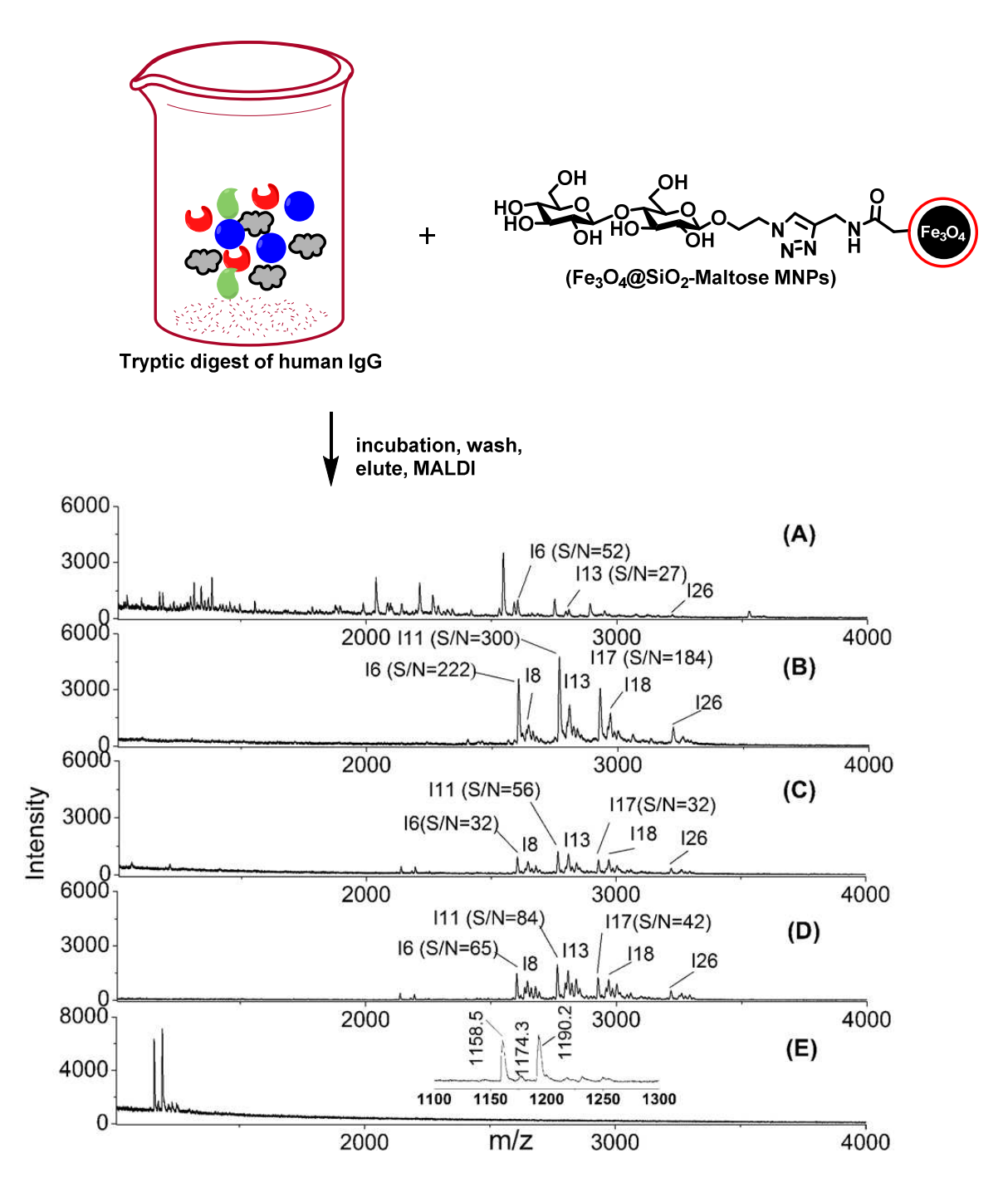


Figure 15: Protein isolation and analysis using maltose functionalized magnetic nanoparticles through MALDI-TOFMS. MALDI-TOFMS spectra of (A) Direct analysis of 5 pmol tryptic digest of human IgG, after enrichment with (B Fe₃O₄@SiO₂@PEGMaltose MNPs, (C) Fe₃O₄@SiO₂@PEG MNPs and (D) Fe₃O₄@SiO₂-Maltose MNPs, (E) After enrichment by Fe₃O₄@SiO₂@PEG-Maltose MNPs and then deglycosylation by PNGase F. Adapted with permission from reference⁶⁹ Copyright 2012, Royal Society of Chemistry

As stated earlier, and demonstrated in the previous example,⁶¹ the dependency of binding of protein on carbohydrate is also best demonstrated by the elution protocols where the elution buffer contains carbohydrate matching the one immobilized on the NP surface. In this work, the bound proteins were eluted at low pH. All the elution buffer combinations had TFA, implying the dissociation of the bound protein was not specifically dependent on its binding to the maltose on the NP surface.⁶⁹

In an effort to investigate carbohydrate binding protein from tumor cells, Wong and coworkers functionalized stage-specific embryonic antigen 4 (SSEA-4) on magnetic IONPs. which they referred to as SSEA-4-conjugated magnetic beads (SSEA-4-MBs) and used it as an affinity probe to isolate and purify SSEA-4 binding protein in breast cancer cells. 155 SSEA-4 has been implicated in the malignancy of cancers such as invasion and metastasis. However its functional role had not been demonstrated due to lack of well-defined SSEA-4 binding proteins. Affinity capture of SSEA-4-binding proteins was performed in the cell lysate of a breast cancer cell line, MCF-7 following standard protocol of incubating the cell lysate with NPs, magnetic separation and elution (dissociation) of bound proteins. The captured and subsequently eluted proteins were subjected to SDS-PAGE and visualized through silver staining. As a control, a parallel affinity capture experiment was performed with NPs that were only functionalized with polyethylene glycol (PEG), methyl-PEG₄ conjugated magnetic beads (MEG-MB). When the protein profile of the SSEA-4-MBs pulled down was compared to the MEG-MB counterpart, it revealed a unique protein band (~60 kDa) on the SDS-PAGE, Figure 16. This protein band was confirmed by LC/MS/MS to be FK-506 binding protein 4 (FKBP4), a cytoplasmic protein that has been found to be highly expressed in breast cancer cell lines MCF-7 and T-47D. 156

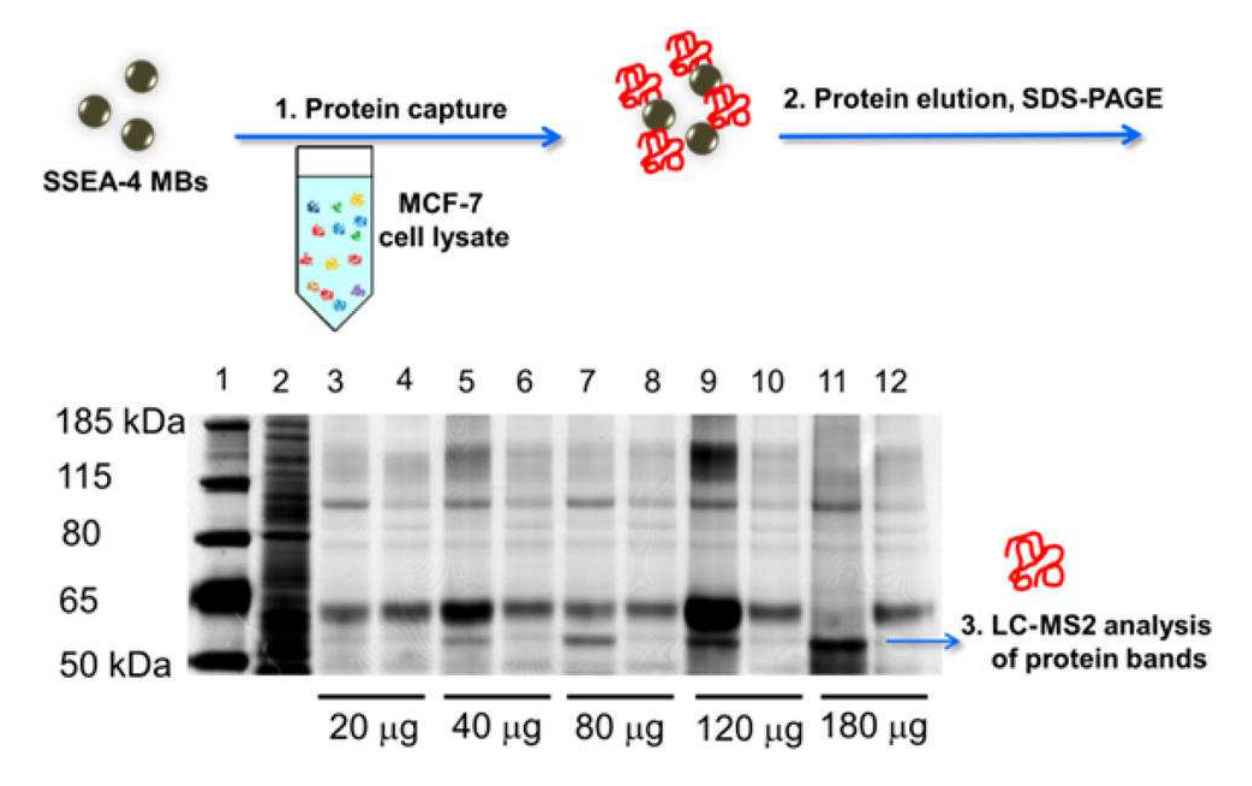


Figure 16: Protein capture from cell lysate using MNPs. Magnetic bead-based capture for the identification of SSEA-4-binding proteins. Different amounts (20, 40, 80, 120, 180 μ g) of MCF-7 total cell lysate were mixed with SSEA-4-MBs or MEG-MBs (100 μ g each), and the bound proteins were eluted, separated by SDS-PAGE, and visualized after silver staining. Lane 1, marker; lane 2, MCF-7 total cell lysate (0.5 μ g); lanes 3, 5, 7, 9, and 11, protein eluted from SSEA-4-MBs; lanes 4, 6, 8, 10, and 12, protein eluted from MEG-MBs for comparison. Reproduced with permission from reference¹⁵⁵ Copyright 2013, American Chemical Society

.

The glycan binding specificity of FKBP4 was confirmed through glycan microarray profiling of 63 glycans with recombinant FKBP4. The results showed that FKBP4 bound to all glycans with Neu5Acα2-3Gal terminus in addition to SSEA-4, **Figure 17 panel A**. They confirmed that the FK-506 inhibited the binding of FKBP4 to SSEA-4, **Figure 17 panel B**. In addition, they showed that inhibition of FKBP4 in MCF-7 significantly influenced the expression of SSEA-4 compared to other glycans containing the Neu5Acα2-3Gal sugar unit, GM2, GD3, and GD2 and globo series glycans, SSEA-3 and Globo H, **Figure 17 panel C**. The glycan microarray and the

inhibition experiments are particularly important because they affirmed the binding specificity and selectivity. Usually this is evaluated through elution protocols where the specific elution buffer contains carbohydrate matching the one immobilized on the NP surface and the results are compared to those obtained from using elution buffer with irrelevant sugar. However, this approach is limited to simple sugars such as monosaccharide and disaccharide. In this work, the bound proteins were eluted by heating the NPs at 95 °C in protein sample buffer, which usually contains at least 1 % SDS. These are strong denaturing conditions, implying there is a possibility that all proteins bound on the NPs whether specifically or non-specifically can be eluted. This is revealed by the SDS-PAGE results where the observed protein profile in the SSEA-4-MBs and MEG-MB fraction are similar and only differ by the degree of protein band intensity.

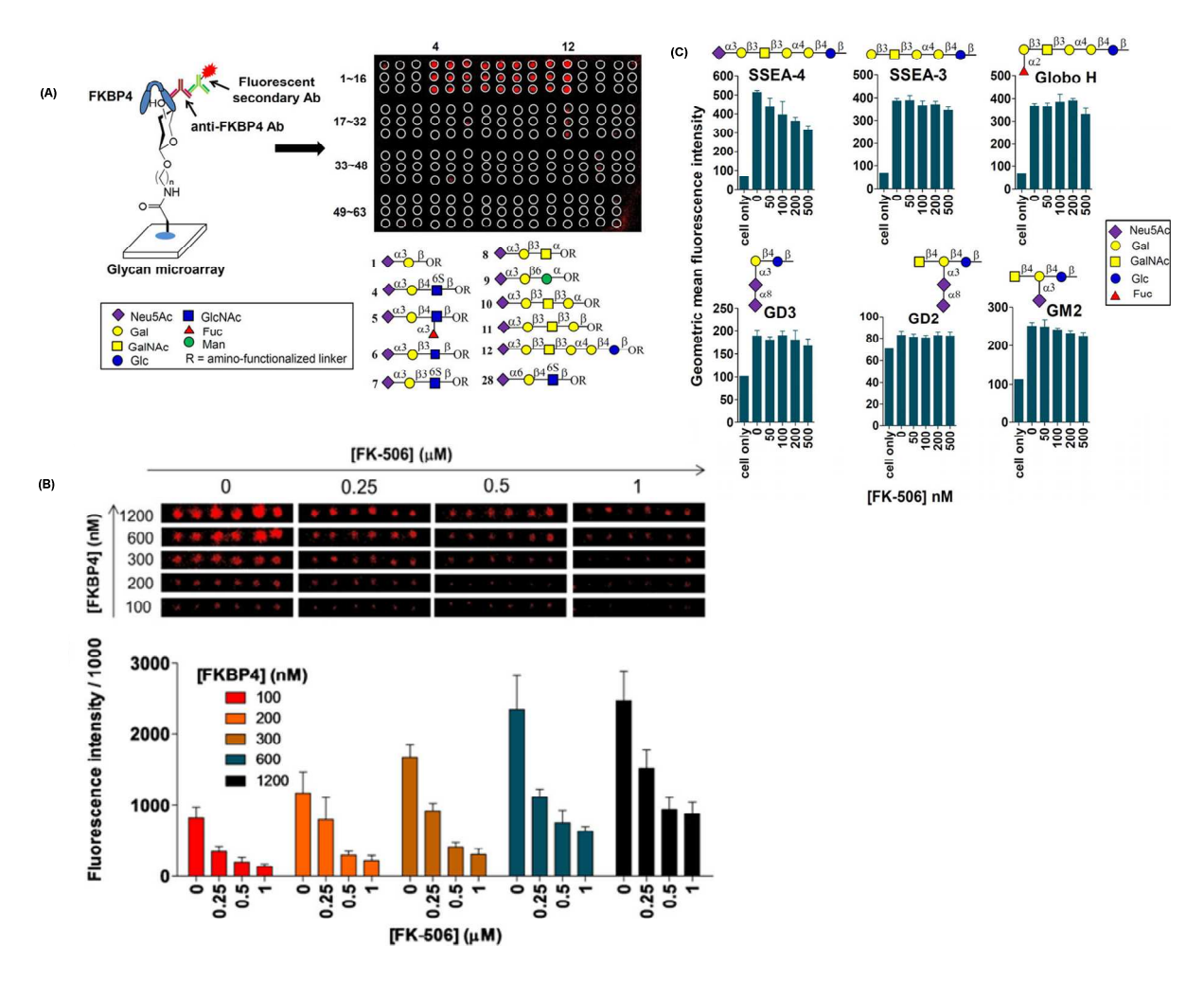


Figure 17: Analysis of FBBP4, SSEA binding protein. (A) Binding analysis of FKBP4 in a printed glycan array with 63 glycans. (B) Competitive inhibition of SSEA-4/FKBP4 interaction by FK-506. (C) Surface expression of the glycan markers of MCF-7 cells analyzed by flow cytometry after FK-506 treatment. "Cell only" means no staining performed, indicating the fluorescence background of the cells. Reproduced with permission from reference 155 Copyright 2013, American Chemical Society

1.4.2: Lectin functionalized MNPs

Lectins are carbohydrate binding proteins that are neither enzymes or antibodies, and they can recognize various carbohydrates attached to proteins and lipids on cell surface and extracellular matrices with high specificities.¹⁵⁸ The interactions between endogenous lectins and carbohydrate mediate a variety of biological processes, some of which are involved in highly

specific events such as cell signaling, 159,160 cell adhesion, 161 immune responses, 162,163 pathogenhost recognition, 164,165 several aspects of tumor growth and development, 150 and in neurotransmission. 166 Lectins have been widely utilized as affinity probes for the efficient detection, separation, and enrichment of glycoproteins in complex biological fluids by virtue of their selective carbohydrate–protein interactions. $^{167-169}$ In addition, lectin-based glycoprotein enrichment combined with mass spectrometric identification has been widely adapted for glycoproteomic profiling to identify disease-associated alterations of glycoprotein as potential biomarker. 170 However, the weak and variable binding affinities of many carbohydrate-lectin interactions ($K_{assoc} = 10^3 - 10^6 \text{ M}^{-1}$) have often compromised the practical utility of lectin in capturing glycoproteins for glycoproteomic applications. 166,170 Most of the well characterized lectins for bioseparation are derived from plants. Concanavalin A (Con A), a mannose and glucose specific lectin, wheat germ agglutinin (WGA), an *N*-acetylglucosamine and sialic acid binding protein and soybean agglutinin (SBA), a galactose binding protein have been widely used. 171

In an effort to simultaneously enrich and detect small molecules using MALDI-TOF-MS, Lin and coworkers developed a straightforward method involving bifunctional MNP system that served as laser desorption/ionization element as well as a solid-phase extraction probe. Their approach involved covalently conjugating a MALDI matrix with protein probe on the same NP to generate MNP@matrix-protein system, **Figure 18.** Their hypothesis behind the fabrication of this system was that besides MNP@matrix-protein ability to purify and enrich the target small molecules from a complex mixture, MNP@matrix can be used as a matrix free additive for MALDI-TOF MS analysis of the enriched molecules. And since the matrix is covalently conjugated to the NP, the MNP@matrix can potentially reduce the interference caused by matrix

ion peaks normally found in low molecular weight range for MALDI-TOF MS. To examine the ability of MNP@matrix-protein to probe a weak biomolecular interaction, the well-defined recognition between mannose and Con A was chosen as a proof-of-concept experiment. MNP system was constructed consisting of dihydroxybenzoic acid (MALDI matrix) and Con A as a probe protein (MNP@DHB-Con A). MNP@DHB-Con A was successfully utilized to enrich mannose spiked in human plasma to mimic complex biological sample. The MNP@DHB-Con A-mannose complex was analyzed directly by MALDI-TOF MS without elution. As low as 0.5 μg of spiked Con A could be detected, enriched, and analyzed by MALDI-TOF-MS in 30 min.

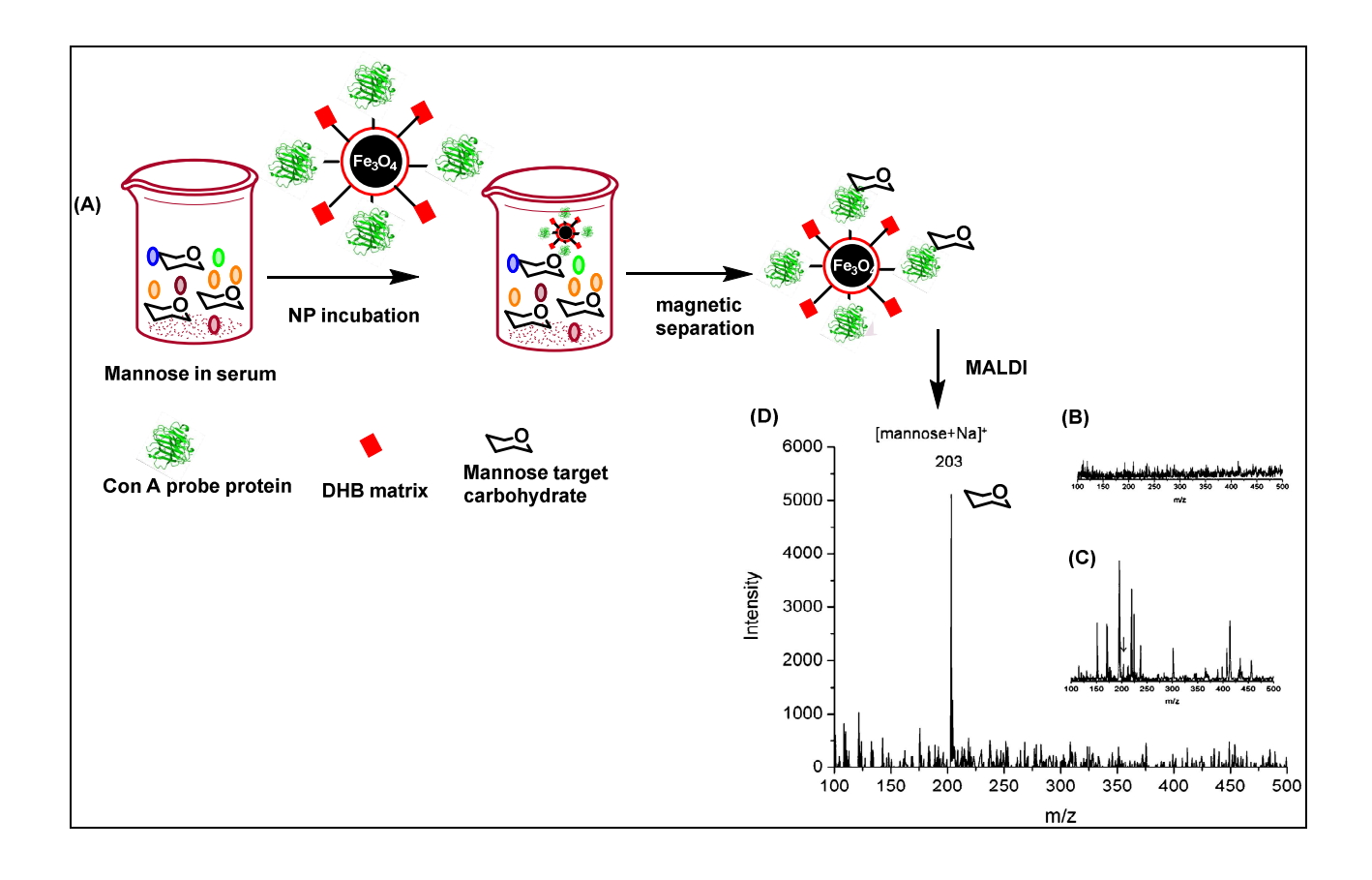


Figure 18: Protein capture and analysis using bifunctional MNP@matrix-Con A. (A) Workflow of functionalized MNP-assisted MALDI-TOF MS. The bifunctional MNP@matrix-Con A serves as an affinity matrix-free additive. Mannose extraction from human plasma by MNP@DHBCon A (B) The background signal of MNP@DHB-Con A; (C) The human serum profile; the black arrow indicates the spiked mannose (D) The mass spectrum of mannose [mannose + Na]⁺ extracted by MNP@DHB-Con A. Adapted and reproduced with permission from reference¹⁷² Copyright 2007, American Chemical Society

Since these systems are often developed with the final goal of being applied in the discovery of new target molecules, additional investigative experiments to confirm binding selectivity and specificity, sensitivity and enrichment efficiency are required. As pertains Lin and coworker work, experiments such as SDS-PAGE, using NPs lacking the target molecule (Con A), or even spiking with irrelevant substrates (add both galactose and mannose, only mannose

peak should be observed on mass spec) would have been desirable. In addition, competitive experiments where free Con A is added to compete with immobilized Con A on the NPs will be desirable in order to reveal the binding specificity of immobilized Con A. Furthermore, elution protocol to release the bound mannose, which can then be analyzed by SDS-PAGE has also been well established as a way to confirm binding specificity. Subsequently, comparing the performance of the lectin functionalized MNP construct with commercially available lectin functionalized beads should be evaluated to assess the improvement and the value added by the NP system.

Such studies to try and qualify the advantages of lectin functionalized MNPs as functional probe for selective separation and enrichment of glycoproteins was reported by Tang et al.¹⁷¹ Con A functionalized MNPs, was similarly used in this study. The first step was to address how lectin are functionalized on the NPs. Normally, the method of choice for immobilization is through amide bond covalent linkage utilizing the amine of the protein's lysine groups as described in previous examples.¹⁷² However, this method can result in the loss of biological activity as the linkage may occur at or next to the carbohydrate binding site. To avoid this potential drawback, Con A was immobilized on the surface of nanospheres that were modified with aminophenylboronic acid forming boronic acid-sugar-Con A bond in a sandwich structure. α-D-mannopyranoside was used as an intermedium as shown in **Figure 19**.

The selectivity, specificity and capacity of these Con A-immobilized MNPs to capture glycoprotein in a protein mixture was demonstrated using standard proteins. Protein mixture consisting of glycoproteins horseradish peroxidase (HRP) and ribonuclease B (RNase B) containing high mannose oligosaccharides and non-glycoproteins bovine albumin (BSA) and myoglobin (MYO) was used. As shown in **Figure 19, panel B**, protein bands on SDS-PAGE

corresponding to HRP and RNase B and not BSA or MYO in the mannose eluted fraction from a mixture of the four proteins. This indicates the potential of the NP in achieving good efficiency and specificity in the isolation of glycoproteins. However, despite the good selective enrichment effect of Con A immobilized NPs, unwanted bands of Con A can be observed on the gel due to the dissociation of Con A during enrichment, **Figure 19 panel B.**

The suitability of Con A-modified MNPs for biomedical application especially for glycoprotein biomarker identification was further tested in cell lysate of human hepatocellular carcinoma (HCC) cell line 7703. After the enrichment procedure, original lysate, supernatant (consist of unbound fraction), and the eluted fraction were resolved on SDS-PAGE. Bands below 25 kDA were discarded to eliminate Con A contamination and the rest of the proteins were subjected to tryptic digestion for LC/MS/MS identification. A total of 101 glycoproteins were identified as searched against protein databases. ¹⁷¹ To assess the performance of the NPs, parallel glycoprotein enrichment experiments from the same cell lysate were performed using commercial Con A magnetic beads (SiMAG Con A magnetic beads) and aminophenylboronic acid functionalized MNPs without Con A functionalization.. More glycoproteins were enriched and purified using Con A MNPs (101 glycoproteins) when compared to commercial Con A magnetic beads (51 glycoproteins) and aminophenylboronic acid functionalized MNPs (12 glycoproteins). The protein profile from the three different experiments is summarized in Figure 19 panel C. It also worth mentioning that boronic acid functionalized MNPs have been proposed as potential tools for glycopeptide and glycoprotein enrichment. 173-175 In this case it showed the weakest performance probably due to its inability to be applied in complicated biological samples. These results provides additional evidence on advantages of biomolecule functionalized magnetic nanoparticles as a tool for the discovery of potential biomarkers.

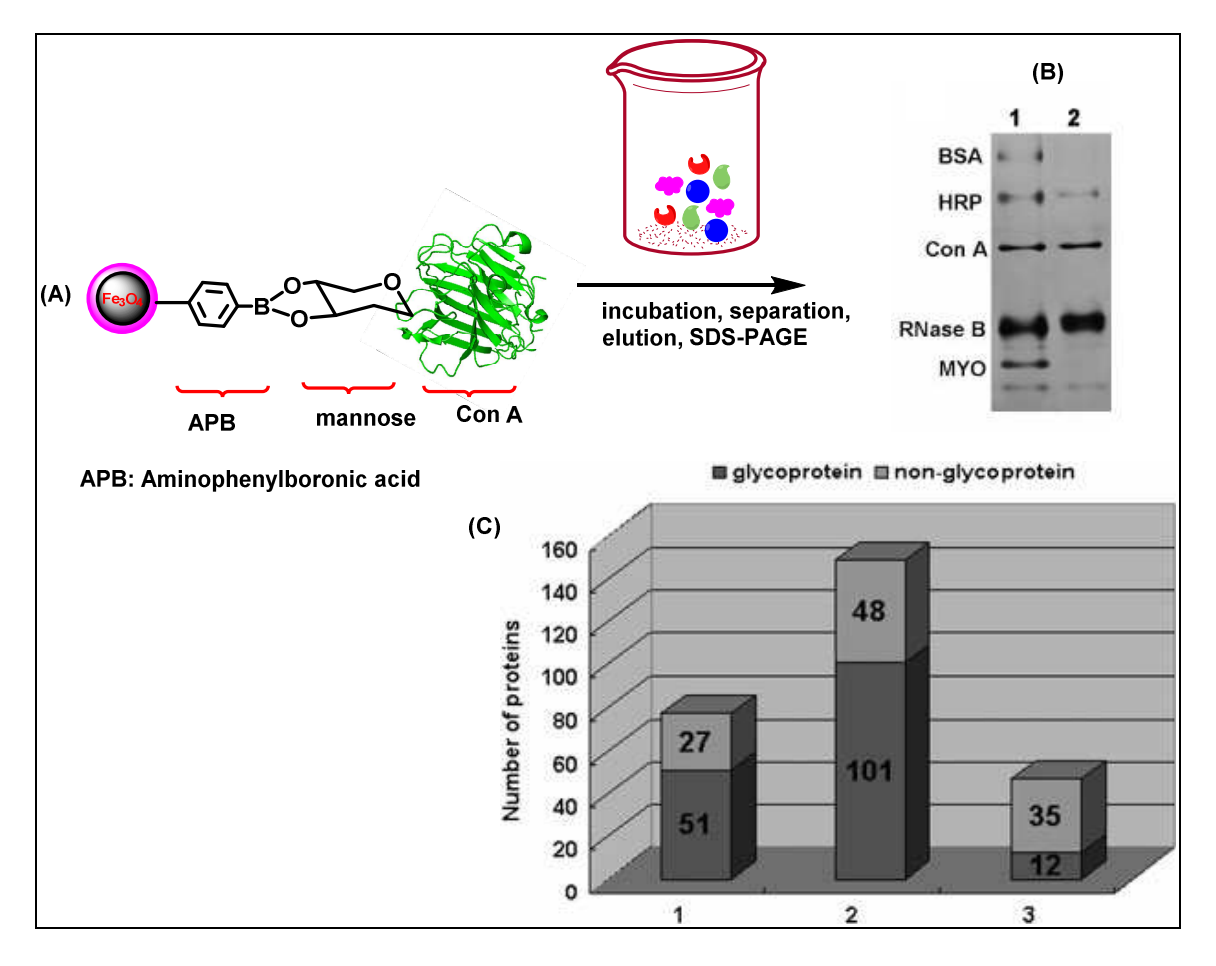


Figure 19: Protein analysis using Con A functionalized MNP through boronic-acid-sugar sandwich. (A) Con A functionalized MNP through boronic-acid-sugar sandwich (B) One-dimensional SDS-PAGE of selective glycoproteins capture by Con A-immobilized MNPs. Lane 1, supernatant of standard protein mixture after enrichment; Lane 2, eluent of nanoparticales after enrichment. (C) Comparison of the three materials for glycoprotein enrichment from cell lysate, indicating the number of glycoproteins identified and the selectivity for glycosylated proteins. Bar 1, proteins identified with commercial Con A magnetic beads; Bar 2, proteins identified with homemade Con A MNPs; Bar 3, proteins identified with aminophenylboronic acid-functionalized MNPs Adapted and reproduced with permission from reference¹⁷¹ Copyright 2010, John Wiley and Sons

This work outline key experiments that need to be undertaken to validate the relevance of functionalized MNP as a potential tool for isolation and enrichment. Despite the success, addressing the leaching of immobilized Con A is key. Also due to the low binding affinity between lectin and carbohydrate, the efficiency of Con A immobilization through this method can be potentially very low. Another possible limitation associated with this immobilization protocol is the risk of cross-linking NPs. Since Con A has four mannose binding sites, an already immobilized Con A can bind three more NPs reducing the available Con A for efficient glycoprotein enrichment. In addition, since boronic acid reacts with the hydroxyl groups and particularly 1,2-diol of the sugar to form boronic ester, such modification may alter its biological recognition towards the respective lectin. For example it has been well established that unmodified hydroxyl groups at C-3, C-4 and C-6 position of α-D-mannopyranose (or α-D-glucopyranose) ring are essential for binding to the active sites of Con A.¹⁷⁶

In an effort to improve on the conjugation of lectins to MNPs while preserving the conformational integrity of their binding site during covalent linkage, Ferrira et al introduced a new concept, based on protection of the lectins' binding sites with their target sugars prior to coupling with MNPs.¹⁷⁷ In addition to Con A, MNPs functionalized with wheat germ agglutinin (WGA), *N*-acetylglucosamine selective lectin and *Maackia amurensis* (MA), lectin with affinity to α -2,3-linked sialic acid residue were synthesized. Con A was incubated with mannose, WGA with *N*-acetylglucosamine, and MA with α -2,3-sialyllactosamine before conjugation and regenerated to remove the protecting sugar prior to glycoprotein enrichment.¹⁷⁷ Using fetuin, a glycoprotein with 5-8 % sialic acid, 3.5 % mannose and 4.8 % acetylglucosamine, thus expected to bind all three lectins, protection of the binding sites showed enhancement in lectin functionality. There was increased recovery in Con A and MA MNPs. There was no statistical

significance to suggest that protection of binding sites had a positive effect on WGA, Figure 20 panel A.

The efficiency of immobilization on supports was evaluated by comparing glycoprotein yields of MNP@ConA with conventional Sepharose support, Sepharose@ConA, which is traditionally immobilized without active site protection. The NPs and Sepharose beads were evaluated based on the same amount of functionalized lectins. In addition to fetuin, ovalbumin, an N-glycoprotein known to bind ConA, which is traditionally immobilized without active site protection. The NPs and Sepharose beads were evaluated based on the same amount of functionalized lectins. In addition to fetuin, ovalbumin, an N-glycoprotein known to bind ConA, which is traditionally immobilized without active site protection. The NPs and Sepharose beads were evaluated based on the same amount of functionalized lectins. In addition to fetuin, ovalbumin, an N-glycoprotein known to bind ConA, which is traditionally immobilized without active site protection. The NPs and Sepharose beads were evaluated based on the same amount of functionalized lectins. In addition to fetuin, ovalbumin, an N-glycoprotein known to bind ConA, which is traditionally immobilized without active site protection. The NPs and Sepharose beads were evaluated based on the same amount of functionalized lectins. In addition to fetuin, ovalbumin, an N-glycoprotein known to bind ConA, which is traditionally immobilized lectins are supported by the same amount of functional sepharose was also used. As shown in Figure 1.20 panel B, Con A functionalized NPs performed better in glycoprotein recovery compared to Sepharose Con A even at 6 times lower amount of Con A.

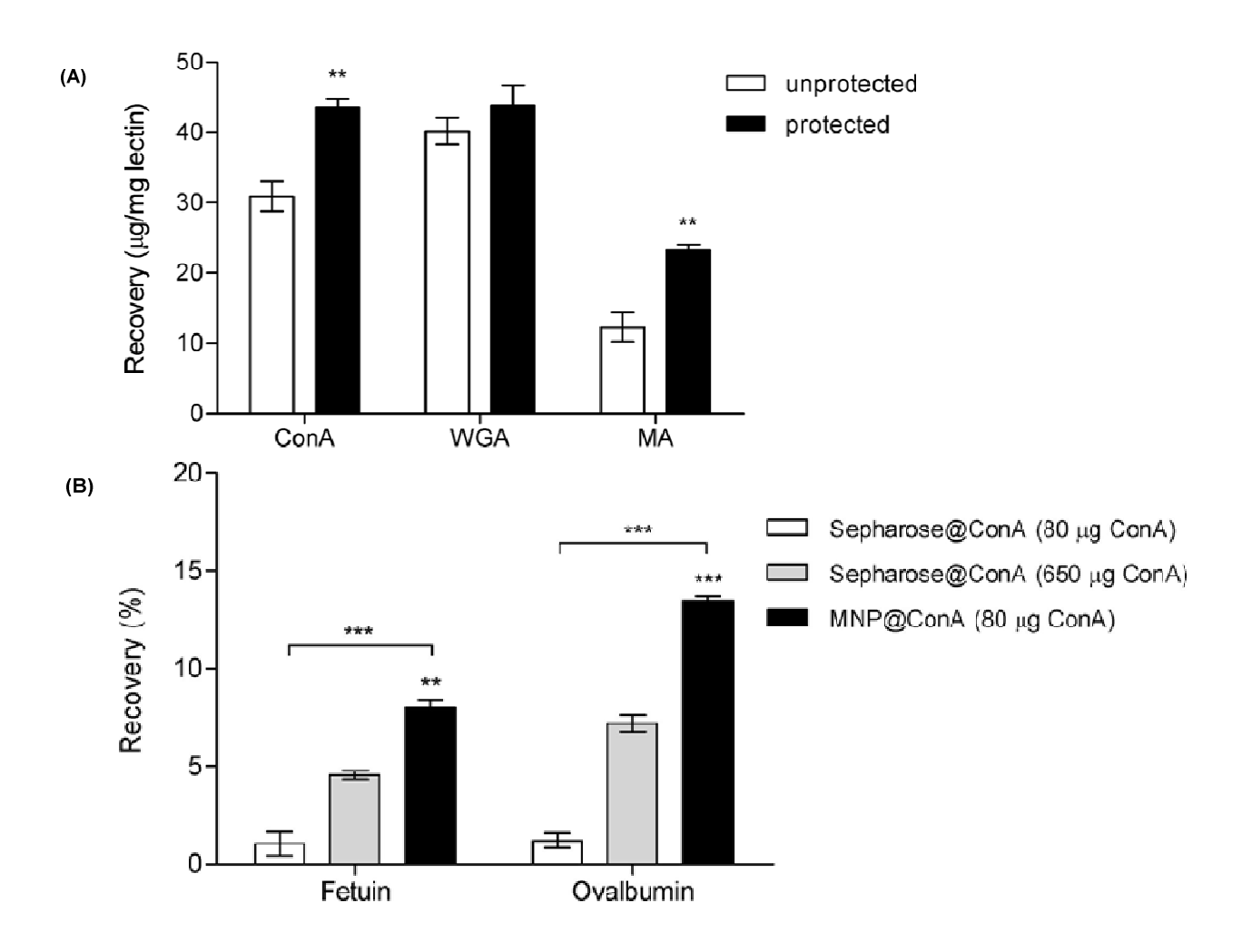


Figure 20: Protein analysis using lectin functionalized MNPs. (A) Fetuin recovery by synthesized MNP@lectins: comparison between unprotected and sugar-protected MNP@lectins. Data are presented as mean standard deviation (SD) of micrograms of fetuin recovered per milligram of MNP@lectin (triplicates of n=3). **p < 0.01. (B) Percentage of glycoprotein recovery of nanobeads MNP@ConA vs Sepharose@ConA. \pm Data are presented as mean SD (triplicates of n=3) upon incubation with 10 μg of fetuin or ovalbumin. **p < 0.01; ***p < 0.001 vs preceding concentration. Reproduced with permission from reference 177 Copyright 2011, American Chemical Society

Besides recovery of standard proteins, the functionalized lectins also exhibited the potential of being developed into analytical tools through selective recovery of glycoproteins from human body fluids (serum, urine and saliva). Similarly these lectin functionalized MNPs

displayed superior performance compared to commercially available lectin beads functionalized through conventional methods that do not involve binding site protection. The superiority was more pronounced in their abilities to minimize nonspecific binding. For example, it was determined in this work that 6 % of the glycoprotein isolated from human urine using MNP@ConA was due to nonspecific binding, which was much less than the 30 % nonspecific recovery using Con A immobilized on agarose beads.¹⁷⁹ The possibility of reducing nonspecificity granted by MNP@lectins is of key importance in bioseparations, as it allows an increased availability of binding sites for ligands of interest and avoids masking target proteins.

As mentioned earlier, the weak and variable binding affinities of many carbohydrate-lectin interactions have often compromised the practical utility of lectin in capturing glycoproteins for glycoproteomic applications. He enrichment protocols provided by the previous examples still utilize the noncovalent interactions of the surface glycans of glycoproteins with lectin. In addition, these studies have also relied on the observation that such weak binding affinities can be compensated by the binding avidity as a results of multiple immobilized lectin ligands on the NP surface. But literature reports have suggested that in some studies, this approach has failed to capture and enrich sufficient quantities of material for mass spectrometry analysis. He

To provide a possible solution, Lu et al. applied boronic acid-decorated lectin (BAD-lectin) in glycoprotein labeling and enrichment.¹⁷⁰ The inclusion of boronic acids (BAs) could have additional benefits: (i) with their chemical affinity for carbohydrates, they will react covalently but reversibly with cis-diol compounds to form stable boronate compounds under basic aqueous conditions. (ii) Unlike lectins, which recognize specific carbohydrates, BAs possess little affinity selectivity for interactions with different glycoforms. BAD-lectin exploits

the initial lectin carbohydrate recognition process, which subsequently facilitates the formation of a boronate ester resulting in a stable covalent lectin-glycoprotein complex. Through this approach, glycoproteins binding weakly and transiently can be isolated and enriched, **Figure 21**.

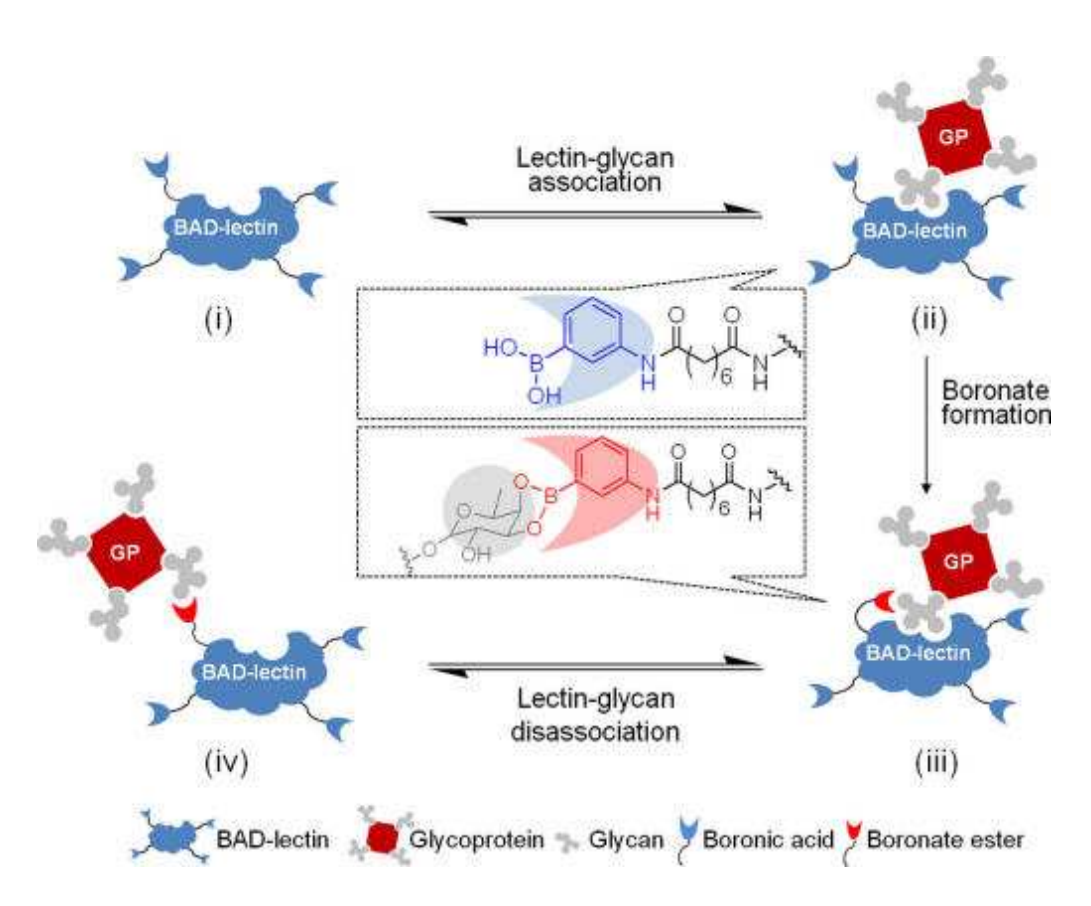


Figure 21: Schematic illustration of the dual binding of a BAD-lectin to a glycoprotein. Schematic illustration of the dual binding of a BAD-lectin to a glycoprotein. (i) A BAD-lectin. (ii) A glycoprotein captured by the lectin by noncovalent glycan-specific recognition. (iii) A glycoprotein captured by both lectin and BA; the latter mediates boronate ester to form a stable covalent lectin-glycoprotein complex. (iv) A glycoprotein captured by a BA ligand alone. Reproduced with permission from reference¹⁷⁰ Copyright 2013, American Chemical Society

The application of BAD-lectin for glycoprotein enrichment and glycoproteomics study was demonstrated on the fabrication of BAD-lectin conjugated MNP (BAD-lectin@MNP). As a proof of concept, *Aleuria aurantia* lectin (AAL), and *Sambucus nigra* lectin (SNA), which are

known to recognize fucosylated glycoproteins, and glycoproteins containing sialic acid linkages (especially $(\alpha$ -2,6) linkages), respectively in addition to concanavalin A (Con A), were fabricated as model systems to detect distinct types of target glycoproteins. Prior to glycoprotein enrichment, it was essential to substantiate the hypothesis that addition of BAs could enhance lectin-carbohydrate binding affinity.

To compare the binding affinity to their cognate glycan ligand of BAD-lectins with that of the free lectins, surface plasmon resonance (SPR) imaging was used for real-time, label-free analysis of the lectin–carbohydrate interactions. As shown in **Figure 22 (B) and (C)**, the steeper association curve for Con A in comparison to BAD-Con A is indicative of a faster initial association, whereas the shallower curve in the dissociation phase for BAD-Con A in comparison to Con A is indicative of a slower dissociation event. Subsequently, the equilibrium dissociation constants (K_D), calculated from the rate constants for free Con A and BAD-Con A, which quantitatively measure their binding strengths on the sugar-functionalized surface, indicated that BAD-Con A had a lower equilibrium dissociation constant than free Con A, 14.3 nM and 80.5 nM respectively. Possible explanation for these observed results was that the presence of BA on the protein's surface might have reduced the initial association between the lectin and the glycan. However, once the lectin binds to the glycan, the subsequent formation of the boronate decreases the rate of dissociation, resulting in an enhanced overall affinity.¹⁷⁰

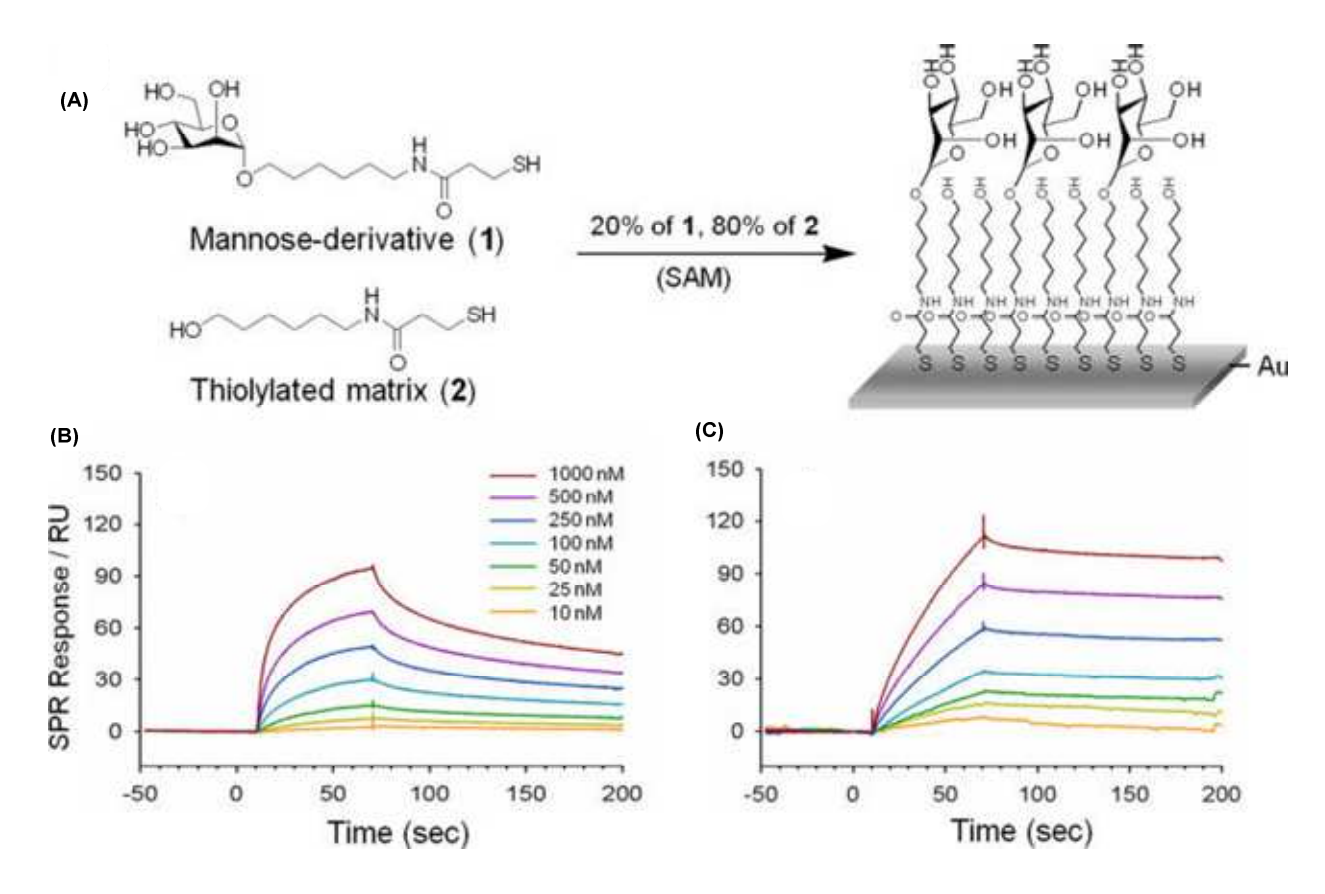


Figure 22: SPR sensing of the affinity of the BAD-lectin probe for a carbohydrate-functionalized self-assembled monolayer (SAM). (A) Mannose functionalized molecules and the corresponding matrices for immobilization on sensor chips. SPR sensorgrams for the binding of (B) ConA and (C) BAD-ConA at a series of concentrations (from 10 to 1000 nM; bottom to top) to a mannose-functionalized SAM chip. Reproduced with permission from reference¹⁷⁰ Copyright 2013, American Chemical Society

In the proof of concept experiment, the performance of BAD-Con A@MNP was compared to Con A@MNP and BA@MNP in the enrichment of ribonuclease B (RNB), a high mannose glycoprotein. BAD-Con A@MNP displayed good performance in comparison with Con A@MNP and BA@MNP. In addition, the BAD-lectin@MNPs were applied in the capture of glycopeptides generated by tryptic digestion of a complex biological sample, which further evaluated the potential application of BAD-lectin@MNPs in the glycoproteomic studies.¹⁷⁰

To further highlight the advantages offered by biomolecule functionalized MNPs, Li and coworkers used Con A functionalized MNPs to isolate and identify native cell membrane glycoproteins from living cells. ¹⁸⁰ In most cases, and as already discussed in previous sections, isolation of target analytes using biomolecule functionalized magentic nanoparticles has been done in cell homogenates. ¹⁵⁵ The use of cell homogenates has potential drawbacks associated with it, the major one being possible protein contamination which may occur during cell lysate preparation and handling. ¹⁸⁰ In a typical isolation experiment, cells were incubated with the Con A MNPs overnight. The cells bound to the surface of the NPs were treated with membrane protein extraction buffer, followed by elution of the membrane glycoprotein bound to Con A on NPs with elution buffer containing 0.5 M methyl-α-D-mannopyranoside. The isolated glycoprotein profile was analyzed by SDS-PAGE and the identity confirmed through LC/MS/MS analysis.

1.4.3: Antibody functionalized MNPs

As one of the well-known affinity probes, antibodies possess strong and specific affinities for epitopes on target antigens. Due to this characteristic, antibodies have been widely used in enzyme linked immunosorbent assays (ELISA),^{181,182} Western blot,^{183,184} immunoaffinity extraction,¹⁸⁵⁻¹⁸⁷ targeted therapeutic delivery,^{188,189} diagnostic arrays,¹⁹⁰⁻¹⁹² and currently in immunotherapy especially for cancer,^{193,194} autoimmune, and inflammatory diseases.¹⁹⁵ When conjugated to nanomaterials as solid support, the high affinity and selectivity of the antigenantibody interactions have allowed the specific extraction, isolation and concentration of analytes of interests¹⁹⁶ including pathogenic bacteria.¹⁹⁷

Major work pioneered in this area involved using antibody functionalized MNPs as affinity probes for protein (antigens) ^{102,198-202} and bacterium^{196,203-205} separation from sample solution. For protein isolation, these probes have been combined with matrix-assisted laser desorption/ionization time-of-flight mass spectrometry (MALDI MS) to profile relevant disease biomarkers from biological fluids. ^{198,200} When compared to antibody functionalized microbeads, antibody conjugated MNPs have demonstrated a better homogeneity with biomolecules and achieved a higher extraction efficiency and sensitivity. ¹⁹⁸ Despite earlier success, these probes still suffered from non-specific binding particularly due to the presence of abundant proteins.

The drawbacks brought about by non-specific binding mainly associated with a decrease in specificity and sensitivity of detection as well as the accuracy of the quantification of target proteins present in low abundance. 199,206 To improve binding specificity of these probes, attention has been focused on both the synthesis of NPs and how antibodies are immobilized on the NPs surface and other solid surfaces. 50,199,207 Lin et al. established that by synthesizing methoxyethyl terminated ethylene glycol (MEG)-protected antibody-conjugated MNPs, nonspecific binding during the separation of protein biomarkers in human plasma was significantly suppressed. 199 This was revealed through MALDI-TOF-MS by monitoring the target signals. As a proof of concept, anti-serum amyloid P component (SAP), a biomarker related to Alzheimer's disease and type 2 diabetes were immobilized on IONPs with ethylene glycol protection. The performance of the NPs was assessed by its ability to specifically detect SAP in human plasma. When this NP system was compared to anti-SAP-MNP prepared by BSA capping or without capping of free unconjugated succinic esters moieties, it was evident that MEG-capping of anti-SAP MNP was able to decrease the non-specific binding of abundant proteins such as human serum albumin (HSA), Figure 1.23. These results highlight key

requirements when constructing biomolecule functionalized NP system in order to minimize non-specific binding; (i) free reactive groups that were initially introduced on the NP surface for a sole purpose of conjugation should be capped, (ii) the capping moieties themselves should have low affinity to other biomolecules.

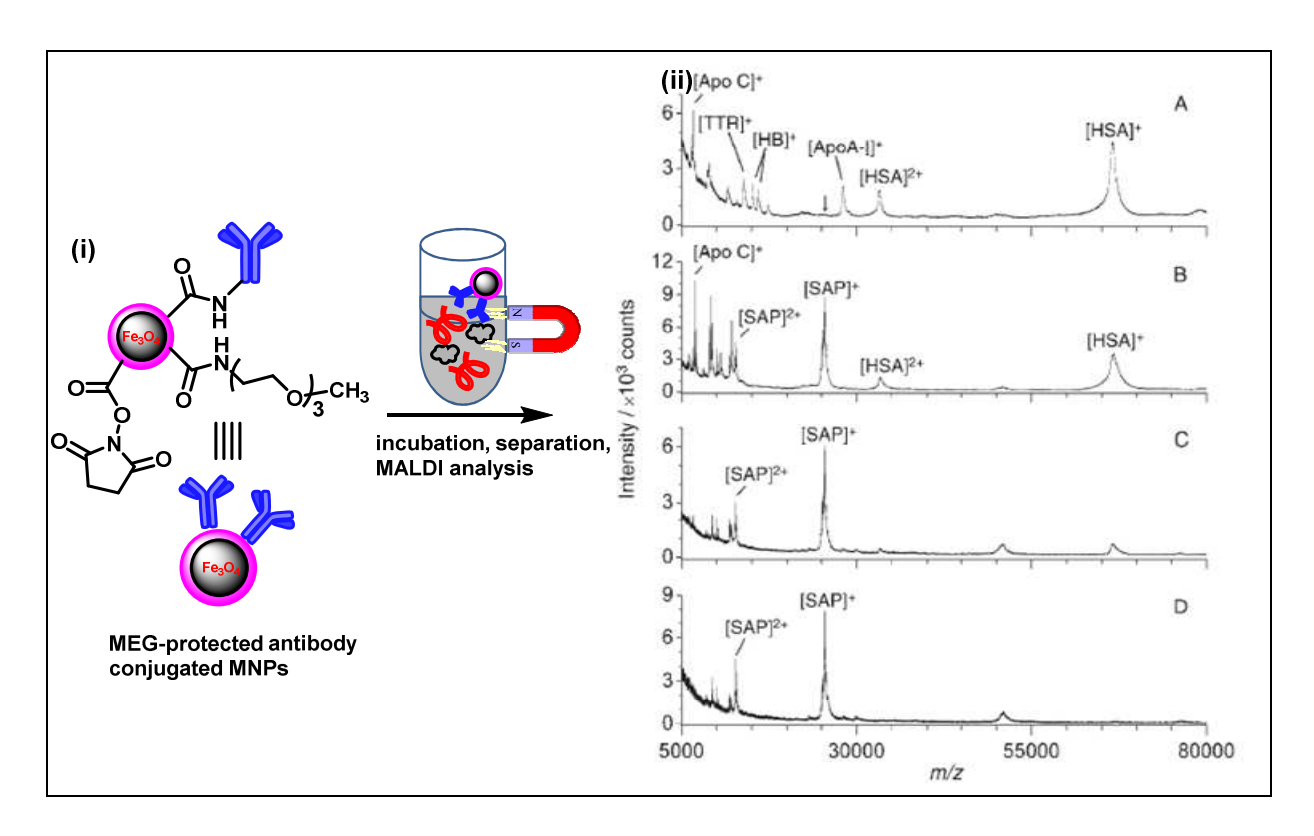


Figure 23: Protein separation using MEG-protected antibody conjugated MNPs. (i) Immunoassay by MEG-protected antibody-conjugated MNPs. ii) MALDI-TOF mass spectra of human plasma (1 mL) from immunoaffinity extraction with anti-SAP MNPs: A) 25-fold dilution of human plasma; B) Extraction with anti-SAP MNPs (without blocking); C) Extraction with anti-SAP MNPs (BSA blocking); D) Extraction with anti-SAP MNPs (40 mm MEG blocking) after 1000-fold dilution. Adapted and reproduced with permission from reference¹⁹⁹ Copyright 2006, John Wiley and Sons

Following similar approach as discussed in previous sections, site specific and chemoselective immobilization of biomolecules on solid surfaces away from their active binding

sites is preferred to achieve superior substrate binding activity. 67,81,100 In most conjugation protocols, antibodies are immobilized on to NPs by random amide bond or Schiff base formation, through modification at their lysine, arginine, aspartate, and glutamate residues.²⁰⁸ These protocols do not guarantee immobilization of the antibodies at a uniform density or in a single orientation, consequently, the immobilized antibodies recognize their antigens with variable efficiency. This may results in unsatisfactory activity in desired application. 209 To achieve site-specific and self-oriented antibody conjugation, methods have been developed that focus on modification at the Fc domain to preserve the antigen binding domain and maintain full immunoactivity. Site-specific modification of the Fc domain have been achieved by targeting the entire Fc or its carbohydrate moiety. Targeting the entire Fc domain can be accomplished by first modifying solid anchorage supports with an intermediate protein (Fc binding proteins commonly, protein G and protein A). These are subsequently used to anchor/immobilize the antibody via the Fc domain in a site-specific manner on the solid support. 49,210,211 This strategy has potential drawbacks associated with it. Firstly, the need for two protein immobilization steps can result in a low density of the immobilized antibody. ²⁰⁹ Secondly, the potential dissociation of the noncovalently linked antibody-protein complex may result in decreased assay sensitivity and increased antibody background. 102

To target the carbohydrate moiety at the Fc region, two approaches have been investigated. Firstly, the vicinal diol groups on the carbohydrate chain of the Fc can be cleaved by periodate oxidation to form aldehyde groups, which are then utilized to attach molecules of interest by Schiff base formation. 98,212 Second approach involves targeting the carbohydrate at the Fc region with boronic acid. 101,102,213 Boronic acids have affinity to vicinal cis-diol compounds such as carbohydrates and glycerol to which they react covalently but reversibly to

form stable boronate compounds under basic aqueous conditions. As a result, boronic acid immobilized on solid supports have been utilized for glycoprotein enrichment and carbohydrate sensing. 173-175,214-217

Taking advantage of this property, Lin and coworkers reported the site-specific and selforiented immobilization of anti-SAP antibodies on MNPs through boronate formation at the carbohydrate moiety of the Fc domain (anti-SAP-BA@MNP). The antibody functionalized MNPs were used as an active immunoprobe for disease biomarker detection from human sera. 102 More importantly, when compared with NP system whose antibodies were randomly immobilized through amide bond formation (anti-SAP-R@MNP) or oriented immobilization through protein G (anti-SAP-G@MNP), the self-oriented immunoprobe via boronic acid (anti-SAP-BA@MNP) provided long-term stability, and improved sensitivity at a low nM range, Figure 24. The observed good performance was presumably through enhanced antibody@MNP activity. Just as in their previous report, ¹⁹⁹ false-positive detections arising from nonspecific binding mainly due to free unconjugated boronic acid that could potentially react with glycoproteins was minimized by effective surface protection using concentration-dependent dextran blocking (anti-SAP-BA-dex@MNP). 102 However, the amount of antigen extracted by anti-SAP-BA-dex@MNP was lower than that extracted by anti-SAP-G@MNP (Figure 24 panel **D, BA vs G)** due to the diol-containing interference of the serum, which could possibly exchange with the immobilized antibody. To improve on this, the serum was pretreated with free boronic acid prior to incubation with anti-SAP-BA-dex@MNP. This dramatically improved the antigen recovery leading to comparable results (Figure 24, panel D, BA1 vs G). On a positive note however, HSA, the most abundant protein in human serum, resulted in high interference in anti-SAP-R@MNP and anti-SAP-G@MNP but not with anti-SAP-BA-dex@MNP even in the

absence of pretreatment with free BA, **Figure 24 panel D**. This demonstrates the high efficiency of the interference-free antigen extraction by BA-oriented antibody MNP in complex biological systems.

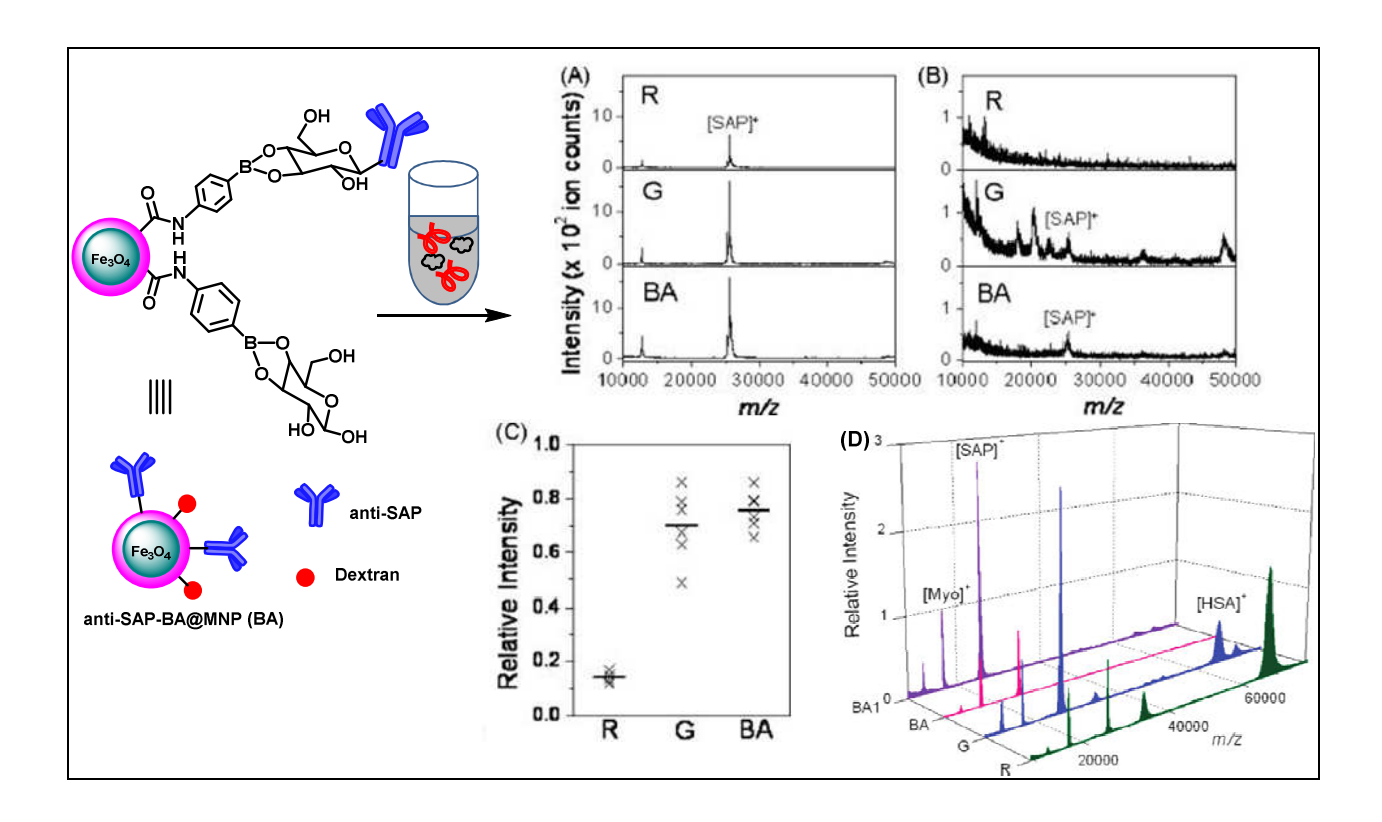


Figure 24: Comparison of the antigen extraction performances of anti-SAP-R@MNP (R), anti-SAP-G@MNP (G), and anti-SAP-BA@MNP (BA) using mass spectrometry. MALDI-TOF MS spectra of the extracted antigen from (A) 16 and (B) 0.4 nM solutions of SAP. (C) Five consecutive measurements of the extracted antigen from a 12 nM SAP solution. Spectrum signal intensities were normalized to that of myoglobin, which was used as a mass spectrum internal standard. (D) MALDI-TOF MS analysis to examine the SAP extraction efficiency of anti-SAP-R@MNP (R), anti-SAP-G@MNP (G), anti-SAPBA-dex@MNP (BA), and anti-SAP-BA-dex@MNP (BA1) from human serum pretreated with 5 mM of *m*-aBA. Spectrum signal intensities (× 102 ion counts) were normalized to that of myoglobin (Myo), which was used as a mass spectrum internal standard. Adapted and reproduced with permission from reference¹⁰² Copyright 2009, American Chemical Society

Since the glycan-boronate ester bonds are formed in a slightly basic pH, it implies that their application is limited in samples whose pH is greater or equal to 7.0. Therefore the development of a site-specific, self-oriented immobilized antibody on solid surfaces through a more stable covalent linkage that can be applied in both acidic and basic pH environment is still desirable. One possible way by which this has been achieved is through UV photo-cross-linking approach that utilizes boronic acid to achieve oriented immobilization of antibody on a surface as reported by Adak et al.²¹³ In a typical experiment, a photoactive boronic acid probe is synthesized. The boronic acid provides good affinity and specificity for the recognition of glycan chains on the Fc region of the antibody, whereas the photoactive probe enables covalent tethering to the antibody upon exposure to UV light, **Figure 25**. Incorporating photoactivatable moieties on affinity probes has been a method of choice when extracting biomolecule binding partners that exhibit weak and transient binding affinities.¹⁶⁶

Figure 25: Light-induced covalent and oriented immobilization of Abs on BA-presenting surfaces. Upon UV irradiation (λ max = 365 nm), the (trifluoromethyl)phenyldiazirine functional groups in 1 generate highly reactive carbenes that spontaneously undergo insertion reactions to permanently tether the antibody on the surface. Adapted and reproduced with permission from reference²¹³ Copyright 2014, American Chemical Society

1.4.4: Aptamers/oligonucleotides functionalized MNPs

Aptamers are short single-strand DNAs (ssDNAs)/RNAs that bind diverse targets beyond DNAs or RNAs from metal ions, organic molecules, to proteins, cells and microorganisms with high affinity and specificity.^{218,219} Typically, the systematic evolution of ligands by exponential enrichment (SELEX) process is used for the isolation of specific, high affinity aptamers. The methodology consists of screening large random oligonucleotide libraries through iterative cycles of *in vitro* selection and enzymatic amplification.²²⁰⁻²²² As an emerging class of recognition elements, aptamers have offered remarkable convenience in the design and modification of their structures. As a result, they offer several advantages when compared to

other recognition molecules such as antibodies. First and as stated earlier, they bind not only to macromolecules such as DNA, RNA,proteins^{223,224} and cells but also to small molecules including organic dyes,²²¹ amino acids,²²⁵⁻²²⁷ carbohydrates,²²⁸ and nucleotides.²²⁹ Therefore aptamers may be a tool of choice in diagnostics and drug delivery when small molecules are the targets. Secondly, since aptamers are selected *in vitro* as opposed to *in vivo* as the case of antibodies, they can be used to select for a wide range of targets.²³⁰ Furthermore, the selection process can be performed under non-physiological condition including high temperatures or pH, making them more stable to heat, pH and organic solvents.²³⁰ In addition, aptamers can be synthesized chemically, and their sequence information can be shared digitally as a blueprint for manufacturing them. This allows cheap and fast production with reproducible properties and very low, if any batch-to-batch variation.²³¹

The combination of aptamers with novel nanomaterials, including nanomaterial-based aptamer bioconjugates has attracted considerable interest and has led to a wide variety of applications. The application has ranged from amplified biosensing, ²³²⁻²³⁴ imaging, ^{235,236} cancer cell-specific recognition, ²³⁷ and targeted drug delivery and diagnostics. ²³⁸ Nanomaterials, including gold, ²³⁹ silica ²⁴⁰ NPs, as well as carbon nanotubes, ²⁴¹ hydrogels, ²⁴² liposomes and micelles, ²⁴³ have been used as carriers of aptamers.

Similarly, aptamers have been immobilized onto MNPs and the application of these functionalized MNPs has been mainly in biosensors, ^{244,245} and MRI imaging agents. ²⁴⁶⁻²⁴⁸ Functionalization of aptamers on MNPs has been accomplished by either streptavidin or avidin-biotin binding chemistry, gold-thiol chelation chemistry on the iron/gold-core/shell NPs, and 'click' chemistry. In streptavidin or avidin-biotin chemistry, the NPs are conjugated with either streptavidin or avidin through covalent bond formation. The aptamer or oligonucleotide to be

immobilized is derivatized with biotin, which is then introduced on the NP surface through the streptavidin-biotin or avidin-biotin binding chemistry. Gold-thiol chelation chemistry is achieved through modification of the oligonucleotide or aptamer with a thiol followed by introduction on the iron/gold-core/shell NPs. On the other hand, 'click' chemistry reaction involves synthesizing NPs with azide on their surfaces and reaction with oligonucleotides modified with alkyne or vice versa. All of these methods as it can be observed do not involve using any functional group native to the oligonucleotide for immobilization on the NPs, implying they are all bio-orthogonal. As a result, the binding specificity and selectivity of the immobilized oligonucleotides are preserved, potentially leading to better and efficient performance. Among the three immobilization strategies, covalent immobilization of the oligonucleotide has the potential to yield more stable attachment and better reproducibility.

The utility of aptamer functionalized MNPs as high efficiency bioseparation and enrichment tools has been realized both in simple and complex biological sample mixtures. To make these nanoprobes usable particularly in biomedical areas, its binding capacity and specificity of interactions with target molecules are paramount. A proof of principle to verify the applicability of aptamer functionalized MNPs has been tested on the basis of their abilities to separate a complementary oligonucleotide from solution. The complimentary oligonucleotide is often modified with a gold NPs or a fluorophore to confirm successful detection and isolation by surface plasmon resonance (SPR) and fluorescence respectively. Labeling also serves as a way to quantify how much of the target complimentary oligonucleotide is isolated, hence revealing their binding capacity. Binding specificity and selectivity is best evaluated through control experiment using fluorescent labeled non-complimentary oligonucleotide that can be tracked during the experimental procedures. Sa

Aptamer functionalized MNPs have shown promising applications in the selective extraction and enrichment of disease cells from complex mixtures including whole blood. Tan and coworkers reported using a two NP systems (fluorescent silica NPs and non-fluorescent MNPs) conjugated with aptamers for the rapid detection and isolation of acute leukemia cells. In their work, oligonucleotide with specific binding recognition for CCRF-CEM acute leukemia cells was attached to fluorophore-doped silica NPs and iron oxide MNPs and used simultaneously as a dual probe for separation and imaging of intact leukemia cells in mixed cell and whole blood samples. The aptamer conjugated MNPs were used for the selective targeting cell extraction whereas aptamer conjugated fluorescent silica NPs were to aid in sensitive cellular detection. The signal intensity corresponding to each aptamer binding event is enhanced upon the interaction of the target cell with the functionalized fluorescent NPs, implying the absence of binding will result in minimal observed fluorescence.²⁵² To determine the extraction and detection capabilities and selectivity in an artificial complex sample, equal amounts of target cells, CEM and non-target cells, Ramos cells (10⁵ each) were mixed, followed by incubation with increasing amounts of the two NPs. The number of cells collected was determined by flow cytometry by the counting of signal events. Similarly individual CEM and Ramos cell solution were incubated with the two NP systems, followed by fluorescent imaging and flow cytometry analysis of the bound cells. Each binding event was expected to result into amplification of fluorescence. On the other hand, to show applicability in real biological samples, whole blood was spiked with CEM cells, incubated with the two NPs followed by fluorescent imaging. As presented in Figure 26, panel B, it is evident that the target cells can be preferentially extracted from both simple and complex sample mixture with minimal non-specific binding.²⁵²

This application was extended for the detection, extraction, and enrichment of multiple cancer cells in simple cell media as well as in serum matrices by conjugating more than one aptamer on one NP.²⁵³ Furthermore, the Tan group has used these aptamer conjugated MNPs as probes for sensitive cancer cell detection, as well as comprehensive cancer cell profiling through pattern recognition based on their expression level of membrane receptors by MRI.²⁵⁴ In addition, since the end goal is to develop a clinical diagnostic tool, parameters that impact the performance of NPs were investigated. This included, the type of fluorophore used to construct fluorescence NPs, the size of MNPs, and the conjugation chemistries.²⁵⁵ It was observed that of the fluorophores doped inside silica NPs, including TMR, RuBpy, FITC, and Cy5, TMR-based particles possessed optimal performance. 60 nm MNPs demonstrated the highest performance compared to 350, 830, 2600 and 8030 that were tested. The conjugation chemistry that was found to be effective in generating functionalized NPs with high selectivity and excellent sensitivity was avidin-coated NPs conjugated to biotinylated aptamers.²⁵⁵.

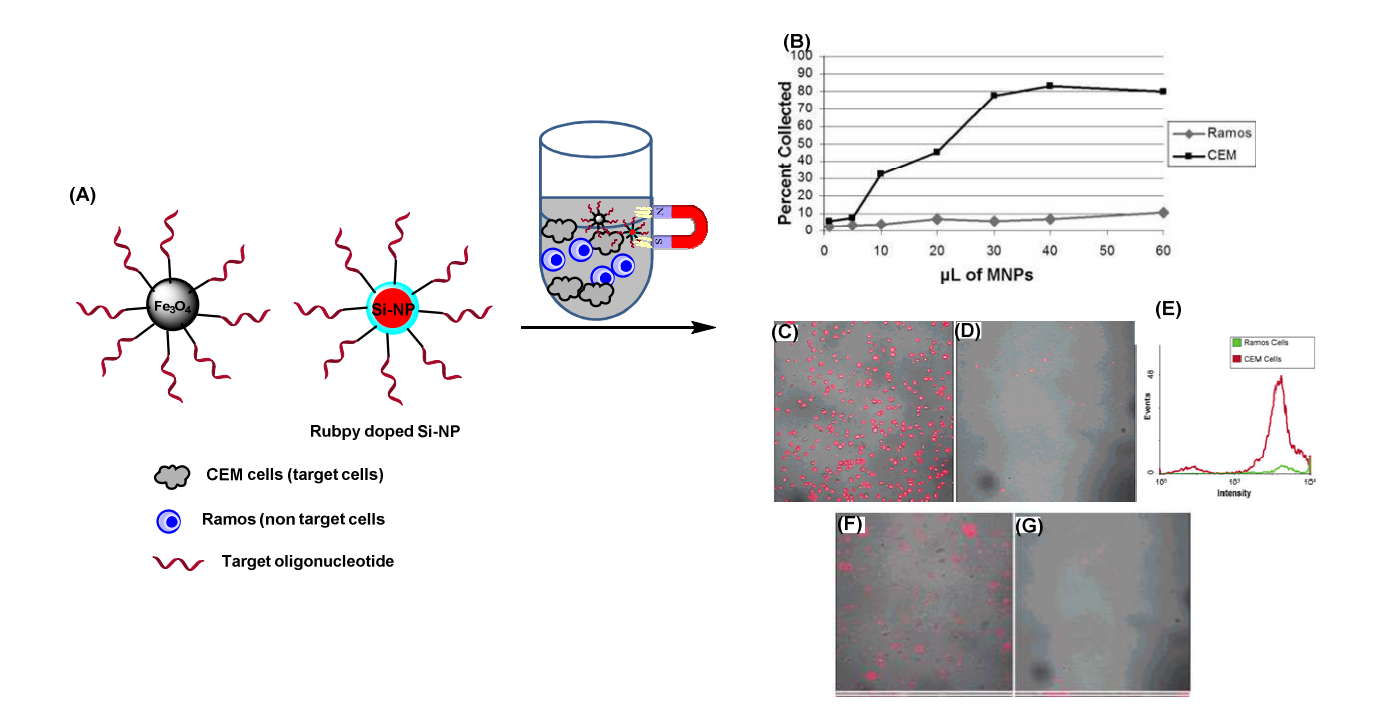


Figure 26: Cancer cell isolation and analysis using two NP systems. (A) cell isolation using two NP systems. (B) Flow cytometric determination of MNP collection and separation efficiencies between target and control cells Images of extracted samples from (C) Target cells and (D) Control cells and (E) Flow cytometric comparison of target and control signal after 5-min incubation with magnetic and fluorescent NPs, followed by three washes by magnetic separation. Confocal images of extractions from whole blood. (F) Extracted sample from target cell spiked whole blood, (G) Extraction from unspiked whole blood. Adapted and reproduced with permission from reference²⁵² Copyright 2006, American Chemical Society

With a similar two NP system, Fang et al. used aptamer conjugated upconversion NPs assisted by MNPs for effective sensitive detection and isolation of circulating tumor cells. Aptamer-biotin-functionalized upconversion NPs (UCNPs) and avidin conjugated MNPs were used. UCNPs are typically nanocrystals containing lanthanide ions, which under excitation by multiple low-energy near-infrared (NIR) photons can emit a high-energy photon at a shorter wavelength, hence acting as excellent optical nanoprobes. One of the most important advantages of UCNPs is the autofluorescence-free nature of upconversion luminescence (UCL)

imaging, a major factor that limits the sensitivity of fluorescence imaging. Hence UCNPs enable imaging with high sensitivity compared to fluorophore-doped NPs.^{256,257} In their work that was a proof of principle, target tumor cells in a mixed cell media or spiked into whole blood were first specifically recognized by aptamer/biotin co-conjugated UCNPs (UCNP– Apt–Biotin). The target tumor cells are then captured by avidin-conjugated MNPs (MNP–Av). After magnetic separation, UCL imaging is conducted to detect the captured-spiked tumor cells. CCRF-CEM cells were used.²⁵⁸ This work represents the first study in which aptamer conjugated UCNPs have been used as nanoprobes to recognize tumor cells, which are then enriched by MNPs, **Figure 27**.²⁵⁸

Besides cells, the combination of aptamer functionalized UCNPs and MNP have been tested for their ability to detect and isolate mycotoxin as reported by Wang and coworkers.²⁴⁵ Protein purification and enrichment using aptamer functionalized MNPs have also been investigated, thus revealing the versatility and diversity of aptamers in terms of bioseparation application.^{259,260}

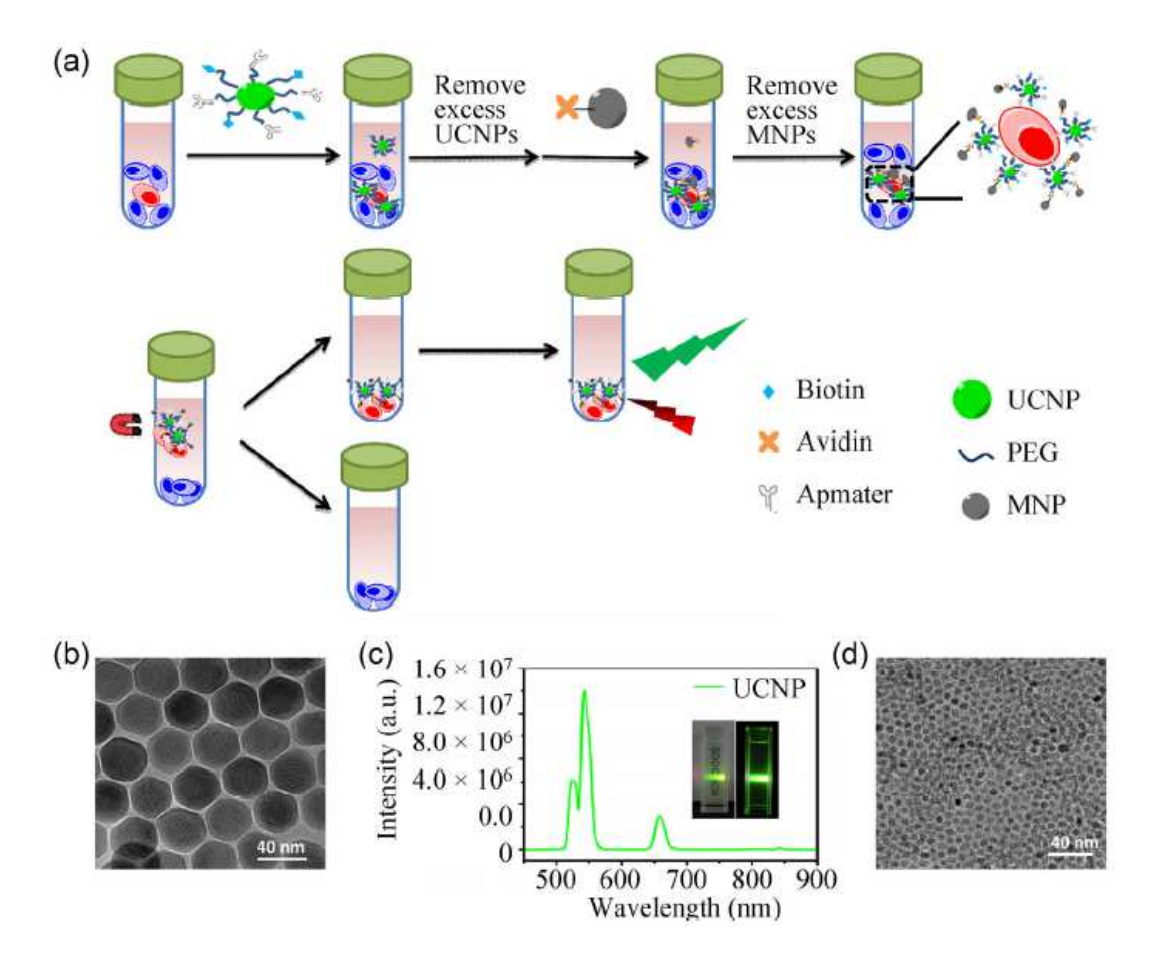


Figure 27: Using UCNP-Apt-Biotin and MNP-Av nanoprobes for CTCs detection and isolation. (a) Schematic illustration of using UCNP-Apt-Biotin and MNP-Av nanoprobes for CTCs detection. Positive tumor cells are recognized by UCNP-Apt-Biotin nanoprobes, which are then specifically attached by MNP-Av NPs for magnetic separation. The UCL signals from UCNPs could be utilized for tumor cell detection. (b) A TEM image of as-made UCNPs (NaYF4:78% Y, 20% Yb, 2% Er). (c) Upconversion luminescence spectrum of PEGylated UCNPs in an aqueous solution. Inset: a photograph of a UCNP aqueous solution excited by a 980-nm laser. (d) A TEM image of as-made MNPs. Reproduced with permission from reference²⁵⁸ Copyright 2014, Springer

1.4.5: Enzyme, protein and peptide functionalized MNPs

1.4.5.1: Enzymes

As catalytic biological macromolecules, enzymes immobilized on novel nanomaterials, including superparamagnetic IONPs have attracted considerable interest and has led to a wide variety of applications especially in proteolysis, 119,120,261 organic synthesis, 117,118,262,263 resolution of chiral intermediates, 264,265, and as biosensors. 266,267 Immobilization of enzymes has been established to be advantageous for these applications because it results into convenience in handling, ease of separation of enzymes from the reaction mixture and reuse, low product cost, increased enzyme activity due to high enzyme loading, and increase in thermal and pH stability compared to free enzymes. 268-271 On the contrary however, few reports are available that describe the utilization of enzymes functionalized on solid support especially MNPs for bioseparation and enrichment of enzyme binding targets. This highlights the need for more work in this area of research.

In one example, Chen and coworkers used xanthine oxidase (XOD) functionalized MNPs to isolate and analyze by HPLC-MS xanthine oxidase binders from plant extract samples.²⁷² The striking part of their results as reported was that XOD functionalized on tetraethyl orthosilicate (TEOS) coated IONPs (Fe₃O₄@SiO₂-XOD) exhibited good specificity for XOD binders, better dispersion in aqueous solution, higher activity and better reusability than that of uncoated NPs (Fe₃O₄-XOD). The amount of XOD immobilized on NPs was calculated by detecting the fluorescent intensity at 334 nm with excitation wavelength at 280 nm. The amount of XOD immobilized on Fe₃O₄ was found to be 302.8 μg/mg. After TEOS coating, the amount of XOD immobilized on Fe₃O₄@SiO₂ increased to 339.9 μg/mg.²⁷² Since immobilization of XOD was done via amine functionalization that was introduced by aminopropyltriethoxysilane (APTES), it

may imply that the presence of initial silica coating may have favored more APTES coating resulting in higher number of amine on the surface. These results confirm the importance of coating NP core. Even though high activity of immobilized enzyme (>95 % through ten cycles of reusability) was observed, its conjugation criteria followed 'randomized conjugation chemistry' using glutaraldehyde linked to amine moieties of the enzymes. The potential drawbacks associated with randomized conjugation have been highlighted in previous sections, which include conjugation occurring at or close to the active binding sites. In addition, enzymes may be denatured due to the random cross-linking to the NPs. Furthermore, there is a possibility of multiple point binding of the enzyme to the NPs. As describe previously, site specific and self-oriented immobilization of biomolecules on solid supports which may include NPs has been proposed as ways to achieve reproducibility from bath to batch production.^{9,33}

One example for oriented immobilization of enzyme on MNPs was reported by Yan and coworkers. In their work, lipase derived from *Yarrowia lipolytica* lipase, LIP2 was covalently immobilized on functionalized IOMNPs in a reverse micelle system (RMS), which resulted in oriented immobilization.²⁷³ The activity of the oriented immobilized lipase was 10 fold more compared to the randomly immobilized lipase when tested in the enrichment of polyunsaturated fatty acids. The advantages of using RMS are due to the fact that the lipase in the oil-water interface get interfacial activation, the active reaction sites that are usually buried in the hydrophobic regions will be exposed and be localized at the hydrophobic spherical surfaces of the micelles. Typically, lipases possess a hydrophobic surface, often containing a 'lid' region associated with the active site, generally inaccessible to the substrate.²⁷⁴ The opening of the lid domain generates a large hydrophobic surface surrounding the lipase active site, and it has been suggested that this surface may be the main site of interaction with the oil-water interface.²⁷⁵

Within a water-in-oil emulsion, these active sites would therefore tend to localize and orientate at the spherical interface of the emulsion droplet.²⁷⁴ Thus in the case of Yan and coworker's system, the aldehyde groups of glutaraldehyde on the surface of the MNP will couple with the now available free amino groups at the reactive site of lipase residues to immobilize lipases on the NPs. As a result, activity loss caused by conformational variation involved in covalent immobilization is profoundly minimized.²⁷³

It has also been reported that site specific immobilization of enzymes on solid supports can be achieved by means of transpeptidase reaction by *Staphylococcus aureus* sortase A.⁹² This similar strategy can be translated to conjugate enzymes on NPs. Enzymatic approaches for the conjugation or immobilization of biomolecules are attractive because the substrate specificity of enzymes enables site-specific biomolecule modification.⁹²

1.4.5.2: Peptides

From the viewpoint of molecular recognition, peptides play key roles in participating in ligand–receptor and protein–protein interactions, since the recognitions mainly involve in the short peptides at the contact interface. Therefore, if the binding affinity of peptides to target proteins can be compared with that of antibodies with possible higher stability, given that it can be massed produced by chemical synthesis in a reproducible manner, peptides could be very promising candidates as recognition biomolecules.²⁷⁶ In that sense, peptides have been immobilized on solid supports including nanomaterials (gold, silica, quantum dots, polymer and iron oxide), and their application has been mainly in fields of diagnosis, imaging, biosensors, and targeted drug delivery for cancer therapy.^{114,277-284}

Among the short peptides, glutathione has received considerable attention, owing to its reactive thiol. It has been conjugated to MNPs and used as an affinity probe to separate and enrich glutathione-S-transferase (GST) tagged protein. Glutathione is a tripeptide with gamma peptide linkage between the carboxyl group of the glutamate side chain and the cysteine which is attached by normal linkage to glycine. It has high affinity for GST. Glutathione functionalized micro-beads are available commercially and have been used extensively in the purification of GST tagged recombinant protein. But due to the advantages offered by MNPs over micro-beads such as low non-specific protein interaction, high binding capacity, and reduced washing steps, research interest has focused on using glutathione immobilized on MNPs.²⁸⁵⁻²⁸⁷

Glutathione has been immobilized on NPs via the free thiol of the cysteine. Lee and coworkers²⁸⁶ functionalized glutathione on the NP surface by first reacting amine ending silica coated IONPs with either *N*-succinimidyl 3-(2-pyridyldithio) propionate for short chain (SC) or succinimidyl 6-(3-[2-pyridyldithio]-propionamido)hexanoate for long chain (LC) to generate SC-SPDP-NP and LC-SDP-NP respectively. Finally, glutathione was introduced by the formation of a new disulfide bond between the cysteine of the reduced glutathione and the SPDP-NP by the displacement of the pyridylthiol moiety. The synthesized glutathione functionalized MNPs were able to purify and enrich GST-tagged protein from complex protein mixture, implying the activity of glutathione was not affected by the conjugation chemistry. More importantly, the functionalized NPs showed superior performance when compared to glutathione functionalized agarose micro-beads. In the purification of GST-tagged ubiquitin (GST-Ub) from a protein mixture of GST-Ub and yeast proteome, and GST-Ub and the human serum proteome, the eluted fraction from the glutathione micro-beads resulted in several non-GST-Ub protein bands as confirmed by SDS-PAGE. The results indicate better capture selectivity of glutathione MNPs

over the conventional micro-beads, as only one prominent band corresponding to the GST-Ub was observed on the SDS-PAGE, **Figure 28**. The main potential drawback for this conjugation method is that the presence of disulfide linkage limits the usage of these NP to buffers that lack reducing agents such as DTT and mercaptoethanol.

In a way to address this shortcoming, Pan et al. reported an alternative immobilization strategy that involves first, coupling dopamine with maleimide followed by reacting with glutathione. Finally, the resultant coupled product was adsorbed onto IONP via the dihydroxyl groups of dopamine, **Figure 29**.²⁸⁵ The glutathione functionalized MNPs were successfully applied in the isolation, and purification of GST-fused protein from *E. coli* lysate that was initially expressed in *E. coli*.

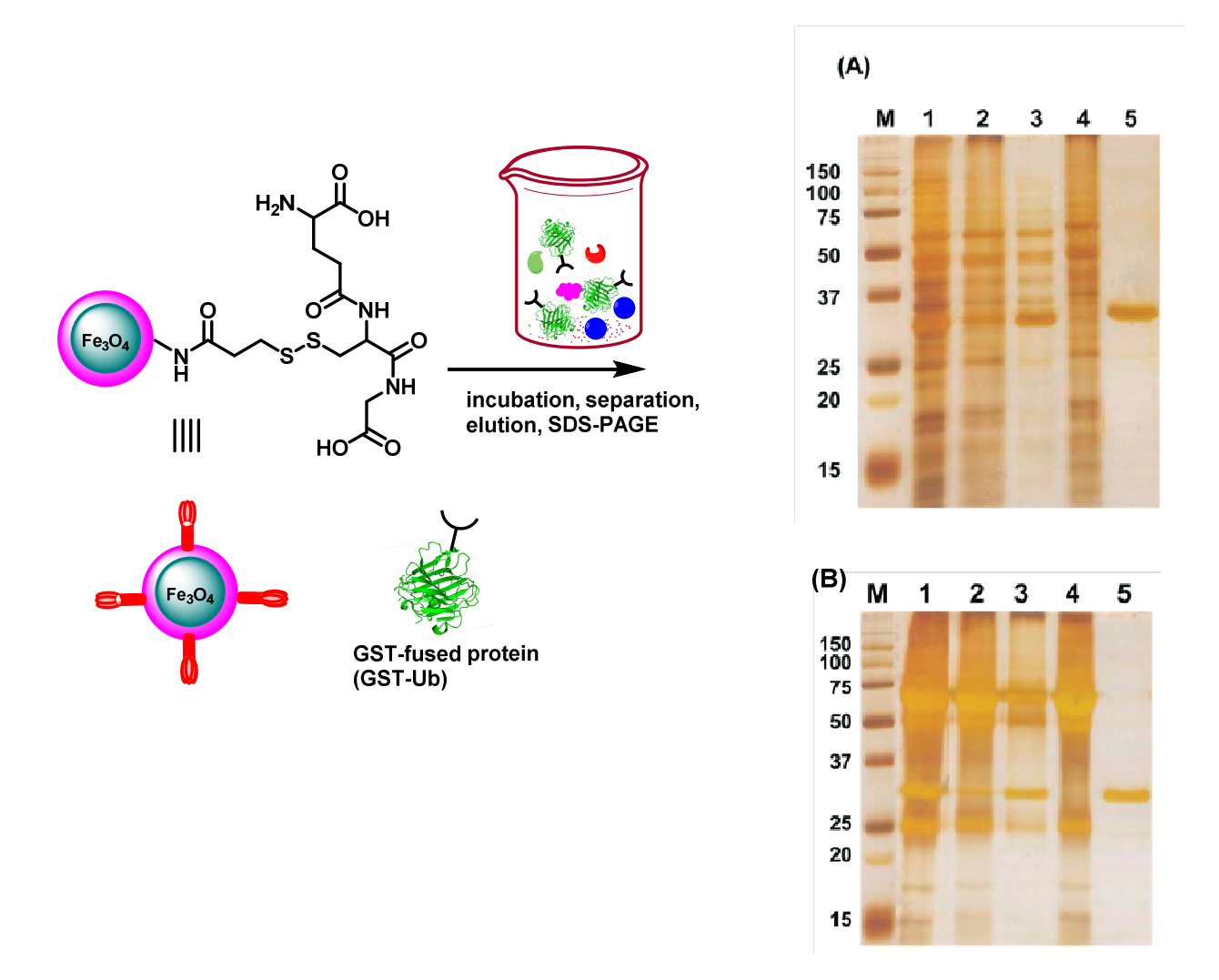


Figure 28: Capture and SDS/PAGE analyses of GST-Ub using SC-GSH-NP. (A) From a protein mixture of GST-Ub and yeast proteome. Molecular weight marker (lane M), yeast proteome and GST-Ub mixture (lane 1), supernatants after mixing with glutathione sepharose 4B beads (lane 2), and capturing and eluting from glutathione sepharose 4B beads (lane 3), supernatants after mixing with SC-GSH-NP (lane 4), and after capturing and eluting from SC-GSH-NP (lane 5) (B) From a mixture of GST-Ub and the human serum proteome. Molecular weight marker (lane M), serum proteome with GST-Ub (lane 1), supernatant after mixing with glutathione sepharose 4B beads (lane 2), and after capturing and eluting from glutathione sepharose 4B beads (lane 3), supernatant after mixing with SC-GSH-NP (lane 4) and after capturing and eluting from SC-GSH-NP (lane 5). Adapted and reproduced with permission from reference²⁸⁶ Copyright 2010, Korean Chemical Society

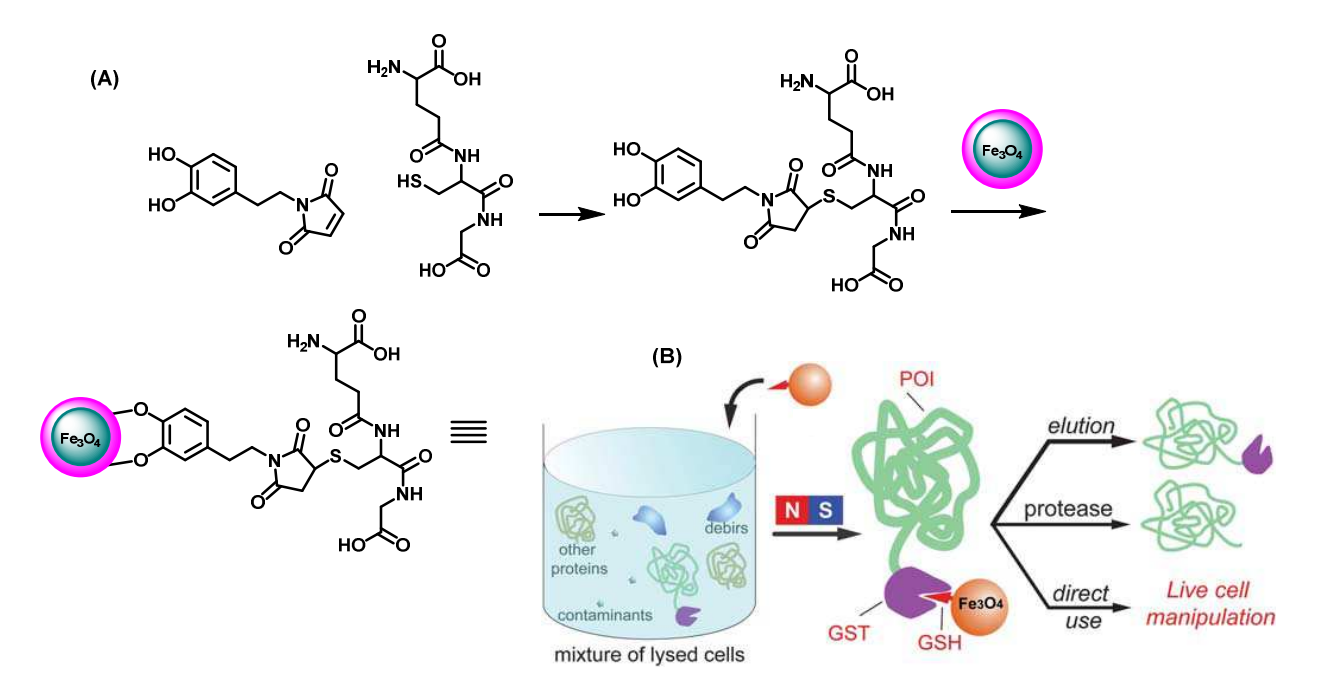


Figure 29: Glutathione functionalized MNPs for isolation of GST-fused proteins. (A) The synthetic route of the glutathione-decorated MNPs. (B) Glutathione-decorated MNPs selectively binds to GST-fused proteins of interest (POI) from a cell lysate and their own downstream applications. Adapted and reproduced with permission from reference²⁸⁵ Copyright 2011, Royal Society of Chemistry

Besides gluthathione, other peptides specific for targeting tumor cells have been conjugated onto MNPs and used as affinity ligands for targeting and extraction of malignant cells both in vivo and in vitro. 276,288 In an effort to provide an alternative method for detection and isolation of circulating tumor cells (CTCs) in the peripheral blood of metastatic cancers, Wang and coworkers developed IONPs immobilized with peptide that could recognize the epithelial cell adhesion molecule (EpCAM), which is usually over-expressed in CTCs. ²⁷⁶ The peptide was selected based on the binding affinity towards EpCAM during the phage display screening The **CTC** recognition procedure. peptide with the sequence VRRDAPRFSMQGLDACGGNNCNN (Pep10), was identified to exhibit high affinity and selectivity towards CTC cells. It was functionalized on the IOMNPs through the biotinstreptavidin interaction. Specificity of the peptide functionalized NPs towards the detection of the CTCs was demonstrated by isolating breast cancer cells (MCF-7) spiked in mixed cell samples. On the other hand, the ability of the peptide functionalized NPs to detect and isolate CTCs in whole blood was demonstrated by isolating MCF-7 spiked in healthy human whole blood. The universality of the peptide NP system was tested in capturing other EpCAM positive tumor cells (SK-BR-3, PC3, and Hep G2 cells) spiked in whole human blood. The performance of the peptide NP CTC isolation was compared to anti-EpCAM conjugated NPs and found to have comparable capture efficiency (over 90%) and purity (over 93%), **Figure 30**. In addition, Pep10 had comparable binding affinity (1.98 x 10⁻⁹ mol L⁻¹) to that of the anti-EpCAM (2.29 x 10⁻¹⁰ mol L⁻¹). The high capture efficiency and binding affinity demonstrated the general applicability of the peptide NP system in CTC detection and isolation.²⁷⁶

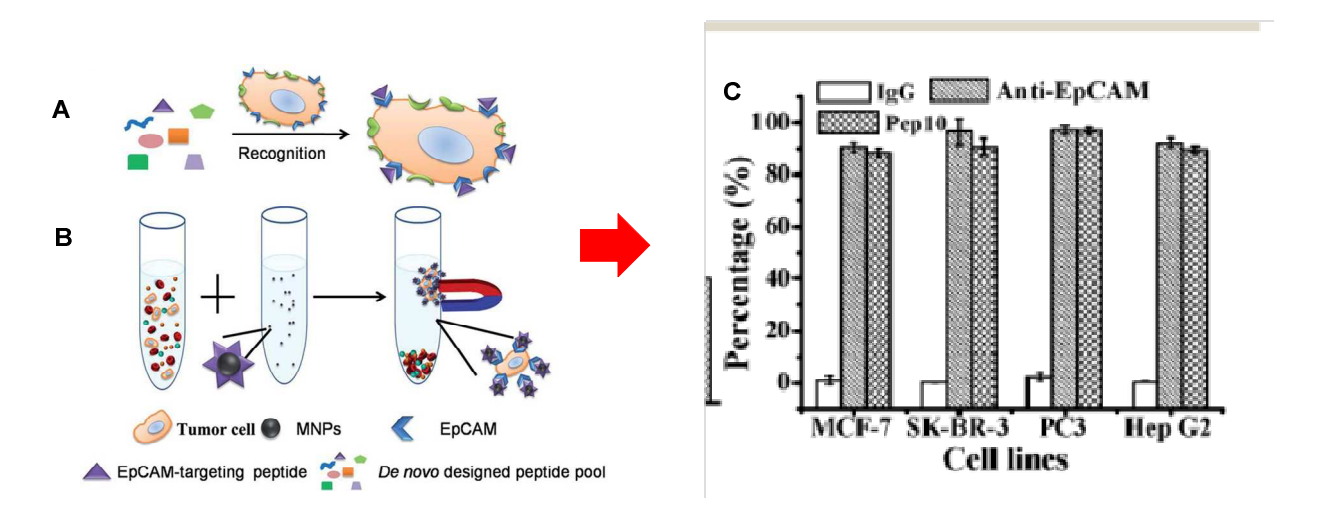


Figure 1.30: Circulating tumor cell isolation with MNPs modified with the EpCAM targeting peptide. (A) Screening of EpCAM targeting peptides from de novo designed peptide pool. (B) Isolation of CTCs in a magnetic field. (C) The binding capacity of IgG, anti-EpCAM and Pep10 on MCF-7, SK-BR-3, PC3 and Hep G2 cell lines was determined by flow cytometry. Percentage refers to the percentage of the cells fluorescence by FITC binding to the total cells. Experiments were done in triplicate and the reported error is the standard deviations. Reproduced with permission from reference²⁷⁶ Copyright 2014, Royal Society of Chemistry

Scarberry et al. reported the clinical viability of peptide functionalized MNPs through the extraction of cancer cells from mouse peritoneal cavity in vivo.²⁸⁸ A polypeptide with the sequence GGGGYSAYPDSVPMMSK was used as a targeting ligand. The peptide core, YSAYPDSVPMMS (YSA) binds specifically to the receptor tyrosine kinase (RTK), EphA2 using the YPDSVP sequence. EphA2 is highly expressed in a majority of ovarian cancers compared with normal ovarian surface epithelium, and predicts poor clinical outcome. ²⁸⁹⁻²⁹¹. The in vivo cancer cell extraction study begun by injecting equal number of fluorescently labeled tumor cells, Hey cells expressing high levels of EphA2 and BG-1 cells expressing low level of EphA2 into the peritoneal cavity of Balb/C female mice. After 5 min of cell incubation and abdominal massage, magnetic nanoparticulate conjugates were injected into the peritoneal cavity and incubated for 5 min. The peritoneal fluid was extracted and filtered magnetically before being examined using a hemocytometer to determine the number of green fluorescent (Hey) and red fluorescent (BG-1) cells. Although the initially mixed cell populations contained 50% Hey and 50% BG-1 cells, Hey cells accounted for 95-100% of extracted cell populations on average from three experimental trials, Figure 30. The scarcity of BG-1 cells in extracted cell populations was consistent with the specificity of YSA peptide-magnetic nanoconjugates. The highly specific binding of the YSA peptide to the EphA2 receptor enabled the magnetic conjugates to differentiate EphA2-rich ovarian carcinoma cells from EphA2-poor cells.

These findings demonstrate that MNP-peptide conjugates can target and remove metastatic cancer cells from the fluid of the abdominal cavity or circulatory system. Such results further suggest the feasibility of a dialysis-like system for the extraction of cancer cells, which,

combined with surgery and chemotherapy, may improve the long-term survival rates for cancer patients.²⁸⁸ In addition to the promising application, the conjugation design of the peptide also highlights the key points to put into account. Firstly, 4 glycines were added at N-terminal through which Rhodamine fluorescence tag was conjugated in order to increase the distance of Rhodamine from the binding region and prevent steric hindrance to receptor binding. Secondly, the lysine on the C-terminal was added to conjugate the peptide onto the NPs through amide bond formation with the carboxylic groups on the NPs, again protecting the binding region. As a result, the activity of the binding region was not affected throughout the conjugation process.²⁸⁸

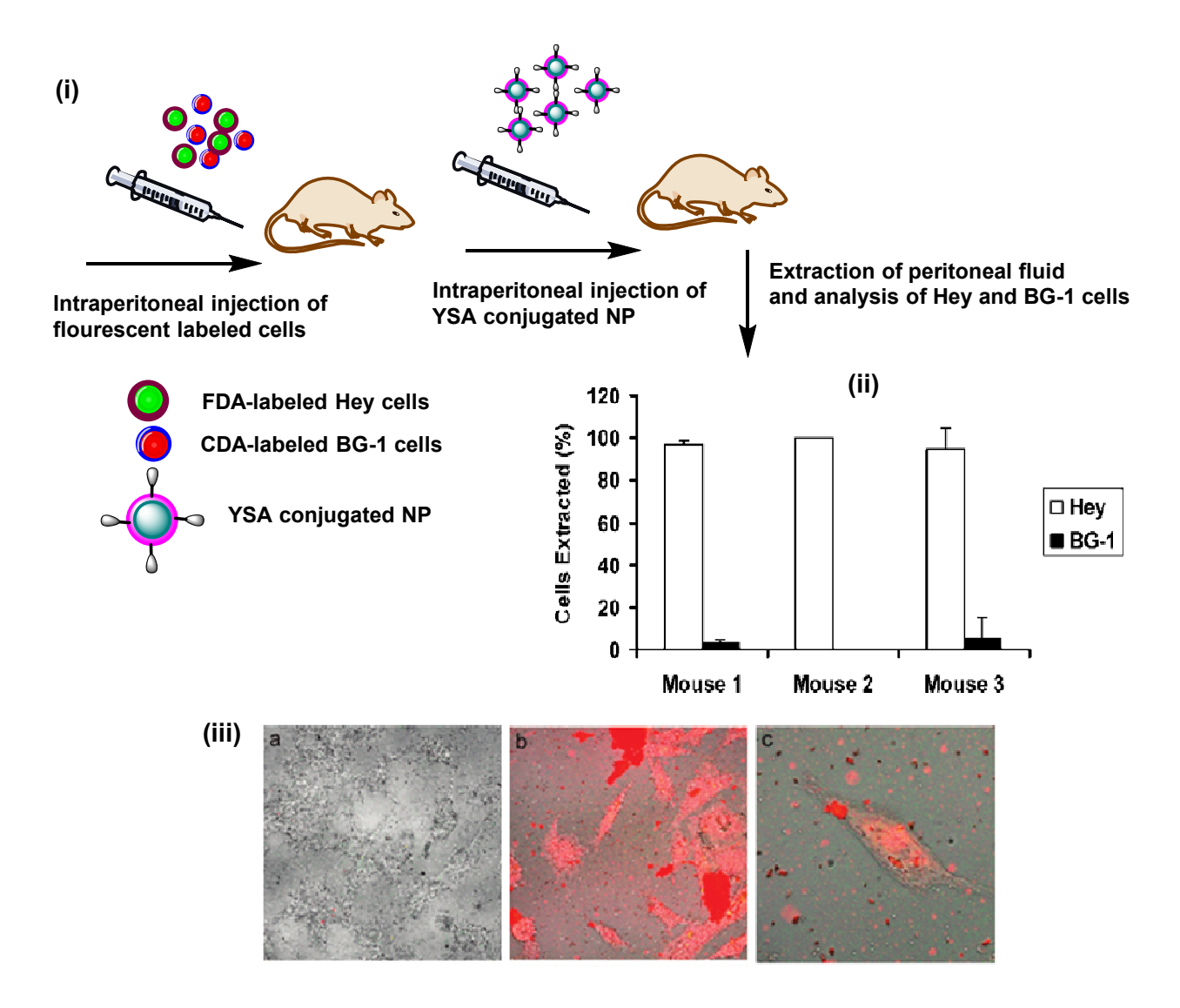


Figure 31: In vivo extraction and analysis of tumor cells with the help of YSA conjugated NPs. (i) *In vivo* incubation of cells with YSA conjugated NPs. (ii) Extraction efficiencies of the Hey and BG-1 cells. Compositions of Hey and BG-1 cells in the cell populations extracted from the peritoneum of three Balb/C female mice. The ratios were averaged from five counts performed on each of three mice. Error bars show the standard deviations. (iii) Confocal microscopic images of *in vitro* targeting of Hey cells. (a) Hey cells incubated with rhodamine-tagged MNPs (200X). (b) Hey cells incubated with rhodamine-tagged NP-YSA peptide conjugates (200×). (c) Higher magnification of Hey cells labeled with rhodamine-tagged NP-YSA peptide conjugates (400×). Adapted and reproduced with permission from reference²⁸⁸ Copyright 2008, American Chemical Society

1.4.5.3: Other proteins

Proteins other than lectins, enzymes, and antibody have also been immobilized on solid supports and used as affinity probes for bioseparation of target molecules. Proteins A and G, which can bind to the Fc region of antibodies (IgG) with high affinities, have been functionalized on microand widely used in the commercial purification of antibodies, immunoprecipitation (IP) techniques. 292-295 However, limitations associated with using protein A or G microbeads such as heterogeneous interface between microbeads and the aqueous medium, considerably reduces the comprehensive interaction and subsequently diminishes the efficiency of the IP technique.²⁹⁶ In addition, immobilized protein A or G have been reported to leach from the affinity resin and co-elute with the bound antibody, hence improved conjugation chemistries are required.²⁹⁴ Furthermore, the high cost of protein A and G microbeads, and low throughput, have initiated the search for more efficient and rapid purification alternatives.²⁹⁷ Due to the uniformity and high dispersity of NPs in aqueous medium, 141 immobilization of these proteins on MNPs for antibody separation and purification has been reported. Lin and coworkers developed protein G and A IOMNP conjugates to facilitate the purification of human IgG antibodies from human serum.²⁹⁶ For conjugation of target proteins, the surface of the core MNP was modified to have amine functionality followed by transformation to activated ester by reacting with the suberic acid bis-N-hydroxysuccinimide ester. 199 Finally, the activated MNPs were conjugated with amine moieties of the proteins. The unreacted activated ester groups were masked by short methoxyethyl ethylene glycol to avoid nonspecific binding of the highly abundant undesired proteins. 199 Protein G and A functionalized MNPs were successfully used to purify human IgG from human serum without contamination by undesired protein.

Besides proteins A and G, other common proteins have been immobilized on MNPs and used for extraction and enrichment of their target molecules. These include, bovine serum albumin (BSA)^{298,299}, biotin/avidin^{300,301}, and hemoglobin (Hb).³⁰² In line with previous discussion, controlling protein orientation on the NP surface during immobilization is of great importance because it influences the optimal molecular recognition of target molecules. As with enzymes, antibodies and lectins discussed earlier, oriented protein immobilization can be achieved by exploring the site-specific and chemoselective conjugation strategies.⁸⁰ Site-specific functionalization is accomplished through the use of functional groups that are not native to protein, hence avoiding possible interference with regions of the proteins that may be involved in interaction with target molecules. As a result, the protein will remain attached to the NPs through a stable linkage, and at the same time maintains its folded state and biological activity.⁸⁰ This has been achieved through noncovalent interaction for example, biotin-streptavidin,^{303,304} and His tag-Ni.⁴⁴ These interactions are commonly utilized for protein purification.

Proteins can be genetically or chemically modified in order to introduce a recognition sequence specific for protein conjugation. Covalent interaction mainly through expressed protein ligation (EPL), ^{78,305} followed by enzymatic ligation reaction ^{91,306} or chemical transformation such as click chemistry, ⁸² Staudinger ligation, ^{81,307} and native chemical ligation (NCL) ^{80,308} has been widely exploited. Since covalent immobilization results in more robust linkage, it is preferred. Enzymatic approaches for the conjugation or immobilization of biomolecules on the other hand are attractive because of the substrate specificity of enzymes. In addition, enzymatic reactions proceed under aqueous conditions without the addition of any further reagents beyond the protein, ligation substrate, and enzyme. Thus it has the potential to provide a means of linking expressed proteins to a wide range of solid supports, which is mild, selective, and can be

carried out in a single step.³⁰⁶ Even though the application of the above mentioned site-specific immobilization of proteins has been on glass surfaces that may be used for the creation of protein microarray, it can be extended to MNPs.

1.5: Summary

Going by the available literature evidence, it is undeniable that detection, isolation, separation, purification, enrichment and profiling of specific biologically active compounds, cells, pathogens is very important because of the role it holds in the areas of biosciences and biotechnology. Achieving this through magnetic based separation techniques, especially biomolecule functionalized MNPS is receiving attention due to the advantages associated with its application. The fact that these systems are inexpensive, simple to use, fast, requires only a few handling steps, where all purification steps can take place in one single separation tube, makes it an even more attractive technology. However despite the appealing and overwhelming advantages, and the progress that has been made over the decades, the use of biomolecule functionalized MNPs to identify novel binding partners is still at its infancy. Besides, the field has stagnated and remains a less attractive area of research. This calls for more incentives in the form of new research ideas for its revival. Based on the available literature information and as presented in this review, a good biomolecule functionalized MNP system for bioseparation can be achieved if all the influencing factors are taken into consideration right from the synthesis step.

Methods for the synthesis of MNP core plus surface coating with stabilizers to minimize aggregation or even make them highly dispersable in aqueous medium are well developed. The segment that seem to require more attention is the biomolecule conjugation step, especially larger protein such as antibodies and lectins. Bioseparation relies on the initial recognition step between the functionalized biomolecule with its target in a medium. Thus maintaining the

biological recognition properties of an immobilized biomolecule is a key requirement. As we have seen, classical protein conjugation chemistries through amide bond formation utilizing free amine moieties of the proteins remains a powerful NP bioconjugation chemistry of choice. However, need for site-specific and regio-specific conjugation chemistries to construct MNPs having well oriented surface biomolecules (protein), has shifted the focus on bioorthogonal conjugation chemistries. The number of bioorthogonal chemistries being evaluated in NP bioconjugation proteins by recombinantly introducing a cognate bioorthogonal reactive group is very encouraging.

Despite the fact that carbohydrates (especially simple sugar, mono- and disaccharides) do not present challenging bioconjugation requirements, the reliance on multivalency to achieve strong binding has not translated to improved enrichment of target sugar binding proteins. Researchers working in this area have shown that addition of covalent functionality through photoactivatable moieties to cross-link the protein(s) bound on the carbohydrate by affinity capture, improves the quantities of the isolated proteins. Therefore, with all the efforts being injected into this research field, we should envision the emergence of efficient biomolecule MNP conjugates that are capable of revolutionizing the field of bioseparation and enrichment.

REFERENCES

REFERENCES

- (1) Morris, V. J., Emerging roles of engineered nanomaterials in the food industry. *Trends Biotechnol.*, **2011**, *29*, 509-516.
- (2) Kreyling, W. G.; Semmler-Behnke, M.; Chaudhry, Q., A complementary definition of nanomaterial. *Nano Today*, **2010**, *5*, 165-168.
- (3) Liden, G., The european commission tries to define nanomaterials. *Ann. Occup. Hyg.*, **2011**, *55*, 1-5.
- (4) Bleeker, E. A. J.; de Jong, W. H.; Geertsma, R. E.; Groenewold, M.; Heugens, E. H. W.; Koers-Jacquemijns, M.; van de Meent, D.; Popma, J. R.; Rietveld, A. G.; Wijnhoven, S. W. P.; Cassee, F. R.; Oomen, A. G., Considerations on the EU definition of a nanomaterial: Science to support policy making. *Regul. Toxicol. Pharm.*, **2013**, *65*, 119-125.
- (5) Auffan, M.; Rose, J.; Bottero, J.-Y.; Lowry, G. V.; Jolivet, J.-P.; Wiesner, M. R., Towards a definition of inorganic nanoparticles from an environmental, health and safety perspective. *Nat. Nanotechnol.*, **2009**, *4*, 634-641.
- (6) Sapsford, K. E.; Algar, W. R.; Berti, L.; Gemmill, K. B.; Casey, B. J.; Oh, E.; Stewart, M. H.; Medintz, I. L., Functionalizing nanoparticles with biological molecules: Developing chemistries that facilitate nanotechnology. *Chem. Rev.*, **2013**, *113*, 1904-2074.
- (7) Oberdorster, G.; Maynard, A.; Donaldson, K.; Castranova, V.; Fitzpatrick, J.; Ausman, K.; Carter, J.; Karn, B.; Kreyling, W.; Lai, D.; Olin, S.; Monteiro-Riviere, N.; Warheit, D.; Yang, H.; Toxicity, I. R. F. R. S. I. N.; Screening Working, G., Principles for characterizing the potential human health effects from exposure to nanomaterials: elements of a screening strategy. *Part. Fibre Toxicol.*, **2005**, *2*, 8-8.
- (8) Pombo, M. L.; Di Fabio, J. L.; Cortes, M. d. L. A., Review of regulation of biological and biotechnological products in Latin American and Caribbean countries. *Biologicals*, **2009**, *37*, 271-276.
- (9) Algar, W. R.; Prasuhn, D. E.; Stewart, M. H.; Jennings, T. L.; Blanco-Canosa, J. B.; Dawson, P. E.; Medintz, I. L., The controlled display of biomolecules on nanoparticles: A challenge suited to bioorthogonal chemistry. *Bioconjugate Chem.*, **2011**, *22*, 825-858.
- (10) De la Fuente, J. M.; Penades, S., Glyconanoparticles: Types, synthesis and applications in glycoscience, biomedicine and material science. *BBA-Gen. Subjects*, **2006**, *1760*, 636-651.
- (11) Reddy, L. H.; Arias, J. L.; Nicolas, J.; Couvreur, P., Magnetic nanoparticles: Design and characterization, toxicity and biocompatibility, pharmaceutical and biomedical applications. *Chem. Rev.*, **2012**, *112*, 5818-5878.

- (12) Massart, R., Preparation of aqueous magnetic liquids in alkaline and acidic media. *IEEE T. Magn*, **1981**, *17*, 1247-1248.
- (13) Gupta, A. K.; Gupta, M., Synthesis and surface engineering of iron oxide nanoparticles for biomedical applications. *Biomaterials*, **2005**, *26*, 3995-4021.
- (14) Laurent, S.; Forge, D.; Port, M.; Roch, A.; Robic, C.; Elst, L. V.; Muller, R. N., Magnetic iron oxide nanoparticles: Synthesis, stabilization, vectorization, physicochemical characterizations, and biological applications. *Chem. Rev.*, **2008**, *108*, 2064-2110.
- (15) El-Boubbou, K.; Huang, X., Glyco-nanomaterials: Translating insights from the "sugar-code" to biomedical applications. *Curr. Med. Chem.*, **2011**, *18*, 2060-2078.
- (16) El-Boubbou, K.; Zhu, D. C.; Vasileiou, C.; Borhan, B.; Prosperi, D.; Li, W.; Huang, X., Magnetic glyco-nanoparticles: A tool to detect, differentiate, and unlock the glycocodes of cancer via magnetic resonance imaging. *J. Am. Chem. Soc.*, **2010**, *132*, 4490-4499.
- (17) El-dakdouki, M. E.-B., K.; Xia, J.; Kavunja, H.; Huang, X., Chemistry of bioconjugates: Synthesis, characterization, and biomedical applications. *John Wiley and Sons, Inc,* **2013**, 281-313.
- (18) Cheng, C.-J.; Lin, C.-C.; Chiang, R.-K.; Lin, C.-R.; Lyubutin, I. S.; Alkaev, E. A.; Lai, H.-Y., Synthesis of monodisperse magnetic iron oxide nanoparticles from submicrometer hematite powders. *Crystal Growth Des.*, **2008**, *8*, 877-883.
- (19) Hyeon, T.; Lee, S. S.; Park, J.; Chung, Y.; Bin Na, H., Synthesis of highly crystalline and monodisperse maghemite nanocrystallites without a size-selection process. *J. Am. Chem. Soc,* **2001**, *123*, 12798-12801.
- (20) Sun, S. H.; Zeng, H.; Robinson, D. B.; Raoux, S.; Rice, P. M.; Wang, S. X.; Li, G. X., Monodisperse MFe2O4 (M = Fe, Co, Mn) nanoparticles. *J. Am. Chem. Soc.*, **2004**, *126*, 273-279.
- (21) Sun, S. H.; Zeng, H., Size-controlled synthesis of magnetite nanoparticles. *J. Am. Chem. Soc.*, **2002**, *124*, 8204-8205.
- (22) Ahniyaz, A.; Seisenbaeva, G. A.; Haggstrom, L.; Kamali, S.; Kessler, V. G.; Nordblad, P.; Johansson, C.; Bergstrom, L., Preparation of iron oxide nanocrystals by surfactant-free or oleic acid-assisted thermal decomposition of a Fe(III) alkoxide. *J. Magn. Magn. Mater.*, **2008**, *320*, 781-787.
- (23) Li, Z.; Chen, H.; Bao, H. B.; Gao, M. Y., One-pot reaction to synthesize water-soluble magnetite nanocrystals. *Chem. Mater.*, **2004**, *16*, 1391-1393.
- (24) Li, Z.; Sun, Q.; Gao, M. Y., Preparation of water-soluble magnetite nanocrystals from hydrated ferric salts in 2-pyrrolidone: Mechanism leading to Fe3O4. *Angew. Chem. Int. Ed.*, **2005**, *44*, 123-126.

- (25) Peng, S.; Wang, C.; Xie, J.; Sun, S., Synthesis and stabilization of monodisperse Fe nanoparticles. *J. Am. Chem. Soc.*, **2006**, *128*, 10676-10677.
- (26) Zhao, F.; Zhang, B.; Feng, L., Preparation and magnetic properties of magnetite nanoparticles. *Mater. Lett.*, **2012**, *68*, 112-114.
- (27) El-Dakdouki, M. H.; El-Boubbou, K.; Zhu, D. C.; Huang, X., A simple method for the synthesis of hyaluronic acid coated magnetic nanoparticles for highly efficient cell labelling and in vivo imaging. *RSC Adv.*, **2011**, *I*, 1449-1452.
- (28) Wei, H.; Insin, N.; Lee, J.; Han, H.-S.; Cordero, J. M.; Liu, W.; Bawendi, M. G., Compact zwitterion-coated iron oxide nanoparticles for biological applications. *Nano Lett.*, **2012**, *12*, 22-25.
- (29) Ehlert, S.; Taheri, S. M.; Pirner, D.; Drechsler, M.; Schmidt, H.-W.; Foerster, S., Polymer ligand exchange to control stabilization and compatibilization of nanocrystals. *Acs Nano*, **2014**, *8*, 6114-6122.
- (30) Narain, R.; Gonzales, M.; Hoffman, A. S.; Stayton, P. S.; Krishnan, K. M., Synthesis of monodisperse biotinylated p(NIPAAm)-coated iron oxide magnetic nanoparticles and their bioconjugation to streptavidin. *Langmuir*, **2007**, *23*, 6299-6304.
- (31) Fasting, C.; Schalley, C. A.; Weber, M.; Seitz, O.; Hecht, S.; Koksch, B.; Dernedde, J.; Graf, C.; Knapp, E.-W.; Haag, R., Multivalency as a chemical organization and action principle. *Angew. Chem. Int. Ed.*, **2012**, *51*, 10472-10498.
- (32) Wang, X.; Ramstrom, O.; Yan, M., Quantitative analysis of multivalent ligand presentation on gold glyconanoparticles and the impact on lectin binding. *Anal. Chem.*, **2010**, *82*, 9082-9089.
- (33) Chen, Y.-X.; Triola, G.; Waldmann, H., Bioorthogonal chemistry for site-specific Labeling and surface immobilization of proteins. *Acc. Chem. Res.*, **2011**, *44*, 762-773.
- (34) Hao, Z.; Hong, S.; Chen, X.; Chen, P. R., Introducing bioorthogonal functionalities into proteins in living cells. *Acc. Chem. Res.*, **2011**, *44*, 742-751.
- (35) Erathodiyil, N.; Ying, J. Y., Functionalization of inorganic nanoparticles for bioimaging applications. *Acc. Chem. Res.*, **2011**, *44*, 925-935.
- (36) Horak, D.; Babic, M.; Jendelova, P.; Herynek, V.; Trchova, M.; Pientka, Z.; Pollert, E.; Hajek, M.; Sykova, E., D-Mannose-modified iron oxide nanoparticles for stem cell labeling. *Bioconjugate Chem.*, **2007**, *18*, 635-644.
- (37) Villanueva, A.; Canete, M.; Roca, A. G.; Calero, M.; Veintemillas-Verdaguer, S.; Serna, C. J.; del Puerto Morales, M.; Miranda, R., The influence of surface functionalization on the enhanced internalization of magnetic nanoparticles in cancer cells. *Nanotechnology*, **2009**, *20*.

- (38) Lee, Y.; Lee, H.; Kim, Y. B.; Kim, J.; Hyeon, T.; Park, H.; Messersmith, P. B.; Park, T. G., Bioinspired surface immobilization of hyaluronic acid on monodisperse magnetite nanocrystals for targeted cancer imaging. *Adv. Mater.*, **2008**, *20*, 4154-4157.
- (39) Haun, J. B.; Devaraj, N. K.; Hilderbrand, S. A.; Lee, H.; Weissleder, R., Bioorthogonal chemistry amplifies nanoparticle binding and enhances the sensitivity of cell detection. *Nat. Nanotechnol.*, **2010**, *5*, 660-665.
- (40) Choi, J.; Lee, J. I.; Lee, Y. B.; Hong, J. H.; Kim, I. S.; Park, Y. K.; Hur, N. H., Immobilization of biomolecules on biotinylated magnetic ferrite nanoparticles. *Chem. Phy. Lett.*, **2006**, *428*, 125-129.
- (41) Gong, P.; Peng, Z.; Wang, Y.; Qiao, R.; Mao, W.; Qian, H.; Zhang, M.; Li, C.; Shi, S., Synthesis of streptavidin-conjugated magnetic nanoparticles for DNA detection. *J. Nanopart. Res.*, **2013**, *15*.
- (42) Chattopadhaya, S.; Tan, L. P.; Yao, S. Q., Strategies for site-specific protein biotinylation using in vitro, in vivo and cell-free systems: toward functional protein arrays. *Nat. Protoc.*, **2006**, *1*, 2386-2398.
- (43) Wingren, C.; Steinhauer, C.; Ingvarsson, J.; Persson, E.; Larsson, K.; Borrebaeck, C. A. K., Microarrays based on affinity-tagged single-chain Fv antibodies: Sensitive detection of analyte in complex proteomes. *Proteomics*, **2005**, *5*, 1281-1291.
- (44) Zhu, H.; Bilgin, M.; Bangham, R.; Hall, D.; Casamayor, A.; Bertone, P.; Lan, N.; Jansen, R.; Bidlingmaier, S.; Houfek, T.; Mitchell, T.; Miller, P.; Dean, R. A.; Gerstein, M.; Snyder, M., Global analysis of protein activities using proteome chips. *Science*, **2001**, *293*, 2101-2105.
- (45) He, M.; Stoevesandt, O.; Palmer, E. A.; Khan, F.; Ericsson, O.; Taussig, M. J., Printing protein arrays from DNA arrays. *Nat. Methods*, **2008**, *5*, 175-177.
- (46) Ganesana, M.; Istarnboulie, G.; Marty, J.-L.; Noguer, T.; Andreescu, S., Sitespecific immobilization of a (His)6-tagged acetylcholinesterase on nickel nanoparticles for highly sensitive toxicity biosensors. *Biosens Bioelectron*, **2011**, *30*, 43-48.
- (47) Zhang, Y.; Yang, Y.; Ma, W.; Guo, J.; Lin, Y.; Wang, C., Uniform magnetic core/shell microspheres functionalized with Ni2+-iminodiacetic acid for one step purification and immobilization of his-tagged enzymes. *Acs Appl. Mater. Inter.*, **2013**, *5*, 2626-2633.
- (48) Ramachandran, N.; Hainsworth, E.; Bhullar, B.; Eisenstein, S.; Rosen, B.; Lau, A. Y.; Walter, J. C.; LaBaer, J., Self-assembling protein microarrays. *Science*, **2004**, *305*, 86-90.
- (49) Ha, T. H.; Jung, S. O.; Lee, J. M.; Lee, K. Y.; Lee, Y.; Park, J. S.; Chung, B. H., Oriented immobilization of antibodies with GST-fused multiple F-c-specific B-domains on a gold surface. *Anal. Chem.*, **2007**, *79*, 546-556.

- (50) Jung, Y.; Lee, J. M.; Kim, J.-w.; Yoon, J.; Cho, H.; Chung, B. H., Photoactivable antibody binding protein: Site-selective and covalent coupling of antibody. *Anal. Chem.*, **2009**, *81*, 936-942.
- (51) Wong, L. S.; Thirlway, J.; Micklefield, J., Direct site-selective covalent protein immobilization catalyzed by a phosphopantetheinyl transferase. *J. Am. Chem. Soc.*, **2008**, *130*, 12456-12464.
- (52) Wang, F.; Shen, H. B.; Feng, J.; Yang, H. F., PNA-modified magnetic nanoparticles and their hybridization with single-stranded DNA target: Surface enhanced Raman scatterings study. *Microchim. Acta*, **2006**, *153*, 15-20.
- (53) Kinoshita, T.; Seino, S.; Mizukoshi, Y.; Nakagawa, T.; Yamamoto, T. A., Functionalization of magnetic gold/iron-oxide composite nanoparticles with oligonucleotides and magnetic separation of specific target. *J. Magn. Magn. Mater.*, **2007**, *311*, 255-258.
- (54) Barrientos, A. G.; de la Fuente, J. M.; Rojas, T. C.; Fernandez, A.; Penades, S., Gold glyconanoparticles: Synthetic polyvalent ligands mimicking glycocalyx-like surfaces as tools for glycobiological studies. *Chem-Eur. J.*, **2003**, *9*, 1909-1921.
- (55) de la Fuente, J. M.; Alcantara, D.; Eaton, P.; Crespo, P.; Rojas, T. C.; Fernandez, A.; Hernando, A.; Penades, S., Gold and gold-iron oxide magnetic glyconanoparticles: Synthesis, characterization and magnetic properties. *J. Phys. Chem. B*, **2006**, *110*, 13021-13028.
- (56) Gallo, J.; Garcia, I.; Padro, D.; Arnaiz, B.; Penades, S., Water-soluble magnetic glyconanoparticles based on metal-doped ferrites coated with gold: Synthesis and characterization. *J. Mater. Chem.*, **2010**, *20*, 10010-10020.
- (57) Garcia, I.; Gallo, J.; Genicio, N.; Padro, D.; Penades, S., Magnetic glyconanoparticles as a versatile platform for selective immunolabeling and imaging of cells. *Bioconjugate Chem.*, **2011**, *22*, 264-273.
- (58) Lartigue, L.; Oumzil, K.; Guari, Y.; Larionova, J.; Guerin, C.; Montero, J.-L.; Barragan-Montero, V.; Sangregorio, C.; Caneschi, A.; Innocenti, C.; Kalaivani, T.; Arosio, P.; Lascialfari, A., Water-soluble rhamnose-coated Fe3O4 nanoparticles. *Org. Lett.*, **2009**, *11*, 2992-2995.
- (59) Lartigue, L.; Innocenti, C.; Kalaivani, T.; Awwad, A.; Duque, M. d. M. S.; Guari, Y.; Larionova, J.; Guerin, C.; Montero, J.-L. G.; Barragan-Montero, V.; Arosio, P.; Lascialfari, A.; Gatteschi, D.; Sangregorio, C., Water-dispersible dugar-coated iron oxide nanoparticles. An evaluation of their relaxometric and magnetic hyperthermia properties. *J. Am. Chem. Soc.*, **2011**, *133*, 10459-10472.
- (60) Earhart, C.; Jana, N. R.; Erathodiyil, N.; Ying, J. Y., Synthesis of carbohydrate-conjugated nanoparticles and quantum dots. *Langmuir*, **2008**, *24*, 6215-6219.

- (61) Zhou, L.; Wu, J.; Zhang, H.; Kang, Y.; Guo, J.; Zhang, C.; Yuan, J.; Xing, X., Magnetic nanoparticles for the affinity adsorption of maltose binding protein (MBP) fusion enzymes. *J. Mater. Chem.*, **2012**, *22*, 6813-6818.
- (62) Liu, H.-Z.; Tang, J.-J.; Ma, X.-X.; Guo, L.; Xie, J.-W.; Wang, Y.-X., Galactose-functionalized magnetic iron-oxide nanoparticles for enrichment and detection of ricin toxin. *Anal. Sci.*, **2011**, *27*, 19-24.
- (63) Kamat, M.; El-Boubbou, K.; Zhu, D. C.; Lansdell, T.; Lu, X.; Li, W.; Huang, X., Hyaluronic acid immobilized magnetic nanoparticles for active targeting and imaging of macrophages. *Bioconjugate Chem.*, **2010**, *21*, 2128-2135.
- (64) El-Dakdouki, M. H.; Zhu, D. C.; El-Boubbou, K.; Kamat, M.; Chen, J.; Li, W.; Huang, X., Development of multifunctional hyaluronan-coated nanoparticles for imaging and drug delivery to cancer cells. *Biomacromolecules*, **2012**, *13*, 1144-1151.
- (65) van Kasteren, S. I.; Campbell, S. J.; Serres, S.; Anthony, D. C.; Sibson, N. R.; Davis, B. G., Glyconanoparticles allow pre-symptomatic in vivo imaging of brain disease. *Proc. Natl. Acad. Sci. USA*, **2009**, *106*, 18-23.
- (66) Valero, E.; Tambalo, S.; Marzola, P.; Ortega-Munoz, M.; Javier Lopez-Jaramillo, F.; Santoyo-Gonzalez, F.; de Dios Lopez, J.; Delgado, J. J.; Calvino, J. J.; Cuesta, R.; Dominguez-Vera, J. M.; Galvez, N., Magnetic nanoparticles-templated assembly of protein subunits: A new platform for carbohydrate-based MRI nanoprobes. *J. Am. Chem. Soc.*, **2011**, *133*, 4889-4895.
- (67) Lin, P.-C.; Ueng, S.-H.; Yu, S.-C.; Jan, M.-D.; Adak, A. K.; Yu, C.-C.; Lin, C.-C., Surface modification of magnetic nanoparticle via Cu(I)-Catalyzed alkyne-azide 2+3 cycloaddition. *Org. Lett.*, **2007**, *9*, 2131-2134.
- (68) Polito, L.; Monti, D.; Caneva, E.; Delnevo, E.; Russo, G.; Prosperi, D., One-step bioengineering of magnetic nanoparticles via a surface diazo transfer/azide-alkyne click reaction sequence. *Chem. Commun.*, **2008**, 621-623.
- (69) Xiong, Z.; Zhao, L.; Wang, F.; Zhu, J.; Qin, H.; Wu, R. a.; Zhang, W.; Zou, H., Synthesis of branched PEG brushes hybrid hydrophilic magnetic nanoparticles for the selective enrichment of N-linked glycopeptides. *Chem. Commun.*, **2012**, *48*, 8138-8140.
- (70) Liang, Y.-Y.; Zhang, L.-M., Bioconjugation of papain on superparamagnetic nanoparticles decorated with carboxymethylated chitosan. *Biomacromolecules*, **2007**, *8*, 1480-1486.
- (71) Li, H.; El-Dakdouki, M. H.; Zhu, D. C.; Abela, G. S.; Huang, X., Synthesis of beta-cyclodextrin conjugated superparamagnetic iron oxide nanoparticles for selective binding and detection of cholesterol crystals. *Chem. Commun.*, **2012**, *48*, 3385-3387.

- (72) Moros, M.; Hernaez, B.; Garet, E.; Dias, J. T.; Saez, B.; Grazu, V.; Gonzalez-Fernandez, A.; Alonso, C.; de la Fuente, J. M., Monosaccharides versus PEG-functionalized NPs: Influence in the cellular uptake. *Acs Nano*, **2012**, *6*, 1565-1577.
- (73) Moros, M.; Pelaz, B.; Lopez-Larrubia, P.; Garcia-Martin, M. L.; Grazu, V.; de la Fuente, J. M., Engineering biofunctional magnetic nanoparticles for biotechnological applications. *Nanoscale*, **2010**, *2*, 1746-1755.
- (74) Pfaff, A.; Schallon, A.; Ruhland, T. M.; Majewski, A. P.; Schmalz, H.; Freitag, R.; Mueller, A. H. E., Magnetic and fluorescent glycopolymer hybrid nanoparticles for intranuclear optical imaging. *Biomacromolecules*, **2011**, *12*, 3805-3811.
- (75) Wang, X.; Liu, L.-H.; Ramstroem, O.; Yan, M., Engineering nanomaterial surfaces for biomedical applications. *Exp. Biol. Med.*, **2009**, *234*, 1128-1139.
- (76) Liu, L.-H.; Dietsch, H.; Schurtenberger, P.; Yan, M., Photoinitiated coupling of unmodified monosaccharides to iron oxide nanoparticles for sensing proteins and bacteria. *Bioconjugate Chem.*, **2009**, *20*, 1349-1355.
- (77) Sletten, E. M.; Bertozzi, C. R., From mechanism to mouse: A tale of two bioorthogonal reactions. *Acc. Chem. Res.*, **2011**, *44*, 666-676.
- (78) Muir, T. W.; Sondhi, D.; Cole, P. A., Expressed protein ligation: A general method for protein engineering. *Proc. Natl. Acad. Sci. USA*, **1998**, *95*, 6705-6710.
- (79) Karagoez, G. E.; Sinnige, T.; Hsieh, O.; Ruediger, S. G. D., Expressed protein ligation for a large dimeric protein. *Protein Eng. Des. Sel.*, **2011**, *24*, 495-501.
- (80) Camarero, J. A.; Kwon, Y.; Coleman, M. A., Chemoselective attachment of biologically active proteins to surfaces by expressed protein ligation and its application for "protein chip" fabrication. *J. Am. Chem. Soc.*, **2004**, *126*, 14730-14731.
- (81) Watzke, A.; Kohn, M.; Gutierrez-Rodriguez, M.; Wacker, R.; Schroder, H.; Breinbauer, R.; Kuhlmann, J.; Alexandrov, K.; Niemeyer, C. M.; Goody, R. S.; Waldmann, H., Site-selective protein immobilization by Staudinger ligation. *Angew. Chem. Int. Ed.*, **2006**, *45*, 1408-1412.
- (82) Lin, P.-C.; Ueng, S.-H.; Tseng, M.-C.; Ko, J.-L.; Huang, K.-T.; Yu, S.-C.; Adak, A. K.; Chen, Y.-J.; Lin, C.-C., Site-specific protein modification through Cu-I-catalyzed 1,2,3-triazole formation and its implementation in protein microarray fabrication. *Angew. Chem. Int. Ed.*, **2006**, *45*, 4286-4290.
- (83) Wang, H.-C.; Yu, C.-C.; Liang, C.-F.; Huang, L.-D.; Hwu, J.-R.; Lin, C.-C., Site-selective proteini immobilization through 2-cyanobenzothiazole-cysteine condensation. *Chembiochem*, **2014**, *15*, 829-835.

- (84) Abdeljabbar, D. M.; Klein, T. J.; Zhang, S.; Link, A. J., A Single genomic copy of an engineered methionyl-tRNA synthetase enables robust incorporation of azidonorleucine into recombinant proteins in E-coli. *J. Am. Chem. Soc.*, **2009**, *131*, 17078-17079.
- (85) Park, H.-S.; Hohn, M. J.; Umehara, T.; Guo, L.-T.; Osborne, E. M.; Benner, J.; Noren, C. J.; Rinehart, J.; Soell, D., Expanding the genetic code of escherichia coli with phosphoserine. *Science*, **2011**, *333*, 1151-1154.
- (86) Wang, L.; Brock, A.; Herberich, B.; Schultz, P. G., Expanding the genetic code of Escherichia coli. *Science*, **2001**, *292*, 498-500.
- (87) van Hest, J. C. M.; Kiick, K. L.; Tirrell, D. A., Efficient incorporation of unsaturated methionine analogues into proteins in vivo. *J. Am. Chem. Soc.*, **2000**, *122*, 1282-1288.
- (88) Deiters, A.; Cropp, T. A.; Mukherji, M.; Chin, J. W.; Anderson, J. C.; Schultz, P. G., Adding amino acids with novel reactivity to the genetic code of Saccharomyces cerevisiae. *J. Am. Chem. Soc.*, **2003**, *125*, 11782-11783.
- (89) Link, A. J.; Vink, M. K. S.; Agard, N. J.; Prescher, J. A.; Bertozzi, C. R.; Tirrell, D. A., Discovery of aminoacyl-tRNA synthetase activity through cell-surface display of noncanonical amino acids. *Proc. Natl. Acad. Sci. USA*, **2006**, *103*, 10180-10185.
- (90) Kiick, K. L.; Saxon, E.; Tirrell, D. A.; Bertozzi, C. R., Incorporation of azides into recombinant proteins for chemoselective modification by the Staudinger ligation. *Proc. Natl. Acad. Sci. USA*, **2002**, *99*, 19-24.
- (91) Parthasarathy, R.; Subramanian, S.; Boder, E. T., Sortase A as a novel molecular "stapler" for sequence-specific protein conjugation. *Bioconjugate Chem.*, **2007**, *18*, 469-476.
- (92) Ito, T.; Sadamoto, R.; Naruchi, K.; Togame, H.; Takemoto, H.; Kondo, H.; Nishimura, S.-I., Highly oriented recombinant glycosyltransferases: Site-specific immobilization of unstable membrane proteins by using staphylococcus aureus Sortase A. *Biochemistry*, **2010**, *49*, 2604-2614.
- (93) Colombo, M.; Mazzucchelli, S.; Montenegro, J. M.; Galbiati, E.; Corsi, F.; Parak, W. J.; Prosperi, D., Protein oriented ligation on nanoparticles exploiting O6-alkylguanine-DNA transferase (SNAP) genetically encoded fusion. *Small*, **2012**, *8*, 1492-1497.
- (94) Keppler, A.; Gendreizig, S.; Gronemeyer, T.; Pick, H.; Vogel, H.; Johnsson, K., A general method for the covalent labeling of fusion proteins with small molecules in vivo. *Nat. Biotechnol.*, **2003**, *21*, 86-89.
- (95) Ericsson, E. M.; Enander, K.; Bui, L.; Lundstrom, I.; Konradsson, P.; Liedberg, B., Site-specific and covalent attachment of his-tagged Proteins by chelation assisted photoimmobilization: A strategy for microarraying of protein ligands. *Langmuir*, **2013**, *29*, 11687-11694.

- (96) Yuan, Y.; Yin, M.; Qian, J.; Liu, C., Site-directed immobilization of antibodies onto blood contacting grafts for enhanced endothelial cell adhesion and proliferation. *Soft. Matter*, **2011**, *7*, 7207-7216.
- (97) Han, H. J.; Kannan, R. M.; Wang, S.; Mao, G.; Kusanovic, J. P.; Romero, R., Multifunctional dendrimer-templated antibody presentation on biosensor surfaces for improved biomarker detection. *Adv. Funct. Mater.*, **2010**, *20*, 409-421.
- (98) Prieto-Simon, B.; Saint, C.; Voelcker, N. H., Electrochemical biosensors featuring oriented antibody immobilization via electrografted and self-assembled hydrazide chemistry. *Anal. Chem.*, **2014**, *86*, 1422-1429.
- (99) Trilling, A. K.; Beekwilder, J.; Zuilhof, H., Antibody orientation on biosensor surfaces: a minireview. *Analyst*, **2013**, *138*, 1619-1627.
- (100) Saerens, D.; Huang, L.; Bonroy, K.; Muyldermans, S., Antibody fragments as probe in biosensor development. *Sensors*, **2008**, *8*, 4669-4686.
- (101) Ho, J.-a. A.; Hsu, W.-L.; Liao, W.-C.; Chiu, J.-K.; Chen, M.-L.; Chang, H.-C.; Li, C.-C., Ultrasensitive electrochemical detection of biotin using electrically addressable site-oriented antibody immobilization approach via aminophenyl boronic acid. *Biosens. Bioelectron.*, **2010**, *26*, 1021-1027.
- (102) Lin, P.-C.; Chen, S.-H.; Wang, K.-Y.; Chen, M.-L.; Adak, A. K.; Hwu, J.-R. R.; Chen, Y.-J.; Lin, C.-C., Fabrication of oriented antibody-conjugated magnetic nanoprobes and their immunoaffinity application. *Anal. Chem.*, **2009**, *81*, 8774-8782.
- (103) Zhuo, Y.; Yuan, P.-X.; Yuan, R.; Chai, Y.-Q.; Hong, C.-L., Bienzyme functionalized three-layer composite magnetic nanoparticles for electrochemical immunosensors. *Biomaterials*, **2009**, *30*, 2284-2290.
- (104) Katz, E.; Willner, I.; Wang, J., Electroanalytical and bioelectroanalytical systems based on metal and semiconductor nanoparticles. *Electroanalysis*, **2004**, *16*, 19-44.
- (105) Braham, Y.; Barhoumi, H.; Maaref, A., Urease capacitive biosensors using functionalized magnetic nanoparticles for atrazine pesticide detection in environmental samples. *Anal. Methods*, **2013**, *5*, 4898-4904.
- (106) Koeber, M.; Moros, M.; Franco Fraguas, L.; Grazu, V.; de la Fuente, J. M.; Luna, M.; Briones, F., Nanoparticle-mediated monitoring of carbohydrate-lectin interactions using transient magnetic birefringence. *Anal. Chem.*, **2014**, *86*, 12159-12165.
- (107) El-Dakdouki, M. H.; El-Boubbou, K.; Kamat, M.; Huang, R.; Abela, G. S.; Kiupel, M.; Zhu, D. C.; Huang, X., CD44 targeting magnetic glyconanoparticles for atherosclerotic plaque imaging. *Pharm. Res.*, **2014**, *31*, 1426-1437.

- (108) Kouyoumdjian, H.; Zhu, D. C.; El-Dakdouki, M. H.; Lorenz, K.; Chen, J.; Li, W.; Huang, X., Glyconanoparticle aided detection of beta-amyloid by magnetic resonance imaging and attenuation of beta-amyloid induced cytotoxicity. *Acs Chem. Neurosci.*, **2013**, *4*, 575-584.
- (109) Cai, W.; Chen, X., Nanoplatforms for targeted molecular imaging in living subjects. *Small*, **2007**, *3*, 1840-1854.
- (110) Glaus, C.; Rossin, R.; Welch, M. J.; Bao, G., In vivo evaluation of Cu-64-labeled magnetic nanoparticles as a dual-modality PET/MR imaging agent. *Bioconjugate Chem.*, **2010**, *21*, 715-722.
- (111) de Rosales, R. T. M.; Tavare, R.; Paul, R. L.; Jauregui-Osoro, M.; Protti, A.; Glaria, A.; Varma, G.; Szanda, I.; Blower, P. J., Synthesis of Cu-64(II)-Bis(dithiocarbamatebisphosphonate) and its conjugation with superparamagnetic iron oxide nanoparticles: In vivo vvaluation as dual-modality PET-MRI agent. *Angew. Chem. Int. Ed.*, **2011**, *50*, 5509-5513.
- (112) Kim, S.-m.; Chae, M. K.; Yim, M. S.; Jeong, I. H.; Cho, J.; Lee, C.; Ryu, E. K., Hybrid PET/MR imaging of tumors using an oleanolic acid-conjugated nanoparticle. *Biomaterials*, **2013**, *34*, 8114-8121.
- (113) Lee, H.-Y.; Li, Z.; Chen, K.; Hsu, A. R.; Xu, C.; Xie, J.; Sun, S.; Chen, X., PET/MRI dual-modality tumor imaging using arginine-glycine-aspartic (RGD) Conjugated radiolabeled iron oxide nanoparticles. *J. Nucl. Med.*, **2008**, *49*, 1371-1379.
- (114) Yang, X.; Hong, H.; Grailer, J. J.; Rowland, I. J.; Javadi, A.; Hurley, S. A.; Xiao, Y.; Yang, Y.; Zhang, Y.; Nickles, R.; Cai, W.; Steeber, D. A.; Gong, S., cRGD-functionalized, DOX-conjugated, and Cu-64-labeled superparamagnetic iron oxide nanoparticles for targeted anticancer drug delivery and PET/MR imaging. *Biomaterials*, **2011**, *32*, 4151-4160.
- (115) Xie, J.; Chen, K.; Huang, J.; Lee, S.; Wang, J.; Gao, J.; Li, X.; Chen, X., PET/NIRF/MRI triple functional iron oxide nanoparticles. *Biomaterials*, **2010**, *31*, 3016-3022.
- (116) Kircher, M. F.; Mahmood, U.; King, R. S.; Weissleder, R.; Josephson, L., A multimodal nanoparticle for preoperative magnetic resonance imaging and intraoperative optical brain tumor delineation. *Cancer Res.*, **2003**, *63*, 8122-8125.
- (117) Xie, W.; Wang, J., Immobilized lipase on magnetic chitosan microspheres for transesterification of soybean oil. *Biomass Bioenerg.*, **2012**, *36*, 373-380.
- (118) Yu, C.-C.; Kuo, Y.-Y.; Liang, C.-F.; Chien, W.-T.; Wu, H.-T.; Chang, T.-C.; Jan, F.-D.; Lin, C.-C., Site-specific immobilization of enzymes on magnetic nanoparticles and their use in organic synthesis. *Bioconjugate Chem.*, **2012**, *23*, 714-724.
- (119) Li, Y.; Xu, X.; Deng, C.; Yang, P.; Zhang, X., Immobilization of trypsin on superparamagnetic nanoparticles for rapid and effective proteolysis. *J. Proteome Res.*, **2007**, *6*, 3849-3855.

- (120) Li, Y.; Yan, B.; Deng, C.; Tang, J.; Liu, J.; Zhang, X., On-plate digestion of proteins using novel trypsin-immobilized magnetic nanospheres for MALDI-TOF-MS analysis. *Proteomics*, **2007**, *7*, 3661-3671.
- (121) Jin, L.; Yang, K.; Yao, K.; Zhang, S.; Tao, H.; Lee, S.-T.; Liu, Z.; Peng, R., Functionalized graphene oxide in enzyme engineering: A selective modulator for enzyme activity and thermostability. *Acs Nano*, **2012**, *6*, 4864-4875.
- (122) El-Dakdouki, M. H.; Pure, E.; Huang, X., Development of drug loaded nanoparticles for tumor targeting. Part 2: Enhancement of tumor penetration through receptor mediated transcytosis in 3D tumor models. *Nanoscale*, **2013**, *5*, 3904-3911.
- (123) Veiseh, O.; Gunn, J. W.; Zhang, M., Design and fabrication of magnetic nanoparticles for targeted drug delivery and imaging. *Adv. Drug Deliver. Rev.*, **2010**, *62*, 284-304
- (124) Bao, G.; Mitragotri, S.; Tong, S., Multifunctional nanoparticles for drug delivery and molecular imaging. *Annu. Rev. Biomed. Eng.*, **2013**, *15*, 253-282.
- (125) Yallapu, M. M.; Othman, S. F.; Curtis, E. T.; Gupta, B. K.; Jaggi, M.; Chauhan, S. C., Multi-functional magnetic nanoparticles for magnetic resonance imaging and cancer therapy. *Biomaterials*, **2011**, *32*, 1890-1905.
- (126) Yigit, M. V.; Moore, A.; Medarova, Z., Magnetic nanoparticles for cancer diagnosis and therapy. *Pharm. Res.*, **2012**, *29*, 1180-1188.
- (127) Brigger, I.; Dubernet, C.; Couvreur, P., Nanoparticles in cancer therapy and diagnosis. *Adv. Drug Deliver. Rev.*, **2002**, *54*, 631-651.
- (128) Yu, M. K.; Jeong, Y. Y.; Park, J.; Park, S.; Kim, J. W.; Min, J. J.; Kim, K.; Jon, S., Drug-loaded superparamagnetic iron oxide nanoparticles for combined cancer imaging and therapy in vivo. *Angew. Chem. Int. Ed.*, **2008**, *47*, 5362-5365.
- (129) Reddy, G. R.; Bhojani, M. S.; McConville, P.; Moody, J.; Moffat, B. A.; Hall, D. E.; Kim, G.; Koo, Y.-E. L.; Woolliscroft, M. J.; Sugai, J. V.; Johnson, T. D.; Philbert, M. A.; Kopelman, R.; Rehemtulla, A.; Ross, B. D., Vascular targeted nanoparticles for imaging and treatment of brain tumors. *Clin. Cancer Res.*, **2006**, *12*, 6677-6686.
- (130) Horak, D.; Babic, M.; Mackova, H.; Benes, M. J., Preparation and properties of magnetic nano- and microsized particles for biological and environmental separations. *J. Sep. Sci.*, **2007**, *30*, 1751-1772.
- (131) Safarik, I.; Safarikova, M., Magnetic techniques for the isolation and purification of proteins and peptides. *Biomagn. Res. Technol.*, **2004**, *2*, 7.
- (132) Safarik, I.; Safarikova, M., Use of magnetic techniques for the isolation of cells. *J. Chromatogr. B*, **1999**, 722, 33-53.

- (133) Franzreb, M.; Siemann-Herzberg, M.; Hobley, T. J.; Thomas, O. R. T., Protein purification using magnetic adsorbent particles. *Appl. Microbiol. Biot.*, **2006**, *70*, 505-516.
- (134) Hage, D. S., Affinity chromatography: A review of clinical applications. *Clin. Chem.*, **1999**, *45*, 593-615.
- (135) Hage, D. S.; Anguizola, J. A.; Bi, C.; Li, R.; Matsuda, R.; Papastavros, E.; Pfaunmiller, E.; Vargas, J.; Zheng, X., Pharmaceutical and biomedical applications of affinity chromatography: Recent trends and developments. *J. Pharmaceut. Biomed.*, **2012**, *69*, 93-105.
- (136) Pfaunmiller, E. L.; Paulemond, M. L.; Dupper, C. M.; Hage, D. S., Affinity monolith chromatography: a review of principles and recent analytical applications. *Anal. Bioanal. Chem.*, **2013**, *405*, 2133-2145.
- (137) Palani, A.; Lee, J.-S.; Huh, J.; Kim, M.; Lee, Y.-J.; Chang, J. H.; Lee, K.; Lee, S.-W., Selective enrichment of cysteine-containing peptides using SPDP-Functionalized superparamagnetic Fe3O4@SiO2 nanoparticles: Application to comprehensive proteomic profiling. *J. Proteome Res.*, **2008**, *7*, 3591-3596.
- (138) Li, Y.; Zhang, X.; Deng, C., Functionalized magnetic nanoparticles for sample preparation in proteomics and peptidomics analysis. *Chem. Soc. Rev.*, **2013**, *42*, 8517-8539.
- (139) Xie, L.; Jiang, R.; Zhu, F.; Liu, H.; Ouyang, G., Application of functionalized magnetic nanoparticles in sample preparation. *Anal. Bioanal. Chem.*, **2014**, *406*, 377-399.
- (140) He, J.; Huang, M.; Wang, D.; Zhang, Z.; Li, G., Magnetic separation techniques in sample preparation for biological analysis: A review. *J. Pharm. Biomed. Anal.*, **2014**.
- (141) Xu, C. J.; Xu, K. M.; Gu, H. W.; Zhong, X. F.; Guo, Z. H.; Zheng, R. K.; Zhang, X. X.; Xu, B., Nitrilotriacetic acid-modified magnetic nanoparticles as a general agent to bind histidine-tagged proteins. *J. Am. Chem. Soc.*, **2004**, *126*, 3392-3393.
- (142) Gu, H. W.; Xu, K. M.; Xu, C. J.; Xu, B., Biofunctional magnetic nanoparticles for protein separation and pathogen detection. *Chem. Commun.*, **2006**, 941-949.
- (143) Gu, H. W.; Ho, P. L.; Tsang, K. W. T.; Wang, L.; Xu, B., Using biofunctional magnetic nanoparticles to capture vancomycin-resistant enterococci and other gram-positive bacteria at ultralow concentration. *J. Am. Chem. Soc.*, **2003**, *125*, 15702-15703.
- (144) Varki, A., Glycan-based interactions involving vertebrate sialic-acid-recognizing proteins. *Nature*, **2007**, *446*, 1023-1029.
- (145) Ernst, B.; Magnani, J. L., From carbohydrate leads to glycomimetic drugs. *Nat. Rev. Drug Discov.*, **2009**, *8*, 661-677.
- (146) Okada, M., Molecular design and syntheses of glycopolymers. *Prog. Polym. Sci.*, **2001**, *26*, 67-104.

- (147) Turnbull, W. B.; Stoddart, J. F., Design and synthesis of glycodendrimers. *J. Biotechnol.*, **2002**, *90*, 231-255.
- (148) Marradi, M.; Chiodo, F.; Garcia, I.; Penades, S., Glyconanoparticles as multifunctional and multimodal carbohydrate systems. *Chem. Soc. Rev.*, **2013**, *42*, 4728-4745.
- (149) Reichardt, N. C.; Martin-Lomas, M.; Penades, S., Glyconanotechnology. *Chem. Soc. Rev.*, **2013**, *42*, 4358-4376.
- (150) Liu, F. T.; Rabinovich, G. A., Galectins as modulators of tumour progression. *Nat. Rev. Cancer*, **2005**, *5*, 29-41.
- (151) Banerjee, S. S.; Chen, D.-H., Glucose-grafted gum arabic modified magnetic nanoparticles: Preparation and specific interaction with concanavalin A. *Chem. Mater.*, **2007**, *19*, 3667-3672.
- (152) El-Boubbou, K.; Gruden, C.; Huang, X., Magnetic glyco-nanoparticles: A unique tool for rapid pathogen detection, decontamination, and strain differentiation. *J. Am. Chem. Soc.*, **2007**, *129*, 13392-13393
- (153) Behra, M.; Azzouz, N.; Schmidt, S.; Volodkin, D. V.; Mosca, S.; Chanana, M.; Seeberger, P. H.; Hartmann, L., Magnetic porous sugar-functionalized PEG microgels for efficient isolation and removal of bacteria from solution. *Biomacromolecules*, **2013**, *14*, 1927-1935.
- (154) Rouhanifard, S. H.; Xie, R.; Zhang, G.; Sun, X.; Chen, X.; Wu, P., Detection and isolation of dendritic cells using Lewis X-functionalized magnetic nanoparticles. *Biomacromolecules*, **2012**, *13*, 3039-3045.
- (155) Hung, T.-C.; Lin, C.-W.; Hsu, T.-L.; Wu, C.-Y.; Wong, C.-H., Investigation of SSEA-4 binding protein in breast cancer cells. *J. Am. Chem. Soc.*, **2013**, *135*, 5934-5937.
- (156) Scammell, J. G.; Hubler, T. R.; Denny, W. B.; Valentine, D. L., Organization of the human FK506-binding immunophilin FKBP52 protein gene (FKBP4). *Genomics*, **2003**, *81*, 640-643.
- (157) Roff, C. F.; Wang, J. L., Endogenous lectins from cultured-cells isolation and characterization of carbohydrate-binding proteins from 3T3-fibroblasts. *J. Biol. Chem.*, **1983**, 258, 657-663.
- (158) Lee, Y. C.; Lee, R. T., Carbohydrate-protein interactions basis of glycobiology. *Acc. Chem. Res.*, **1995**, *28*, 321-327.
- (159) Hebert, E., Endogenous lectins as cell surface transducers. *Biosci. Rep.*, **2000**, *20*, 213-237.

- (160) Lorenzon, P.; Vecile, E.; Nardon, E.; Ferrero, E.; Harlan, J. M.; Tedesco, F.; Dobrina, A., Endothelial cell E- and P-selectin and vascular cell adhesion molecule-1 function as signaling receptors. *J.Cell Biol.*, **1998**, *142*, 1381-1391.
- (161) Zanetta, J. P.; Badache, A.; Maschke, S.; Marschal, P.; Kuchler, S., Carbohydrates and soluble lectins in the regulation of cell-adhesion and proliferation. *Histolo. Histopathol.*, **1994**, *9*, 385-412.
- (162) Sato, S., Galectins as molecules of Danger signal, which could evoke an immune response to infection. *Trends Glycosci. Glyc.*, **2002**, *14*, 285-301.
- (163) Virginia Tribulatti, M.; Gabriela Figini, M.; Carabelli, J.; Cattaneo, V.; Campetella, O., Redundant and antagonistic functions of galectin-1,-3, and-8 in the elicitation of T-cell responses. *J. Immunol.*, **2012**, *188*, 2991-2999.
- (164) Spear, G. T.; Zariffard, M. R.; Xin, J.; Saifuddin, M., Inhibition of DC-SIGN-mediated trans infection of T cells by mannose-binding lectin. *Immunology*, **2003**, *110*, 80-85.
- (165) Chemani, C.; Imberty, A.; de Bentzmann, S.; Pierre, M.; Wimmerova, M.; Guery, B. P.; Faure, K., Role of LecA and LecB lectins in Pseudomonas aeruginosa-induced lung injury and effect of carbohydrate ligands. *Infect. Immun.*, **2009**, *77*, 2065-2075.
- (166) Wibowo, A.; Peters, E. C.; Hsieh-Wilson, L. C., Photoactivatable glycopolymers for the proteome-wide identification of fucose-alpha(1-2)-galactose binding proteins. *J. Am. Chem. Soc.*, **2014**, *136*, 9528-9531.
- (167) Drake, R. R.; Schwegler, E. E.; Malik, G.; Diaz, J.; Block, T.; Mehta, A.; Semmes, O. J., Lectin capture strategies combined with mass spectrometry for the discovery of serum glycoprotein biomarkers. *Mol. Cell Proteomics*, **2006**, *5*, 1957-1967.
- (168) Kaji, H.; Yamauchi, Y.; Takahashi, N.; Isobe, T., Mass spectrometric identification of N-linked glycopeptides using lectin-mediated affinity capture and glycosylation site-specific stable isotope tagging. *Nat. Protoc.*, **2006**, *1*, 3019-3027.
- (169) Ahn, Y. H.; Kim, J. Y.; Yoo, J. S., Quantitative mass spectrometric analysis of glycoproteins combined with enrichment methods. *Mass. Spectrom. Rev.*, **2015**, *34*, 148-165.
- (170) Lu, Y.-W.; Chien, C.-W.; Lin, P.-C.; Huang, L.-D.; Chen, C.-Y.; Wu, S.-W.; Han, C.-L.; Khoo, K.-H.; Lin, C.-C.; Chen, Y.-J., BAD-lectins: Boronic acid-decorated lectins with enhanced binding affinity for the selective enrichment of glycoproteins. *Anal. Chem.*, **2013**, *85*, 8268-8276.
- (171) Tang, J.; Liu, Y.; Yin, P.; Yao, G.; Yan, G.; Deng, C.; Zhang, X., Concanavalin A-immobilized magnetic nanoparticles for selective enrichment of glycoproteins and application to glycoproteomics in hepatocelluar carcinoma cell line. *Proteomics*, **2010**, *10*, 2000-2014.

- (172) Lin, P.-C.; Tseng, M.-C.; Su, A.-K.; Chen, Y.-J.; Lin, C.-C., Functionalized magnetic nanoparticles for small-molecule isolation, identification, and quantification. *Anal. Chem.*, **2007**, *79*, 3401-3408.
- (173) Qi, D.; Zhang, H.; Tang, J.; Deng, C.; Zhang, X., Facile synthesis of mercaptophenylboronic acid-functionalized core-shell structure Fe3O4@C@Au magnetic microspheres for selective enrichment of glycopeptides and glycoproteins. *J. Phys. Chem. C*, **2010**, *114*, 9221-9226.
- (174) Wang, Y.; Liu, M.; Xie, L.; Fang, C.; Xiong, H.; Lu, H., Highly efficient enrichment method for glycopeptide analyses: Using specific and nonspecific nanoparticles synergistically. *Anal. Chem.*, **2014**, *86*, 2057-2064.
- (175) Wang, H.; Bie, Z.; Lu, C.; Liu, Z., Magnetic nanoparticles with dendrimer-assisted boronate avidity for the selective enrichment of trace glycoproteins. *Chem. Sci*, **2013**, *4*, 4298-4303.
- (176) Goldstein, I. J.; Hollerma, C. E.; Smith, E. E., Protein-carbohydrate interaction .2. Inhibition studies on interaction of Concanavalin A with polysaccharides. *Biochemistry*, **1965**, *4*, 876-&.
- (177) Ferreira, J. A.; Daniel-da-Silva, A. L.; Alves, R. M. P.; Duarte, D.; Vieira, I.; Santos, L. L.; Vitorino, R.; Amado, F., Synthesis and optimization of lectin functionalized nanoprobes for the selective recovery of glycoproteins from human body fluids. *Anal. Chem.*, **2011**, *83*, 7035-7043.
- (178) Ohyama, Y.; Kasai, K. I.; Nomoto, H.; Inoue, Y., Frontal affinity-chromatography of ovalbumin glycoasparagines on a concanavalin a-sepharose column a quantitative study of the binding-specificity of the lectin. *J. Biol. Chem.*, **1985**, *260*, 6882-6887.
- (179) Wang, L. J.; Li, F. X.; Sun, W.; Wu, S. Z.; Wang, X. R.; Zhang, L.; Zheng, D. X.; Wang, J.; Gao, Y. H., Concanavalin A-captured glycoproteins in healthy human urine. *Mol. Cell Proteomics*, **2006**, *5*, 560-562.
- (180) Yang, G.; Cui, T.; Chen, Q.; Ma, T.; Li, Z., Isolation and identification of native membrane glycoproteins from living cell by concanavalin A-magnetic particle conjugates. *Anal. Biochem.*, **2012**, *421*, 339-341.
- (181) Friguet, B.; Chaffotte, A. F.; Djavadiohaniance, L.; Goldberg, M. E., Measurements of the true affinity constant in solution of antigen-antibody complexes by enzyme-linked immunosorbent-assay. *J. Immunol. Methods*, **1985**, *77*, 305-319.
- (182) Seubert, P.; Vigopelfrey, C.; Esch, F.; Lee, M.; Dovey, H.; Davis, D.; Sinha, S.; Schlossmacher, M.; Whaley, J.; Swindlehurst, C.; McCormack, R.; Wolfert, R.; Selkoe, D.; Lieberburg, I.; Schenk, D., Isolation and quantification of soluble alzheimers beta-peptide from biological-fluids. *Nature*, **1992**, *359*, 325-327.

- (183) Burnette, W. N., Western blotting electrophoretic transfer of proteins from sodium dodecyl sulfate-polyacrylamide gels to unmodified nitrocellulose and radiographic detection with antibody and radioiodinated protein-A. *Anal. Biochem*, **1981**, *112*, 195-203.
- (184) Hossenlopp, P.; Seurin, D.; Segoviaquinson, B.; Hardouin, S.; Binoux, M., Analysis of serum insulin-like growth-factor binding-proteins using western blotting use of the method for titration of the binding-proteins and competitive-binding studies. *Anal. Biochem.*, **1986**, *154*, 138-143.
- (185) Hennion, M. C.; Pichon, V., Immuno-based sample preparation for trace analysis. *J. Chromatogr. A*, **2003**, *1000*, 29-52.
- (186) Delaunay-Bertoncini, N.; Hennion, M. C., Immunoaffinity solid-phase extraction for pharmaceutical and biomedical trace-analysis-coupling with HPLC and CE-perspectives. *J. Pharmaceut. Biomed.*, **2004**, *34*, 717-736.
- (187) Degan, P.; Shigenaga, M. K.; Park, E. M.; Alperin, P. E.; Ames, B. N., Immunoaffinity isolation of urinary 8-hydroxy-2'-deoxyguanosine and 8-hydroxyguanine and quantitation of 8-hydroxy-2'-deoxyguanosine in DNA by polyclonal antibodies. *Carcinogenesis*, **1991**, *12*, 865-871.
- (188) Junutula, J. R.; Raab, H.; Clark, S.; Bhakta, S.; Leipold, D. D.; Weir, S.; Chen, Y.; Simpson, M.; Tsai, S. P.; Dennis, M. S.; Lu, Y.; Meng, Y. G.; Ng, C.; Yang, J.; Lee, C. C.; Duenas, E.; Gorrell, J.; Katta, V.; Kim, A.; McDorman, K.; Flagella, K.; Venook, R.; Ross, S.; Spencer, S. D.; Wong, W. L.; Lowman, H. B.; Vandlen, R.; Sliwkowski, M. X.; Scheller, R. H.; Polakis, P.; Mallet, W., Site-specific conjugation of a cytotoxic drug to an antibody improves the therapeutic index. *Nat. Biotechnol.*, **2008**, *26*, 925-932.
- (189) Chari, R. V. J.; Miller, M. L.; Widdison, W. C., Antibody-drug Conjugates: An emerging concept in cancer therapy. *Angew. Chem. Int. Ed.*, **2014**, *53*, 3796-3827.
- (190) Huang, R. P., Detection of multiple proteins in an antibody-based protein microarray system. *J. Immunol. Methods*, **2001**, *255*, 1-13.
- (191) Cahill, D. J., Protein and antibody arrays and their medical applications. *J. Immunol. Methods*, **2001**, *250*, 81-91.
- (192) Belov, L.; de la Vega, O.; dos Remedios, C. G.; Mulligan, S. P.; Christopherson, R. I., Immunophenotyping of leukemias using a cluster of differentiation antibody microarray. *Cancer Res.*, **2001**, *61*, 4483-4489.
- (193) Melero, I.; Hervas-Stubbs, S.; Glennie, M.; Pardoll, D. M.; Chen, L., Immunostimulatory monoclonal antibodies for cancer therapy. *Nat. Rev. Cancer*, **2007**, *7*, 95-106.
- (194) Weiner, L. M.; Surana, R.; Wang, S., Monoclonal antibodies: versatile platforms for cancer immunotherapy. *Nat. Rev. Immunol.*, **2010**, *10*, 317-327.

- (195) Chan, A. C.; Carter, P. J., Therapeutic antibodies for autoimmunity and inflammation. *Nat. Rev. Immunol.*, **2010**, *10*, 301-316.
- (196) Freitas, M.; Viswanathan, S.; Nouws, H. P. A.; Oliveira, M. B. P. P.; Delerue-Matos, C., Iron oxide/gold core/shell nanomagnetic probes and CdS biolabels for amplified electrochemical immunosensing of Salmonella typhimurium. *Biosens. Bioelectron.*, **2014**, *51*, 195-200.
- (197) Bhattacharya, D.; Chakraborty, S. P.; Pramanik, A.; Baksi, A.; Roy, S.; Maiti, T. K.; Ghosh, S. K.; Pramanik, P., Detection of total count of Staphylococcus aureus using antitoxin antibody labelled gold magnetite nanocomposites: a novel tool for capture, detection and bacterial separation. *J. Mater. Chem.*, **2011**, *21*, 17273-17282.
- (198) Chou, P. H.; Chen, S. H.; Liao, H. K.; Lin, P. C.; Her, G. R.; Lai, A. C. Y.; Chen, J. H.; Lin, C. C.; Chen, Y. J., Nanoprobe-based affinity mass spectrometry for selected protein profiling in human plasma. *Anal. Chem.*, **2005**, *77*, 5990-5997.
- (199) Lin, P. C.; Chou, P. H.; Chen, S. H.; Liao, H. K.; Wang, K. Y.; Chen, Y. J.; Lin, C. C., Ethylene glycol-protected magnetic nanoparticles for a multiplexed immunoassay in human plasma. *Small*, **2006**, *2*, 485-489.
- (200) Sanford, J. R.; Coutinho, P.; Hackett, J. A.; Wang, X.; Ranahan, W.; Caceres, J. F., Identification of nuclear and cytoplasmic mRNA targets for the shuttling protein SF2/ASF. *PLoS One*, **2008**, *3*, e3369.
- (201) Park, H.-Y.; Schadt, M. J.; Wang, L.; Lim, I. I. S.; Njoki, P. N.; Kim, S. H.; Jang, M.-Y.; Luo, J.; Zhong, C.-J., Fabrication of magnetic core @ shell Fe oxide @ Au nanoparticles for interfacial bioactivity and bio-separation. *Langmuir*, **2007**, *23*, 9050-9056.
- (202) Nash, M. A.; Waitumbi, J. N.; Hoffman, A. S.; Yager, P.; Stayton, P. S., Multiplexed enrichment and detection of malarial biomarkers using a stimuli-responsive iron oxide and gold nanoparticle reagent system. *ACS Nano*, **2012**, *6*, 6776-6785.
- (203) Ho, K. C.; Tsai, P. J.; Lin, Y. S.; Chen, Y. C., Using biofunctionalized nanoparticles to probe pathogenic bacteria. *Anal. Chem.*, **2004**, *76*, 7162-7168.
- (204) Reddy, P. M.; Chang, K.-C.; Liu, Z.-J.; Chen, C.-T.; Ho, Y.-P., Functionalized magnetic iron oxide (Fe₃O₄) nanoparticles for capturing gram-positive and gram-negative bacteria. *J. Biomed. Nanotechnol.*, **2014**, *10*, 1429-1439.
- (205) Yang, H.; Li, H.; Jiang, X., Detection of foodborne pathogens using bioconjugated nanomaterials. *Microfluid. Nanofluid.*, **2008**, *5*, 571-583.
- (206) Tang, N.; Tornatore, P.; Weinberger, S. R., Current developments in SELDI affinity technology. *Mass Spectrom. Rev.*, **2004**, *23*, 34-44.

- (207) Prieto-Simon, B.; Saint, C.; Voelcker, N. H., Electrochemical biosensors featuring oriented antibody immobilization via electrografted and self-assembled hydrazide chemistry. *Anal Chem*, **2014**, *86*, 1422-1429.
- (208) Vashist, S. K.; Lam, E.; Hrapovic, S.; Male, K. B.; Luong, J. H. T., Immobilization of antibodies and enzymes on 3-aminopropyltriethoxysilane-functionalized bioanalytical platforms for biosensors and diagnostics. *Chem. Rev.*, **2014**, *114*, 11083-11130.
- (209) Kwon, Y.; Han, Z. Z.; Karatan, E.; Mrksich, M.; Kay, B. K., Antibody arrays prepared by cutinase-mediated immobilization on self-assembled monolayers. *Anal. Chem.*, **2004**, *76*, 5713-5720.
- (210) Kaittanis, C.; Naser, S. A.; Perez, J. M., One-step, nanoparticle-mediated bacterial detection with magnetic relaxation. *Nano Lett*, **2007**, *7*, 380-383.
- (211) Jung, Y.; Lee, J. M.; Jung, H.; Chung, B. H., Self-directed and self-oriented immobilization of antibody by protein G-DNA conjugate. *Anal. Chem.*, **2007**, *79*, 6534-6541.
- (212) Hage, D. S.; Wolfe, C. A. C.; Oates, M. R., Development of a kinetic model to describe the effective rate of antibody oxidation by periodate. *Bioconjugate Chem.*, **1997**, *8*, 914-920.
- (213) Adak, A. K.; Li, B.-Y.; Huang, L.-D.; Lin, T.-W.; Chang, T.-C.; Hwang, K. C.; Lin, C.-C., Fabrication of antibody microarrays by light-induced covalent and oriented immobilization. *Acs Appl. Mater. Inter.*, **2014**, *6*, 10452-10460.
- (214) Zhang, X.; He, X.; Chen, L.; Zhang, Y., A combination of distillation-precipitation polymerization and click chemistry: fabrication of boronic acid functionalized Fe₃O₄ hybrid composites for enrichment of glycoproteins. *J. Mater. Chem.*, **2014**, *2*, 3254-3262.
- (215) Zhang, X.; He, X.; Chen, L.; Zhang, Y., Boronic acid modified magnetic nanoparticles for enrichment of glycoproteins via azide and alkyne click chemistry. *J. Mater. Chem.*, **2012**, *22*, 16520-16526.
- (216) Zhou, W.; Yao, N.; Yao, G.; Deng, C.; Zhang, X.; Yang, P., Facile synthesis of aminophenylboronic acid-functionalized magnetic nanoparticles for selective separation of glycopeptides and glycoproteins. *Chem. Comm.*, **2008**, 5577-5579.
- (217) Lin, Z.-A.; Zheng, J.-N.; Lin, F.; Zhang, L.; Cai, Z.; Chen, G.-N., Synthesis of magnetic nanoparticles with immobilized aminophenylboronic acid for selective capture of glycoproteins. *J Mater Chem*, **2011**, *21*, 518-524.
- (218) Wang, G.; Wang, Y.; Chen, L.; Choo, J., Nanomaterial-assisted aptamers for optical sensing. *Biosens. Bioelectron.*, **2010**, *25*, 1859-1868.
- (219) Torres-Chavolla, E.; Alocilja, E. C., Aptasensors for detection of microbial and viral pathogens. *Biosens. Bioelectron.*, **2009**, *24*, 3175-3182.

- (220) Ellington, A. D.; Szostak, J. W., *In vitro* selection of RNA molecules that bind specific ligands. *Nature*, **1990**, *346*, 818-822.
- (221) Ellington, A. D.; Szostak, J. W., Selection *in vitro* of single-stranded-dna molecules that fold into specific ligand-binding structures. *Nature*, **1992**, *355*, 850-852.
- (222) Lou, X.; Qian, J.; Xiao, Y.; Viel, L.; Gerdon, A. E.; Lagally, E. T.; Atzberger, P.; Tarasow, T. M.; Heeger, A. J.; Soh, H. T., Micromagnetic selection of aptamers in microfluidic channels. *Proc. Natl. Acad. Sci. USA*, **2009**, *106*, 2989-2994.
- (223) Bock, L. C.; Griffin, L. C.; Latham, J. A.; Vermaas, E. H.; Toole, J. J., Selection of single-stranded-DNA molecules that bind and inhibit human thrombin. *Nature*, **1992**, *355*, 564-566.
- (224) Sarell, C. J.; Karamanos, T. K.; White, S. J.; Bunka, D. H. J.; Kalverda, A. P.; Thompson, G. S.; Barker, A. M.; Stockley, P. G.; Radford, S. E., Distinguishing closely related amyloid precursors using an RNA aptamer. *J. Biol. Chem.*, **2014**, *289*, 26859-26871.
- (225) Famulok, M., Molecular recognition of amino-acids by RNA-aptamers an L-citrulline binding RNA motif and its evolution into an L-arginine binder. *J. Am. Chem. Soc.*, **1994**, *116*, 1698-1706.
- (226) Geiger, A.; Burgstaller, P.; vonderEltz, H.; Roeder, A.; Famulok, M., RNA aptamers that bind L-arginine with sub-micromolar dissociation constants and high enantioselectivity. *Nucleic Acids Res.*, **1996**, *24*, 1029-1036.
- (227) Mannironi, C.; Scerch, C.; Fruscoloni, P.; Tocchini-Valentini, G. P., Molecular recognition of amino acids by RNA aptamers: The evolution into an L-tyrosine binder of a dopamine-binding RNA motif. *RNA*, **2000**, *6*, 520-527.
- (228) Yang, K.-A.; Barbu, M.; Halim, M.; Pallavi, P.; Kim, B.; Kolpashchikov, D. M.; Pecic, S.; Taylor, S.; Worgall, T. S.; Stojanovic, M. N., Recognition and sensing of low-epitope targets via ternary complexes with oligonucleotides and synthetic receptors. *Nat. Chem.*, **2014**, *6*, 1003-1008.
- (229) Sassanfar, M.; Szostak, J. W., An RNA motif that binds ATP. *Nature*, **1993**, *364*, 550-553.
- (230) Lee, J. H.; Yigit, M. V.; Mazumdar, D.; Lu, Y., Molecular diagnostic and drug delivery agents based on aptamer-nanomaterial conjugates. *Adv. Drug Deliver. Rev.*, **2010**, *62*, 592-605.
- (231) Famulok, M.; Mayer, G., Aptamers and SELEX in chemistry & biology. *Chem. Biol.*, **2014**, *21*, 1055-1058.
- (232) Xu, H.; Mao, X.; Zeng, Q.; Wang, S.; Kawde, A.-N.; Liu, G., Aptamer-functionalized gold nanoparticles as probes in a dry-reagent strip biosensor for protein analysis. *Anal. Chem.*, **2009**, *81*, 669-675.

- (233) Chiu, T.-C.; Huang, C.-C., Aptamer-Functionalized Nano-Biosensors. *Sensors*, **2009**, *9*, 10356-10388.
- (234) Liu, J., Oligonucleotide-functionalized hydrogels as stimuli responsive materials and biosensors. *Soft Matter.*, **2011**, *7*, 6757-6767.
- (235) Lee, J. H., Conjugation approaches for construction of aptamer-modified nanoparticles for application in imaging. *Curr. Top. Med. Chem.*, **2013**, *13*, 504-512.
- (236) Kim, D.; Jeong, Y. Y.; Jon, S., A drug-loaded aptamer-gold nanoparticle bioconjugate for combined CT imaging and therapy of prostate cancer. *ACS Nano*, **2010**, *4*, 3689-3696.
- (237) Pu, Y.; Zhu, Z.; Liu, H.; Zhang, J.; Liu, J.; Tan, W., Using aptamers to visualize and capture cancer cells. *Anal. Bioanal. Chem.*, **2010**, *397*, 3225-3233.
- (238) Yang, L.; Zhang, X.; Ye, M.; Jiang, J.; Yang, R.; Fu, T.; Chen, Y.; Wang, K.; Liu, C.; Tan, W., Aptamer-conjugated nanomaterials and their applications. *Adv. Drug. Deliver. Rev.*, **2011**, *63*, 1361-1370.
- (239) Pavlov, V.; Xiao, Y.; Shlyahovsky, B.; Willner, I., Aptamer-functionalized Au nanoparticles for the amplified optical detection of thrombin. *J. Am. Chem. Soc.*, **2004**, *126*, 11768-11769.
- (240) Wang, Y.; Liu, B., Conjugated polyelectrolyte-sensitized fluorescent detection of thrombin in blood serum using aptamer-immobilized silica nanoparticles as the platform. *Langmuir*, **2009**, *25*, 12787-12793.
- (241) So, H.-M.; Park, D.-W.; Jeon, E.-K.; Kim, Y.-H.; Kim, B. S.; Lee, C.-K.; Choi, S. Y.; Kim, S. C.; Chang, H.; Lee, J.-O., Detection and titer estimation of Escherichia coli using aptamer-functionalized single-walled carbon-nanotube field-effect transistors. *Small*, **2008**, *4*, 197-201.
- (242) Helwa, Y.; Dave, N.; Froidevaux, R.; Samadi, A.; Liu, J., Aptamer-functionalized hydrogel microparticles for fast visual detection of mercury(II) and adenosine. *Acs Appl. Mater. Interfaces*, **2012**, *4*, 2228-2233.
- (243) Kang, H.; O'Donoghue, M. B.; Liu, H.; Tan, W., A liposome-based nanostructure for aptamer directed delivery. *Chem. Commun.*, **2010**, *46*, 249-251.
- (244) Kouassi, G. K.; Wang, P.; Sreevatan, S.; Irudayaraj, J., Aptamer-mediated magnetic and gold-coated magnetic nanoparticles as detection assay for prion protein assessment. *Biotechnol. Progr.*, **2007**, *23*, 1239-1244.
- (245) Wu, S.; Duan, N.; Wang, Z.; Wang, H., Aptamer-functionalized magnetic nanoparticle-based bioassay for the detection of ochratoxin a using upconversion nanoparticles as labels. *Analyst*, **2011**, *136*, 2306-2314.

- (246) Yigit, M. V.; Mazumdar, D.; Lu, Y., MRI detection of thrombin with aptamer functionalized superparamagnetic iron oxide nanoparticles. *Bioconjugate Chem.*, **2008**, *19*, 412-417.
- (247) Yigit, M. V.; Mazumdar, D.; Kim, H.-K.; Lee, J. H.; Dintsov, B.; Lu, Y., Smart "Turn-on" magnetic resonance contrast agents based on aptamer-functionalized superparamagnetic iron oxide nanoparticles. *Chembiochem*, **2007**, *8*, 1675-1678.
- (248) Bamrungsap, S.; Shukoor, M. I.; Chen, T.; Sefah, K.; Tan, W., Detection of lysozyme magnetic relaxation switches based on aptamer-functionalized superparamagnetic nanoparticles. *Anal. Chem.*, **2011**, *83*, 7795-7799.
- (249) Lee, C. W.; Huang, K. T.; Wei, P. K.; Yao, Y. D., Conjugation of gamma-Fe₂O₃ nanoparticles with single strand oligonucleotides. *J. Magn. Magn. Mater.*, **2006**, *304*, E412-E414.
- (250) Thomson, D. A. C.; Tee, E. H. L.; Tran, N. T. D.; Monteiro, M. J.; Cooper, M. A., Oligonucleotide and polymer functionalized nanoparticles for amplification-free detection of DNA. *Biomacromolecules*, **2012**, *13*, 1981-1989.
- (251) Horak, D.; Spanova, A.; Tvrdikova, J.; Rittich, B., Streptavidin-modified magnetic poly(2-hydroxyethyl methacrylate-co-glycidyl methacrylate) microspheres for selective isolation of bacterial DNA. *Eur. Polym. J.*, **2011**, *47*, 1090-1096.
- (252) Herr, J. K.; Smith, J. E.; Medley, C. D.; Shangguan, D. H.; Tan, W. H., Aptamer-conjugated nanoparticles for selective collection and detection of cancer cells. *Anal. Chem.*, **2006**, *78*, 2918-2924.
- (253) Smith, J. E.; Medley, C. D.; Tang, Z.; Shangguan, D.; Lofton, C.; Tan, W., Aptamer-conjugated nanoparticles for the collection and detection of multiple cancer cells. *Anal. Chem.*, **2007**, *79*, 3075-3082.
- (254) Bamrungsap, S.; Chen, T.; Shukoor, M. I.; Chen, Z.; Sefah, K.; Chen, Y.; Tan, W., Pattern recognition of cancer cells using aptamer-conjugated magnetic nanoparticles. *Acs Nano*, **2012**, *6*, 3974-3981.
- (255) Medley, C. D.; Bamrungsap, S.; Tan, W.; Smith, J. E., Aptamer-conjugated nanoparticles for cancer cell detection. *Anal. Chem.*, **2011**, *83*, 727-734.
- (256) Lin, M.; Zhao, Y.; Wang, S.; Liu, M.; Duan, Z.; Chen, Y.; Li, F.; Xu, F.; Lu, T., Recent advances in synthesis and surface modification of lanthanide-doped upconversion nanoparticles for biomedical applications. *Biotechnol. Adv.*, **2012**, *30*, 1551-1561.
- (257) Gu, Z.; Yan, L.; Tian, G.; Li, S.; Chai, Z.; Zhao, Y., Recent advances in design and fabrication of upconversion nanoparticles and their safe theranostic applications. *Adv. Mater.*, **2013**, *25*, 3758-3779.

- (258) Fang, S.; Wang, C.; Xiang, J.; Cheng, L.; Song, X.; Xu, L.; Peng, R.; Liu, Z., Aptamer-conjugated upconversion nanoprobes assisted by magnetic separation for effective isolation and sensitive detection of circulating tumor cells. *Nano Res.*, **2014**, *7*, 1327-1336.
- (259) Shukoor, M. I.; Natalio, F.; Tahir, M. N.; Ksenofontov, V.; Therese, H. A.; Theato, P.; Schroeder, H. C.; Mueller, W. E. G.; Tremel, W., Superparamagnetic gamma-Fe2O3 nanoparticles with tailored functionality for protein separation. *Chem. Commun.*, **2007**, 4677-4679.
- (260) Zhang, X.; Zhu, S.; Deng, C.; Zhang, X., Highly sensitive thrombin detection by matrix assisted laser desorption ionization-time of flight mass spectrometry with aptamer functionalized core-shell Fe3O4@C@Au magnetic microspheres. *Talanta*, **2012**, *88*, 295-302.
- (261) Fan, C.; Shi, Z.; Pan, Y.; Song, Z.; Zhang, W.; Zhao, X.; Tian, F.; Peng, B.; Qin, W.; Cai, Y.; Qian, X., Dual matrix-based Immobilized trypsin for complementary proteolytic digestion and fast proteomics analysis with higher protein sequencecCoverage. *Anal. Chem.*, **2014**, *86*, 1452-1458.
- (262) Dang-Thuan, T.; Chen, C.-L.; Chang, J.-S., Immobilization of Burkholderia sp lipase on a ferric silica nanocomposite for biodiesel production. *J. Biotechnol.*, **2012**, *158*, 112-119.
- (263) Xie, W.; Ma, N., Enzymatic transesterification of soybean oil by using immobilized lipase on magnetic nano-particles. *Biomass Bioenerg.*, **2010**, *34*, 890-896.
- (264) Lehmann, S. V.; Breinholt, J.; Bury, P. S.; Nielsen, T. E., Enzymatic resolution to (-)-ormeloxifene intermediates from their racemates using immobilized Candida rugosa lipase. *Chirality*, **2000**, *12*, 568-573.
- (265) Bhushan, I.; Parshad, R.; Qazi, G. N.; Ingavle, G.; Rajan, C. R.; Ponrathnam, S.; Gupta, V. K., Lipase enzyme immobilization on synthetic beaded macroporous copolymers for kinetic resolution of chiral drugs intermediates. *Proc. Biochem.*, **2008**, *43*, 321-330.
- (266) Rossi, L. M.; Quach, A. D.; Rosenzweig, Z., Glucose oxidase-magnetite nanoparticle bioconjugate for glucose sensing. *Anal. Bioanal. Chem.*, **2004**, *380*, 606-613.
- (267) Wu, Y.; Chen, C.; Liu, S., Enzyme-functionalized silica nanoparticles as sensitive labels in biosensing. *Anal. Chem.*, **2009**, *81*, 1600-1607.
- (268) Ansari, S. A.; Husain, Q., Potential applications of enzymes immobilized on/in nano materials: A review. *Biotechnol. Adv.*, **2012**, *30*, 512-523.
- (269) Swarnalatha, V.; Esther, R. A.; Dhamodharan, R., Immobilization of alphaamylase on gum acacia stabilized magnetite nanoparticles, an easily recoverable and reusable support. *J. Mol. Catal. B-Enzym.*, **2013**, *96*, 6-13.
- (270) Talbert, J. N.; Goddard, J. M., Characterization of lactase-conjugated magnetic nanoparticles. *Process Biochem.*, **2013**, *48*, 656-662.

- (271) Sohrabi, N.; Rasouli, N.; Torkzadeh, M., Enhanced stability and catalytic activity of immobilized alpha-amylase on modified Fe₃O₄ nanoparticles. *Chem. Eng. J.*, **2014**, *240*, 426-433.
- (272) Liu, L.; Shi, S.; Zhao, H.; Yu, J.; Jiang, X.; Chen, X., Selective fishing and analysis of xanthine oxidase binders from two Fabaceae species by coupling enzyme functionalized core-shell magnetic nanoparticles with HPLC-MS. *J. Chromatogr. B*, **2014**, *945*, 163-170.
- (273) Liu, T.; Zhao, Y.; Wang, X.; Li, X.; Yan, Y., A novel oriented immobilized lipase on magnetic nanoparticles in reverse micelles system and its application in the enrichment of polyunsaturated fatty acids. *Bioresource Technol.*, **2013**, *132*, 99-102.
- (274) Brady, D.; Jordaan, J.; Simpson, C.; Chetty, A.; Arumugam, C.; Moolman, F. S., Spherezymes: A novel structured self-immobilisation enzyme technology. *BMC Biotechnol.*, **2008**, *8*.
- (275) Aloulou, A.; Rodriguez, J. A.; Fernandez, S.; van Oosterhout, D.; Puccinelli, D.; Carriere, F., Exploring the specific features of interfacial enzymology based on lipase studies. *BBA-Mol. Cell. Biol. L.*, **2006**, *1761*, 995-1013.
- (276) Bai, L.; Du, Y.; Peng, J.; Liu, Y.; Wang, Y.; Yang, Y.; Wang, C., Peptide-based isolation of circulating tumor cells by magnetic nanoparticles. *J. Mater. Chem. B*, **2014**, *2*, 4080-4088.
- (277) Chen, W.; Jarzyna, P. A.; van Tilborg, G. A. F.; Nguyen, V. A.; Cormode, D. P.; Klink, A.; Griffioen, A. W.; Randolph, G. J.; Fisher, E. A.; Mulder, W. J. M.; Fayad, Z. A., RGD peptide functionalized and reconstituted high-density lipoprotein nanoparticles as a versatile and multimodal tumor targeting molecular imaging probe. *FASEB. J.*, **2010**, *24*, 1689-1699.
- (278) Deshayes, S.; Maurizot, V.; Clochard, M.-C.; Baudin, C.; Berthelot, T.; Esnouf, S.; Lairez, D.; Moenner, M.; Deleris, G., "Click" conjugation of peptide on the surface of polymeric nanoparticles for targeting tumor angiogenesis. *Pharm. Res.*, **2011**, *28*, 1631-1642.
- (279) Qin, M.; Zong, H.; Kopelman, R., Click conjugation of peptide to hydrogel nanoparticles for tumor-targeted drug delivery. *Biomacromolecules*, **2014**, *15*, 3728-3734.
- (280) Arosio, D.; Manzoni, L.; Araldi, E. M. V.; Scolastico, C., Cyclic RGD functionalized gold nanoparticles for tumor targeting. *Bioconjugate Chem.*, **2011**, *22*, 664-672.
- (281) Morales-Avila, E.; Ferro-Flores, G.; Ocampo-Garcia, B. E.; De Leon-Rodriguez, L. M.; Santos-Cuevas, C. L.; Garcia-Becerra, R.; Medina, L. A.; Gomez-Olivan, L., Multimeric system of Tc-99m-labeled gold nanoparticles conjugated to c RGDfK(C) for molecular imaging of tumor alpha(v)beta(3) expression. *Bioconjugate Chem.*, **2011**, *22*, 913-922.
- (282) Kinnari, P. J.; Hyvonen, M. L. K.; Makila, E. M.; Kaasalainen, M. H.; Rivinoja, A.; Salonen, J. J.; Hirvonen, J. T.; Laakkonen, P. M.; Santos, H. A., Tumour homing peptide-functionalized porous silicon nanovectors for cancer therapy. *Biomaterials*, **2013**, *34*, 9134-9141.

- (283) Scari, G.; Porta, F.; Fascio, U.; Avvakumova, S.; Dal Santo, V.; De Simone, M.; Saviano, M.; Leone, M.; Del Gatto, A.; Pedone, C.; Zaccaro, L., Gold nanoparticles capped by a GC-containing peptide functionalized with an RGD motif for integrin targeting. *Bioconjugate Chem.*, **2012**, *23*, 340-349.
- (284) Todorova, N.; Chiappini, C.; Mager, M.; Simona, B.; Patel, I. I.; Stevens, M. M.; Yarovsky, I., Surface presentation of functional peptides in solution determines cell Internalization efficiency of TAT conjugated nanoparticles. *Nano Lett.*, **2014**, *14*, 5229-5237.
- (285) Pan, Y.; Long, M. J. C.; Li, X.; Shi, J.; Hedstrom, L.; Xu, B., Glutathione (GSH)-decorated magnetic nanoparticles for binding glutathione-S-transferase (GST) fusion protein and manipulating live cells. *Chem. Sci.*, **2011**, *2*, 945-948.
- (286) Lee, Y.-J.; Park, J.-M.; Huh, J.; Kim, M.; Lee, J.-S.; Palani, A.; Lee, K.; Lee, S.-W., Ultra-specific enrichment of GST-tagged protein by GSH-modified nanoparticles. *B. Kor. Chem. Soc.*, **2010**, *31*, 1568-1572.
- (287) Ni, K.; Yang, J.; Ren, Y.; Wei, D., Facile synthesis of glutathione-functionalized Fe3O4@polydopamine for separation of GST-tagged protein. *Mater. Lett.*, **2014**, *128*, 392-395.
- (288) Scarberry, K. E.; Dickerson, E. B.; McDonald, J. F.; Zhang, Z. J., Magnetic nanoparticle-peptide conjugates for in vitro and in vivo targeting and extraction of cancer cells. *J Am Chem Soc*, **2008**, *130*, 10258-10262.
- (289) Lin, Y. G.; Han, L. Y.; Kamat, A. A.; Merritt, W. M.; Landen, C. N., Jr.; Deavers, M. I.; Fletcher, M. S.; Urbauer, D. L.; Kinch, M. S.; Sood, A. K., EphA2 overexpression is associated with angiogenesis in ovarian cancer. *Cancer*, **2007**, *109*, 332-340.
- (290) Thaker, P. H.; Deavers, M.; Celestino, J.; Thornton, A.; Fletcher, M. S.; Landen, C. N.; Kinch, M. S.; Kiener, P. A.; Sood, A. K., EphA2 expression is associated with aggressive features in ovarian carcinoma. *Clin. Cancer Res.*, **2004**, *10*, 5145-5150.
- (291) Han, L. Q.; Dong, Z. M.; Qiao, Y. H.; Kristensen, G. B.; Holm, R.; Nesland, J. M.; Suo, Z. H., The clinical significance of EphA2 and Ephrin A-1 in epithelial ovarian carcinomas. *Gynecol. Oncol.*, **2005**, *99*, 278-286.
- (292) Koguma, I.; Yamashita, S.; Sato, S.; Okuyama, K.; Katakura, Y., Novel purification method of human immunoglobulin by using a thermo-responsive protein A. *J. Chromatogr. A*, **2013**, *1305*, 149-153.
- (293) McLean, M. D.; Chen, R.; Yu, D.; Mah, K.-Z.; Teat, J.; Wang, H.; Zaplachinski, S.; Boothe, J.; Hall, J. C., Purification of the therapeutic antibody trastuzumab from genetically modified plants using safflower Protein A-oleosin oilbody technology. *Transgenic Res.*, **2012**, *21*, 1291-1301.
- (294) Zhu-Shimoni, J.; Gunawan, F.; Thomas, A.; Vanderlaan, M.; Stults, J., Trace level analysis of leached protein A in bioprocess samples without interference from the large excess of rhMAb IgG. *J. Immunol. Methods*, **2009**, *341*, 59-67.

- (295) Hober, S.; Nord, K.; Linhult, M., Protein A chromatography for antibody purification. *J. Chromatogr. B*, **2007**, *848*, 40-47.
- (296) Lin, P.-C.; Yu, C.-C.; Wu, H.-T.; Lu, Y.-W.; Han, C.-L.; Su, A.-K.; Chen, Y.-J.; Lin, C.-C., A Chemically functionalized magnetic nanoplatform for rapid and specific biomolecular recognition and separation. *Biomacromolecules*, **2013**, *14*, 160-168.
- (297) Ghose, S.; Zhang, J.; Conley, L.; Caple, R.; Williams, K. P.; Cecchini, D., Maximizing binding capacity for protein A chromatography. *Biotechnol. Progress*, **2014**, *30*, 1335-1340.
- (298) Qing, L.-S.; Xue, Y.; Zheng, Y.; Xiong, J.; Liao, X.; Ding, L.-S.; Li, B.-G.; Liu, Y.-M., Ligand fishing from Dioscorea nipponica extract using human serum albumin functionalized magnetic nanoparticles. *J. Chromatogr. A*, **2010**, *1217*, 4663-4668.
- (299) Liu, L.; Ma, Y.; Chen, X.; Xiong, X.; Shi, S., Screening and identification of BSA bound ligands from Puerariae lobata flower by BSA functionalized Fe3O4 magnetic nanoparticles coupled with HPLC-MS/MS. *J. Chromatogr. B*, **2012**, *887*, 55-60.
- (300) Magro, M.; Faralli, A.; Baratella, D.; Bertipaglia, I.; Giannetti, S.; Salviulo, G.; Zboril, R.; Vianello, F., Avidin functionalized maghernite nanoparticles and their application for recombinant human biotinyl-SERCA purification. *Langmuir*, **2012**, *28*, 15392-15401.
- (301) Wang, W.; Jing, Y.; He, S.; Wang, J.-P.; Zhai, J.-P., Surface modification and bioconjugation of FeCo magnetic nanoparticles with proteins. *Colloid. Surface B*, **2014**, *117*, 449-456.
- (302) Sun, B.; Huang, L.; Na, N.; He, D.; Ouyang, J., Applications of multifunctional magnetic nanoparticles for the enrichment of proteins for PAGE separation. *Electrophoresis*, **2011**, *32*, 2091-2098.
- (303) Tan, L. P.; Chen, G. Y. J.; Yao, S. Q., Expanding the scope of site-specific protein biotinylation strategies using small molecules. *Bioorg. Med. Chem. Lett.*, **2004**, *14*, 5735-5738.
- (304) Girish, A.; Sun, H. Y.; Yeo, D. S. Y.; Chen, G. Y. J.; Chua, T. K.; Yao, S. Q., Site-specific immobilization of proteins in a microarray using intein-mediated protein splicing. *Bioorg. Med. Chem. Lett.*, **2005**, *15*, 2447-2451.
- (305) Reynolds, N. P.; Tucker, J. D.; Davison, P. A.; Timney, J. A.; Hunter, C. N.; Leggett, G. J., Site-specific immobilization and micrometer and nanometer scale photopatterning of yellow fluorescent protein on glass surfaces. *J. Am. Chem. Soc.*, **2009**, *131*, 896-897.
- (306) Chan, L.; Cross, H. F.; She, J. K.; Cavalli, G.; Martins, H. F. P.; Neylon, C., Covalent attachment of proteins to solid supports and surfaces via sortase-mediated ligation. *PLoS One*, **2007**, *2*, e1164.
- (307) Kalia, J.; Abbott, N. L.; Raines, R. T., General method for site-specific protein immobilization by staudinger ligation. *Bioconjugate Chem.*, **2007**, *18*, 1064-1069.

(308) Helms, B.; van Baal, I.; Merkx, M.; Meijer, E. W., Site-specific protein and peptide immobilization on a biosensor surface by pulsed native chemical Ligation. *Chembiochem*, **2007**, *8*, 1790-1794.

CHAPTER 2: Identification of lectins from metastatic cancer cells through magnetic glyconanoparticles

2.1: Abstract

Cancer cells can have characteristic carbohydrate binding properties. Previously, it was shown that a highly metastatic melanoma cell line B16F10 bound to galactoside functionalized nanoparticles much stronger than the corresponding less metastatic B16F1 cells. In order to better understand the carbohydrate binding properties of cancer cells, herein, we report the isolation and characterization of endogenous galactose binding proteins from B16F10 cells using magnetic glyconanoparticles. The galactose coated magnetic glyconanoparticles could bind with lectins present in the cells and be isolated through magnet mediated separation. Through Western blot and mass spectrometry, arginine/serine rich splicing factor Sfrs1 was identified as a galactose selective endogenous lectin overexpressed in B16F10 cells compared to B16F1 cells. In addition, galectin-3 was found in higher amounts in B16F10 cells. Finally, the glyconanoparticles exhibited a superior efficiency in lectin isolation, from both protein mixtures as well as live cells, than the more traditional micro-particles functionalized with carbohydrates. The magnetic glyconanoparticles present a useful tool for discovery of endogenous lectins as well as binding partners of lectins without prior knowledge of protein identities.

2.2: Introduction

Lectins are carbohydrate binding proteins that are neither enzymes nor antibodies, and they can recognize various carbohydrates attached to proteins and lipids with high specificity.¹ The interactions between endogenous lectins and carbohydrates mediate a variety of biological processes, including cell signaling,^{2,3} cell adhesion,⁴ immune responses,^{5,6} and pathogen-host recognition.^{7,8} On cancer cells, some lectins have been found to be overexpressed, which

contributes to neoplastic transformation, angiogenesis, tumor invasion and metastasis, antiapoptosis, and escape from immune surveillance. 9-14 As a result, cancer cells can have very different carbohydrate binding properties compared to normal cells. Thus, methods that can aid in the detection, isolation, and purification of endogenous lectins from cancer cells, preferably from their native environments, are highly desired. 15

A new tool that has been developed in the recent decade for studying carbohydrate protein interaction is functionalized magnetic nanoparticles. ¹⁶⁻²⁴ Compared to micron-sized beads or resins, ^{22,25} nanoparticles have high surface area to volume ratios. As a result, high density glycans can be immobilized onto the nanoparticles leading to increased avidity due to the polyvalency effect. ²⁵ The magnetic properties of the nanoparticles can enable not only the detection of binding via magnetic resonance imaging, ²⁴ but also separation of target proteins from bulk media aided by a magnet. ^{18,20,21}

Previously, using a panel of magnetic glyconanoparticles (MGNPs), we discovered that a range of cells including malignant versus normal cells and closely related tumor cells, can be readily distinguished based on their characteristic signatures in carbohydrate binding.²⁴ For example, even though the B16F10 and B16F1 melanoma cells are derived from the same parent cell line (isogenic cells), the highly metastatic B16F10 binds much stronger to galactose (Gal) functionalized magnetic nanoparticles than the less metastatic B16F1 cells. However, it was unclear which lectins were responsible for the enhanced galactoside binding by B16F10 cells. In this work, we aim to identify the galactoside binding lectins endogenous to B16F10 cells using MGNPs.

Although glyco-nanoparticles have been extensively utilized to analyze carbohydratelectin interactions,^{26,27} the majority of studies were performed using pure lectins with only a few reports on lectin purification and characterization from complex mixtures.^{20,28,29} We demonstrate that MGNPs can be useful in isolation and identification of lectins from the whole cell environment much more effectively than traditional micro-particles.

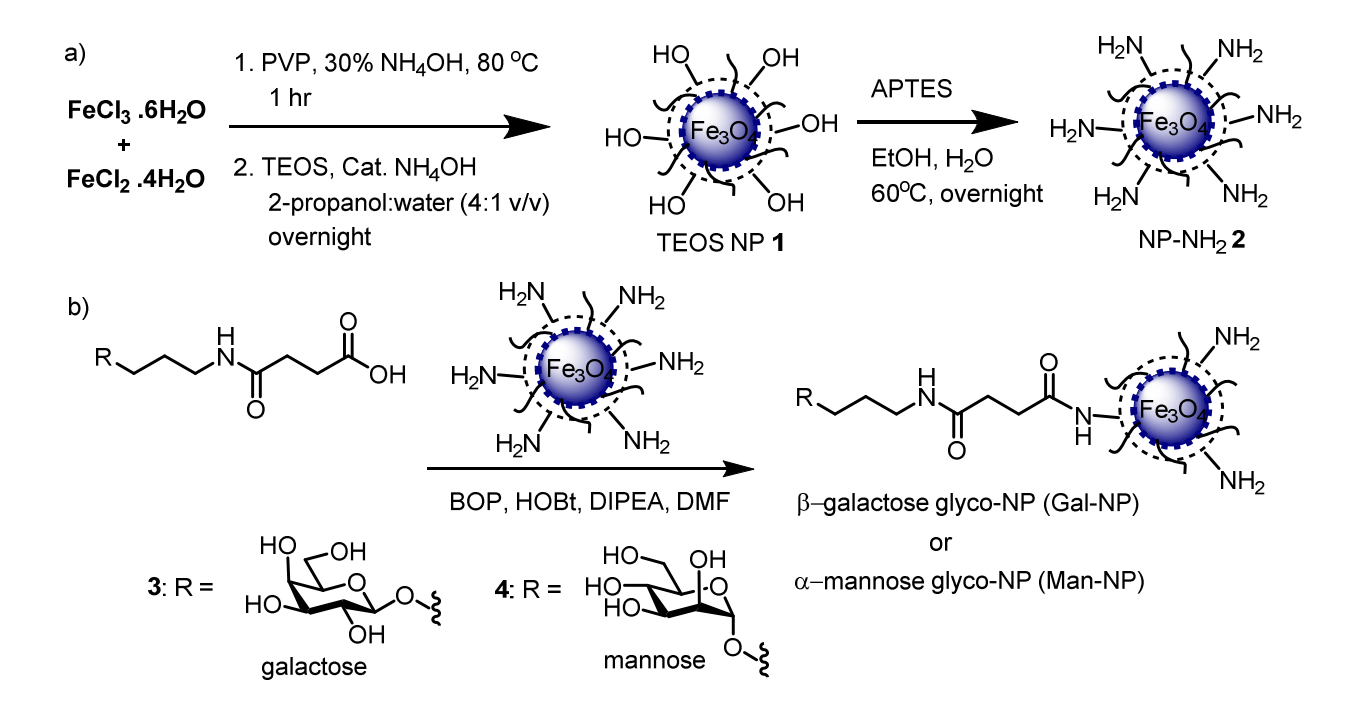
2.3: Results

2.3.1: Synthesis and lectin binding specificity of MGNPs

Fe₃O₄ magnetite NPs were synthesized via the co-precipitation method from a mixed solution of ferric chloride and ferrous chloride, which were subsequently coated with silica to protect the magnetic core (**Scheme 1a**). The NP **1** was then functionalized with amine and derivatized with galactose and mannose carboxylic acids **3** and **4** leading to Gal-NP and Man-NP respectively (**Scheme 1b**).

We found that zeta potential was a convenient method to monitor the progress of the NP functionalization. The zeta potential of TEOS-NP 1 was -23.1 mV. Upon successful amine functionalization, the zeta potential NP-2 became +17.4 mV presumably due to protonation of amines at neutral pH. Amide formation with the galactosyl and mannosyl acids reduced the amount of ammonium ions on the surface rendering a more negative zeta potential value of -11.7 mV and -6.04 mV respectively. The NPs were characterized by TEM, DLS and TGA. TEM image yielded core diameters of 10 nm, **Figure 32**, while TGA yielded a weight percentage of 3.8 % of galactose and 5.5 % of mannose on Gal-NP and Man-NP respectively, **Figure 33**.

Scheme 1: Synthesis of glyco-NP



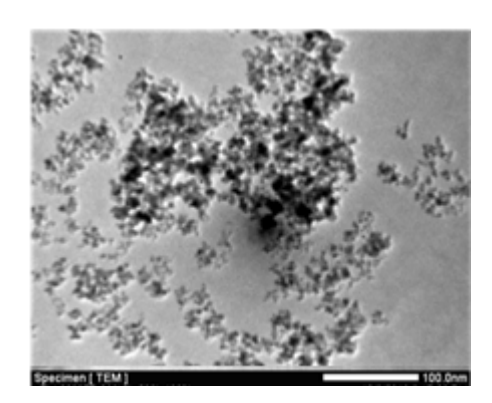


Figure 32: TEM image of Gal-NPs, scale bar is 100 nm

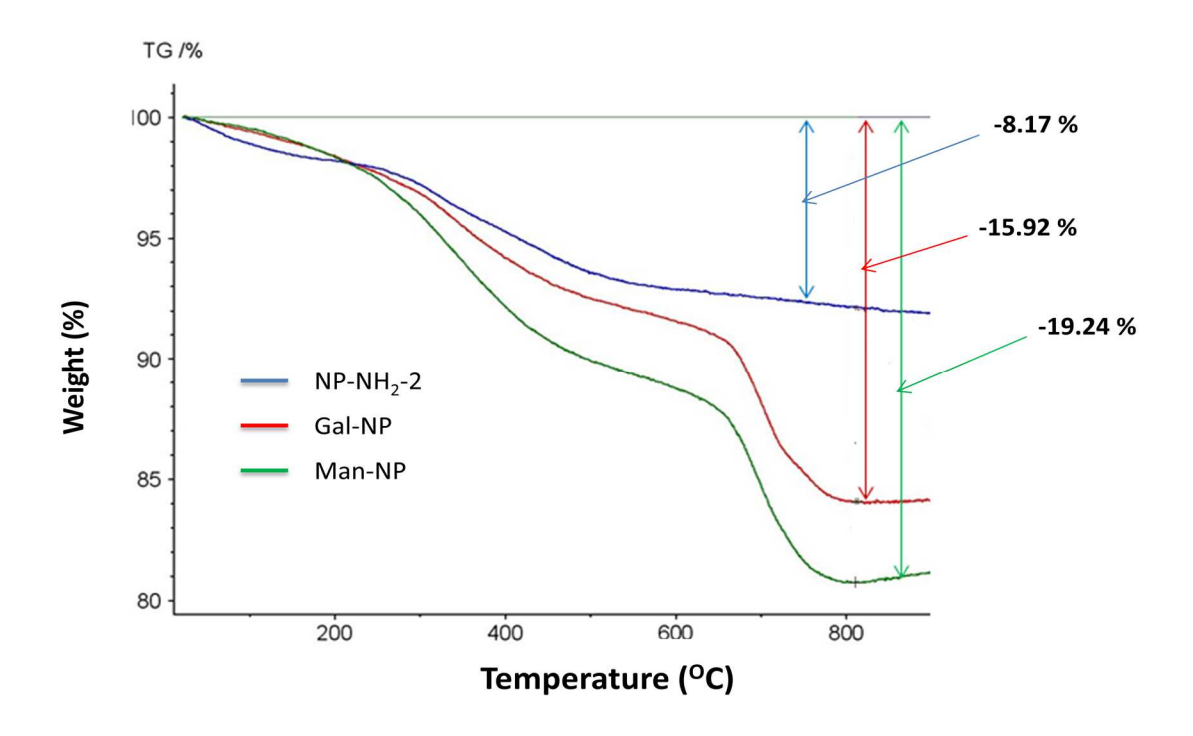


Figure 33: curves for NP-NH2 2(dark blue), Gal-NPs (red) and Man-NPs (green)

The carbohydrates immobilized on NPs retain recognition specificities, as demonstrated by lectin binding experiments. Gal-NP (4 mg of NP corresponding to 0.15 mg of Gal) was incubated with a fluorescently labeled galactose selective lectin, TRITC labeled *Bandeiraea simplicifolia* lectin (BSI) in buffer. Upon applying a desktop magnet, NPs were removed from the mixture. The amount of protein in supernatant was quantified showing a reduction of 78% in fluorescence intensity, **Figure 34**. Incubation of the isolated Gal-NPs with a large quantity (375 mg) of free galactose eluted the bound BSI from NPs (~ 65 % of originally bound BSI). A similar experiment was carried out by incubating FITC-Con A, a mannose selective lectin with Man-NP. Man-NP showed a reduction of 80% in fluorescence intensity and addition of 375 mg of free mannose led to the recovery of about 50 % of the originally bound Con A, **Figure 35**.

The eluted fractions of BSI and Con A were resolved on SDS-PAGE to confirm that the lectins were indeed recovered from the NPs, **Figure 36**.

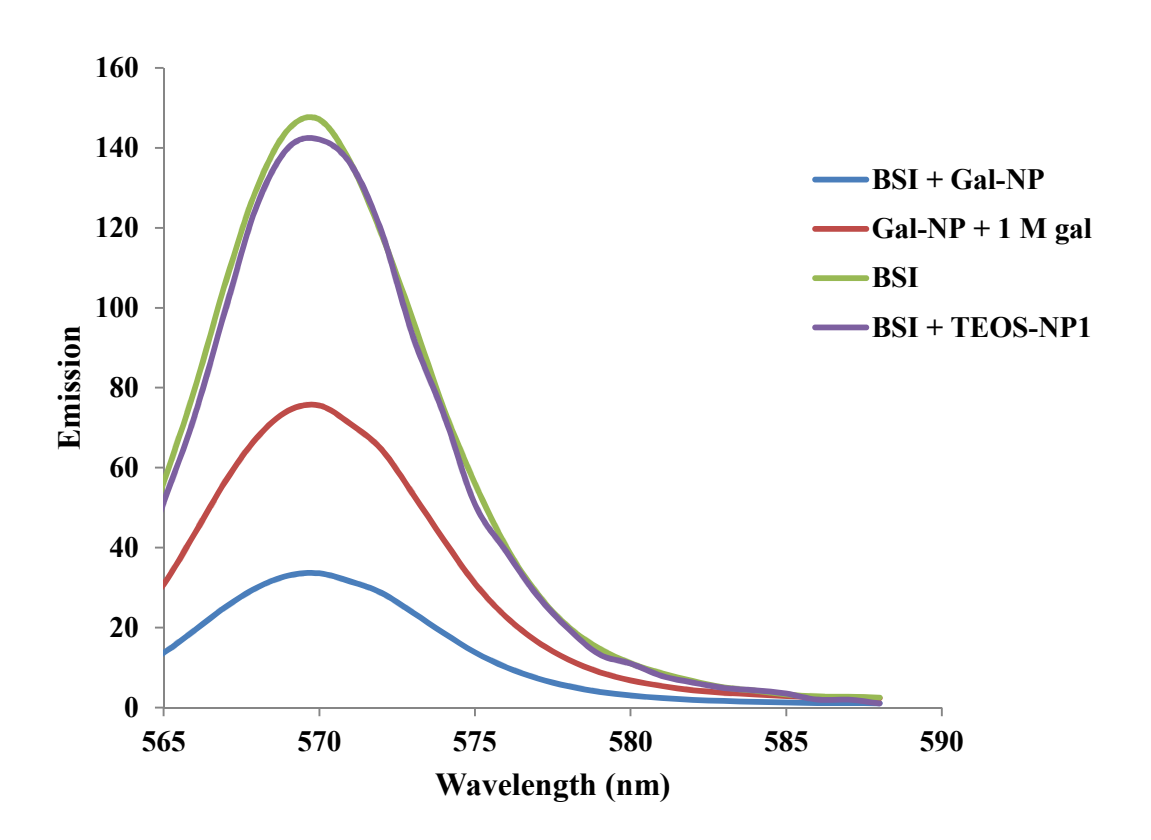


Figure 34: Fluorescent emission spectra of the supernatant of TRITC labeled BS-I solutions after incubation with Gal-NP and magnetic mediated separation

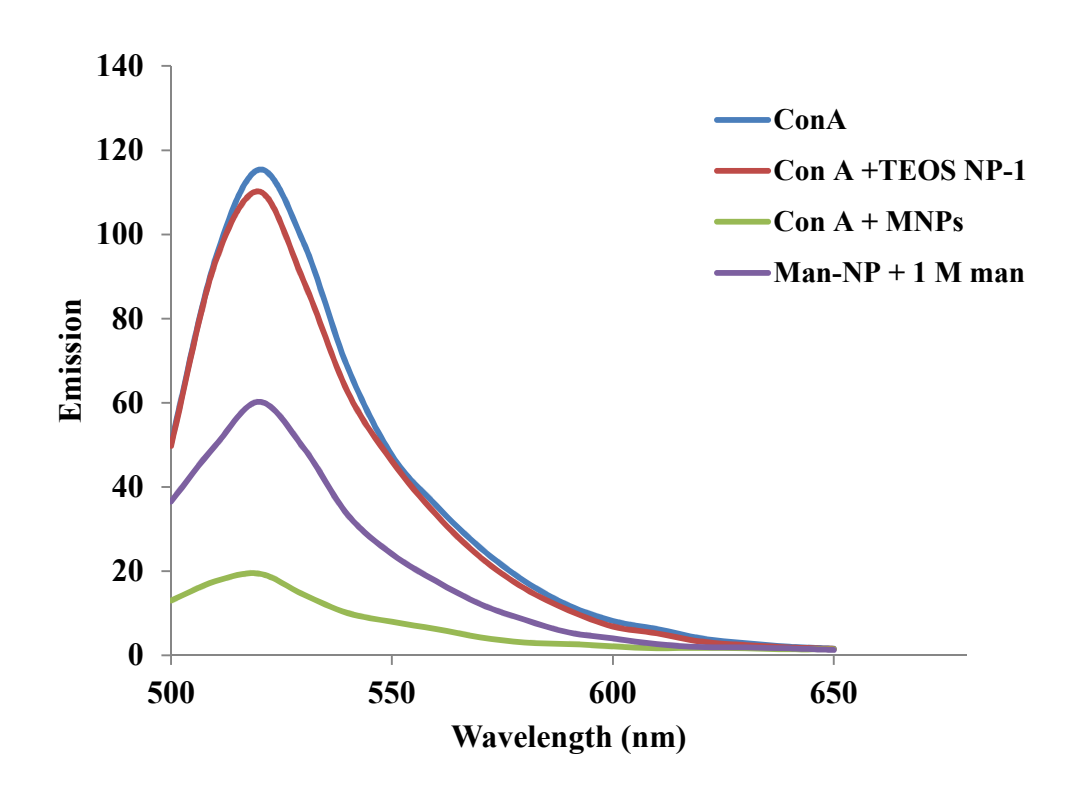


Figure 35: Fluorescent emission spectra of the supernatant of FITC labeled Con A solutions after incubation with Man-NP and magnetic mediated separation

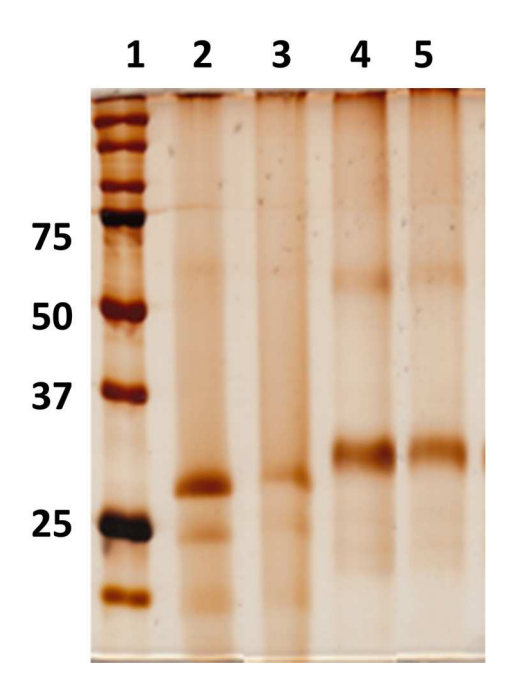


Figure 36: SDS-PAGE of lectins before addition of NP and after elution with 1 M sugar solutions. Lane 1: Molecular marker, lane 2: Con A before addition of Man-NP, lane 3: Con A eluted by 1 M mannose solution, lane 4: BS-I before addition of Gal-NP, lane 5: BS-I eluted by 1 M galactose solution

2.3.2: Isolation of exogenous lectin added to cell lysate

Our goal is to identify lectins from cancer cells. As cellular proteins can potentially non-specifically bind with the glyco-NPs and block the glycans from biological interactions, the ability of the MGNPs to separate lectins from other cancer cell contents was first tested by spiking a galactose binding lectin soybean agglutinin (SBA) into the lysate of B16F10 melanoma cells. After incubating the lysate with Gal-NP (500 µg of NP corresponding to 19 µg, 1.06 x 10⁻⁷ mol of immobilized galactose), a magnet was applied to the mixture to collect the NPs, followed by thorough washing with PBS buffer. The galactose binding proteins on the NPs were then released by incubation with a concentrated solution of free galactose (18 mg of Gal). The presence of SBA in supernatant, PBS wash and galactose eluted solution was detected and

quantified by Western blot using an anti-SBA antibody. When SBA was blotted, two bands were observed: (a) a prominent band at ~30 kD, corresponding to the molecular weight of the SBA polypeptide; and (b) a band at ~60 kD, corresponding to the SBA dimer, **Figure 37**, **Panel A**, **lane 1**, consistent with previous report of this lectin. The unbound supernatant fraction yielded very little SBA (**Figure 37**, **Panel A**, **lane 2** ~ **9% of SBA added**). The majority of SBA (~78% of SBA added) was found in the galactose eluted fraction, **Figure 37**, **Panel A**, **lane 4** and **Table 1**, suggesting that most of the exogenously added lectin was bound to the Gal-NP and could be released through galactose elution. This demonstrated that cellular proteins did not significantly impact lectin binding abilities of Gal-NPs.

2.3.3: Isolation of endogenous lectin from cell lysate

The isolation of lectins endogenous to B16F10 cells was explored next. The lysate of B16F10 cells was incubated with Gal-NP (500 µg of NP corresponding to 19 µg, 1.06 x 10⁻⁷ mol of immobilized galactose) and the NPs were isolated through magnet induced precipitation. To establish the lectin binding specificity to the NPs, the NPs were first washed with a solution of mannose followed by galactose elution. The various fractions were collected and analyzed by SDS-PAGE.

B16F10 is known to express a galactoside binding lectin, galectin-3 (Gal3), which is a member of galectin family.³¹ Gal3 has been associated with cell migration and invasion in melanoma and induction of metastasis.^{31,32} The presence of Gal3 in B16F10 is confirmed by a ~30 kD band on SDS-PAGE of lysates with immunoblotting by an anti-Gal3 antibody, **Figure 37**, **Panel B, lane 1**. The unbound supernatant fraction yielded a faint Gal3 band, **Figure 37**, **Panel B, lane 2**, suggesting that most of the Gal3 in the lysate was bound to the Gal-NPs. No

Gal3 could be detected in the PBS wash fraction, **Figure 37**, **Panel B**, **lane 3**, while a minute amount of the protein was found in the mannose eluted fraction, **Figure 37**, **Panel B**, **lane 4**. The bulk of Gal3, accounting for 68% of the Gal-3 in the original lysate, could be recovered in the galactose-eluted fraction, **Figure 37**, **Panel B**, **lane 5** and **Table 2**. The near depletion of Gal3 in the unbound supernatant fraction of the lysate incubated with Gal-NP, **Figure 37**, **Panel B**, **lane 2**, suggested that the MGNPs had a high capacity for lectins.

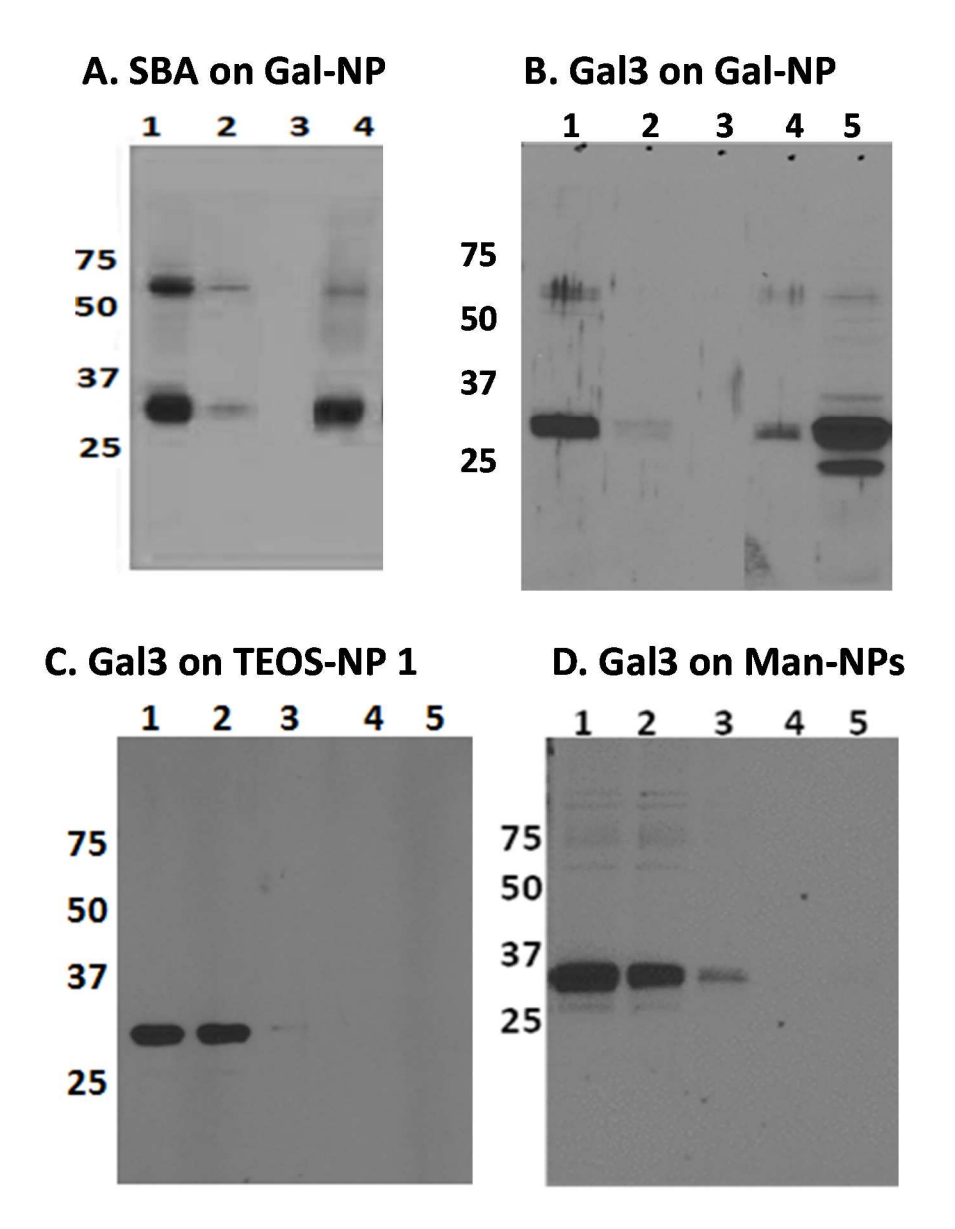


Figure 37: Binding of galactose specific lectins to Gal-NP, Man-NP and TEOS-NP 1 as detected by Western blot using anti-SBA or anti-Gal3 antibodies respectively. Panel A: Isolation of exogenous lectin (SBA) spiked in B16F10 lysate using Gal-NP. Lane 1: before addition of glyco-NPs, Lane 2: unbound fraction (supernatant); Lane 3: PBS wash; Lane 4: galactose elution. Panel B: Blotting for Gal3 isolated from B16F10 cell lysate using Gal-NP. Lane 1: B16F10 lysate, Lane 2: unbound fraction (supernatant); Lane 3: PBS wash; Lane 4: mannose elution; Lane 5: galactose eluted fraction. Panel C: Isolation of Gal3 using TEOS-NP 1. Lane 1: B16F10 lysate; Lane 2: unbound fraction (supernatant); Lane 3: PBS wash; Lane 4: mannose elution; Lane 5: galactose elution. Panel D: Isolation of Gal3 using Man-NPs. Lane 1: B16F10 lysate; Lane 2: unbound fraction (supernatant); Lane 3: PBS wash; Lane 4: galactose elution; Lane 5: mannose elution. The numbers on left side of each panel indicate the positions of the corresponding molecular weight markers

Gal3 is selective towards galactose with no mannose affinity.³³ To confirm the binding selectivity, TEOS NP 1 with no carbohydrates, **Figure 37**, **Panel C** and Man-NP, **Figure 37**, **Panel D**, were incubated with B16F10 cell lysate followed by magnet induced separation, PBS wash as well as mannose and galactose elutions. Western blot showed that most of the Gal3 were found in the unbound fractions, **Figure 37**, **Panel C**, **lane 2** and **Panel D**, **lane 2**. No Gal3 was detected in the mannose or galactose eluted fractions of NP 1, **Figure 37**, **Panel C**, **lane 4** and 5 or Man-NP, **Figure 37**, **Panel D**, **lane 4** and 5, indicating the depletion of Gal3 from the lysate requires a Gal3 binding carbohydrate on the NP.

Table 1: Quantification of SBA in fraction after incubation with Gal-NP

Fractions	Band intensity (From Fig. 1 Panel A)	Volume (μL)	Amounts of SBA (Arbitrary units corrected for volume)	% of SBA in fraction
Before Gal-NP	53	1000	5301	
Unbound 5		1000	482	9
Wash 1		500	91	2
Galactose elution	41	500	4126	78

Table 2: Quantification of Gal3 in fraction after incubation with Gal-NP

Fractions	Band intensity (From Fig. 1 Panel B)	Volume (μL)	(Arbitrary units corrected)	
Before Gal-NP	26	450	2329	
Unbound	5	450	451	19
Wash	1	250	25	1
Mannose elution	5	250	118	5
Galactose elution	63	250	1586	68

To demonstrate the advantages of using NPs vs the more traditional resins and beads, commercially available magnetic micro-particles (average diameter 3.13 µm) were derivatized with galactose. The efficiency of Gal-3 isolation by galactose micro-particles was compared to that of Gal-NP at equal amounts of galactose. Gal-NP showed superior performance compared to the micro-particles presumably due to their smaller sizes and larger surface to volume ratio resulting in enhanced rate and capacity for lectin binding, **Figure 38, and Table 3**.

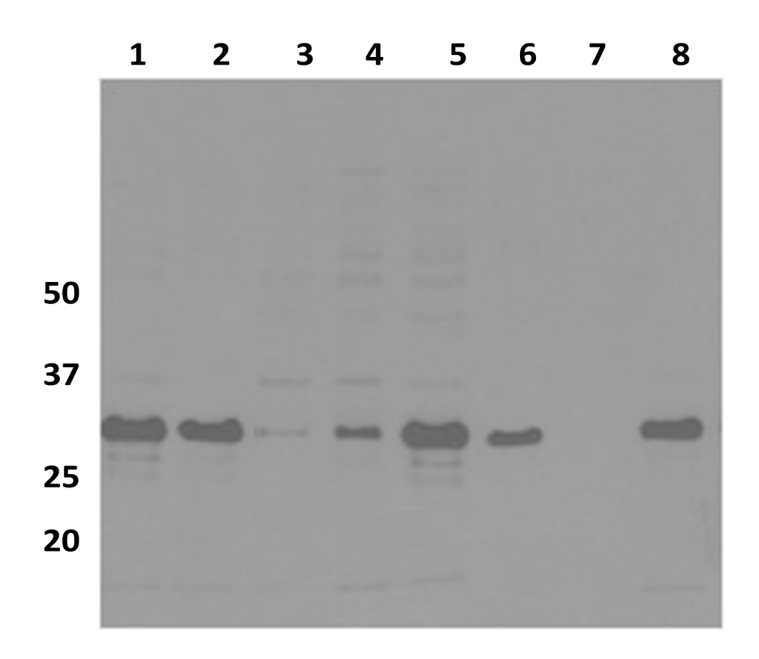


Figure 38: Comparing commercial galactose micro-nanoparticles with Gal-NPs in Gal-3 isolation from B16F10 cell lysate. Lane 1-4 commercial gal-microparticles, lane 5-8 gal-NPs. Lane 1 and 5: lyaste, lane 2 and 6: unbound fraction, lane 3 and 7: mannose eluted fraction, lane 4 and 8: galactose eluted fraction

Table 3: Quantification of Gal3 fraction using ImageJ after incubation of cell lysate with particles from **Figure 38**

Commercial galactose micro-particles				Gal-NPs			
			Amount of				Amount
			Gal3				of Gal3
	Band	Volume	(arbitrary		Band	Volume	(arbitrary
Fractions	intensity	(µL)	units)	Fractions	intensity	(µL)	units)
Before				Before			
Gal-NPs	21.1	450	9477	Gal-NPs	21.1	450	9492
Unbound	17.4	450	7848	Unbound	10.7	450	4824
Mannose				Mannose			
elution	1.1	250	273	elution	0.1	250	27
Galactose				Galactose			
elution	6.6	250	1648	elution	18.5	250	4636

2.3.4: Proteomic analysis of proteins bound to Gal-NP

Using cell lysate to study endogenous lectin can have some drawbacks as the cell lysis procedures utilize detergents to disrupt cellular membranes, which may denature some candidate proteins. It is desirable to use live cells since the lectins are in their native environments allowing binding study under physiological conditions. NPs are compatible with whole cell analysis as Gal-NPs have been found to enter B16F10 cells and do not cause cytotoxicity,²⁴ thus providing a platform for lectin discovery in live cells.

To establish the possibility of identifying endogenous lectins from live cells, B16F10 cells were incubated with Gal-NPs overnight at 37 °C. Overnight incubation was established as the optimal incubation time with large quantities of Gal-NP endocytosed into the cells, **Figure** 39.

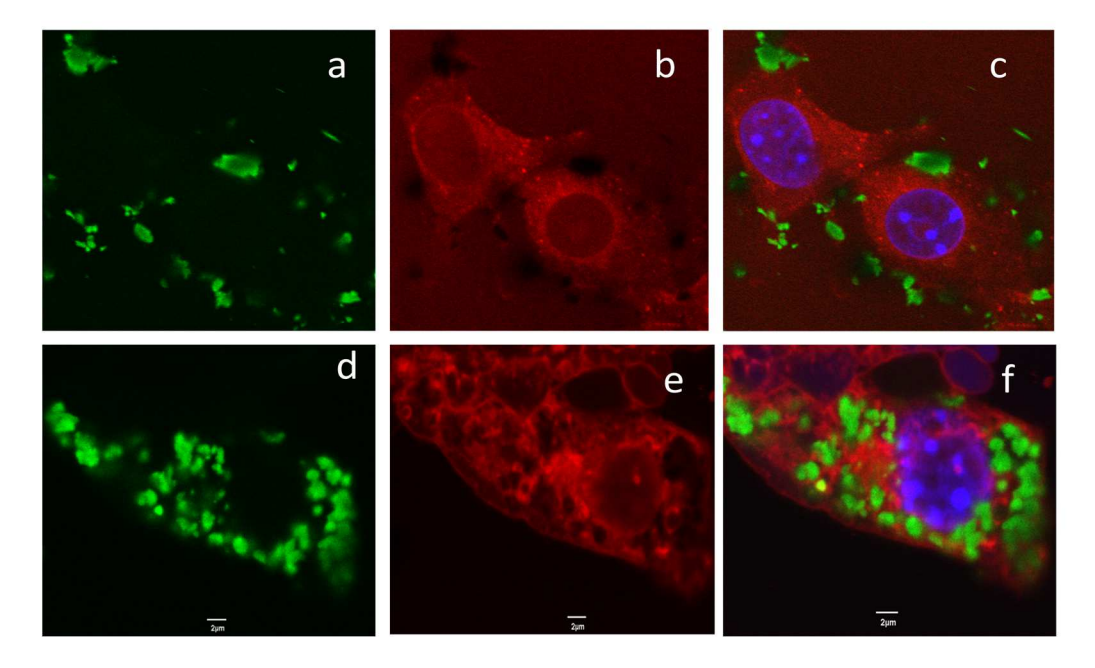


Figure 39: Binding of FITC labeled Gal-NPs to B16F10 cells incubated for 1 h or 12 hr. Incubation for 1 h (a, b, c) or 12 hr (d, e, f). Green channel showing FITC-labeled Gal-NPs, red channel for lysosome tracker and blue channel for DAPI showing nuclear staining

The unbound particles were washed off and the cells were lysed. NPs were then recovered by magnetic separation, which was followed by PBS, mannose and galactose washes. The various fractions were resolved on a SDS-PAGE gel and analyzed via silver staining. While many bands were present in (a) the supernatant after magnetic separation, representing the unbound fraction; and (b) PBS wash fraction, **Figure 40, Panel A, lanes 1 and 2**, the galactose-eluted fraction yielded two prominent sets of bands at 15-20 kD and 30-35 kD respectively, **Figure 40, Panel A, lane 4**. To confirm the abilities of proteins in the galactose-eluted fraction to bind with galactose, this fraction was subjected to gel filtration to remove bound galactose and incubated with a fresh batch of Gal-NP. The bound proteins were eluted with free galactose again and analyzed via SDS-PAGE. Similar patterns of bands were observed as those from the

first affinity selection, **Figure 40**, **Panel B**, **lane 4**, thus confirming the bindings of those proteins with Gal-NPs were galactose dependent.

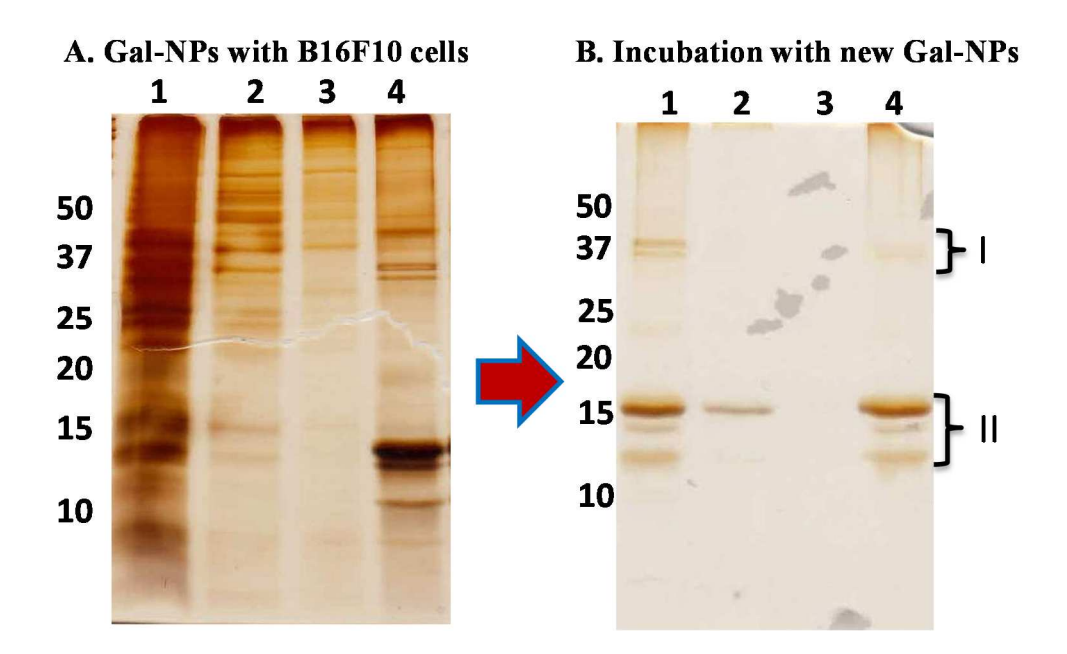


Figure 40: Identification of endogenous proteins bound to Gal-NPs. Identification of endogenous proteins bound to Gal-NPs. Panel A: B16F10 cells were incubated with Gal-NPs overnight, lysed, subjected to magnetic separation followed by elution of bound proteins. Lane 1: Supernatant after magnetic separation; Lane 2: PBS wash fraction; Lane 3: mannose eluted fraction; Lane 4: galactose eluted fraction. Panel B: Galactose eluted fraction passed through a desalting column to remove free galactose and subjected to fresh Gal-NP binding followed by sequential elutions. Lane 1: before addition of Gal-NPs, Lane 2: PBS wash; Lane 3: mannose eluted fraction; Lane 4: galactose eluted fraction. The bands around 37 kD and 15 kD were subjected to trypsinic digestion followed by LC/MS/MS analysis. The numbers on left side of each panel indicate the positions of the corresponding molecular weight markers

To determine the identities of the proteins bound to Gal-NPs, proteomic analysis was performed. The gel slice containing bands at ~37 kD (area I highlighted in **Figure 40, Panel B, lane 5** was cut out and digested with trypsin. LC-MS-MS analysis of the tryptic digest

fragments revealed two distinct polypeptides: (a) there were 12 matches, representing 10 distinct tryptic peptides (each with a carboxyl terminal lysine or arginine), with the amino acid sequence of murine homolog of splicing factor 2 (SF2)/alternative splicing factor (ASF), hereafter designated as Sfrs1. (b) There were 37 matches, representing 25 tryptic peptides, with the amino acid sequence of murine annexin V. A similar proteomic analysis was carried out on the gel slice containing the bands at ~15 kD (area II highlighted for **Figure 40, Panel B, lane 5**. Three histone proteins (H4, H2B, H2A) were identified as the polypeptides accounting for the bands in area II.

As a comparison, proteomic analysis was also performed on the corresponding regions of the SDS-PAGE from the mannose eluted fraction of Gal-NP isolation, as well as the galactose eluted fraction of TEOS-NP 1 isolation. From these samples, all derived from B16F10 cells, no proteins corresponding to Sfrs1, annexin V or histone proteins were identified by LC-MS suggesting isolation of these proteins required galactose on the NPs.

2.3.5: Confirmation of Sfrs1 in the galactose-eluted fraction of Gal-NP by Western blot

To confirm the presence of Sfrs1, the various fractions from Gal-NP binding with B16F10 cells were developed on a SDS-PAGE gel and immunoblotted with anti-Sfrs1. There was little Sfrs1 in the unbound, PBS wash and mannose elution fractions, **Figure 41**, **Panel A**, **lanes 1-4**. However, a prominent positive band was observed in the material bound to Gal-NP and eluted with galactose (Fig. 3, Panel A, lane 5). In contrast, antibodies against an irrelevant protein, Sfrs5, failed to yield a positive immunoblot in the galactose-eluted fraction (data not shown). Therefore, the identification of Sfrs1 in the galactose-eluted fraction by LC-MS was confirmed by Western blot analysis.

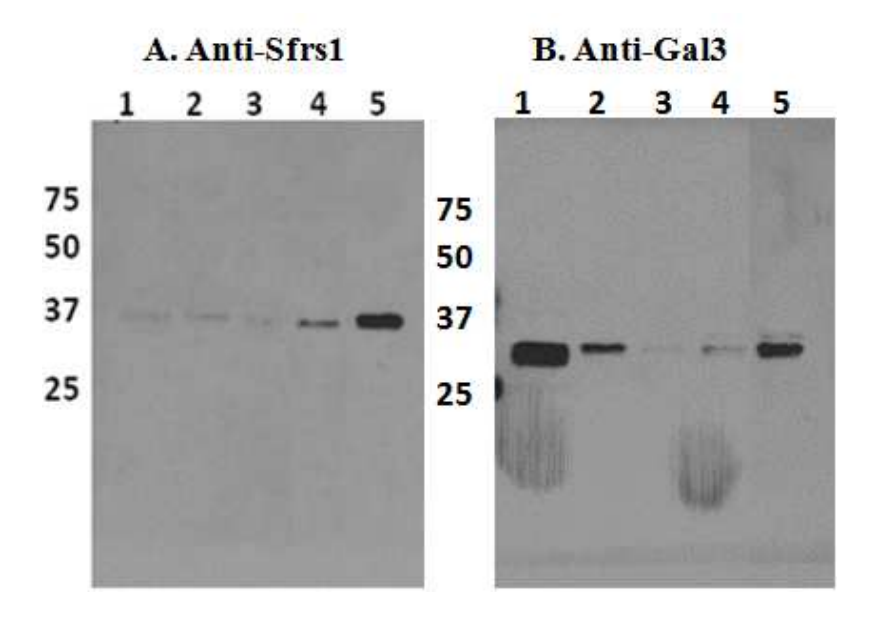


Figure 41: Blotting for endogenous lectins from whole cells bound to Gal-NP. B16F10 cells were incubated with Gal-NPs overnight. Blotting for endogenous lectins from whole cells bound to Gal-NP. B16F10 cells were incubated with Gal-NPs overnight. After incubation, cells were lysed through homogenization, followed by the elution protocols described above. Panel A: Blotting for Sfrs1. Lane 1: Residual lysis buffer after magnetic separation (supernatant); Lanes 2 and 3: PBS wash fraction, Lane 4: mannose eluted fraction; Lane 5: galactose eluted fraction. Panel B: Blotting for Gal3. Lane 1: Residual lysis buffer after magnetic separation (supernatant); Lanes 2 and 3: PBS wash fraction; Lane 4: mannose eluted fraction; Lane 5: galactose eluted fraction. The numbers on left side of each panel indicate the positions of the corresponding molecular weight markers

Besides the detection of Sfrs1, the gel was also immunoblotted with anti-Gal3. In this case, the supernatant fraction after magnetic separation, representing the unbound fraction, yielded a prominent Gal3 band, **Figure 41**, **Panel B**, **lane 1**. As Gal-NP was able to deplete completely Gal3 from the lysate of B16F10 cells, the presence of large amount of Gal3 in the unbound fraction suggests that some Gal3 molecules were sequestered in the cells in locations not accessible by Gal-NPs. A significant amount of Gal3 was found in the galactose-eluted fraction, **Figure 41**, **Panel B**, **lane 5**, consistent with the results of **Figure 37**. The reason that

Gal3 was not identified in the proteomics studies was most likely because Gal3 (~30 kD) migrated to just below the ~37 kD region (area I in Figure 40, panel B) excised for analysis.

The performance of Gal micro-particles in isolation of lectins from live cells was also compared to Gal-NP. Equal amounts of Gal micro-particles and NPs were incubated with B16F10 cells. After removing the free particles in the extracellular space, the amounts of particles endocytosed by the cells were quantified by inductively coupled plasma optical emission spectrometry (ICP-OES). With Gal-NP, about two-fold increase in the amount of intracellular iron was observed indicating more facile uptake of the NPs vs the micro-particles, **Table 5**. In addition, the lectin isolation experiments were performed from the whole cells using both Gal NPs and micro-particles. Consistent with the experiment using lysate, **Figure 38**, Gal-NP showed superior efficiency in purifying Gal3 from the whole cell compared to the Gal micro-particles, **Figure 42 and Table 4**.

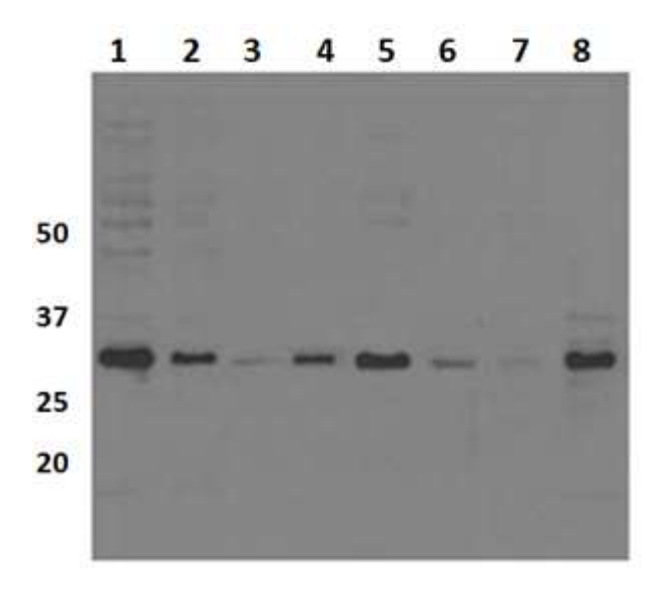


Figure 42: Comparing commercial gal-microparticles with Gal-NPs in Gal-3 isolation from whole cell. Lane 1-4 commercial gal-microparticles, Lane 5-8 gal-NPs. Lane 1 and 5: Residual lysis buffer after magnetic separation (supernatant), lane 2 and 6: wash fraction, lane 3 and 7: mannose eluted fraction, lane 4 and 8: galactose eluted fraction. The numbers on left side indicate the positions

Table 4: Quantification of Gal3 in fraction using ImageJ after incubation of cells with particles, from **Figure 42**

Commercial galactose micro-particles				Gal-NPs			
			Amount			Amount	
			of Gal3				of Gal3
	Band	Volume	(arbitrary		Band	Volume	(arbitrary
Fractions	intensity	(µL)	units)	Fractions	intensity	(µL)	units)
Supernata				Supernat			
nt	28.0	500	13994	ant	19.6	500	9792
Wash	12.8	300	3848	Wash	4.6	300	1366
Mannose				Mannose			
elution	2.0	250	511	elution	1.1	250	271
Galactose				Galactose			
elution	10.6	250	2642	elution	21.4	250	5339

Table 5: Amount of iron in cells after Gal-NPs and commercial micro-particles were incubated with B16F10 cells

Experiment	Same amount of particles (500µg), 6			Same amount of galactose (19 ug), 6		
	hour incubation			hour incubation		
Sample	Total Iron	Iron	% uptake	Total Iron	Iron	% uptake
		uptaken			uptaken	
Gal-NPs	340	129	38	544	185	34
Commercial	129	22	17	360	64	18
micro-particles						

2.3.6: Binding properties of Sfrs1 expressed as a fusion protein with GST

In the above experiments, Sfrs1 was observed in the galactose-eluted fraction after the whole cells were incubated with Gal-NP. It was possible that the observed binding of Sfrs1

occurred via its association with a galactose binding protein for which we had neither an antibody reagent nor mass spectrometry information. A major challenge in specific isolation and purification of proteins is the co-purification of highly abundant proteins with low affinity for the immobilized compound leading to false positive results.³⁴ To test for direct binding of Sfrs1 with Gal-NP, Sfrs1 was expressed and purified as a fusion protein with glutathione S-transferase (GST) following a similar procedure as for the preparation of GST-Gal3.³⁵

When GST alone was incubated with Gal-NP, almost all of the protein was recovered in the unbound fraction, **Figure 43**, **Panel A**, **lanes 1-3**. Therefore, GST (M_r ~27 kD) by itself does not interact with the Gal-NP serving as a negative control. The positive control was GST-Gal3 (M_r ~57 kD). Although small amounts of GST-Gal3 were present in both the unbound and wash fractions, the majority of the fusion protein was found in the galactose bound fraction, **Figure 43**, **Panel B**, **lane 3**. When the binding experiments were performed using GST-Sfrs1, all the GST-Sfrs1 incubated with Gal-NP was recovered in the bound fraction with no GST-Sfrs1 in the unbound or the wash fraction, **Figure 43**, **Panel C**, **lanes 1-3**.

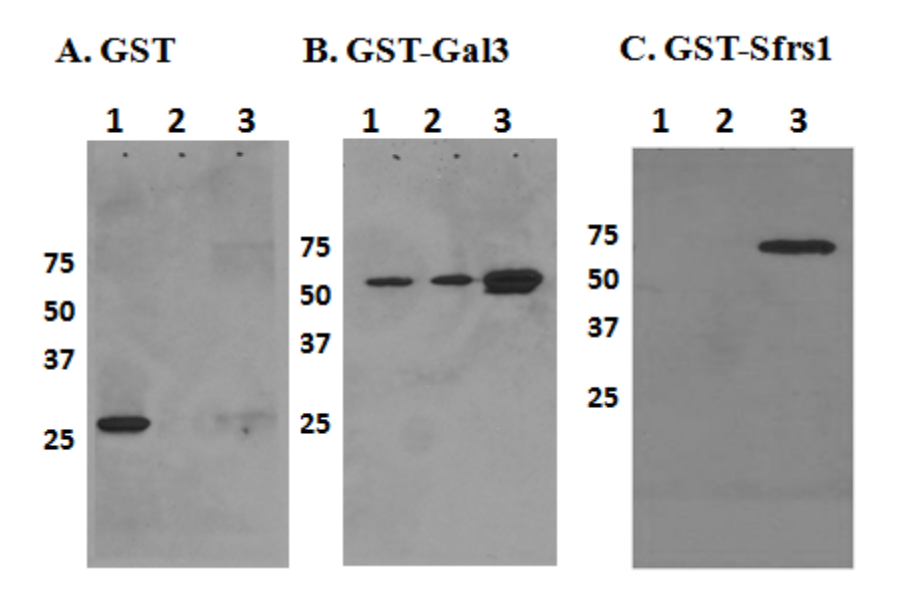


Figure 43: Binding of GST, GST-Gal3, and GST-SFRS1 to Gal-NPs. Panel A: Binding of GST to Gal-NPs. Lane 1: Unbound fraction (supernatant), Lane 2: Wash fraction, Lane 3: Bound fraction. Panel B: Binding of GST-Gal3 to Gal-NPs. Lane 1: Unbound fraction (supernatant), Lane 2: Wash fraction, Lane 3: Bound fraction. Panel C: Binding of GST-Sfrs1 to Gal-NPs. Lane 1: Unbound fraction (supernatant), Lane 2: Wash fraction, Lane 3: Bound fraction. All of the blotting were carried out with the same anti-GST antibodies. The numbers on left side of each panel indicate the positions of the corresponding molecular weight markers

To test for the specificity of GST-Sfrs1 binding to Gal-NP, the binding experiment between GST-Sfrs1 and Gal-NP was repeated but this time the bound GST-Sfrs1 was subjected to sequential elution with mannose solution followed with galactose solution after PBS wash. The decrease in GST-Sfrs1 band intensity in the unbound fraction as compared to before addition of Gal-NP is an indicator for binding but not for specificity, **Figure 44**, **Panel A**, **lanes 1 and 2**. After eluting with mannose and galactose solution, the blotting results revealed the presence of GST-Sfrs1 protein band in the galactose eluted fraction but very minimal in the mannose eluted fraction or the PBS wash fraction supporting binding dependence on galactose, **Figure 44**, **Panel A**, **lanes 3-5**.

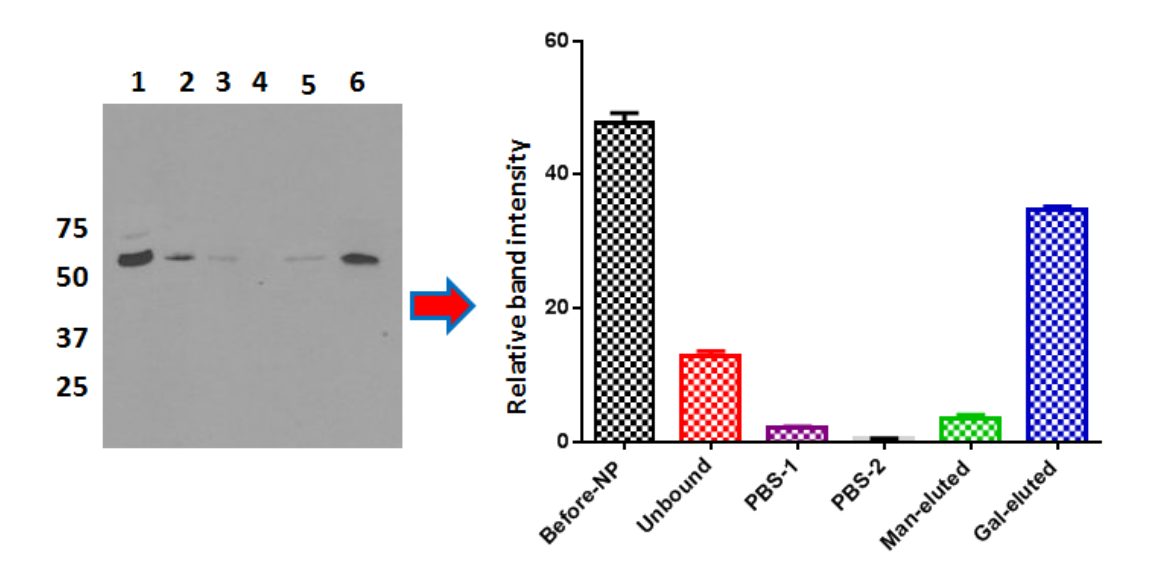


Figure 44: Further confirmation for the binding specificity of GST-Sfrs1 to Gal-NPs. Western blot results with anti-Sfrs1, and histogram representation of band intensities as determined by ImageJ. Lane 1: Before addition of Gal-NP; Lane 2: unbound fraction (supernatant); Lanes 3 and 4: PBS wash fraction; Lane 5: mannose eluted fraction; Lane 6: galactose eluted fractions. The numbers on left side of Western blot results indicate the positions of the corresponding molecular weight markers

To further substantiate the binding specificity of GST-Sfrs1 to Gal-NP, the binding experiment was repeated with TEOS-NP 1 as a negative control to demonstrate the binding was not due to non-specific absorption by NPs, Figure 45. As indicated by the blotting results, majority of GST-Sfrs1 failed to bind to the nanoparticles, Figure 45, lanes 1 and 2. In addition, there were no GST-Sfrs1 protein bands in the mannose or galactose eluted fractions, Figure 45, lanes 4 and 5.

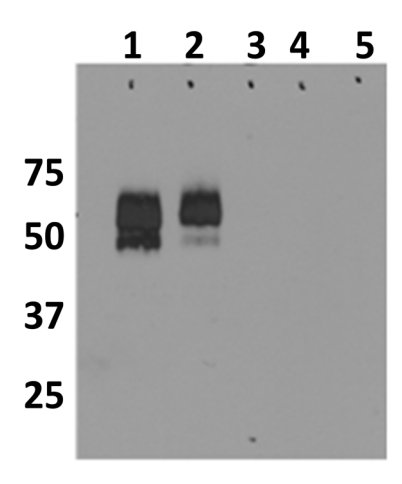


Figure 45: Further confirmation for the binding specificity of Sfrs1 to Gal-NPs. Binding of GST-Sfrs1 to TEOS-NPs as determined by Western blot using anti-GST. Lane 1: Before addition of TEOS-NP 1; Lane 2: Unbound fraction (supernatant); Lane 3: Wash fraction; Lane 4: mannose eluted fraction; Lane 5: galactose eluted fractions; Lanes 5 and 6: galactose eluted fractions. The numbers on left side of indicate the positions of the corresponding molecular weight markers

Glycan microarray is a powerful high throughput technique to decipher the carbohydrate binding activities of proteins.³⁶ Recently, Fukuda and coworkers performed glycan microarray screening and ELISA assay of Sfrs1.³⁷ Sfrs1 has been shown to bind with a wide range of glycans including LacNAc and sialyl Lewis X, which contain galactose at the non-reducing terminal. Our results on Gal-NP binding by Sfrs1 are consistent with the findings from the Fukuda group.

As presented above, besides Sfrs1, annexin V and histone proteins have been identified via proteomics from the galactose eluted fractions of Gal-NP bound proteins. To test the glycan binding properties of these proteins, recombinant annexin V and histones (a mixture of H3, H4, H2B, H2A from chicken) were submitted to the Consortium for Functional Glycomics (CFG) and screened on a 610 member glycan microarray covering a wide range of mammalian glycans at multiple concentrations. Interestingly, no significant binding signals were observed on the

microarray, suggesting that these proteins exhibited little affinity to any of the glycan components up to 0.1 mM. All the measured relative fluorescence was less than 1000 units which is considered 'negative' binding according to the current microarray assay, **Figures 61 and 62**. In a separate experiment, histone proteins were incubated with Gal-NPs, which was followed by magnetic separation and PBS wash. Subsequent elution with a concentrated solution of galactose eluted little histone proteins. These results confirmed the low affinity of histones for galactoside.

2.3.7: Comparison of the amount of Sfrs1 isolated on Gal-NP from B16F10 versus B16F1 cells

Our previous studies had documented that there was a higher binding of Gal-NP to B16F10, a more metastatic melanoma cancer cell line compared to its less metastatic isogenic counterpart B16F1.²⁴ It is possible that the quantitative difference in Gal-NP binding observed between B16F10 and B16F1 cell lines could be explained in part by the difference in the expression levels of Sfrs1. To determine this equal number of either B16F10 and B16F1 cells, 2.5 × 10⁵ cells were cultured overnight, Gal-NP was added and cultured for an addition 12 hrs. Cells were lysed, subjected to magnetic separation, washed with PBS and the bound fraction eluted sequentially with mannose and galactose solution. The galactose eluted fractions were blotted for Sfrs1, which showed elevated level of Sfrs1 in B16F10 as compared to B16F1, **Figure 46, Panel A,** demonstrating higher amounts of Sfrs1 accessible to Gal-NP in B16F10 cells. In separate experiments, lysate was prepared from 5 ×10⁵ cells of each cell line, equal amounts of lysates from these two cell lines were resolved on a SDS-PAGE gel and blotted for

Sfrs-1 and GAPDH. B16F10 was found to express more Sfrs1 as compared to its isogenic counterpart B16F1, **Figure 46**, **Panel B**.

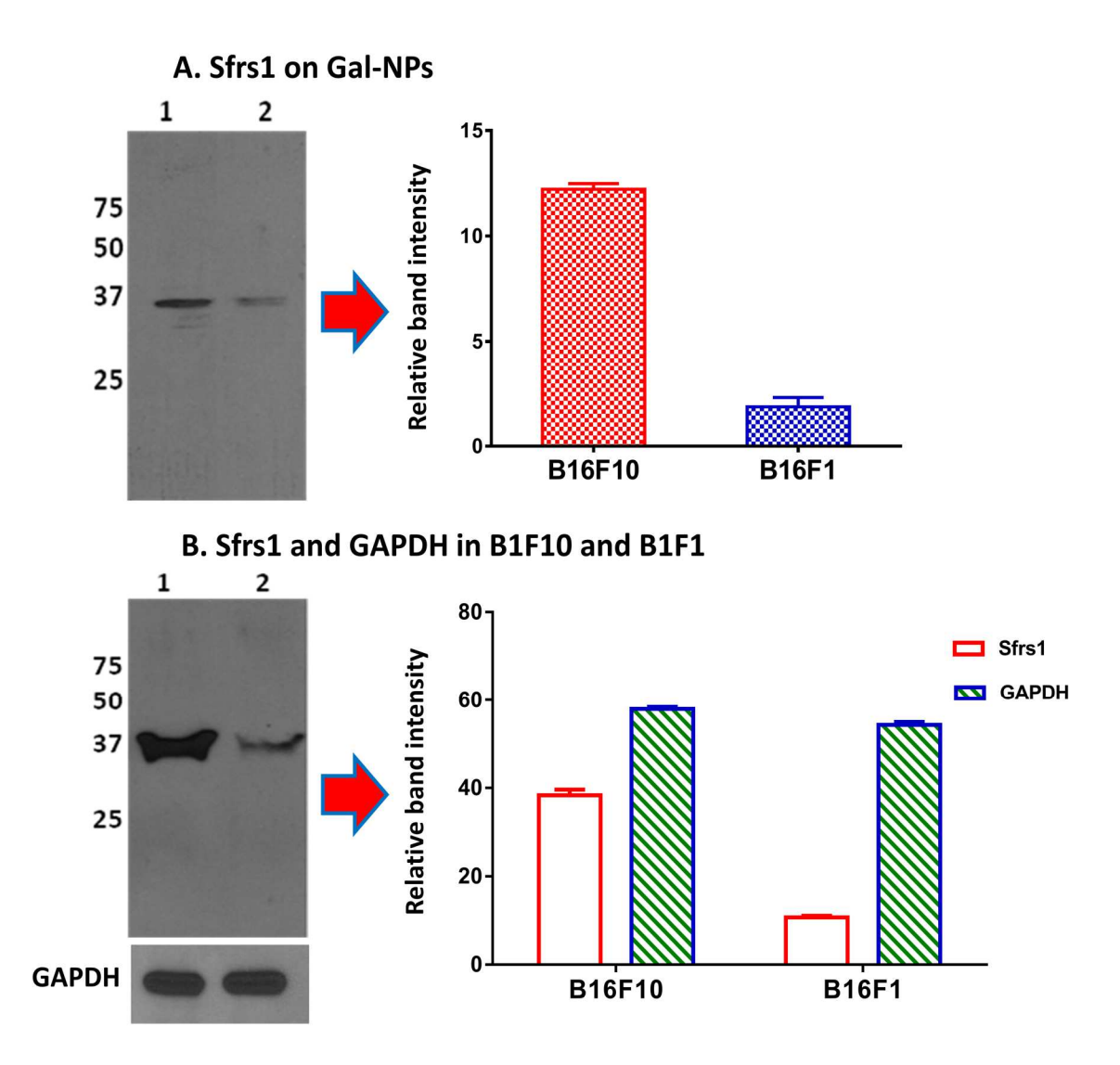


Figure 46: Comparison of Sfrs1 in B16F10 and B16F1 cells. Western blot results and histogram representation of the band intensities as analyzed by ImageJ software is shown. Lane 1: B16F10, Lane 2: B16F1. Panel B: Equal volume of the lysate prepared from equal number of B16F10 and B16F1 cells was resolved on SDS-PAGE and blotted for Sfrs1 and GAPDH. Western blot results and histogram representation of the band intensities as analyzed by ImageJ is shown. Lane 1: B16F10. Lane 2: B16F1. Blotting for glyceraldehyde 3-phosphate dehydrogenase (GAPDH) was used as loading control. The numbers on left side of Western blot results indicate the positions of the corresponding molecular weight markers

2.4: Discussion

Splicing factors are normally present in the nucleus mediating RNA splicing. Fukuda group recently reported the novel finding that Sfrs1 exists on cell surface of endothelial cells, functioning as a cell adhesion molecule to facilitate cancer cell metastasis.³⁷ As discussed above, recombinant Sfrs1 can bind to a variety of glycans including those terminated with galactose at the non-reducing end. It is important to note that the splicing factors binding to carbohydrate was calcium dependent, a characteristic exhibited by C-type lectins.³⁷ Besides cell surface presence and their well-known site of action, i.e., in the nucleus, Sfrs proteins can be present in the cytoplasm. Cytoplasmic accumulation of Sfrs1 was reported to be controlled by arginine methylation. Mutations that block methylation and remove positive charges result in the cytoplasmic accumulation of Sfrs1.³⁸ The carboxy-terminal arginine/serine-rich domain and the presence of active RNA-recognition motifs is required for Sfrs1 shuttling to the cytoplasm.³⁹ Once in the cytoplasm, Sfrs1 was found to stimulate translation and the cytoplasmic mRNA targets for shuttling Sfrs1 have been identified. 16,40 These properties of Sfrs1 proteins are consistent to those observed with Gal1 and Gal3, two galectins that have been reported to be present in the nucleus, cytoplasm and on cell surface, modulate pre-mRNA splicing activities, are overexpressed in metastatic cancer cells, play a role in tumor growth and development, and are able to bind carbohydrates.33,35,41-45 Taken together, Sfrs1 has high similarities to Gal3 in functions and joins a growing list of carbohydrate binding proteins that are multi-functional and exist in multiple cellular locations.

From our studies, higher levels of Sfrs1 have been isolated from the highly metastatic B16F10 cells compared to those from the less metastatic counterpart B16F1 cells. The role of Sfrs1 in promoting cancer growth and development through alternative splicing has been

reported.^{46,47} Sfrs1 was found to be upregulated in various human tumors relative to their respective normal controls including tumors of the colon, thyroid, small intestine, kidney, and lung.^{47,48} Its overexpression was found to be sufficient to transform immortalized cell lines. Moreover, Sfrs1 was shown to control the alternative splicing of the tumor suppressor BIN1 and the resulting BIN1 isoform lacked tumor suppressor activity. The oncogenic activity of Sfrs1 may also be due to its implication in multiple cellular programs as it regulates the alternative splicing of genes implicated in proliferation, apoptosis and cell motility, an activity important for tumor metastasis.^{47,49} These findings imply Sfrs1 has a significant role in cancer growth and development and therefore a potential target for the development of cancer therapies and diagnostics.

The glycan microarray screening results of annexin V and histone proteins suggest that they have weak affinities with all components including galactosides on the array. It should be pointed out that some members of the annexin family including annexin V have been documented to bind with carbohydrates. For example, annexins IV, V and VI can bind with glycosaminoglycan affinity columns to facilitate purification although the binding constants are not known.^{50,51} Annexin V has been reported to bind to sugar chains containing bisecting *N*-acetylglucosamine with relatively low affinity of 0.2 mM.⁵² Highly sulfated heparan sulfate/heparin were identified as preferred ligands for annexin A1.⁵³ The CFG microarray does not contain glycosaminoglycans and binding with Kd values higher than 0.1 mM could not be detected well. Thus, the lack of binding signals from annexin V and histones most likely reflect the weak affinities of these proteins with the components on the current glycan microarray under the experimental conditions.

The isolation of annexin and histone proteins by Gal-NP can be potentially explained by the interactions of these proteins with galactoside binding proteins, forming protein-protein complexes on the Gal-NPs. Related to our results, it has been reported that splicing factors including Sfrs1 co-localizes and interacts with histones contributing to the regulation of alternative splicing. Annexins have been shown to directly interact with Gal3. Thus, it is possible that the isolation of histones and annexin may be as a result of their complexations with Sfrs1 or Gal3 on the Gal-NP, resulting in their co-isolation by magnet mediated separation. The exact identity of the binding partners and the physiological importance of these interactions will require further investigations.

2.5: Conclusions

In this study, we report the utilization of MGNP to isolate endogenous lectins from B16F10 melanoma cancer cell line using both the whole cell and cell lysate. Gal-NP facilitated the purification of endogenous Gal3 through a magnet induced purification protocol. The identity of Gal3 was confirmed by Western blot and the specificity of Gal-NP binding to Gal3 was verified using carbohydrate elution protocols. The successful isolation of a well-known galactose binding lectin Gal3 using Gal-NP implies the possibility of finding other lectins (either known or unknown) in B16F10 cell line that can interact with galactose. Indeed, Sfrs1 has been isolated by Gal-NP, which was confirmed by mass spectrometry, Western blot, carbohydrate elution protocol, and direct binding of GST fused Sfrs1. The caveat to note is that not all proteins isolated by MGNPs are lectins, as some proteins may be co-isolated through their complexations with the lectins bound to the MGNPs. MGNPs have also been shown to be superior to the corresponding glyco micro-particles in lectin isolation from both live cells and cell lysates. Therefore, MGNPs can be a useful tool for the field of glyco-proteomics by providing exciting

opportunities to discover novel lectins endogenous to cells as well as the identification of the binding partners of the lectins.

2.6: Future directions

Weak binding affinities of carbohydrate-lectin interactions has compromised practical applications of glyconanoparticles in capturing lectins. Despite the fact that this weak binding affinities can be compensated through multivalent presentation of carbohydrate ligands on the NP surface, at some instance this method has not been able to capture enough lectin quantities for mass spectrometry analysis. In one successful example, Hsieh-Wilson and coworkers demonstrated that lectin enrichment based on the combination of affinity capture and covalent tethering of captured lectin to the probe generated enough material for mass spectrometry analysis. The key feature of their probe was a glycopolymer that carried multivalent sugar epitopes and photoreactive nitrophenylazide moieties to enable covalent cross-linking of the associated lectins.

Following a similar approach, we propose the incorporation of photoreactive moiety together with the carbohydrate affinity ligand. The synthetic design will follow closely the work reported by Lin and coworkers.⁵⁹ The probe carrying both the carbohydrate ligand that will provide the required affinity and specificity for the recognition of the lectins, and the photoactive group for covalent tethering of the captured lectin upon exposure to UV will be synthesized. This probe will also contain a biotin handle to facilitate affinity isolation and enrichment of the bound lectin using streptavidin functionalized MNPs, **Figure 47**. These probes could be applied in the isolation of lectin from both the cell lysate (protein mixture), and live cell as shown in **Figures 48 and 49** respectively.

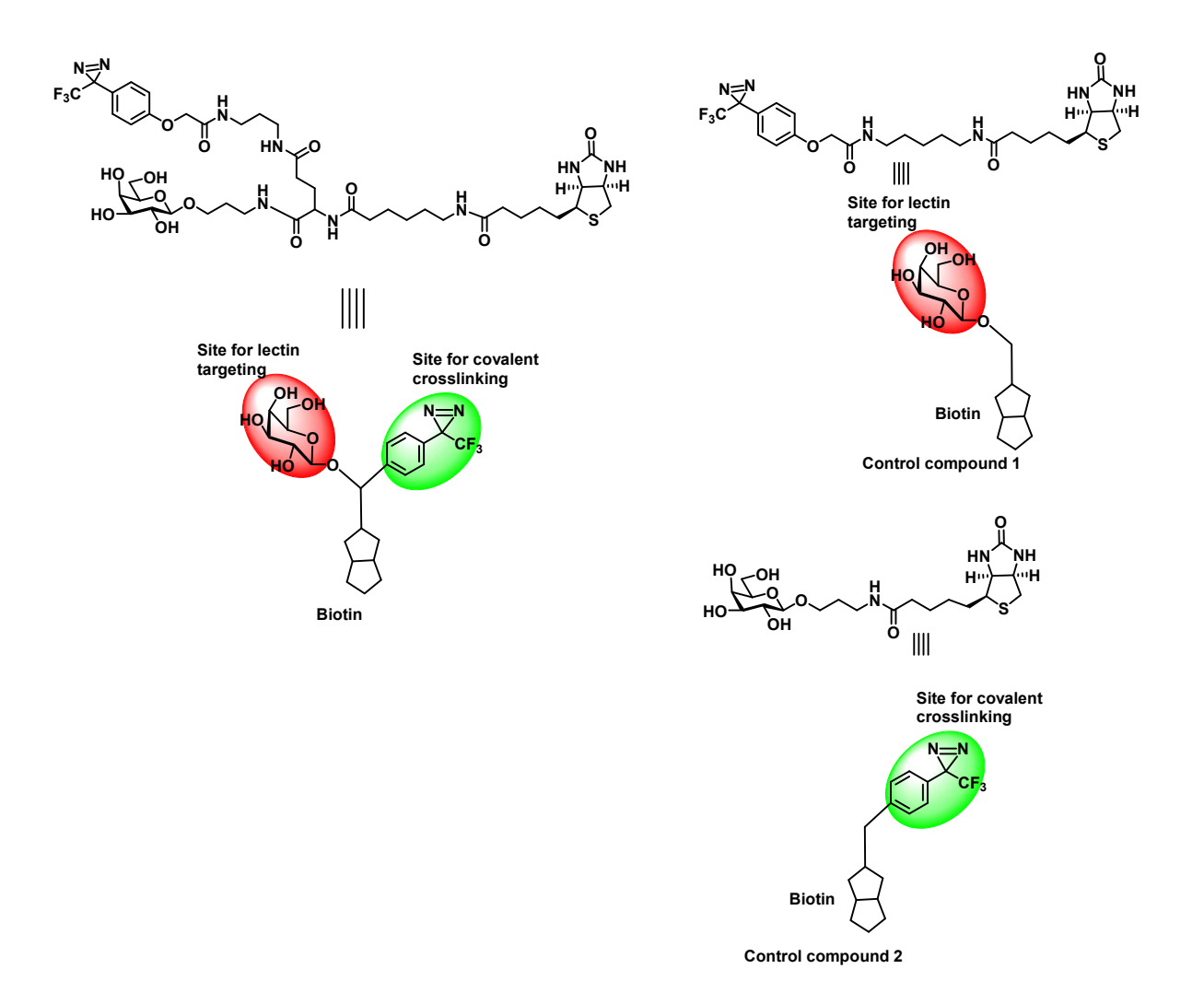


Figure 47: The probe carrying both the carbohydrate ligand that will provide the required affinity and specificity for the recognition of the lectins, and the photoactive group for covalent tethering of the captured lectin upon UV irradation

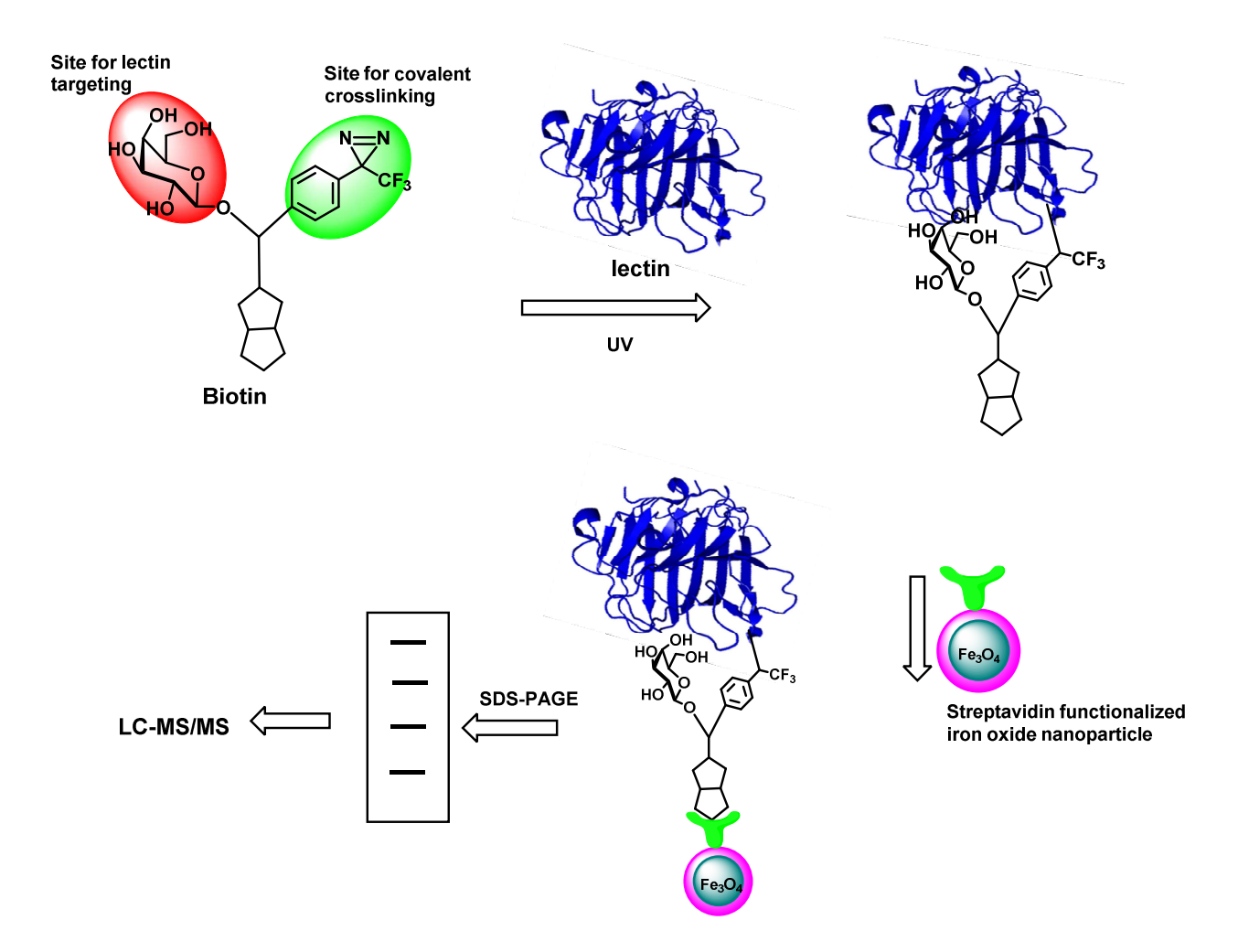


Figure 48: Lectin isolation from cell lysate using a carbohydrate affinity probe combinined with photoactivatable moiety

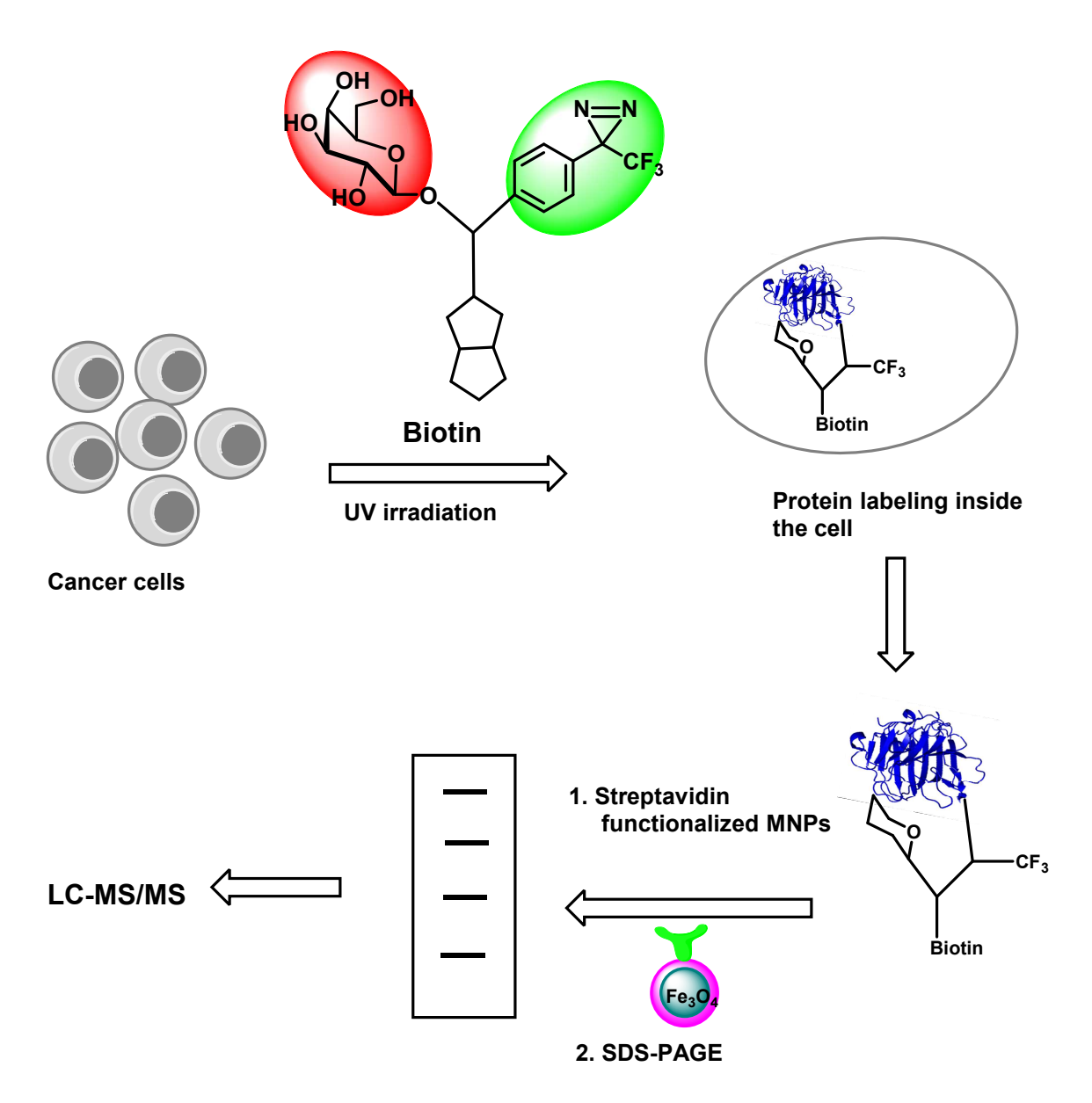


Figure 49: Lectin isolation from live cells using a carbohydrate affinity probe combinined with photoactivatable moiety

2.6: Experimental Section

2.6.1: Materials and instrumentation

All chemicals were reagent grade and were used as received from the manufacturer unless otherwise indicated. Iron (III) chloride hexahydrate (FeCl₃.6H₂O) was purchased from Honeywell Riedel-de Haen, Iron (II) chloride tetrahydrate (FeCl₂.4H₂O), polyvinylpyrrolidone (PVP), fetal bovine serum (FBS), phosphate buffered saline (PBS), high glucose Dulbecco's modified Eagle medium (DMEM), Fluorescein isothiocyanate labeled Concanavalin A (FITC, Con A) from Canavalia ensiformis, tetramethyl-rhodamine-isothiocyanate labeled lectin from Bandeiraea simplicifolia (TRITC-BS-I), HEPES, phenylmethanesulfonyl fluoride (PMSF), inhibitor cocktail. sodium sulfate N,N,N',N'protease dodecyl (SDS), tetramethylethylenediamine (TEMED), Tween-20, Triton X-100, reduced gluthathione, sodium azide (NaN₃) were purchased from Sigma Aldrich. Fluorescein isothiocyanate labeled annexin V was purchased from SouthernBiotech Aposcreeen. Chemiluminescent HRP antibody detection reagent was purchased from Denville Scientific Inc. Ammonium hydroxide was purchased from Scientific, tetraethoxy-silane (TEOS), aminopropyl triethoxysilane (APTES), Fisher dithiothreitol (DTT), iodoacetamide were purchased from Acros. Benotriazole-1-yl-oxy-tris-(dimethlyamino)-phosphonium hexafluorophosphate (BOP) was purchased from Peptides International, while hydroxybenzotriazole (HOBt) was purchased from Chem Impex International. Sodium chloride (NaCl), potassium chloride (KCl), sodium thiosulfate (Na₂S₂O₃), calcium chloride (CaCl₂) were purchased from CCI. Sodium carbonate (Na₂CO₃), ammonium bicarbonate (NH₄HCO₃) were purchased from Jade Scientific. Piperazine di-hydrochloride monohydrate was purchased from Alfa Aesar. Immobilized gluthathione beads were purchased from Thermo Scientific. Carboxylic acid functionalized magnetic micro-particle with mean diameter of 3.13 µm was purchased from Bangs Laboratories, Inc.

B16F10 and B16F1 melanoma cancer cell lines were purchased from American Type Culture Collection (ATCC). L-glutamine, streptomycin, and penicillin were purchased from Gibco. UltraPure Tris, ethylenediaminetetracetic acid (EDTA), and UltraPure glycine were purchased from Invitrogen. 30% Acrylamide/0.8% bisacrylamide solution and ammonium persulphate were purchased from BioRad. Sequencing grade modified porcine trypsin was purchased from Promega. Isopropyl-β-D-thiogalactopyranoside (IPTG) was bought from Research Organic, ampicillin from Roche, and chloramphenicol from United States Biochemical Corporation.

The purification of *Soybean agglutinin* (SBA) and the generation and characterization of anti-SBA antibodies have been previously reported.³⁰ The constructs for the expression of proteins from pGEX vectors (Pharmacia), including gluthatione S-transferases (GST), gluthatione S-transferases fused galectin-3 (GST-Gal3), and rabbit polyclonal antibody reagents against GST and Gal3 have also been described.³⁵ The pGEX vector for the expression of Sfrs1was a kind gift of Dr. Benoit Chabot (Universite de Sherbrooke, Sherbrooke, Quebec, Canada).⁶⁰ Polyclonal antibodies directed against Sfrs1 (rabbit) and Sfrs5 (mouse) were purchased from Novus Biologicals. Mouse monoclonal anti-glyceraldehyde 3-phosphate dehydrogenase (GAPDH) was purchased from Biodesign. *E. coli* BL-21 codon plus (DE3) cells were from Stratagene.

Zeta potential was performed on a Zetasizer Nano zs apparatus (Malvern, UK), Fourier Transform Infrared Spectroscopy (FT-IR) was carried out on a Mattson spectrometer, Galaxy series, FTIR 3000, Thermogravimetric Analysis (TGA) was carried out on a Thermal advantage

(TA-Instruments-Waters LLC) TGA-Q500 series while Transmission Electron Microscope (TEM) was carried on a JEOL JEM-2200FS. Inductively coupled plasma (ICP) analysis was carried out on Varian 710-ES Axial ICP-OES.

2.6.2: Synthesis and characterization of iron oxide magnetic glyconanoparticles

Gal-NP, Man-NP, and TEOS-NP were prepared following previously reported procedures. Priefly, a solution of iron (III) chloride hexahydrate, FeCl₃.6H₂O (20.01 mmol, 5.41 g, 5ml), iron (II) chloride tetrahydrate, FeCl₂.4H₂O (10.01 mmol, 2.00 g, 2.5 ml), 28 % ammonium hydroxide (20 ml) and polyvinylpyrrolidone (PVP) (0.0256 g/ml, 0.65 ml) were stirred for one hour at 80 °C. The resulting black precipitate (nanoparticles) was isolated by an external magnet and washed with deionized water (DI) and ethanol. The nanoparticles were coated with silica by reacting with tetraethoxy-silane (TEOS) (4.50 mmol, 1.0 ml) in 2-propanol:water (4:1 v/v, 150 ml) and ammonium hydroxide (0.2 % v/v, 0.3 ml) for 1 hour to yield silica coated magnetic nanoparticles (TEOS-NP). To prepare amine functionalized nanoparticle, TEOS-NP was suspended in ethanol (150 ml), sonicated for 30 minutes and reacted with aminopropyl triethoxysilane (APTES) (2 % w/v, 12.8 mmol, 3.0 mL) at 60 °C for 18 hours. The resulting amine functionalized nanoparticles (APTES-NP) were isolated by an external magnet, washed with deionized water and ethanol, and dried under a vacuum pump.

Mannose and galactose monosaccharide with carboxylic acid linkers were synthesized following reported procedures.²³ They were conjugated to the APTES-NP by amide bond formation using BOP and HOBt coupling chemistry to generate Gal-NP and Man-NP respectively. The resulting carbohydrate functionalized NP were characterized by Zeta potential,

FT-IR, TGA, TEM, and fluorescent labeled plant lectin binding studies as described previously.^{23,24}

To confirm that the immobilized carbohydrate preserved its biological recognition ability, magnetic glyco-NP lectin binding studies were carried out as reported.²⁴ FITC labeled Con A (a mannose selective lectin) and TRITC labeled BSI (a galactose selective lectin) were used. Fluorescent labeled lectins (4 mg) were dissolved in 0.1 M NaHCO₃ solution (40 mL) to obtain 100 ug/mL lectin solution. The lectin solutions were incubated with their respective glyco-NP or with TEOS-NP 1 at 4 °C for 12 hours. A magnetic field was applied to the mixture inducing aggregation of NPs on the side of the vial. The supernatant was carefully pipetted out and the residual fluorescence of the supernatant was recorded. If the NPs could bind the lectin, removal of the fluorescence lectin from the solution would lead to a reduction of fluorescent intensity of the supernatant.

2.6.3: Lysate preparation

Lysate was prepared following reported procedures with slight modifications.⁶¹ Briefly, B16F10 melanoma cell line was cultured in 100 mm cell culture plates at 37 °C and 5% carbon dioxide in a high glucose DMEM growth medium supplemented with 10% FBS, 1% L-glutamine, and 1% streptomycin penicillin. At 80% confluence (approximately six million cells), the growth medium was removed and the cells were washed with PBS. 300 μL of low salt homogenization buffer (20 mM Hepes-NaOH pH 7.4, 0.2 mM EDTA pH 8.0, 1 mM PMSF, Protease inhibitor cocktail) was added. Cells were scraped and collected in a 1.5 mL microcentrifuge tube. Another 300 μL of low salt homogenization buffer was added to the dish, scraped again and pooled with the first fraction in the microcentrifuge tube. The cells were incubated on ice for 5 minutes and then subject to 10 strokes in a tight-fitting Dounce

homogenizer. Equal volume of high salt homogenization buffer (300 mM NaCl, 200 mM Hepes-NaOH pH 7.4, 0.2 mM EDTA, 1 mM DTT, 1 mM PMSF, Protease inhibitor cocktail) was added in the homogenizer followed by 10 additional strokes. The cell homogenate was centrifuged at 1000 g for 10 minutes at 4 °C and supernatant was collected.

2.6.4: Silver staining, Coomassie blue staining, and Western blot

2.6.4.1: Silver staining

Silver staining protocols⁶² were followed. Briefly, the proteins were resolved on a non-reducing 12% SDS-PAGE. The gel was fixed overnight at room temperature in 50% methanol, 12% acetic acid and 0.05% formaldehyde in deionized water. The gel was washed with 50% ethanol (3 times 20 minutes each) then pretreated in freshly made Na₂S₂O₃.5H₂O (0.2 g/L) for 1 minute. After washing thoroughly with deionized water, the gel was impregnated in freshly prepared silver nitrate-formaldehyde solution (0.2 g AgNO₃ + 75 μ L of 37% formaldehyde in 100 mL of water) for 20 minutes, washed with deionized water and developed in freshly prepared solution of Na₂CO₃ (60 g), Na₂S₂O₃.5H₂O (25 mg) and 37% formaldehyde (500 μ L) in 1 liter. Once the bands were visible, the staining was stopped by immersing the gel in a solution consisting 50% methanol and 12% acetic acid for 10 minutes followed by washing in 50% methanol for 30 minutes.

2.6.4.2: Coomassie blue staining

The proteins were resolved on a 12% SDS-PAGE after which the gel was fixed overnight at room temperature in 40% methanol, 7% acetic acid in deionized water. The fixing solution was discarded and 1X working solution of brilliant blue G-colloidal concentrate (16%)

concentrate, 20% methanol and 64% deionized water) added, and rocked for at least two hours. The staining chamber was tilted to check if protein bands of interest were visible; if not, the staining was allowed to proceed for a longer time till the bands were visible. The staining solution was recycled, and wash solution #1 (10% acetic acid, 25% methanol and 65% deionized water) was added and washed for 30 seconds. Wash solution #2 (25% acetic acid, 75% deionized water) was added and washed for 5 minutes. This procedure was repeated until the gel background was clear and protein bands clearly visible.

2.6.4.3: Western blot

After gel electrophoresis, the proteins were electrophoretically transferred onto Immun-Blot PVDF membrane (Bio-RAD). 63 The PVDF membrane and the gel were briefly equilibrated in the transfer buffer (25 mM Tris, 193 mM glycine, and 20% methanol) and put into the transfer cassette. After the transfer the membrane was blocked overnight in 10% Spartan dry milk in Tris-buffered saline containing Tween 20, pH 7.6 (50 mM Tris, 0.5M NaCl, 0.02% Tween 20, (T-TBS)) and rocked overnight at room temperature. Finally the membrane was incubated with primary antibody followed by HRP-conjugated secondary antibody and the proteins visualized using chemiluminescence HRP detection reagent in the dark room. Antibodies for immunoblotting were diluted in T-TBS containing 1% Spartan dry milk. Primary antibodies, rabbit anti-Gal-3, rabbit anti-Sfrs1, rabbit anti-Sfrs5 and rabbit anti-SBA were used at a 1:1000 dilution while secondary antibody, horseradish peroxidase-conjugated goat anti-rabbit IgG at 1:10000 dilution.

2.6.5: Isolation of endogenous and exogenous lectins

For endogenous lectin, 300 µL of lysate was transferred into 1.5 mL microcentrifuge tube and the volume brought to 450 µL with buffer D+ (Buffer D: 10 mM HEPES, pH 7.9, 20%) glycerol, 0.1 M KCl, 0.2 mM EDTA, 0.5 mM PMSF, 0.5 mM DTT, D+: 60% Buffer D and 40% H₂O). 50 μL was saved and the rest was incubated with 0.5 mg Gal-NP for 2 hrs at 4 °C. After 2 hrs, magnetic batch separation of the nanoparticles was carried out using a magnetic separator (Dexter Magnetic LifeSep 50SX). The field gradient at full field is approximately 23.3 T/m. The separation process involved the placement of the tube containing the magnetic sample in the magnetic separator. After 15 minutes, the initially homogeneous solution became heterogeneous and a black deposit forms on the back wall where the gradient field is the highest. The supernatant which contained unbound fraction was saved. NP were washed 3 times with buffer D+ followed by sequential elution with 250 µL of 0.5 M mannose solution, and 0.5 M galactose solution. The saved fraction (5 μ L), supernatant (5 μ L), wash fraction (10 μ L) and the eluted fraction (10 µL each) were resolved on 12% cross-linked SDS-PAGE followed by blotting for Gal-3. As a control, the same experiment as above was repeated using Man-NP and TEOS-NP. For exogenous lectin, 500 µL of lysate was spiked with 10 µL (5 mg/mL); Soybean agglutinin (SBA), a galactose binding plant lectin in a 1.5 mL Eppendorf tube and the volume brought to 1000 μL with buffer D+. 50 μL was saved and the rest incubated with 0.5 mg Gal-NPs for 2 hrs at 4 °C After 2 hrs, magnetic separation was done and the supernatant which contained unbound fraction was saved. NPs were washed 3 times with buffer D+ followed elution by with 500 µL, 0.5 M galactose solution. The saved fraction (10 μ L), supernatant (10 μ L), wash fraction (5 μ L) and the elution fraction (5 µL) were resolved on 12% cross-linked SDS-PAGE followed by blotting for SBA and Gal3.

2.6.6: Isolation of lectins after binding Gal-NP to intact cells

Cells were cultured and at 80% confluence (approximately six million cells), the growth media was removed and the cells were washed with PBS. 10 mL of 100 µg/mL of Gal-NP in serum free DMEM medium was added and the cells incubated with the NP for 12 hr at 37 °C, 5% CO₂ incubator. The cell lysate was prepared either by Triton X-100 based lysis buffer or homogenization in a dounce homogenizer. For Triton X-100 based lysis buffer, the media was aspirated out and cells washed 3 times with PBS (0.5 mL) to remove any unbound nanoparticles. 500 μL lysis buffer (0.1% Triton X-100, 75 mM Tris, pH 7.2, 55 mM CaCl₂, 10 mM NaN₃, PMSF and protease inhibitor) was added and rocked at 4°C for 20 minutes). The lysate was transferred into a 1.5 mL microcentrifuge tube and subjected to magnetic separation to separate the supernatant from nanoparticles. The supernatant contained proteins that did not bind to nanoparticles. In the homogenization protocol, the procedures described in the lysate preparation section were followed. The lysate was transferred into a 1.5 mL microcentrifuge tube and subjected to magnetic separation. The nanoparticles were washed 3 times with PBS followed by sequential elution with 0.5M mannose solution and 0.5M galactose solution. The supernatant, PBS wash fraction, mannose and galactose eluted fractions were resolved by SDS-PAGE and protein bands visualized through silver and Coomassie staining.

2.6.7: LC/MS/MS

After SDS-PAGE, the gel was stained with Coomassie Brilliant Blue G (Brilliant Blue G colloidal concentrate). Protein bands of interest were excised from the gel and subjected to tryptic digestion according to reported procedures with slight modifications.⁶⁴ Briefly, gel slices

were dehydrated using 100% acetonitrile and incubated with 10 mM dithiothreitol in 100 mM ammonium bicarbonate, pH~8, at 56 °C for 45 min, dehydrated again and incubated in the dark with 50 mM iodoacetamide in 100 mM ammonium bicarbonate for 20 min. Gel slices were then washed with ammonium bicarbonate and dehydrated again. Sequencing grade modified typsin was prepared to 0.01 μg/μL in 50 mM ammonium bicarbonate and ~50 μL of this was added to each gel band so that the gel was completely submerged. Bands were then incubated at 37 °C overnight. Peptides were extracted from the gel by water bath sonication in a solution of 60% acetonitrile, 1% trifluoroacetic acid and vacuum dried to ~2 μL. Peptides were then re-suspended in 2% acetonitrile, 0.1% trifluoroacetic acid to 20 µL and submitted for proteomic analysis. From this, 10 µL were injected by a Waters nanoAcquity Sample Manager (www.waters.com) and loaded for 5 minutes onto a Waters Symmetry C18 peptide trap (5 µm, 180 µm x 20 mm) at 4 μL/min in 5% acetonitrile, 0.1% formic Acid. The bound peptides were then eluted onto a Waters BEH C18 nanoAcquity column (1.7µm, 100 µm x 100mm) over 16 minutes with a gradient of 5% B to 30% B in 9 min using a Waters nanoAcquity ultra performance liquid chromatography (UPLC) (Buffer A = 99.9% water/0.1% formic acid, Buffer B = 99.9% acetonitrile/0.1% formic acid) with an initial flow rate of 1 µL/min.

Eluted peptides were sprayed into a ThermoFisher LTQ Linear Ion trap mass spectrometer outfitted with a MICHROM Bioresources advance nano-spray source. The top five ions in each survey scan were then subjected to data-dependant zoom scans followed by low energy collision induced dissociation (CID) and the resulting MS/MS spectra are converted to peak lists using BioWorks Browser v 3.3.1 (ThermoFisher) using the default LTQ instrument parameters. Peak lists were searched against the SwissProt mouse protein sequence database, using the Mascot searching algorithm, v2.4 (www.matrixscience.com). The Mascot output was

then analyzed using Scaffold, v3.6.5 (www.proteomesoftware.com) to probabilistically validate protein identifications using the ProteinProphet computer algorithm. Assignments validated above the Scaffold 95% confidence filter are considered true. Mascot parameters for all databases were as follows: allow up to 2 missed tryptic sites, fixed modification of carbamidomethyl cysteine, variable modification of oxidation of methionine, MS/MS tolerance of 0.6 Da, and peptide charge state limited to +2/+3.

2.6.8: Binding of GST and GST fused proteins to Gal-NP

GST-Sfrs1 was expressed and purified as a fusion protein with glutathione S-transferase (GST) in the same fashion as the method reported previously for the preparation of GST-Gal3 ³⁵ with modifications. Briefly, the E-coli strain BL21(DE3) carrying GST-Sfrs1 plasmid was grown in LB (10 g/L tryptone, 5 g/L yeast extract, 5 g/L NaCl) containing 100 μg/mL ampicillin and 34 chloramphenicol followed by induction with 0.1 μg/mL mM isopropyl-β-Dthiogalactopyranoside for 3 hrs at 37 °C. Cells were then centrifuged, the pellet was resuspended in lysis buffer (20 mM piperazine-HCl, pH 9.5, 0.5 M NaCl, 1 mM DTT, 1 mM PMSF, and protease inhibitor cocktail. Lysozyme was added to a final concentration of 100 mg/L followed by incubation on ice for 30 min. The cells were lysed using a probe sonicator, carefully avoiding foaming the sample. Triton X-100 was added to a final concentration of 1% and the sample rocked for 30 mins at 4 °C. The lysate was centrifuged at 10000 rpm for 10 min at 4 °C and the supernatant was purified on the basis of GST binding to glutathione agarose beads (Thermo Scientific). First, the supernatant was incubated with glutathione agarose beads at 4 °C for 2 hrs. centrifuged at 500g for 2 min to remove the unbound protein, washed 4 times with lysis buffer and thereafter transferred into a column. The bound protein was eluted from the glutathione column with the lysis buffer containing 20 mM reduced glutathione.

In the experiment to test the binding of GST-Sfrs1 to Gal-NP, 300 μ g of Gal-NP, corresponding to 11.4 μ g, 6.36 x 10⁻⁸ mol of immobilized galactose was incubated with 380 ng of GST-Sfrs1 for 30 min at 4 $^{\circ}$ C in the presence of 60% buffer D+. Magnetic separation was performed to isolate the supernatant and saved as unbound fraction (UF). The nanoparticles were washed 3 times with 100 μ L buffer D, and saved as wash fraction (WF). The nanoparticles were then solubilized in 40 μ L of sample loading buffer (contains 1% SDS) to dissociate the bound protein, followed by magnetic separation to isolate the bound fraction (BF) from nanoparticles. Same experiment was repeated with GST (negative control) and GST-Gal3 (positive control). The UF, WF and BF of GST, GST-Gal3 and GST-Sfrs were subjected to SDS-PAGE analysis and blotted for GST, Gal3 and Sfrs1 respectively.

To test for the binding specificity of Sfrs1 to Gal-NP, 12 μL (10 μg of GST-Sfrs1) was added to 490 μL of buffer D (500 μL total volume). 20 μL was saved and the remaining (480 μL) was incubated with 500 μg of Gal-NP, corresponding to 19 μg, 1.05 x 10⁻⁷ mol of immobilized galactose at 4 °C for 1 hr. Magnetic separation was performed to isolate the supernatant and saved as unbound fraction (UF). The nanoparticles were washed 3 times with 100 μL buffer D, and saved as wash fraction (WF). The bound protein was eluted with 0.5 M mannose solution followed by 0.5 M galactose solution and saved as eluted fraction (EF). The saved fraction, UF, WF, and eluted fractions was subjected to SDS-PAGE analysis and blotted for Sfrs1. As a negative control, the same experiment was repeated using TEOS-NP.

2.6.9: Comparison of Sfrs1 from F10 and F1 using Gal-NP

Using Gal-NP, the amount of Sfrs1 in B16F10 was compared to that in B16F1. Each cell line, seeded at a density of 2.5 x 10⁵ cells/cm² in 60 x 15 mm dishes, was cultured at 37 °C, 5% CO₂ overnight. The growth media was removed and the cells were washed with 3 times with PBS (2 mL). 4 mL of 100 μg/mL of Gal-NPs (400 μg NP, corresponding to 15 μg, 8.48 x 10⁻⁸ mol of immobilized galactose) in serum free DMEM medium was added and the cells incubated with the NP for 12 hr at 37 °C, 5% CO₂ incubator. The medium was aspirated out and cells washed 3 times with PBS (2 mL) to remove any unbound nanoparticles. Cells were lysed using Triton X-100 lysis buffer as described above. The lysate was transferred into a 1.5 mL microcentrifuge tube and subjected to magnetic separation. The nanoparticles were washed 3 times with PBS followed by sequential elution with 0.5M mannose solution and 0.5M galactose solution. Only galactose eluted fractions were subjected to SDS-PAGE analysis and blotted for Sfrs1 as we were interested in Sfrs1 that was specifically bound to Gal-NP.

The amounts of Sfrs1 in B16F10 and B16F1 were compared in a quantitative experiment. Cell lysate was prepared from equal amount of B16F10 or B16F1 cells (5 x 10⁵ cells were used). Equal volumes of the two lysates was resolved by SDS-PAGE and blotted for Sfrs1 and the amount of Sfrs1 represented by the band intensity was quantified using ImageJ software.

2.6.10: Quantification of Western blot protein gel band using ImageJ software

The quantification process follows the Beer - Lambert's law, i.e., the band intensity is proportional to the protein concentration. First, the protein band intensities were measured as areas and converted to percentage of the total area of the measured peaks following procedures described in the ImageJ user guide.⁶⁵ This area was taken to represent arbitrary units of protein

contained in the volume of the sample that was loaded on the SDS-PAGE. Total amount of protein was obtained by taking into account the total volume for each fraction. The fraction 'before Gal-NP' was taken to represent the total protein present before depletion with Gal-NP, and therefore the percentage protein was calculated using this value as the base value.

REFERENCES

REFERENCES

- (1) Lee, Y. C.; Lee, R. T., Carbohydrate-protein interactions basis of glycobiology. *Acc. Chem. Res.*, **1995**, *28*, 321-327.
- (2) Hebert, E., Endogenous lectins as cell surface transducers. *Biosci. Rep.*, **2000**, *20*, 213-237.
- (3) Lorenzon, P.; Vecile, E.; Nardon, E.; Ferrero, E.; Harlan, J. M.; Tedesco, F.; Dobrina, A., Endothelial cell E- and P-selectin and vascular cell adhesion molecule-1 function as signaling receptors. *J.Cell Biol.*, **1998**, *142*, 1381-1391.
- (4) Zanetta, J. P.; Badache, A.; Maschke, S.; Marschal, P.; Kuchler, S., Carbohydrates and soluble lectins in the regulation of cell-adhesion and proliferation. *Histolo. Histopathol.*, **1994**, *9*, 385-412.
- (5) Sato, S., Galectins as molecules of Danger signal, which could evoke an immune response to infection. *Trends Glycosci. Glyc.*, **2002**, *14*, 285-301.
- (6) Virginia Tribulatti, M.; Gabriela Figini, M.; Carabelli, J.; Cattaneo, V.; Campetella, O., Redundant and antagonistic functions of galectin-1,-3, and-8 in the elicitation of T-cell responses. *J. Immunol.*, **2012**, *188*, 2991-2999.
- (7) Spear, G. T.; Zariffard, M. R.; Xin, J.; Saifuddin, M., Inhibition of DC-SIGN-mediated trans infection of T cells by mannose-binding lectin. *Immunology*, **2003**, *110*, 80-85.
- (8) Chemani, C.; Imberty, A.; de Bentzmann, S.; Pierre, M.; Wimmerova, M.; Guery, B. P.; Faure, K., Role of LecA and LecB lectins in Pseudomonas aeruginosa-induced lung injury and effect of carbohydrate ligands. *Infect. Immun.*, **2009**, *77*, 2065-2075.
- (9) Liu, F. T.; Rabinovich, G. A., Galectins as modulators of tumour progression. *Nat. Rev. Cancer*, **2005**, *5*, 29-41.
- (10) Danguy, A.; Camby, I.; Kiss, R., Galectins and cancer. *BBA-Gen. Subjects*, **2002**, *1572*, 285-293.
- (11) Krause, T.; Turner, G. A., Are selectins involved in metastasis? *Clin. Exp. Metastasis*, **1999**, *17*, 183-192.
- (12) Hebert, E., Mannose-6-phosphate/Insulin-like growth factor II receptor expression and tumor development. *Biosci. Rep.*, **2006**, *26*, 7-17.
- (13) Foulstone, E.; Prince, S.; Zaccheo, O.; Burns, J. L.; Harper, J.; Jacobs, C.; Church, D.; Hassan, A. B., Insulin-like growth factor ligands, receptors, and binding proteins in cancer. *J. Pathol.*, **2005**, *205*, 145-153.

- (14) Hill, A.; McFarlane, S.; Johnston, P. G.; Waugh, D. J. J., The emerging role of CD44 in regulating skeletal micrometastasis. *Cancer Lett.*, **2006**, *237*, 1-9.
- (15) La Belle, J. T.; Gerlach, J. Q.; Svarovsky, S.; Joshi, L., Label-free impedimetric detection of glycan-lectin interactions. *Anal. Chem.*, **2007**, *79*, 6959-6964.
- (16) Sanford, J. R.; Coutinho, P.; Hackett, J. A.; Wang, X.; Ranahan, W.; Caceres, J. F., Identification of nuclear and cytoplasmic mRNA targets for the shuttling protein SF2/ASF. *PLoS One*, **2008**, *3*, e3369.
- (17) Chou, P. H.; Chen, S. H.; Liao, H. K.; Lin, P. C.; Her, G. R.; Lai, A. C. Y.; Chen, J. H.; Lin, C. C.; Chen, Y. J., Nanoprobe-based affinity mass spectrometry for selected protein profiling in human plasma. *Anal. Chem.*, **2005**, *77*, 5990-5997.
- (18) Samra, Z. Q.; Athar, M. A., Novel synthesis of mannosamine conjugated magnetic nanoparticles for purification and stabilization of human lysosomal beta-mannosidase. *Biotechnol. Bioproc. Eng.*, **2009**, *14*, 651-661.
- (19) Chen, Y. J.; Chen, S. H.; Chien, Y. Y.; Chang, Y. W.; Liao, H. K.; Chang, C. Y.; Jan, M. D.; Wang, K. T.; Lin, C. C., Carbohydrate-encapsulated gold nanoparticles for rapid target-protein identification and binding-epitope mapping. *Chembiochem*, **2005**, *6*, 1169-+.
- (20) Hung, T.-C.; Lin, C.-W.; Hsu, T.-L.; Wu, C.-Y.; Wong, C.-H., Investigation of SSEA-4 binding protein in breast cancer cells. *J. Am. Chem. Soc.*, **2013**, *135*, 5934-5937.
- (21) Zhou, L.; Wu, J.; Zhang, H.; Kang, Y.; Guo, J.; Zhang, C.; Yuan, J.; Xing, X., Magnetic nanoparticles for the affinity adsorption of maltose binding protein (MBP) fusion enzymes. *J. Mater. Chem.*, **2012**, *22*, 6813-6818.
- (22) Ferreira, J. A.; Daniel-da-Silva, A. L.; Alves, R. M. P.; Duarte, D.; Vieira, I.; Santos, L. L.; Vitorino, R.; Amado, F., Synthesis and optimization of lectin functionalized nanoprobes for the selective recovery of glycoproteins from human body fluids. *Anal. Chem.*, **2011**, *83*, 7035-7043.
- (23) El-Boubbou, K.; Gruden, C.; Huang, X., Magnetic glyco-nanoparticles: A unique tool for rapid pathogen detection, decontamination, and strain differentiation. *J. Am. Chem. Soc.*, **2007**, *129*, 13392-+.
- (24) El-Boubbou, K.; Zhu, D. C.; Vasileiou, C.; Borhan, B.; Prosperi, D.; Li, W.; Huang, X., Magnetic glyco-nanoparticles: A tool to detect, differentiate, and unlock the glycocodes of cancer via magnetic resonance imaging. *J. Am. Chem. Soc.*, **2010**, *132*, 4490-4499.
- (25) Xu, C. J.; Xu, K. M.; Gu, H. W.; Zhong, X. F.; Guo, Z. H.; Zheng, R. K.; Zhang, X. X.; Xu, B., Nitrilotriacetic acid-modified magnetic nanoparticles as a general agent to bind histidine-tagged proteins. *J. Am. Chem. Soc.*, **2004**, *126*, 3392-3393.
- (26) Marradi, M.; Chiodo, F.; Garcia, I.; Penadés, S., Glyconanoparticles as multifunctional and multimodal carbohydrate systems. *Chem. Soc. Rev.*, **2013**, *42*, 4728-4745.

- (27) El-Boubbou, K.; Huang, X., Glyco-nanomaterials: Translating insights from the "sugar-code" to biomedical applications. *Curr. Med. Chem.*, **2011**, *18*, 2060-2078.
- (28) Nakamura-Tsuruta, S.; Kishimoto, Y.; Nishimura, T.; Suda, Y., One-Step Purification of Lectins from Banana Pulp Using Sugar-Immobilized Gold Nano-Particles. *J. Biochem.*, **2008**, *143*, 833-839.
- (29) Carrizales Alvarez, S. A.; Ilyina, A.; Gregorio Jauregui, K. M.; Martinez Hernandez, J. L.; Vazquez Gutierrez, B. B.; Segura Ceniceros, E. P.; Cruz, A. Z.; Caballero, H. S.; Lopez Campos, R. G., Isolation and immobilization of influenza virus-specific N-SA-alpha-2,3-gal receptors using magnetic nanoparticles coated with chitosan and maackia amurensis lectin. *Appl. Biochem. Biotechnol.*, **2014**, *174*, 1945-1958.
- (30) Malek-Hedayat, S.; Meiners, S. A.; Metcalf, T. N.; Schindler, M.; Wang, J. L.; Ho, S. C., Endogenous lectin from cultured soybean cells chemical characterization of the lectin of SB-1 cells. *J. Biol. Chem.*, **1987**, *262*, 7825-7830.
- (31) Wang, Y.-G.; Kim, S.-J.; Baek, J.-H.; Lee, H.-W.; Jeong, S.-Y.; Chun, K.-H., Galectin-3 increases the motility of mouse melanoma cells by regulating matrix metalloproteinase-1 expression. *Exp. Mol. Med.*, **2012**, *44*, 387-393.
- (32) Braeuer, R. R.; Zigler, M.; Kamiya, T.; Dobroff, A. S.; Huang, L.; Choi, W.; McConkey, D. J.; Shoshan, E.; Mobley, A. K.; Song, R.; Raz, A.; Bar-Eli, M., Galectin-3 contributes to melanoma growth and metastasis via regulation of NFAT1 and autotaxin. *Cancer Res.*, **2012**, *72*, 5757-5766.
- (33) Roff, C. F.; Wang, J. L., Endogenous lectins from cultured-cells isolation and characterization of carbohydrate-binding proteins from 3T3-fibroblasts. *J. Biol. Chem.*, **1983**, 258, 657-663.
- (34) Rix, U.; Superti-Furga, G., Target profiling of small molecules by chemical proteomics. *Nat. Chem. Biol.*, **2009**, *5*, 616-624.
- (35) Voss, P. G.; Gray, R. M.; Dickey, S. W.; Wang, W.; Park, J. W.; Kasai, K.-i.; Hirabayashi, J.; Patterson, R. J.; Wang, J. L., Dissociation of the carbohydrate-binding and splicing activities of galectin-1. *Arch. Biochem. Biophys.*, **2008**, *478*, 18-25.
- (36) Park, S.; Lee, M.-R.; Shin, I., Fabrication of carbohydrate chips and their use to probe protein-carbohydrate interactions. *Nat. Protoc.*, **2007**, *2*, 2747-2758.
- (37) Hatakeyama, S.; Sugihara, K.; Nakayama, J.; Akama, T. O.; Wong, S.-M. A.; Kawashima, H.; Zhang, J.; Smith, D. F.; Ohyama, C.; Fukuda, M.; Fukuda, M. N., Identification of mRNA splicing factors as the endothelial receptor for carbohydrate-dependent lung colonization of cancer cells. *Proc. Natl. Acad. Sci. USA*, **2009**, *106*, 3095-3100.
- (38) Sinha, R.; Allemand, E.; Zhang, Z.; Karni, R.; Myers, M. P.; Krainer, A. R., Arginine methylation controls the subcellular localization and functions of the oncoprotein splicing factor SF2/ASF. *Mol. Cell. Biol.*, **2010**, *30*, 2762-2774.

- (39) Caceres, J. F.; Screaton, G. R.; Krainer, A. R., A specific subset of SR proteins shuttles continuously between the nucleus and the cytoplasm. *Genes Dev.*, **1998**, *12*, 55-66.
- (40) Sanford, J. R.; Gray, N. K.; Beckmann, K.; Caceres, J. F., A novel role for shuttling SR proteins in mRNA translation. *Genes Dev.*, **2004**, *18*, 755-768.
- (41) Haudek, K. C.; Patterson, R. J.; Wang, J. L., SR proteins and galectins: what's in a name? *Glycobiology*, **2010**, *20*, 1199-1207.
- (42) Moutsatsos, I. K.; Davis, J. M.; Wang, J. L., Endogenous lectins from cultured-cells isolation and characterization of carbohydrate-binding proteins from 3T3-fibroblasts. *J. Cell Biol.*, **1986**, *102*, 477-483.
- (43) Moutsatsos, I. K.; Wade, M.; Schindler, M.; Wang, J. L., Endogenous lectins from cultured-cells nuclear-localization of carbohydrate-binding protein 35 in proliferating 3T3-fibroblasts. *Proc. Natl. Acad. Sci. USA*, **1987**, *84*, 6452-6456.
- (44) Voss, P. G.; Haudek, K. C.; Patterson, R. J.; Wang, J. L., Inhibition of cell-free splicing by saccharides that bind galectins and SR proteins. *J. Carbohyd. Chem.*, **2012**, *31*, 519-534.
- (45) Vyakarnam, A.; Dagher, S. F.; Wang, J. L.; Patterson, R. J., Evidence for a role for galectin-1 in pre-mRNA splicing. *Mol. Cell. Biol.*, **1997**, *17*, 4730-4737.
- (46) Ghigna, C.; Giordano, S.; Shen, H.; Benvenuto, F.; Castiglioni, F.; Comoglio, P. M.; Green, M. R.; Riva, S.; Biamonti, G., Cell motility is controlled by SF2/ASF through alternative splicing of the Ron protooncogene. *Mol. Cell*, **2005**, *20*, 881-890.
- (47) Karni, R.; de Stanchina, E.; Lowe, S. W.; Sinha, R.; Mu, D.; Krainer, A. R., The gene encoding the splicing factor SF2/ASF is a proto-oncogene. *Nat. Struct. Mol. Biol.*, **2007**, *14*, 185-193.
- (48) Piekielko-Witkowska, A.; Wiszomirska, H.; Wojcicka, A.; Poplawski, P.; Boguslawska, J.; Tanski, Z.; Nauman, A., Disturbed expression of splicing factors in renal cancer affects alternative splicing of apoptosis regulators, oncogenes, and tumor suppressors. *PLoS ONE*, **2010**, *5*, e13690.
- (49) Moore, M. J.; Wang, Q.; Kennedy, C. J.; Silver, P. A., An alternative splicing network links cell-cycle control to apoptosis. *Cell*, **2010**, *142*, 625-636.
- (50) Kojima, K.; Yamamoto, K.; Irimura, T.; Osawa, T.; Ogawa, H.; Matsumoto, I., Characterization of carbohydrate-binding protein p33/41 Relation with annexin IV, molecular basis of the doublet forms (p33 and p41), and modulation for the carbohydrate binding activity phospholipids. *J. Biol. Chem.*, **1996**, *271*, 7679-7685.
- (51) Ishitsuka, R.; Kojima, K.; Utsumi, H.; Ogawa, H.; Matsumoto, I., Glycosaminoglycan binding properties of annexin IV, V, and VI. *J. Biol. Chem*, **1998**, *273*, 9935-9941.

- (52) Gao-Uozumi, C.-X.; Uozumi, N.; Miyoshi, E.; Nagai, K.; Ikeda, Y.; Teshima, T.; Noda, K.; Shiba, T.; Honke, K.; Taniguchi, N., A novel carbohydrate binding activity of annexin V toward a bisecting N-acetylglucosamine. *Glycobiology*, **2000**, *10*, 1209-1216.
- (53) Horlacher, T.; Noti, C.; de Paz, J. L.; Bindschaedler, P.; Hecht, M. L.; Smith, D. F.; Fukuda, M. N.; Seeberger, P. H., Characterization of annexin A1 glycan binding reveals binding to highly sulfated glycans with preference for highly sulfated heparan sulfate and heparin. *Biochemistry*, **2011**, *50*, 2650-2659.
- (54) Pradeepa, M. M.; Sutherland, H. G.; Ule, J.; Grimes, G. R.; Bickmore, W. A., Psip1/Ledgf p52 Binds Methylated Histone H3K36 and Splicing Factors and Contributes to the Regulation of Alternative Splicing. *PLoS Genet.*, **2012**, *8*, e1002717.
- (55) Long, L.; Thelen, J. P.; Furgason, M.; Haj-Yahya, M.; Brik, A.; Cheng, D.; Peng, J.; Yao, T., The U4/U6 Recycling Factor SART3 Has Histone Chaperone Activity and Associates with USP15 to Regulate H2B Deubiquitination. *J. Biol. Chem.*, **2014**, *289*, 8916-8930.
- (56) Song, L.; Mao, J.; Zhang, J.; Ibrahim, M. M.; Li, L.-H.; Tang, J.-W., Annexin A7 and its binding protein galectin-3 influence mouse hepatocellular carcinoma cell line in vitro. *Biomed. Pharmacother.*, **2014**, *68*, 337-384.
- (57) Yu, F.; Finley, R. L.; Raz, A.; Kim, H. R. C., Galectin-3 translocates to the perinuclear membranes and inhibits cytochrome c release from the mitochondria. A role for synexin in galectin-3 translocation. *J. Biol. Chem.*, **2002**, *277*, 15819-15827.
- (58) Wibowo, A.; Peters, E. C.; Hsieh-Wilson, L. C., Photoactivatable glycopolymers for the proteome-wide identification of fucose-alpha(1-2)-galactose binding proteins. *Journal of the American Chemical Society*, **2014**, *136*, 9528-9531.
- (59) Adak, A. K.; Li, B.-Y.; Huang, L.-D.; Lin, T.-W.; Chang, T.-C.; Hwang, K. C.; Lin, C.-C., Fabrication of antibody microarrays by light-induced covalent and oriented immobilization. *Acs Appl. Mater. Inter.*, **2014**, *6*, 10452-10460.
- (60) Paradis, C.; Cloutier, P.; Shkreta, L.; Toutant, J.; Klarskov, K.; Chabot, B., HnRNP I/PTB can antagonize the splicing repressor activity of SRp30c. *RNA*, **2007**, *13*, 1287-1300.
- (61) Liu, X.; Fagotto, F., A method to separate nuclear, cytosolic, and membrane-associated signaling molecules in cultured cells. *Sci. Signal.*, **2011**, *4*, 1-12.
- (62) Blum, H.; Beier, H.; Gross, H. J., Improved silver staining of plant-proteins, RNA and DNA in polyacrylamide gels. *Electrophoresis*, **1987**, *8*, 93-99.
- (63) Towbin, H.; Staehelin, T.; Gordon, J., Electrophoretic transfer of proteins from polyacrylamide gels to nitrocellulose sheets procedure and some applications. *Proc. Natl. Acad. Sci. USA*, **1979**, *76*, 4350-4354.

- (64) Shevchenko, A.; Wilm, M.; Vorm, O.; Mann, M., Mass spectrometric sequencing of proteins from silver stained polyacrylamide gels. *Anal. Chem.*, **1996**, *68*, 850-858.
 - (65) Ferreira, T.; Rasband, W., ImageJ user guide 1.46r. *IJ 1.46r*, **2012**.

CHAPTER 3: Acid responsive nanoparticle mediated antigen delivery for tumor immunotherapy

3.1: Abstract

Cytotoxic T lymphocyte (CTL) therapy has clinically shown the potential to treat cancer patients. For CTL therapy to be successful, cancers should express antigens that are targets for specific CTLs. However, it has been established that due to genetic instability of cancer cells, subpopulation of cancer cells may fail to express the target antigen, possibly leading to escape from CTL destruction, hence tumor grows progressively. These antigen-loss variant (ALV) cancer cells can be eliminated as bystanders by targeting tumor associated stromal cells, but only if the cancer cells express sufficient antigens to be effectively cross-presented by the stromal cells. Here, we investigated whether acid responsive nanoparticles can be used to deliver CTL-specific antigen to the cancer microenvironment to enhance tumor eradication by activated antigenspecific CTLs in a mouse model. Our results show that model CTL antigen (OVA peptide, SIINFEKL) encapsulated in pH sensitive acetalated dextran nanoparticles (OVA_(P)-Ac-Dx-NPs) could be successfully delivered to tumor cells in vitro and tumor microenvironment in vivo. The uptake and presentation of the peptide antigen by major histocompatibility molecules class I (MHC-I) in vitro and in vivo was confirmed by flow cytometry and confocal laser scanning microscopy through antibody staining. In addition, solid tumor bearing mice treated with OVA_(P)-Ac-Dx-NPs showed much slower tumor growth compared to mice treated with free OVA, empty Ac-Dx-NPs, or PBS. Taken together, these findings offer a promising new direction for treating established solid tumors using CTL therapy.

Keywords

Cytotoxic T lymphocytes (CTL), antigen, nanoparticles, cancer.

3.2: Introduction

Strategies aiming to stimulate the immune system to eradicate tumor cells are highly attractive for tumor prevention and therapy. Over the past few decades, new forms of cancer therapy have evolved that take advantage of unique or overexpressed cell surface antigens or receptors on tumor cells as therapeutic targets.¹ One such approach has been the use of neutralizing monoclonal antibodies to target some of these antigens or receptors, either alone or in combination with chemotherapeutic free drug or conjugate drug (antibody-drug conjugates).²⁻¹⁰ As such, antibody-based therapy for cancer has been successful and is an important strategy for treating patients with haematological malignancies and solid tumors.⁹

Besides antibody therapy, the use of immune system's cytotoxic T lymphocyte (CTL, generally CD8⁺ T cells) to eliminate tumor cells expressing CTL target antigens has been fronted as an alternative for cancer therapy. ¹¹ Each CTL expresses a unique T-cell-antigen receptor (TCR) that has specificity for a particular target antigen. The antigens recognized by CTLs consist of peptide fragments (usually 8-10 amino acids), which are bound within the major clefts of MHC-I molecules on the cell surface. The outcome of engagement of a TCR by complementary MHC-I/antigen complexes on the target-cell surface triggers the CTL's effector functions, which can result in the destruction of the target cell. CTLs can induce target cell destruction through the release of inflammatory cytokines, the induction of apoptosis inducing proteins, and cytotoxic degranulation, which lead to perforin mediated lysis. ^{11,12}

The efficacy of CTL therapy has been demonstrated through adoptive cell transfer (ACT), as pioneered by Rosenberg and coworker in treatment of metastatic tumors.¹³ Adoptive transfer involves isolation of highly active tumor specific T cells from tumor mass, referred to as tumor infiltrating lymphocytes (TIL).¹⁴ These T cells are activated and expanded *ex vivo* and

subsequently administered back into same patient with cytokines (IL-2, in order to increase the number of effector cells *in vivo*) with or without lymphodepletion.¹⁵⁻²⁰ Lymphodepletion leads to improved persistence and repopulation of T cells with the transferred cells proliferating *in vivo*, displaying functional activity, and trafficking to tumor sites.¹⁸ A drawback to this approach is the requirement that patients or experimental animals should have preexisting tumor-reactive cells that can be expanded *ex vivo*.¹⁵ In addition, it may be difficult to identify these tumor-reactive lymphocytes especially in some less accessible cancers than melanoma.²¹ A potential solution to this limitation was first reported by Morgan et al. when they demonstrated that normal human lymphocytes can be genetically engineered to recognize cancer antigens and mediate cancer regression *in vivo*.²¹ Collectively, reported results on adoptive transfer of tumor-specific CTL show it can mediate tumor regression and prevention of tumor outgrowth, both in clinical studies and animal models.

However, despite the success of adoptive T cells transfer, the existence of tumor reactive CD8+ T cells in the peripheral circulation of a patient or an experimental animal has not been sufficient to cause complete rejection of an established tumor.^{11,22} Relevant to the present work, rejection of tumor growth by activated T cells may fail due to down-regulation of CTL-recognized target antigen and antigen presenting MHC-I complex molecules by some sub-population of tumor cells.^{23,24} Since the MHC-I molecules are required for the presentation of antigens on tumor cells to the CTLs, the absence of MHC-I/antigen complex from the cell surface may lead to the escape of these tumors from immunosurveillance.²⁵ These tumor cells have been referred to as antigen loss variants (ALVs),²⁶ and they can be eliminated as bystanders by targeting the tumor stroma as reported by Schreiber and coworkers.²⁷ However, for indirect and rapid elimination of resistant ALVs to induce complete rejection of established tumors,

tumor cells should express sufficiently high levels of antigens to be locally cross-presented by the non-malignant tumor stromal cells.^{24,27-30} To determine the requirement of stromal cells to eliminated ALV, C3H *Rag2*^{-/-} mice in which the MHC molecules of the tumor stromal cells would not present the CTL specific model tumor antigen (SIYRYYGL, SIY peptide antigen), were inoculated with solid tumors, whose parental cancer cells had high levels of SIY antigen (SIY-2Hi). The study was compared to C57BL/6 *Rag1*^{-/-} mice in which the MHC molecules of the tumor stromal cells would present the SIY antigen. Whereas all C57BL/6 *Rag1*^{-/-} mice that received activated 2CT cells (SIY specific CTL) rejected SIY-2Hi tumors, all C3H *Rag2*^{-/-} mice that received activated 2CT cells did not. More importantly, cells recovered from tumors in C3H *Rag2*^{-/-} mice that received 2CT cells were ALVs. Thus, ALVs subpopulation of cancer cells present in SIY-2Hi tumors escaped when the stromal cells did not present the SIY antigen.²⁷

The rising challenge is how to present the tumor microenvironment to the immune system as a region with high concentrations of CTL antigens to make the tumor more susceptible for CTLs. Herein we propose the use of 'smart' nanoparticles that can selectively deliver the CTL specific antigen to the tumor microenvironment. Subsequent uptake will induce sensitization of tumor stroma leading to eradication of established tumors by CTLs. Tumor microenvironment presents several properties that make them distinguishable from their normal counterparts. One of these difference is variation in biological environmental stimuli. This has led to the development of 'intelligent' nanoparticle carrier systems that offer an alternative type of 'active targeting' delivery of therapeutics to tumors.³¹ One of the stimuli that stands out and has formed an area of active research in the past decades, presenting opportunities to design and construct potential cancer therapeutics is the pH.³² Compared to normal tissues (pH 7.4), the microenvironment of tumor tissues typically exhibit mildly acidic pH (~ pH 6.5-6.8). The low

pH has been implicated to favor cancer progression by promoting proliferation, the evasion of apoptosis, metabolic adaptation, migration, and invasion.³³ Owing to this unusual acidity of the tumor extracellular microenvironment, several pH-responsive nano-systems have been reported that are capable of increasing the efficacy of tumor therapy.³⁴

We are interested in pH responsive 'smart' nanoparticles that can encapsulate, deliver, and control the release of CTL-specific antigen at the tumor site, based on intrinsic differences in the pH between tumor and normal tissues.^{35,36} This nanoparticle should remain stable in the circulation, but then become strongly activated in response to the low extracellular pH in tumors.³⁷ And once in the tumor, the hyperpermeability of tumor blood vessels to circulating macromolecules and the partially impaired lymphatic drainage will lead to enhanced permeability and retention (EPR) effect for the nanoparticle delivery system.³⁸⁻⁴⁰ With high retention, it is possible to achieve high local concentration of the delivered CTL-antigen.

Various polymeric materials that can be used to construct pH sensitive 'smart' nanoparticles have been actively pursued in the past decades. 34,37,41-52 In our case we are interested in dextran whose hydroxyl groups have been protected with acetal groups (acetalated dextran, Ac-Dx), first developed by Frechet and coworkers, 53 who established that Ac-Dx-nanoparticles (Ac-Dx-NPs) can encapsulate model protein (OVA). In addition, after being uptaken by cells, OVA was released, processed, and subsequently its antigenic epitopes were presented on MHC-I molecules. More importantly, Ac-Dx-NPs were found to be non-toxic to cells. 53 In their follow up work, they demonstrated that Ac-Dx could be synthetically tuned to generate nanoparticles that have different payload release profiles based on the degree of acetalation. 54 Since then, Ac-Dx derived nanoparticles have found many applications both *in vitro* and *in vivo* ranging from imaging, 55 gene delivery, 56 siRNA delivery, 57 and as a platform

for delivery of drugs and other therapeutics.⁵⁸⁻⁶⁹ However, there is no report on the application of Ac-Dx-NPs as a CTL short peptide antigen delivery platform *in vivo*.

In this chapter, we report the encapsulation of CTL model antigen, $OVA_{(257-264)}$ (SIINFEKL) peptide, $OVA_{(P)}$ in Ac-Dx-NPs and their application in tumor therapy using mouse model. Our results show that the encapsulated peptide was delivered to the tumor microenvironment as confirmed by flow cytometry and scanning confocal microscopy. In addition we observed that the growth of established solid tumor was slower when mice were treated with $OVA_{(P)}$ encapsulated in Ac-Dx-NPs compared to other treatment groups comprising of free $OVA_{(P)}$ empty Ac-Dx-NPs, and PBS.

3.3: Results

3.3.1: Synthesis and characterization of nanoparticles containing $OVA_{(P)}$ encapsulated by acetalated dextran nanoparticles

OVA_(P) was synthesized through solid phase peptide synthesis (SPPS) using Fmoc chemistry, scheme 3.1. Successful coupling of the amino acids was monitored by electrospray ionization mass spectrometry (ESI) of the product cleaved from the resin. After synthesis, the OVA_(P) was purified by HPLC, and analyzed by ESI to confirm the isolated product. The results of the analysis are presented in Figures 63 and 64 respectively. Preparation of acetalated dextran nanoparticles encapsulating OVA_(P) followed reported procedures.⁵³ The nanoparticles were characterized by scanning electron microscopy (scheme 3.2). In order to quantify the amount of encapsulated OVA_(P), a standard curve was generated from HPLC. Various amounts of OVA_(P)-Ac-Dx-NPs (1, 2, and 3 mg) were hydrolyzed in 500 µL, 0.1% TFA, followed by HPLC analysis. The peak areas corresponding to $OVA_{(P)}$ were determined and the amount of $OVA_{(P)}$ was calculated from the standard curve. The value was reported as the average of the three independent measurements. The amount of encapsulated OVA(P) was estimated to be 20 µg peptide per 1 mg nanoparticle (2% by weight of nanoparticle was made up of OVA_(P)). In addition, OVA_(P)-Ac-Dx-NPs were resuspended in either PBS or in a solution containing 0.1% TFA in deionized water to a final concentration of 1 mg/mL in 1.5 mL microcentrifuge tubes overnight. The tubes were centrifuged and the supernatant was analyzed by ESI to determine the amount of OVA_(P) released. The peak corresponding to OVA_(P) 963 single charged or 482 double charged was not observed when OVA_(P)-Ac-Dx-NPs were resuspended in PBS (Figure 65), when compared to resuspension in 0.1 % TFA solution (Figure 66).

Scheme 2: Synthesis of OVA(P) through solid phase peptide synthesis (SPPS)

- 30% SPPS
- A) Fmoc-cleavage: 20% piperidine/DMF
- B) Amino acid-coupling: 5 eq. Fmoc-AA-OH, 4.9 eq. HBTU, HOBT 10 eq. DIEPA/ DMF
- C) Deprotection: 95% AcOH, 5% Water 5% TIPS

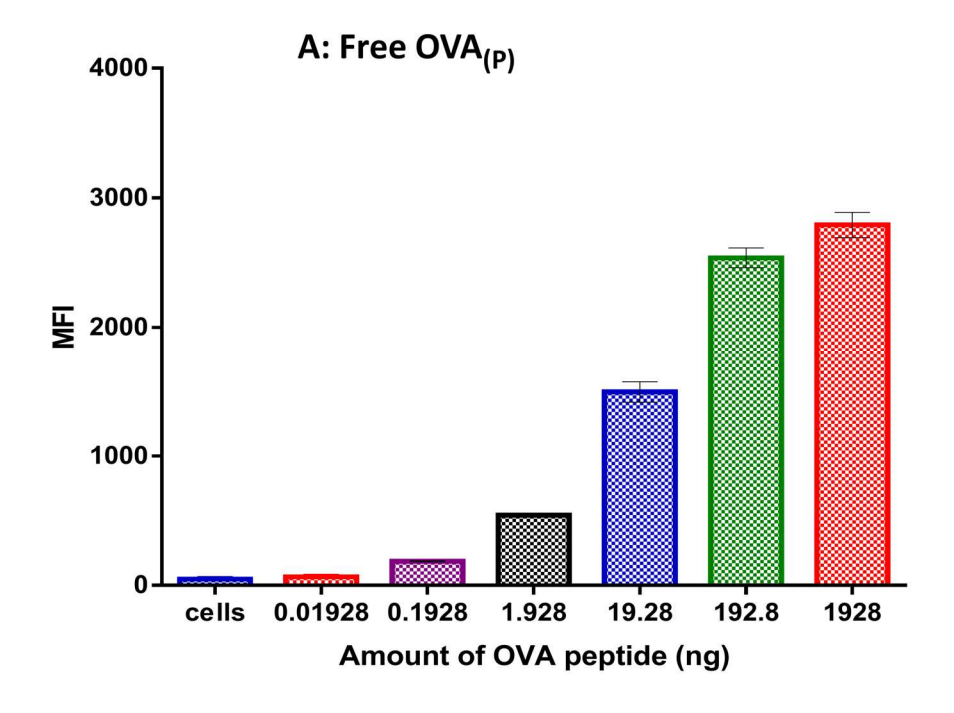
Scheme 3: Synthesis of OVA(P)-Ac-Dx-NPs

Scanning electron micrograph (SEM) of OVA_(P) encapsulated acetalated dextran nanoparticles

3.3.2: Assessing the presentation of OVA(P) peptide by MHC I molecules

The presentation of $OVA_{(P)}$ peptide by MHC I molecules was evaluated using EL4 tumor cells. For an antigen to elicit any noticeable immune response, it should be uptaken by the target cells, processed and presented on the MHC class I molecules. As already established, tumor cells are

genetically unstable and may present low or no MHC class I molecules on their surfaces, which may result in evasion of immune surveillance. 70 Various amounts of free OVA(P) or OVA(P)-Ac-Dx-NPs were incubated with EL4 cells for one hours at 37 °C, followed by FACS analysis after staining with anti-mouse H-2K^b bound to SIINFEKL (that specifically recognized OVA_(P) bound to MHC class I molecules but not free unbound OVA(P)). From Figure 50, it was established that both free OVA_(P) and encapsulated OVA_(P) were processed by the cells and presented on the MHC-I molecules. Next, free OVA_(P) and OVA_(P) encapsulated NP bearing the same amount of $OVA_{(P)}$ (normalized to 54 ng) were incubated by the cells in a period of 24 hrs and the presentation of $OVA_{(P)}$ at various time period was evaluated. As shown in **Figure 51**, the optimal incubation time was established to be 6 hrs for both free OVA_(P) and OVA_(P)-Ac-Dx-NPs. When the results of this optimal time was analyzed by t-test, it was established that the amount presented was comparable with no statistical significance. The duration at which the OVA_(P)remains presented on the MHC class I molecules was also evaluated for a period of 24 hrs. In this case, EL-4 cells were pulsed with either OVA(P) or OVA(P)-Ac-Dx-NP (amount of OVA_(P) normalized to 54 ng) and incubated for 1 hour. The growth medium was removed by centrifugation, cells washed and re-incubated in fresh growth medium for 1, 3, 6, 12, 18, and 24 hrs respectively) and analyzed by FACS after staining with OVA_(P) antibody, anti-mouse H-2K^b bound to SIINFEK, Figure 52. The results show that free OVA_(P) was uptaken and processed by cells quicker than encapsulated OVA_(P) (0 to 3 hrs). However, greater presentation of OVA_(P) was observed after 12 hrs when cells were pulsed with OVA_(P)-Ac-Dx-NPs, suggesting the slow release of the encapsulated $OVA_{(P)}$.



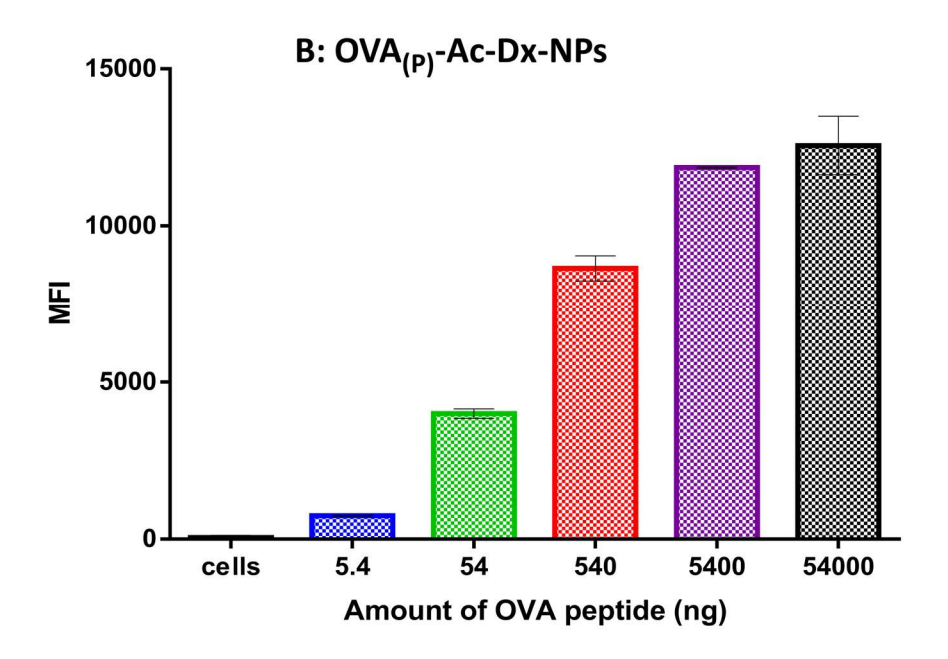


Figure 50: In vitro presentation of OVA antigenic peptide by MHC-I of EL-4 cancer cells. Panel A: 2.0×10^5 EL-4 cells were pulsed with free OVA_(P), panel B: 3.0×10^5 EL-4 cells were pulsed with encapsulated OVA_(P) (OVA_(P)-Ac-Dx-NPs). The high mean fluorescence intensity (MFI) values in panel B corresponds with the high number of cells used

..

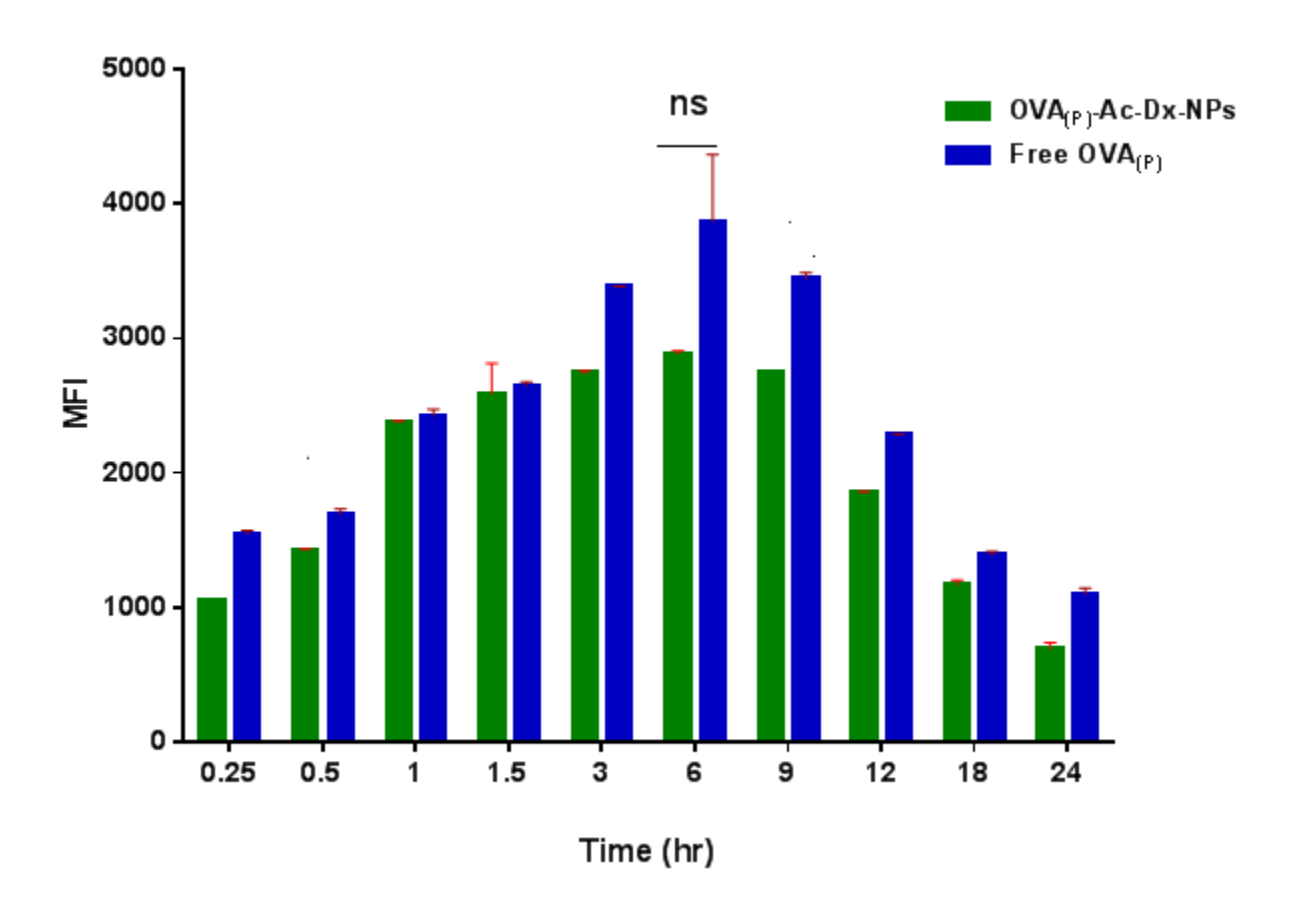


Figure 51: Effect of incubation time on OVA(P) antigen presentation by MHC-I of EL-4 cells. Amount of $OVA_{(P)}$ was normalized to 54 ng. ns: not significant

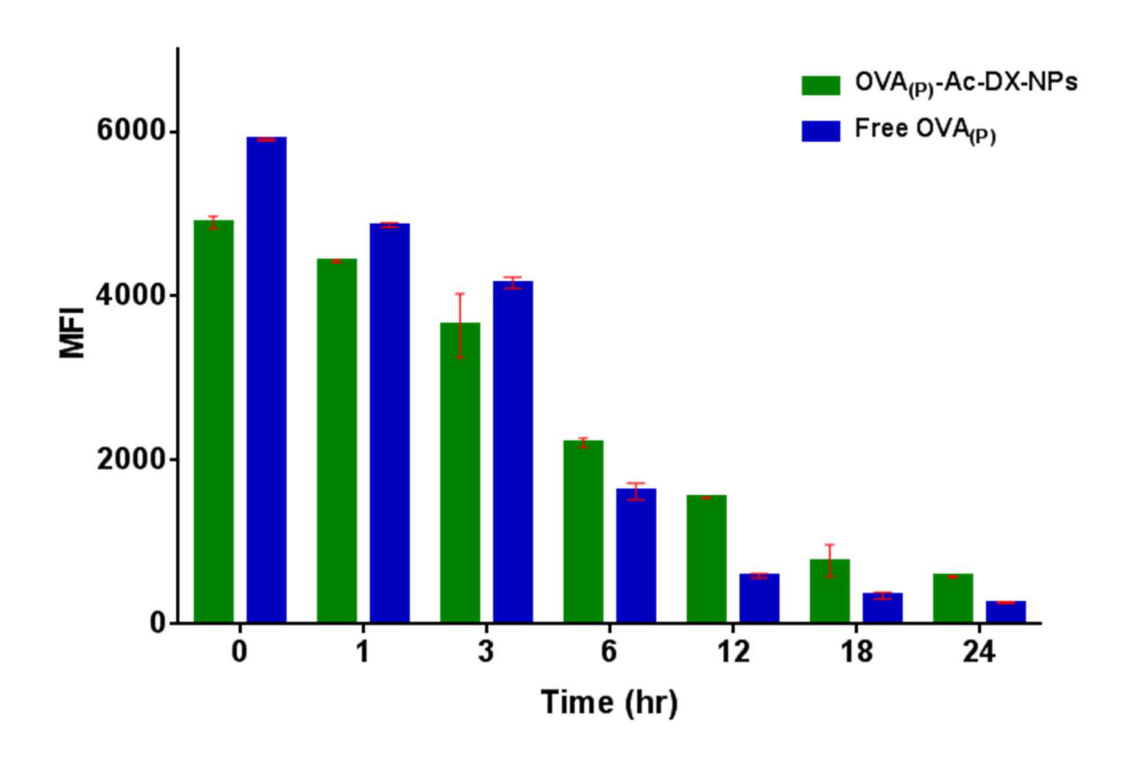


Figure 52: Duration at which OVA antigen remained on MHC-I when cells were pulsed with either free OVA(P) or OVA(P)-Ac-Dx-NPs. Amount of OVA(P) was normalized to 54 ng

3.3.3: B3Z assay

To assess whether $OVA_{(P)}$ antigen presented by the MHC-I molecules of EL-4 tumor cells were capable of activating cytotoxic T-cells, B3Z assay was carried out.⁵³ B3Z is a lacZ-inducible CD8+ T cell expressing TCR specific for $OVA_{(P)}$ presented on the murine H-2K^b MHC class I molecules.⁷¹ Once the TCR engages $OVA_{(P)}$ -H-2K^b complex, β -galactosidase is secreted, which cleaves its substrate chlorophenol red- β -D-galactopyranoside (CPRG) and give a colorimetric readout. EL-4 cells were pulsed with $OVA_{(P)}$ or $OVA_{(P)}$ -Ac-Dx-NPs for 6 hours, then co-cultured with B3Z cells for an additional 16 hours. CPRG was added and after 6 hours, the absorbance

was read at 595 nm. As shown in **Figure 53**, incubation of EL-4 tumor cells with $OVA_{(P)}$ -Ac-Dx-NPs led to increased MHC-I presentation of the $OVA_{(P)}$ epitope by a factor of 20 relative to free $OVA_{(P)}$. This drastic increase in presentation was an indicator that $OVA_{(P)}$ -Ac-Dx-NPs harbors the potential to be used as vaccines against tumors.

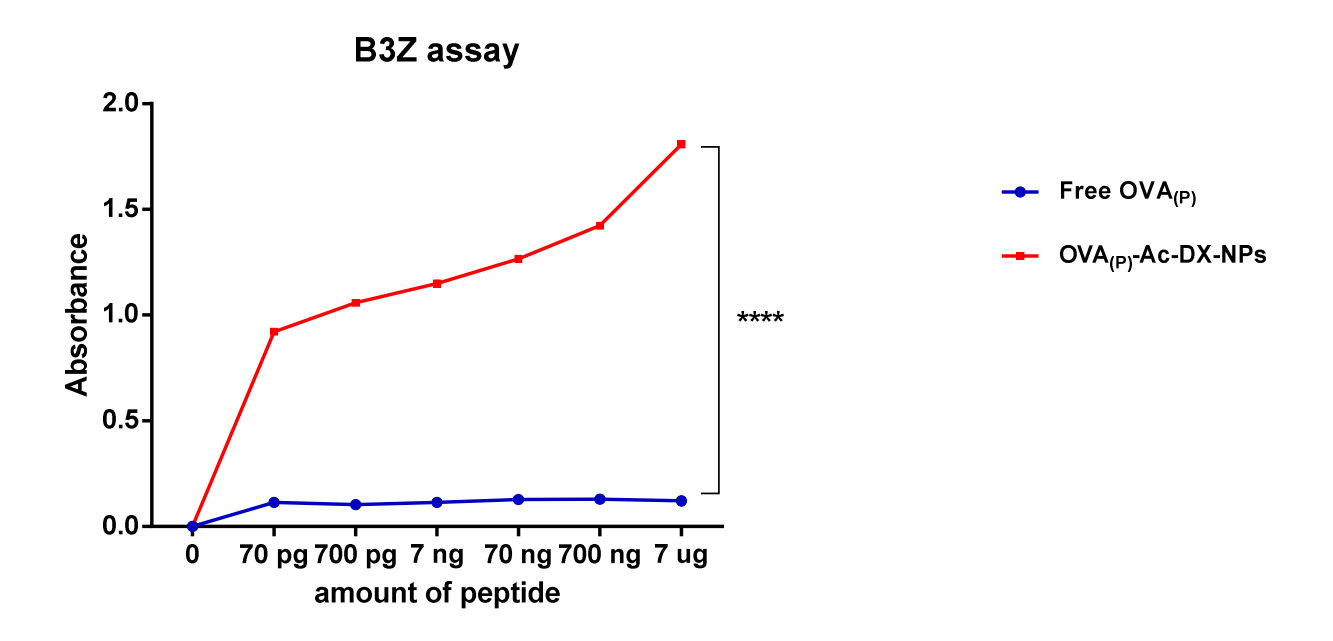


Figure 53: B3Z assay measuring OVA antigen presentation of EL-4 cells pulsed with free OVA(P) or OVA(P)-Ac-Dx-NPs. The t-test method was used for analysis, ****, $P \le 0.0001$. Absorbance was measured at 595 nm

3.3.4: $OVA_{(P)}$ antigen delivery to tumor environment by the assistance of acetalated dextran nanoparticles

Aiming at further investigating whether $OVA_{(P)}$ -Ac-Dx-NPs can be used as a vaccine to treat tumors, the ability of these nanoparticles to deliver $OVA_{(P)}$ antigen to tumor environment was evaluated. Mice were inoculated with EL-4 tumors on the left flank. When the tumor size was about 300 mm³, mice were administered with $OVA_{(P)}$ -Ac-Dx-NPs (14 μ g OVA peptide), via

intravenous tail vein injection. The mice were sacrificed 9 h post injection with the tumors were harvested and divided into two halves. For one half, single suspension cells were generated by digesting in collagenase type IV enzyme solution, stained with anti-OVA or its isotype and analyzed by FACS. The second half was subjected to histopathology antibody staining and subsequently analyzed by confocal microscopy imaging. Both results from FACS and confocal microscopy results confirmed the delivery and presentation of OVA(P) on MHC-I molecules, which was specifically detected by anti-OVA antibody, **Figures 54 and 55**.

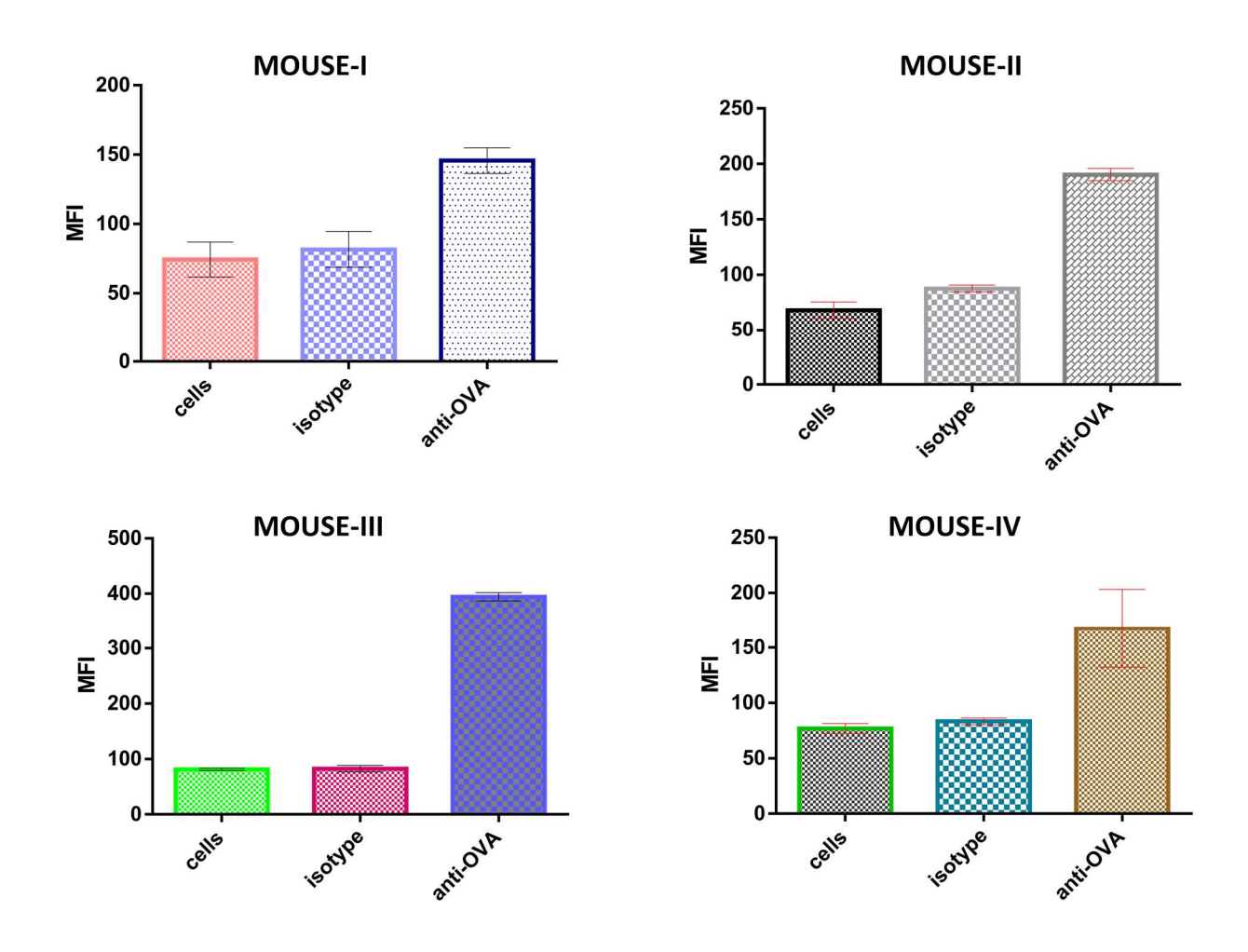


Figure 54: In vivo presentation of OVA-antigen on MHC-I by the cell population in the tumor microenvironment. The cell population was analyzed by FACS after staining with $OVA_{(P)}$ antibody, detecting anti-mouse MHC-I H-2K^b bound to SIINFEK antigen

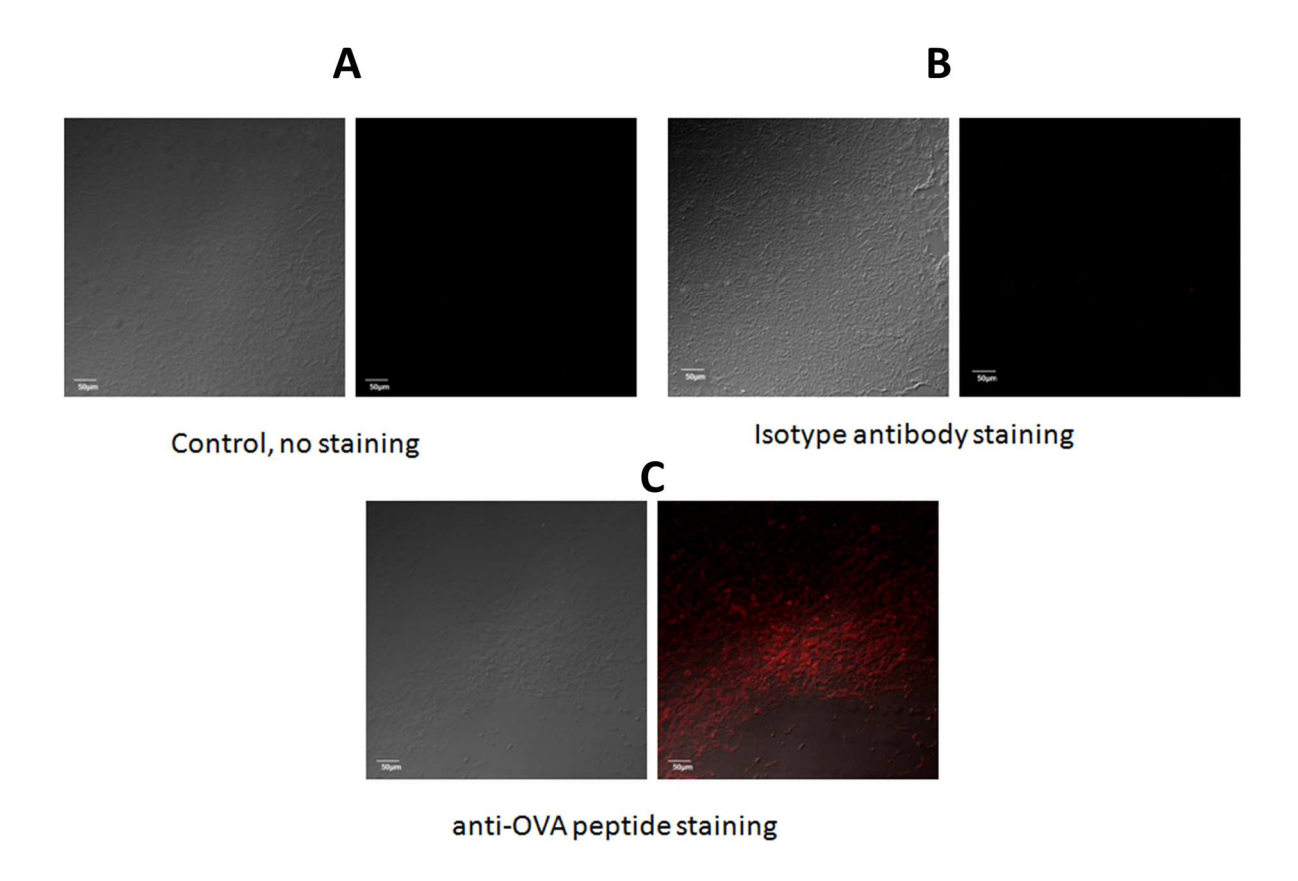
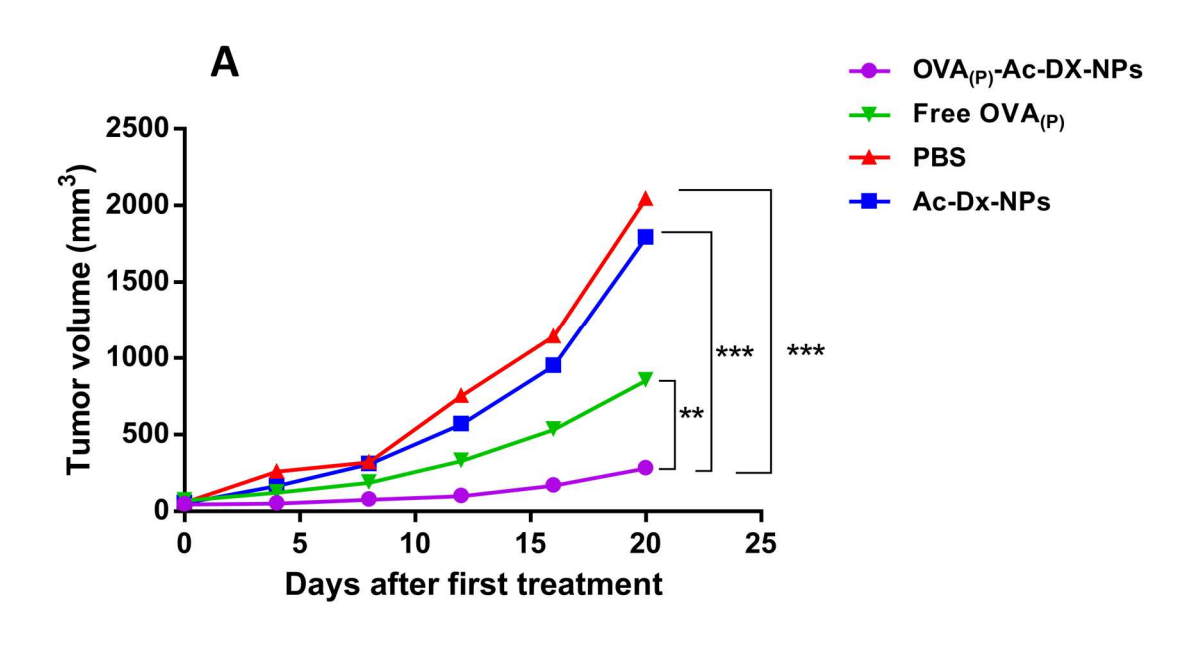


Figure 55: *In vivo* presentation of OVA(P) antigen on MHC-I by the cell population in the tumor microenvironment. The cell population was analyzed by confocal microscopy. Panel A: Tumor tissue slice was not subjected to any antibody staining. Panel B: Tumor tissue slice was stained with isotype control antibody. Panel C: Tumor tissue slice was stained with OVA_(P) antibody, detecting anti-mouse MHC-I H-2K^b bound to SIINFEK antigen. Scale bar is 50 μM

3.3.5: In vivo tumor protection

Further tests were carried out to determine if the delivery of the antigen can offer protection against tumor growth. C57BL/6 wild type mice were immunized subcutaneously under the scruff on day 0 with 100 μ L of OVA protein (50 μ g of OVA) as an emulsion in complete Freund's adjuvant. Booster were given on days 14 and 28 with emulsions in incomplete Freund's adjuvant (IFA). Subcutaneous (sc) tumors were established by administering sc 2 x 10⁵ EL-4 cells in 100 μ L of PBS per mouse into the left flank. When the tumor size was about 20-30 mm³, mice were

vaccinated via intra-tumor injection with either free OVA_(P), OVA_(P)-Ac-Dx-NPs (amount of OVA was normalized to 7 μg), empty Ac-Dx-NPs or PBS (100 μL final injected volumes). A total of 3 treatments were administered (every other day from the first vaccination). Tumor growth was monitored by taking dimensions with calipers, and mice with tumor volume over 1000 mm³ were removed from the experiment and euthanized. Mice were also removed if they showed other signs of pain or distress, such as immobility, a hunched posture, lack of eating or ulcers developing at the tumor area. Based on the tumor volume, it is evident that treatment with OVA_(P)-Ac-Dx-NPs offered protection against established tumor, as the tumor growth rate was significantly slower when compared to treatment with either free OVA_(P), empty Ac-Dx-NPs or PBS, **Figure 56**. Throughout the study, mice in the OVA_(P)-Ac-Dx-NPs group maintained the highest probability of survival compared to all other groups, **Figure 56 panel B**. All mice in PBS and Ac-Dx-NPs group died 20 days into the study, 20 % of the mice in free OVA_(P) study group were still alive. However, there were no mortalities found in the OVA_(P)-Ac-Dx-NPs study group. Study was stopped at day 26 after mice started showing lesions at the tumor area.



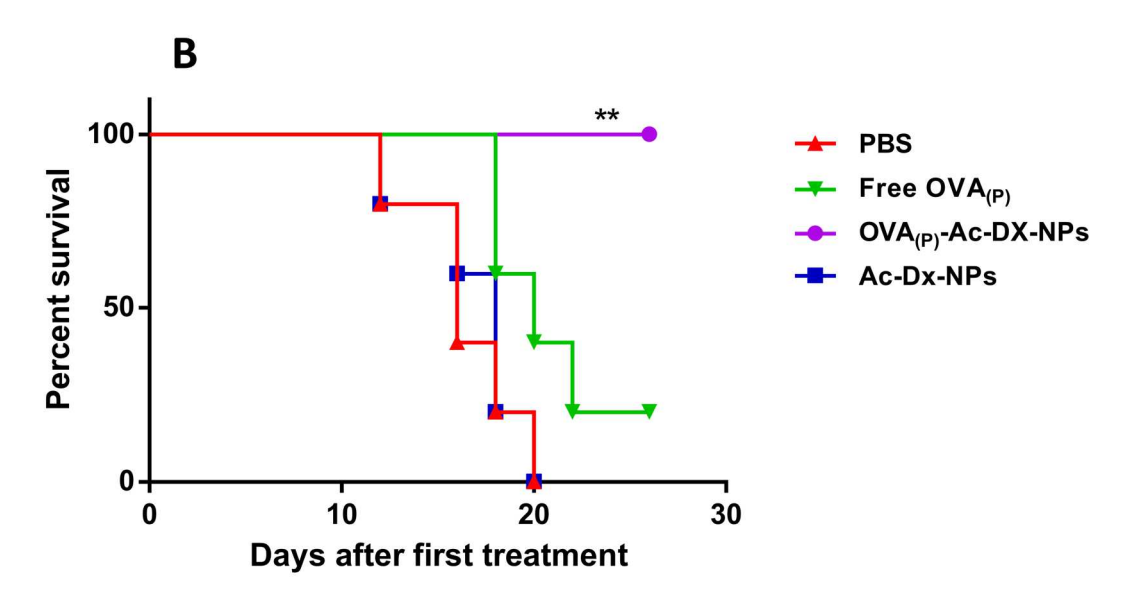


Figure 56: Tumor challenge studies of wild type mice bearing established s.c solid tumors. Panel A: Tumor growth progress after intra-tumor treatment with PBS, free OVA_(P), empty Ac-Dx-NPs and OVA_(P)-Ac-Dx-NPs. Panel B: Mice survival curve. Data shown is the mean of 5 mice per group. The Log-rank and the t-test methods were used for analysis. In A, **, $P \le 0.0042$; ***, $P \le 0.005$, while in B **, $P \le 0.005$ compared with free OVA_(P) group

Next we asked whether mice with already established solid tumors could be protected if the vaccination was carried out via intravenous injection as opposed to intra-tumor injection. A

preliminary study was done using OT-I transgenic mice, in which CD8⁺ T cells express TCR specific for the OVA_(P) presented on MHC-I molecules (OT-I cells).^{72,73} Mice were immunized following similar protocols as wild type stated above. Similarly, sc solid tumors were inoculated on the left flank and when the tumor volume was between 20-30 mm³, mice were treated intravenously via tail vein. Only a single dose of either OVA_(P)-Ac-Dx-NPs, free OVA_(P), empty Ac-Dx-NPs or PBS was given on day zero. The amount of OVA_(P) was normalized to 20 μg in 100 μL total volume formulated in PBS. Similar results were observed where mice treated with OVA_(P)-Ac-Dx-NP had slow tumor growth rate. PBS and empty particles treated mice had similar tumor growth rate with no mortality reported, confirming that Ac-Dx-NPs are not toxic.⁵³

The use of OT-I mice however posed some potential limitation. Due to the high levels of activated OVA_(P) specific T-cells, any off target delivery of the peptide would potentially lead to the death of the mice. This came to be evident when all the mice in the study group treated with free OVA_(P) died two days after vaccination, while two mice from the OVA_(P)-Ac-Dx-NPs group also died. These results gave an eye opening observations; (i) mice were safer when treated with OVA_(P) antigen encapsulated in Ac-Dx-NPs (ii) the concentration of the peptide administered to OT-I mice (20 μg OVA_(P)) could be potentially too high (iii) there is off target delivery of the encapsulated OVA_(P) (iv) only single dose treatment was necessary to produce a reduced rate of tumor growth compared to intra-tumor injection experiment, implying high number of antigenspecific CTLs is required to cause tumor regression. Mice in PBS and empty nanoparticle group were sacrificed 13 days after first treatment, after tumor sizes were over 1000 mm³. On the other hand, mice treated with OVA_(P)-Ac-Dx-NPs showed tumor regression, but progressive growth started 10 days after first single dose treatment on day zero, **Figure 57, panel A**.

After preliminary success with OT-I mice model, we next performed the study in wild type mice. Similarly, solid tumors were inoculated on the left flank, and after tumor had established, mice were treated via tail vein with either OVA_(P)-Ac-Dx-NPs, free OVA_(P), Ac-Dx-NPs or PBS. The injected OVA_(P) was normalized to 20 µg and a total of three injection were administered every other day. As shown in **Figure 58**, mice treated with OVA_(P)-Ac-Dx-NPs had slow rate of tumor growth, and showed high chances of survival throughout the study. None of the free OVA_(P) treated mice died from OVA_(P) injection implying the amount of OVA_(P)-specific CTL generated in wild type mice after immunization is low. All the ten mice in the PBS and Ac-Dx-NPs study groups died 15 days into the study from tumor. Over 50 % of the mice in the free OVA_(P) study group had died by this day. However, they all died 18 days into the study, the same day the first mortality from the OVA_(P)-Ac-Dx-NPs study was reported, **Figure 58**, **panel B**.

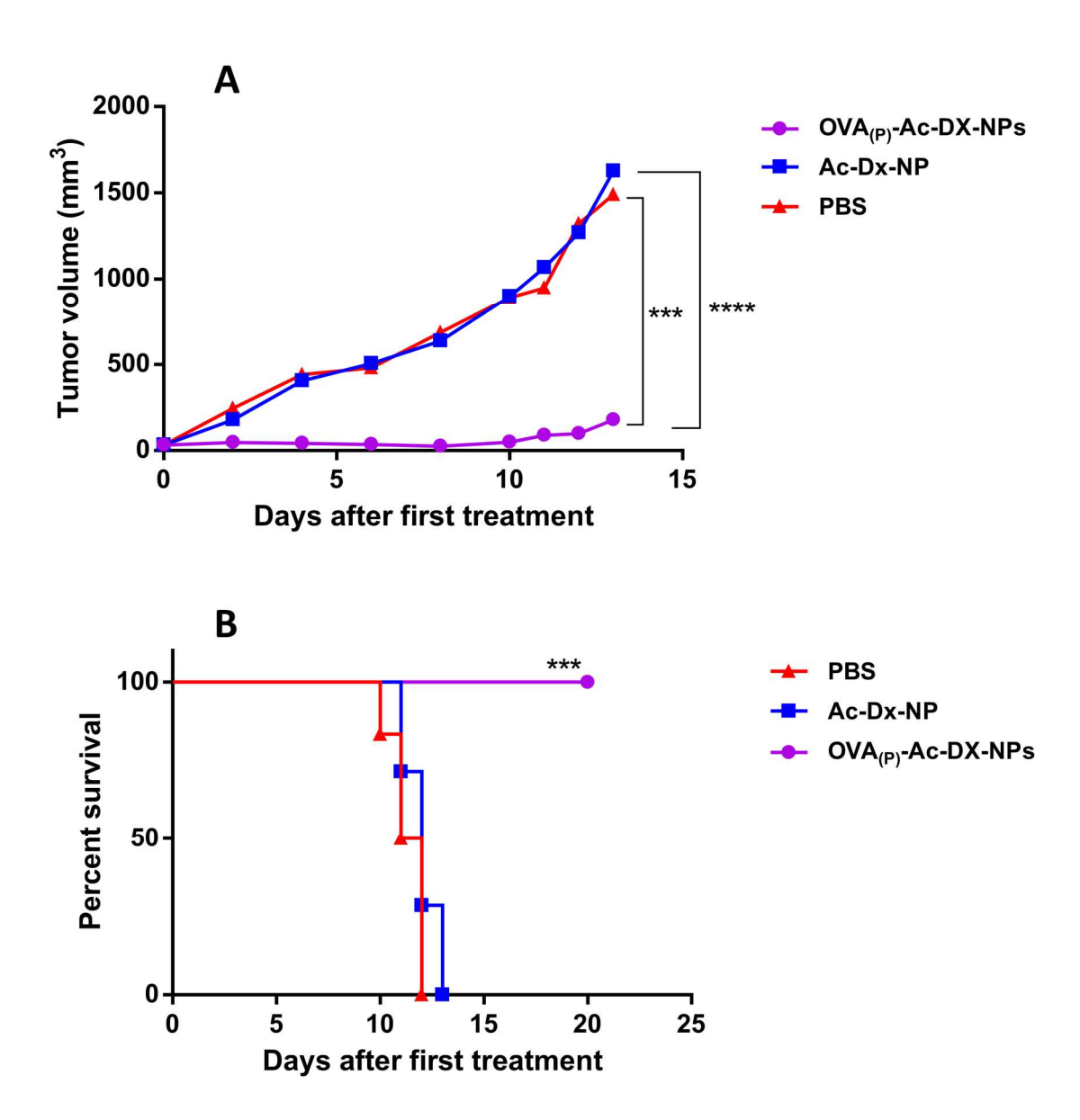


Figure 57: Tumor challenge studies of OT-I transgenic mice bearing sc solid tumors. Panel A: Tumor growth progress after i.v. treatment with PBS, free OVA_(P) antigen, empty Ac-Dx-NPs and Ac-Dx-NPs encapsulating OVA antigen (OVA_(P)-Ac-Dx-NPs). Panel B: Mice survival curve. Data shown is the mean of 7 mice per group. The Log-rank and the t-test methods were used for analysis. In A ***, $P \le 0.002$; ****, $P \le 0.0001$, while in B, ***, $P \le 0.001$ compared with Ac-Dx-NPs group

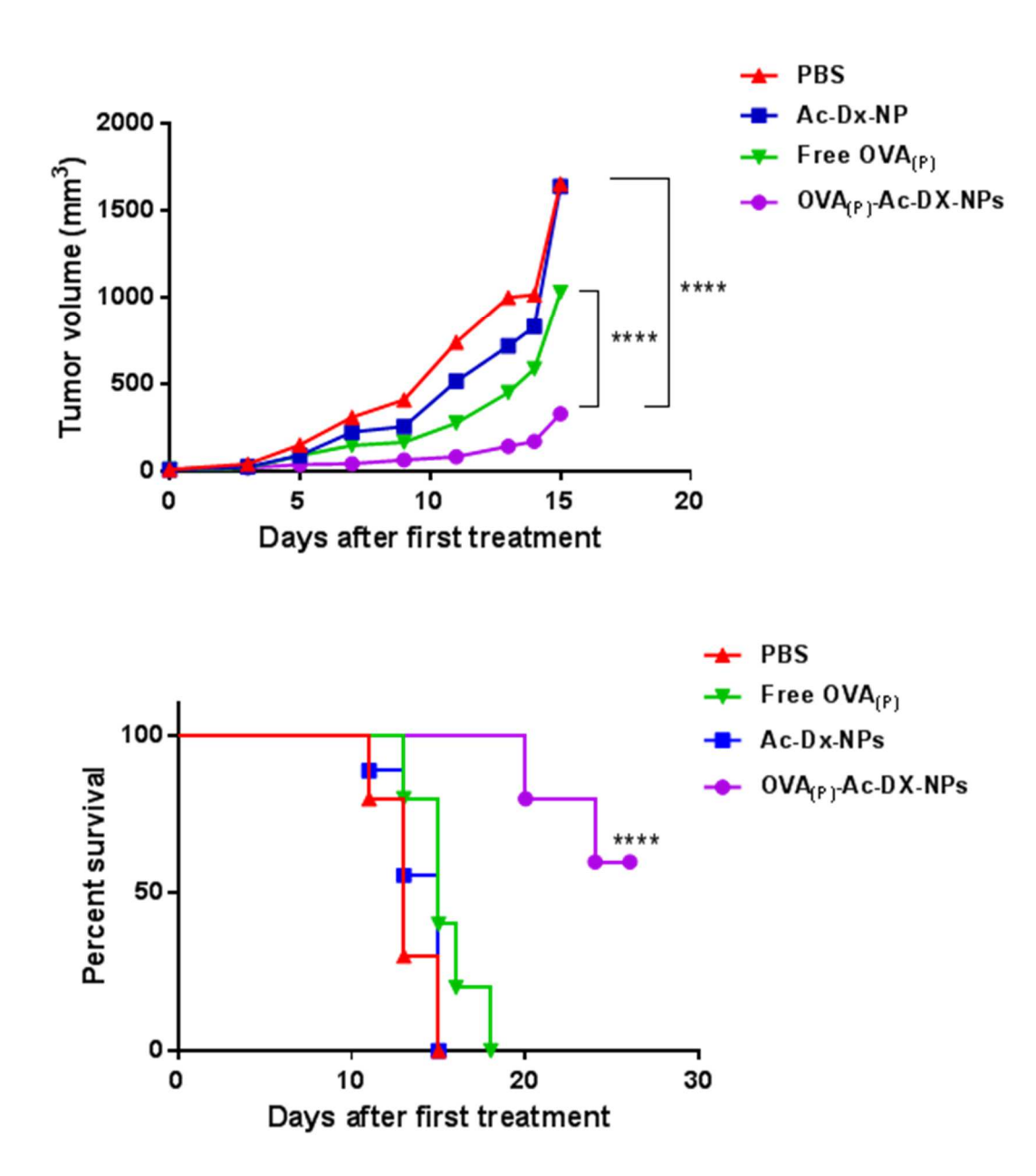


Figure 58: Tumor challenge studies of wild type mice bearing sc solid tumors. Panel A: Tumor growth progress after i.v. treatment with PBS, free $OVA_{(P)}$ antigen, empty Ac-Dx-NPs and Ac-Dx-NPs encapsulating OVA antigen ($OVA_{(P)}$ -Ac-Dx-NPs). Panel B: Mice survival curve. Data shown are the mean of 10 mice per group. The Log-rank and the t-test methods were used for analysis. In A, ****, $P \le 0.0001$, while in B, ****, $P \le 0.0002$ compared with free $OVA_{(P)}$ group

3.4: Discussion

Immune response and /or immunotherapy often fail to cause rejection of progressively or established tumors even when effective CTL responses are generated. It has been established that one way in which tumors may escape immune surveillance is failure by a subpopulation of tumor cells to express the target antigen, resulting in diminished MHC-I/peptide interactions. The direct outcome is the diminished recognition of the MHC-I/peptide complex by the TCR leading to cancer cell escape from destruction by CTL, hence tumor grows progressively. ^{23,26,30,70,74} Cancer cells with diminished MHC-peptide complex have been referred to as antigen loss variant (ALV). Schreiber and coworkers demonstrated that these ALV can be indirectly eliminated as bystanders by CTL if the cancer antigens are effectively cross-presented by the tumor associated stromal cells. ^{24,27-30}

Therefore increasing the concentration of tumor antigen in the tumor microenvironment may require targeted delivery of the tumor antigen by an external vehicle, in the event that parental cancer cells lack enough antigens to be cross-presented by stromal cells. The delivery vehicle of choice should be designed such that it takes advantage of the unique properties of the tumor microenvironment. pH-responsive nanostructures/nanoparticles hold the promise as a viable delivery vehicle because of the low pH nature of the tumor microenvironment. ^{32,34,37} Here we show using two experimental approachs that OVA_(P) antigen encapsulated in dextran nanoparticles was successfully delivered to the tumor microenvironment. Furthermore, our results indicated that the antigen was uptaken by the cell population in the tumor microenvironment, and presented on to MHC - I molecules, which were detected by the antibody staining as confirmed by both FACS and confocal microscopy, **Figures 54 and 55**. A good antigen delivery system should possess enhanced permeability and retention (EPR)

characteristics. 75-79 Once they enter tumor environment, they should stay there sufficiently long and release their payload relatively slowly thereby increasing their therapeutic effect.⁷⁶ The results obtained from the B3Z assays suggest that there was prolonged availability of OVA_(P) at significantly higher concentration when cells were exposed to OVA_{(P)-}Ac-Dx-NPs as compared to free OVA_(P), Figure 53. The advantage of prolonged availability implies that once delivered, majority of the cell population in the tumor microenvironment, including stromal cells, will have a chance to uptake the antigen, present on MHC-I molecules, subsequently sensitize the tumor environment for destruction by CTL. This was evident from our results that show slowed tumor growth after mice were treated with OVA_(P)-Ac-Dx-NPs, Figures 56, 57 and 58. This is particularly attractive because it provides a confirmation that besides full length proteins, 47 therapeutically relevant short peptides⁸⁰ too can be encapsulated in acid responsive nanoparticles, and successfully delivered to their intended destinations. In addition, short peptides are easier to synthesize and purify, and they can be produced in high quantities with high degree of reproducibility, further highlighting the advantages of working with short peptides antigens. Besides, if whole proteins are encapsulated, cells will have the extra burden to proteolytically degrade protein to the required short CTL-peptide antigens to be presented on the MHC-I molecules.

Despite promising results obtained from the current study, we were not able to achieve complete eradication of the established solid tumor. Several other mechanisms other than ALV can potentially explain why the presence of high levels of tumor activated CD8⁺ T-cells have failed to cause complete rejection of established tumor has been proposed. Some of them are related to the inability of the activated T-cells (either adoptively transferred or generated through immunization) to access the tumor, or even some instance the activated T cells migrate away

from the tumor site. 85,86 In our current study it can also be explained by the inability of OVA(P)-Ac-Dx-NP to access all tumor cells due to limited penetration of OVA(P)-Ac-Dx-NP in tumor tissues. One potential direction is to enhance tumor penetrating abilities of the NPs. Our current results agree with previous reports, which suggest that even in transgenic mice, which were engineered to enable every T cell to express a tumor-antigen reactive TCR (such as OT-I mice), tumors still grew progressively after initial regression was observed.^{22,87} In an attempt to provide a solution to the inability of the adoptively transferred T cells to fully access the tumor, Stephan et al. demonstrated that activated tumor specific T cells together with the necessary costimulatory molecules, can be delivered efficiently by harboring them in bioengineered polymer matrices. As opposed to adoptive transfer via intravenous administration, the polymer material is designed to deliver and stimulate the T cells when placed in tumor resection sites or close to inoperable tumors. When at the tumor site, it acts as an active reservoir from which the propagating cells are released as the material biodegrades. In a multifocal ovarian cancer model, they demonstrate that polymer-delivered T cells triggered regression, whereas injected tumorreactive lymphocytes had little curative effect. 88 Therefore, if our proposed CTL-antigen delivery method is used together with these already available and established methods for activated T cell delivery, eradication of established tumor is possible.

3.5: Conclusion

Tumor cells often evoke specific immune responses that however, fail to eliminate all the tumor cells. The development of cancer immunotherapies over the decades, has mostly focused on the generation of large numbers of activated anti-tumor effector cells through vaccination or adoptive T cell transfer. However, this has not been able to be translated into clinical successes for cancer therapy because even where tumor regression or complete responses were achieved

there is usually relapse of the disease. By the establishment that subpopulation of tumor cells fail to display T cell specific antigen required for tumor destruction, efforts should also focus on how to improve antigen presentation on cancer cells. Other than hoping that tumor cells should present antigens high enough to be cross-presented by the tumor stromal cells, methods need to be developed that will aid in delivery of CTL specific antigens to the tumor microenvironment in optimal quantities. We have shown here that 'intelligent' pH responsive nanoparticle systems capable of delivering CTL specific antigen to the tumor microenvironment holds the promise. Just as adoptive transfer or polymer assisted delivery is capable of saturating the tumor microenvironment with CTL of high activity, nanoparticle-antigen delivery systems can also enhance tumor treatment efficacy. If these (CTL and antigen delivery methods) are used in combination, it is likely that we can achieve both activated CTL and their corresponding antigens at high concentrations in the tumor microenvironment, which could potentially translate to efficient tumor eradication. We are currently working on improving the encapsulation of OVA_(P) antigen to eliminate the potential antigen leak as evident by the death of two OT-I mice from the $OVA_{(P)}$ -Ac-Dx-NPs group. We are also exploring the possibility of covalently linking the OVA antigen to acetalated dextran through pH or enzymatic sensitive linkers prior to emulsification to form nanoparticle. The enzymatic sensitive linkers should target enzymes that are highly overexpressed in the tumor microenvironment compared to normal tissues. Through covalent linkage, antigen leakage and subsequently off targeting can be minimized and higher concentration of the vaccines can be administered to study dose dependent treatments.

3.6: Future directions

Encapsulation of CTL specific $OVA_{(P)}$ antigen in acid responsive dextran nanoparticles provided an alternative direction towards cancer immunotherapy. Despite the promising results, the death of two OT-1 mice treated with $OVA_{(P)}$ -Ac-Dx-NPs revealed the potential drawback of the current encapsulation technology. It is possible that some of the $OVA_{(P)}$ antigen leaked out during $OVA_{(P)}$ -Ac-Dx-NPs blood circulation ending up in vital organs resulting to off-target toxicity. In addition, an attempt to account for the amount of $OVA_{(P)}$ antigen that was delivered to the tumor and other vital body organs such as the liver, kidney, spleens, etc was experimentally unsuccessful. To circumnavigate the leakage problem, covalent linkage of the $OVA_{(P)}$ to Ac-Dx-NPs through linkers that can be cleaved without altering the $OVA_{(P)}$ sequence was proposed.

Cathepsin B enzyme cleavable linker have been fronted as the emerging candidate to accomplish the covalent linkage due to the success it has shown in other applications, ⁸⁹⁻⁹¹ and especially in the construction of antibody drug conjugate. ⁹² Consequently, the choice of cathepsin B cleavable linkers fits perfectly with the general hypothesis of this work whereby we are targeting biological stimuli that are overexpressed in the tumor microenvironment. Cathepsin B, a lysosomal protease (lysosome pH = 5.0-5.5) has been found to be overexpressed in various tumors where it has been implicated in tumor invasion and metastasis. ⁹³ It is never found in the extracellular matrix, except the extracellular matrix of tumor microenvironment. The extracellular activity of cathepsin B in tumors is supported partly by the low pH as a result of acidified environment around the cancer (pH = 6.4-6.8). Cleavable peptide sequences for cathepsin B are well developed: Ala-Leu-Ala-Leu, Gly-Phe-Leu-Gly, Phe-Arg, Phe-Lys, and Val-Cit are some of the linkers that have been highlighted. Out of these, Phe-Arg, Phe-Lys and

Val-Cit have been shown to perform better in the delivery of chemotherapeutic drug conjugates. 90

To successfully construct OVA_(P)-Ac-Dx-NP conjugates, literature reports on the modification of acetalated dextran will be explored. Firstly, the diol of the dextran can be partially oxidized to generate carbonyl groups followed by protection of the free hydroxyl groups.⁵⁷ The partially oxidized dextran is then conjugated with OVA_(P) antigen modified with cathepsin B cleavable linkers through reductive amination, **Figure 59**. Alternatively, carbohydrate reducing chain ends present at the surface of the acetalated dextran nanoparticles could be exploited to form stable oxime conjugates with alkoxyamine bearing OVA_(P) modified with cathepsin B cleavable linkers,⁵⁵ **Figure 60**. With these conjugates, it is possible to achieve decreased off-targeting toxicity due to premature OVA_(P) leakage, and also carry out organ distribution and dose dependent studies, even in OT-1 mice. Besides acetalated dextran nanoplatforms, these cathepsin B-peptide antigen constructs can be modified to fit onto other novel polymer derived nanoparticles.

Figure 59: Conjugation of cathepsin B linkers-OVA(p) antigen construct on partially oxidized dextran polymer through reductive amination

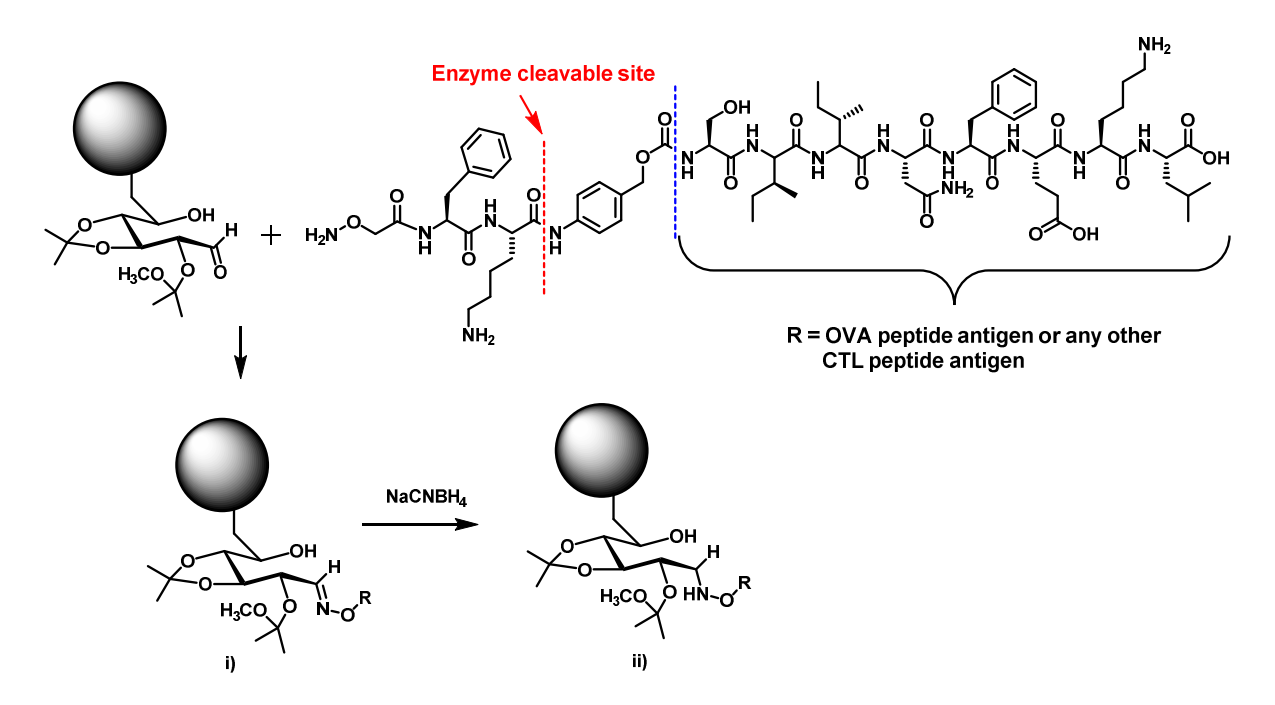


Figure 60: Conjugation of cathepsin B linkers-OVA(p) antigen construct by taking advantage of the reducing end equilibrium between hemiacetal and straight chain forms of carbohydrate present at the surface of the Ac-Dx-NPs through reductive amination

3.6: Experimental Section

3.6.1: Materials and instrumentation

All chemicals were reagent grade and were used as received from the manufacturer unless otherwise indicated. Fetal bovine serum (FBS), phosphate buffered saline (PBS), high glucose Dulbecco's modified Eagle medium (DMEM), Dulbecco's modified Eagle medium nutrient mixture F-12 Ham (DMEM/F12), complete Freund's adjuvant (CFA), incomplete Freund's adiuvant (IFA). RPMI-1640, ovalbumin (OVA). chlorophenol red-β-Dgalactopyranoside (CPRG), dimethyl sulfoxide cell culture grade, pyruvate, acetonitrile HPLC grade, pyridium p-toluenesulfonate, triisopropylsilane (TIPS), dextran (Mw = 9 000 - 10 500 g/mol), sodium azide (NaN₃), N,N-dimethylformamide (DMF), dichloromethane (DCM) were purchased from Sigma Aldrich. Methoxypropene, anhydrous DMSO. N.Ndiisopropylethylamine, were purchased from Acros. Hydroxybenzotriazole (HOBt), O-(Benzotriazol-1-yl)-*N*,*N*,*N*′,*N*′-tetramethyluronium hexafluorophosphate (HBTU), protected amino acids were was purchased from Chem Impex international. Piperidine, polyvinyl alcohol (PVA, Mw = 13 000 - 23 000 g/mol, 86-89% hydrolyzed) was purchased from Alfa Aesar. Regular and HPLC grade trifluoroacetic acid (TFA) was purchased from EMD millipore. L-glutamine, streptomycin, penicillin, collagenase type IV and Hank's balanced salt solution were purchased from Gibco.

Scanning electron microscopy (SEM) images were acquired on The 7500F ultra-high resolution scanning electron microscope, flow cytometry (FACS) data was acquired using LSR II flow cytometer analyzer and analyzed by FlowJo_V10 software. Confocal microscopy images were acquired using an Olympus FluoView 1000 LSM confocal microscope, dynamic light scattering (DLS) was performed on a Zetasizer Nano zs apparatus (Malvern, UK).

3.6.2: Animals and cell lines

Pathogen free female C57BL/6 mice age 6 - 10 weeks were obtained from Charles River. OT-I mice were generously donated by Norbert E. Kaminski (Pharmacology and Toxicology department, Michigan State University). The mice were maintained in the University Laboratory Animal Resource facility of Michigan State University. All animal care procedures and experimental protocols have been approved by the Institutional Animal Care and Use Committee (IACUC) of Michigan State University. EL4 cells were generously donated by Gendler J. Sandra (Mayo clinic). Cells were cultured in RPMI medium 1640 supplemented with 10 % FBS, 1% L-glutamine, and 1% streptomycin penicillin. B3Z (CD8⁺) cells was generously donated by Nilabh Shastri (University of California, Berkeley). Cells were cultured in RPMI-1640 supplemented with 10% FBS, 1 mM pyruvate, 50 μM 2-mercaptoethanol, 1% L-glutamine, and 1% streptomycin penicillin. The two cell lines were grown at 37 °C in a 5% CO₂/air incubator.

3.6.3: OVA peptide synthesis

The OVA-derived (H-2K^b, SIINFEKL) peptide was synthesized through solid phase peptide synthesis using Fmoc chemistry. The leucine resin in a syringe was swollen overnight in DCM at room temperature. Lysine's free carboxylic acid was activated with HBTU, HOBt and DIPEA base in anhydrous DMF (10 mL) for 30 minutes. The DCM was discarded from the syringe and the activated lysine added and the coupling reaction left to proceed for 10 h at room temperature. After the reaction, the solution in the syringe was discarded and the resin washed 3 times with DMF followed by 3 times with DCM. Fmoc was deprotected by adding a solution containing 20% piperidine in DMF, this was done twice, 20 minutes each with constant rotation. After the

end of the 40 minutes, the resin was wash 4 times with DMF and 4 times with DCM. The next activated amino acid was added and the procedure was repeated until all the amino acids had been coupled. Fmoc on the final amino acid was removed as previous described, the peptide was cleaved from the resin by a solution containing 95% TFA, 5% MilliQ water, and 5% TIPS. At this acidic condition, all the protecting groups were cleaved. Excess TFA was removed by evaporation on a rotavap followed by precipitation in diethylether and centrifugation until the resultant diethylether supernatant was clear. The peptide was air dried in the hood, dissolved in minimum amount of DMSO and purified by HPLC using 0.1% TFA MilliQ water and acetonitrile over a C18 column. Successful coupling was confirmed by ESI mass spectrometry.

3.6.4: Preparation of acetalated dextran nanoparticles containing OVA peptide ($OVA_{(P)}$ -Ac-Dx-NPs)

Acetalated dextran nanoparticles containing OVA peptide was prepared by double emulsion water/oil/water as previously reported with modification.⁵³ Briefly OVA peptide, OVA_(P) (10 mg) was dissolved in DMSO (50 μL). Acetalated dextran (200 mg) was dissolved in DCM (1 mL) and added to the OVA_(P) solution in a 15 mL centrifuge tube. This mixture was emulsified by sonicating for 30 s on ice using a probe sonicator (Branson digital sonifier, 250) with a duty cycle of 20%. This primary emulsion was added to an aqueous solution of poly(vinyl alcohol) (2 mL, 3% w/v in PBS) and sonicated for an additional 30 s on ice using the same setting except the duty cycle was increased to 30%. The resulting double emulsion was immediately poured into a second PVA solution (10 ml, 0.3% w/v in PBS) and stirred for 4 h allowing the organic solvent to evaporate. The particles were isolated by centrifugation (10 000 RPM, 20 min) and washed with PBS (30 mL) and MilliQ-H₂O (2 x 30 mL, pH 8) by vortexing and sonication followed by

centrifugation and removal of the supernatant. The washed particles were resuspended in MilliQ- H_2O (2 mL, pH 8) and lyophilized to yield a white fluffy solid. Empty particles without the peptide were prepared following the same procedures omitting the $OVA_{(P)}$.

3.6.5: OVA peptide presentation on MHC-I by flow cytometry (FACS)

EL4 cells were pulsed with different concentrations of either free OVA_(P), 2.0 x 10⁵ cells or acetalated dextran nanoparticles encapsulating OVA_(P), (OVA_(P)-Ac-Dx-NPs), 3.0 x 10⁵ cells at 37 °C in a 5% CO₂/air incubator for 1 h. Cells were washed 3 times with FACS buffer (1 % FBS, 0.5 % NaN₃ in PBS), stained with either anti-mouse H-2Kb bound to SIINFEKL (subsequently referred to as anti-OVA) or anti-mouse IgG1K (isotype control) for 30 minutes in FACS buffer on ice followed by FACS analysis. After the titration curves were generated, similar experiment was repeated but this time the amount of OVA_(P) was normalized to 54 ng and the incubation was carried out in 24 h period to for kinetic studies to determine time of maximum antigen presentation by MHC-I molecules on the cells surface.

To determine the duration at which the antigen remains presented on MHC-I molecules, EL-4 cells were pulsed with either free OVA_(P) or OVA_(P)-Ac-Dx-NPs (OVA_(P) was normalized to 54 ng), and incubated at 37 °C in a 5% CO₂/air incubator for 1 h in FACS tubes. Cells were centrifuged, the supernatant was discarded, washed twice in RPMI-1640 culture medium, followed by incubation in fresh medium for 0, 1, 3, 6, 12, 18, and 24 hrs. Cells were washed and stained with anti-OVA followed FACS analysis.

3.6.6: B3Z T cell activation assay

B3Z cell is a CD8⁺ T cell hybridoma expressing a T cell receptor (TCR) that specifically recognizes OVA₍₂₅₇₋₂₆₄₎ (SIINFEKL), OVA_(P) presented on the H-2K^b MHC class I molecules. The cells carry a β-galactosidase (lacZ) construct, hence they secrete β-galactosidase when its T-cell receptor (TCR) engages an OVA₍₂₅₇₋₂₆₄₎:H-2K^b complex. Reported procedures were closely followed.⁵³ Briefly, 2 x 10^4 EL-4 cells were cultured overnight in a 96 well plate and subsequently incubated with OVA_(P)-Ac-Dx-NPs or free OVA_(P) at increasing concentration . After 6 h, the cells were washed and $1x10^5$ B3Z cells were added to the EL-4 cells and co-cultured for an additional 16 h. The medium was removed and 100 μL of CPRG buffer (9.1 mg of CPRG, 0.125 mg of NP40 and 90 mg MgCl₂ in 100 mL of PBS) was added to each well. After 6 hrs, the absorbance at 595 nm was measured using a microplate reader. The results are presented as a mean quadruplicate.

3.6.7: Assessing the delivery of OVA to tumor environment by FACS and confocal microscopy

3.6.7.1: FACS

Solid tumor was inoculated on the left flank by injecting 5 x 10^5 EL4 cells subcutaneously. When the tumors were about 300 mm³, the mice were injected with OVA_(P)-Ac-Dx-NPs (amount of OVA_(P) was normalized to 7 µg based on B3Z assay). The mice were sacrificed 9 h post injection, tumors were harvested and divided into two halves. One half was digested in collagenase type IV enzyme solution to generate single suspension cells while the other half was subjected to histopathology antibody staining prior to confocal microscopy imaging. Briefly, the mice were euthanized with isoflurane and CO₂. Tumors were removed carefully avoiding the

skin and put into a labeled Petri dish (60 x 15 mm). Tumors were cut into two halves, one piece was frozen in the embedding medium at -80 °C for histology. The remaining half on Petri dish was minced into very fine pieces using sterile scalpels. 1 mL of collagenase solution (1g/mL, collagenase type IV in DMEM/F12 supplemented with 5% FBS) was added into the minced tumor tissues and transferred into a 50 mL centrifuge tube. The collagenase solution was brought to a final volume 10 mL. The tubes were placed in a 37 °C water bath, and every 30 minutes the samples were pipetted with a 10 mL pipette and then placed back in the water bath for a total of 3 h. 10 mL of cold Hank's balanced salt solution (HBSS) modified supplemented with 2% FBS was added to the sample tubes and cell suspension filtered through a 70 µm cell strainer into a new labeled 50 mL centrifuge tube. The tubes were centrifugation at 1600 RPM for 5 min. The supernatant was discarded. The pellet was washed in additional 10 mL of HBSS, centrifuged again and the supernatant discarded. Finally the pellet was resuspended in 1 mL FACS buffer and divided into three parts in FACS. Two tubes were stained with either isotype control antibody or anti-OVA and the remaining tube used to set the background. The tubes were incubated on ice for 30 minutes, centrifuged at 1600 RPM for 5 minutes, and washed twice with FACS buffer by gentle vortexing and centrifugation. Finally the pellet was resuspended in 350 uL of FACS buffer and analyzed by FACS.

3.6.7.2: Histopathology staining

Frozen tumor sections were generated and put on slides and allowed to reach room temperature from -80 $^{\circ}$ C. The samples were fixed in pre-chilled acetone for 2 minutes and rinsed 3 times in tris buffered saline (TBS) buffer without Tween 20 with no incubation, followed by incubation in the same buffer for 5 minutes. The slides were transferred into TBS with Tween 20 (TBST)

buffer for additional 5 minutes, loaded onto autostainer followed by flooding the autostainer with TBST for 5 minutes. The slides were stained with either anti-mouse H-2K^b PE conjugate bound to SIINFEK or with isotype control antibody, anti-mouse IgG1K PE conjugate at 1:100 for 60 minutes, or no antibody staining. The slides were rinsed in TBST, cover-slipped with ProLong Gold anti-fade mounting media and confocal microscopy images acquired

3.6.8: Tumor immunotherapy

C57BL/6 wild type or OT-1 mice were immunized subcutaneously under the scruff on day 0 with 0.1 mL of OVA protein (50 µg of OVA) as an emulsion in complete Freund's adjuvant. Boosters were given on days 14 and 28 with emulsion in incomplete Freund's adjuvant (IFA). The mice were inoculated with subcutaneous tumor (2 x 10^5 , EL-4 cells were injected) on the left flank. When the tumor size was about 70-90 mm³, intra-tumor injection of either OVA_(P)-Ac-Dx-NPs, free OVA_(P), empty Ac-DX-NPs, or PBS was done. For the study groups where treatement was via intravenous injection, mice were treated when tumor size were about 20-25 mm³. The amount of injected OVA_(P) was normalized to 7 µg for intra-tumoral injection and 20 µg for intravenous injection. Tumor volume was determined prior to injection using the formula: volume (cm)³ = $\frac{1}{2}$ (L × W × H). Phase of the study group which received only one injection. Tumor growth was monitored by measuring the tumor volume every other day. Mice were sacrificed when the tumor volume was over 1 cm³.

APPENDIX

APPENDIX

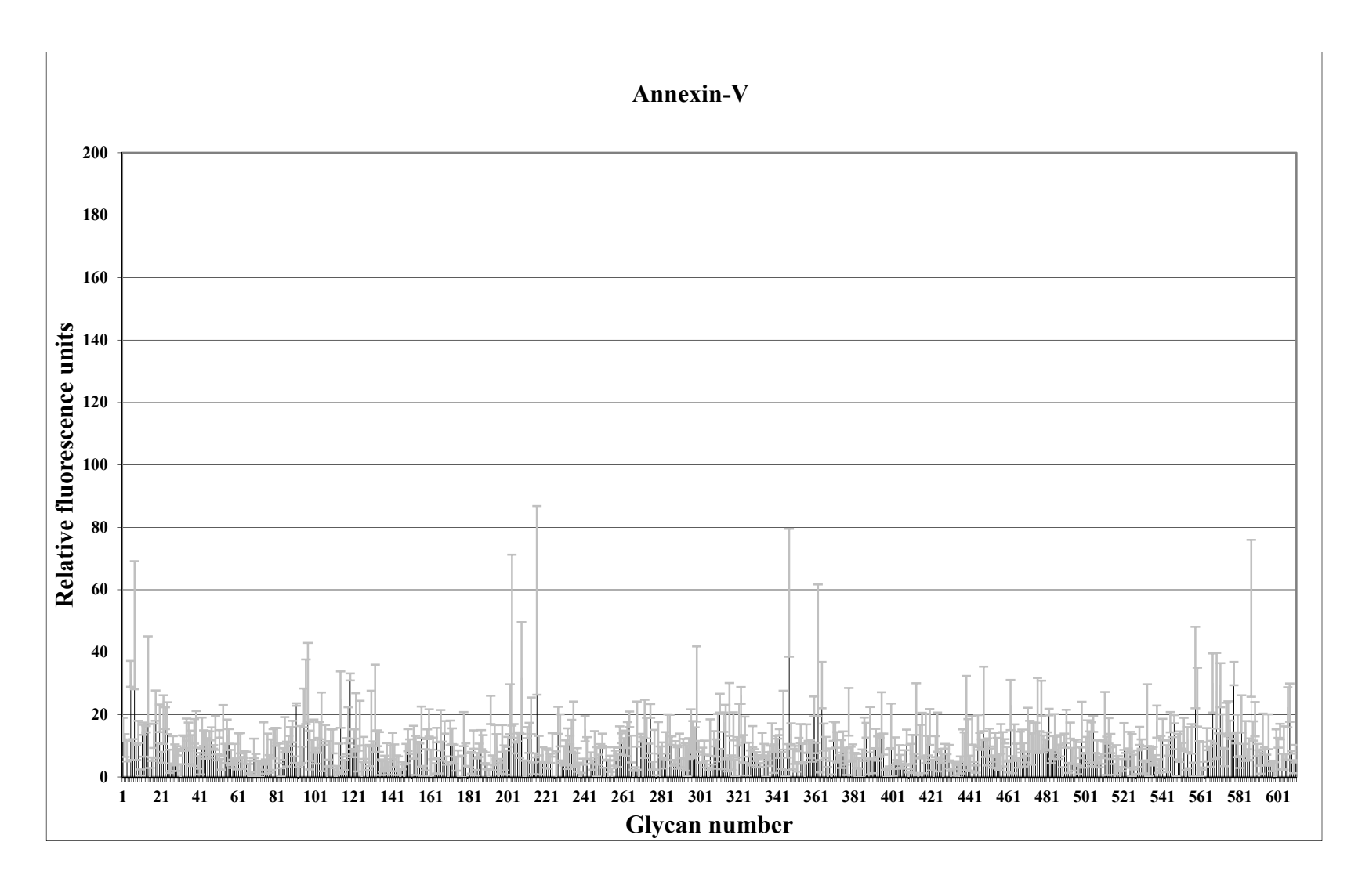


Figure 61: Glycan microarrays by FITC labeled annexn-V

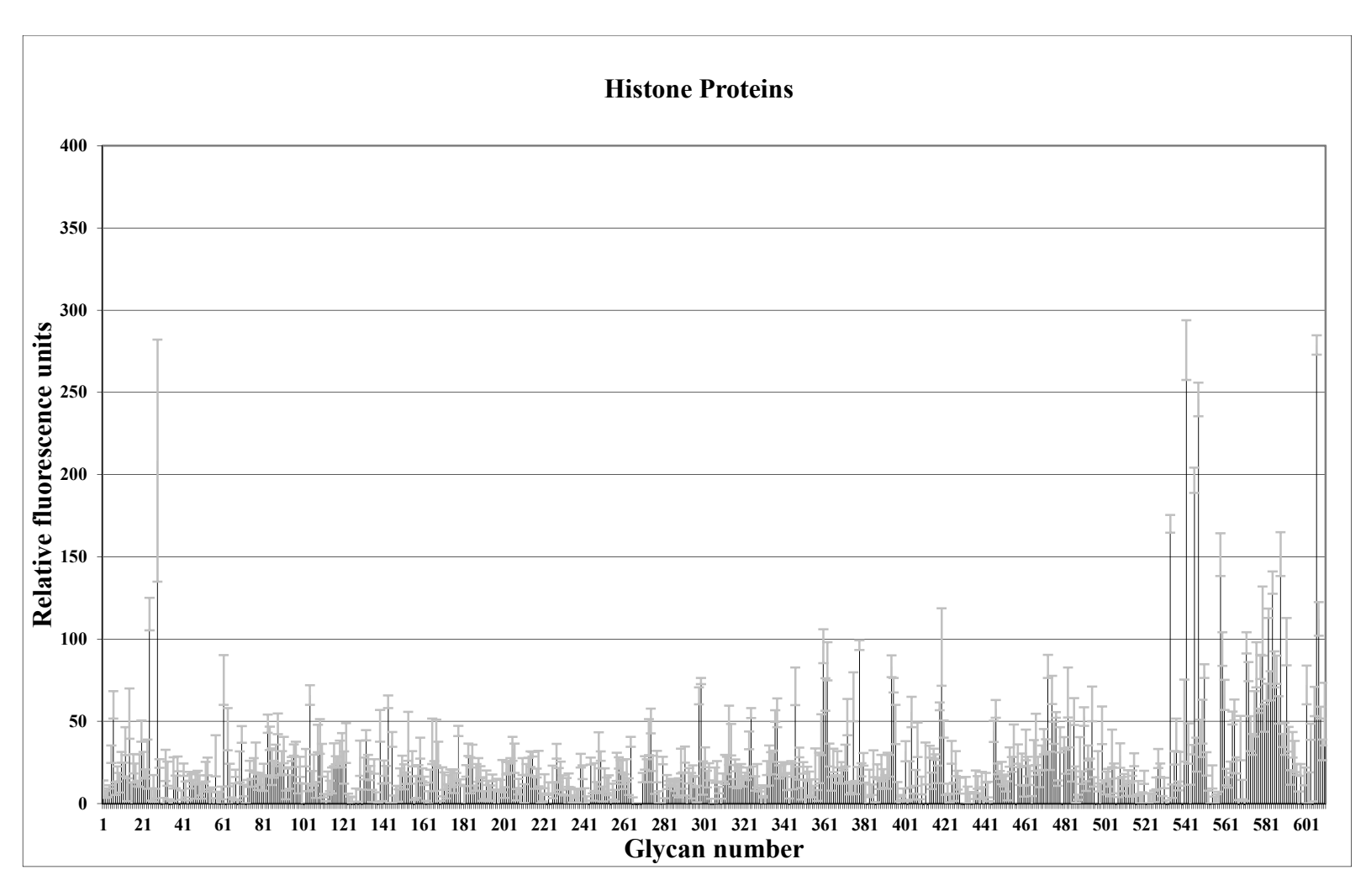


Figure 62: Glycan microarrays by FITC labeled histone protein.

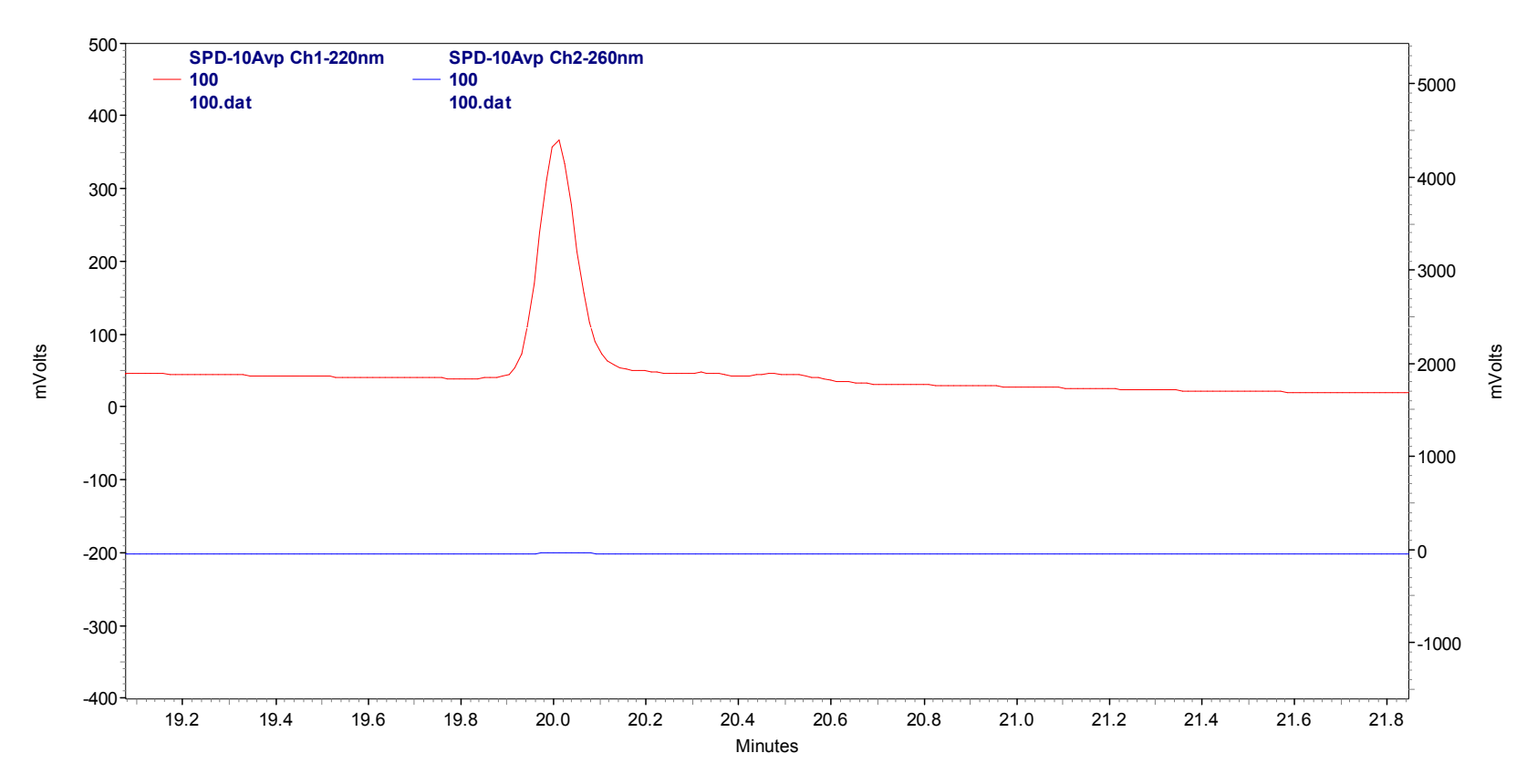


Figure 63: HPLC chromatogram of purified OVA peptide

.

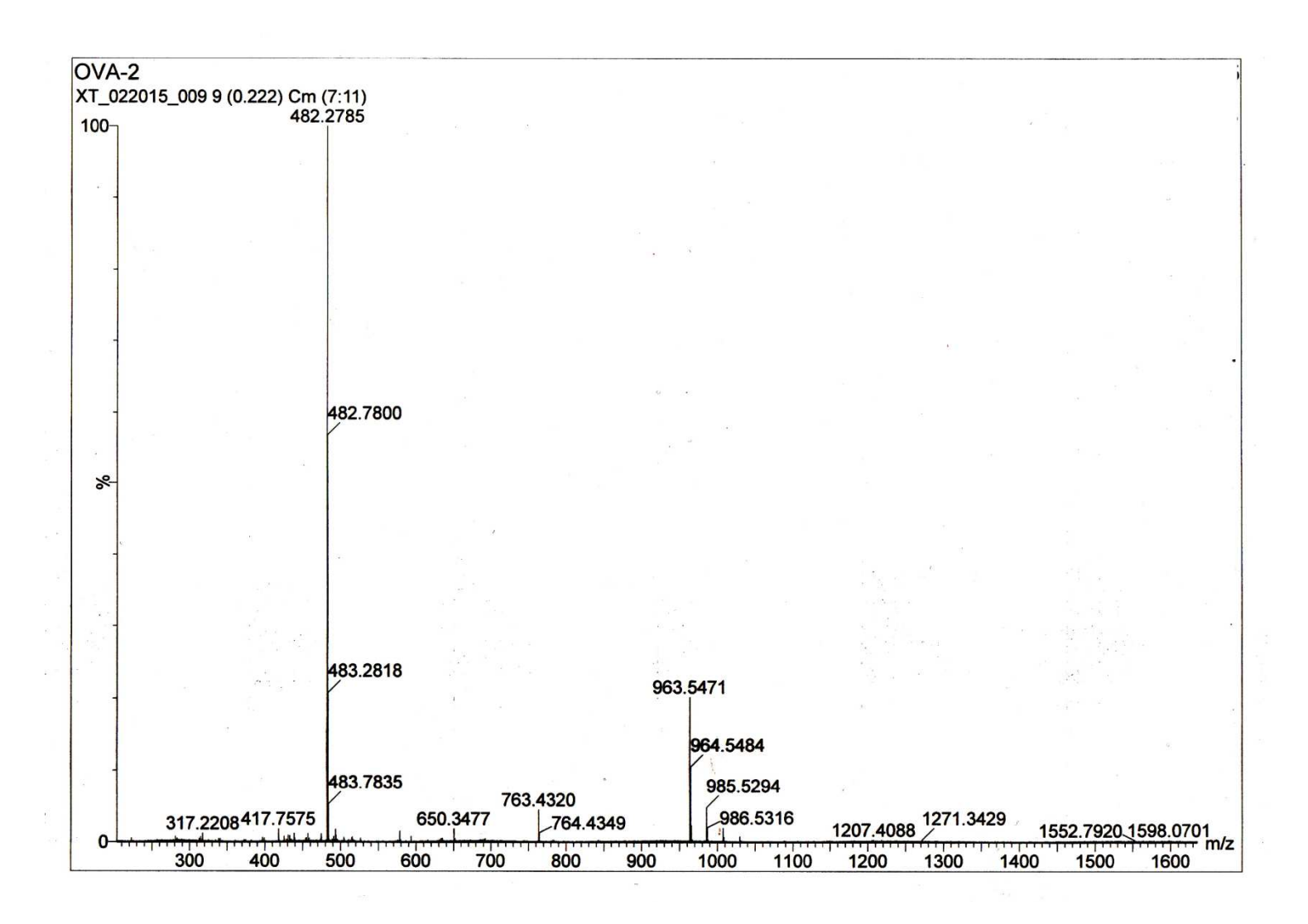


Figure 64: ESI spectrum of purified OVA peptide, OVA_(P).

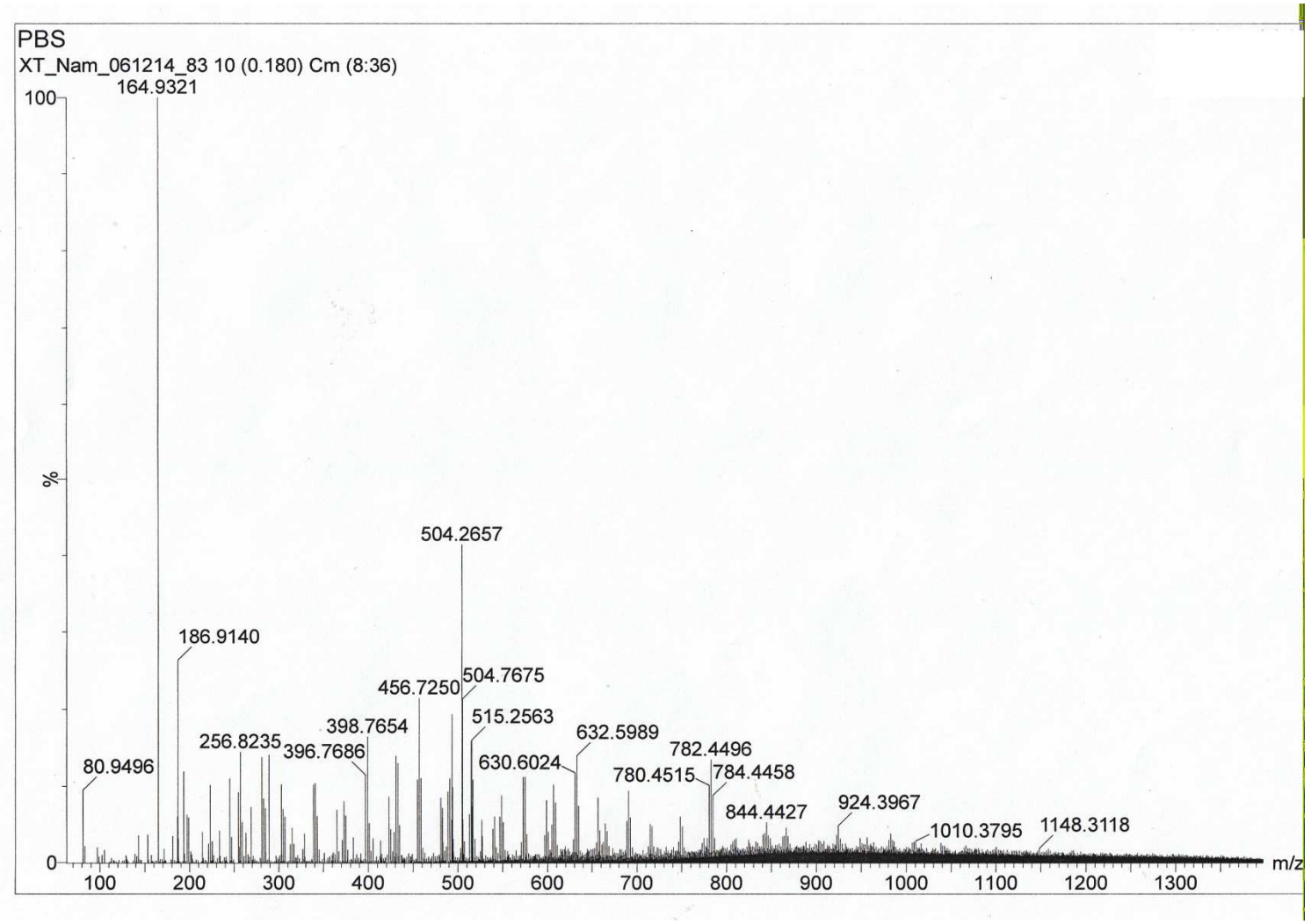


Figure 65: ESI spectrum of the supernatant after OVA_(P)-Ac-Dx-NPs were resuspended in PBS overnight

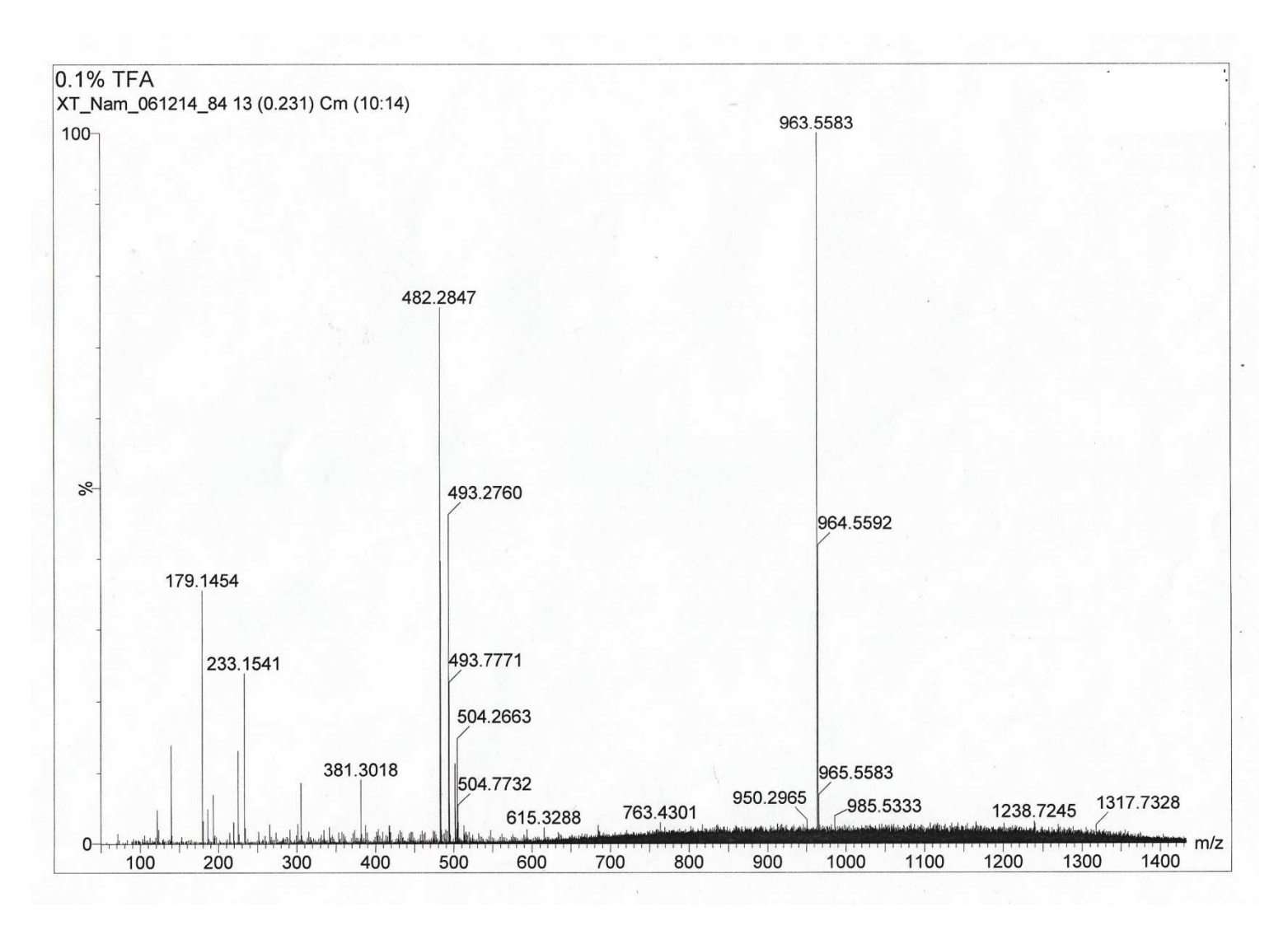


Figure 66: ESI spectrum of the supernatant after OVA(P)-Ac-Dx-NPs were resuspended in 0.1% TFA overnight.

REFERENCES

REFERENCES

- (1) Kawakami, K.; Terabe, M.; Kioi, M.; Berzofsky, J. A.; Puri, R. K., Intratumoral therapy with IL13-PE38 results in effective CTL-mediated suppression of IL-13R alpha 2-expressing contralateral tumors. *Clin. Cancer. Res.*, **2006**, *12*, 4678-4686.
- (2) Junutula, J. R.; Flagella, K. M.; Graham, R. A.; Parsons, K. L.; Ha, E.; Raab, H.; Bhakta, S.; Nguyen, T.; Dugger, D. L.; Li, G.; Mai, E.; Phillips, G. D. L.; Hiraragi, H.; Fuji, R. N.; Tibbitts, J.; Vandlen, R.; Spencer, S. D.; Scheller, R. H.; Polakis, P.; Sliwkowski, M. X., Engineered thio-trastuzumab-DM1 conjugate with an improved therapeutic index to target human epidermal growth factor receptor 2-positive breast cancer. *Clin. Cancer Res.*, **2010**, *16*, 4769-4778.
- (3) Yang, J. C.; Haworth, L.; Sherry, R. M.; Hwu, P.; Schwartzentruber, D. J.; Topalian, S. L.; Steinberg, S. M.; Chen, H. X.; Rosenberg, S. A., A randomized trial of bevacizumab, an anti-vascular endothelial growth factor antibody, for metastatic renal cancer. *New Engl. J. Med.*, **2003**, *349*, 427-434.
- (4) Feldman, A. M.; Lorell, B. H.; Reis, S. E., Trastuzumab in the treatment of metastatic breast cancer Anticancer therapy versus cardiotoxicity. *Circulation*, **2000**, *102*, 272-274.
- (5) von Mehren, M.; Adams, G. P.; Weiner, L. M., Monoclonal antibody therapy for cancer. *Annu. Rev. Med.*, **2003**, *54*, 343-369.
- (6) Slamon, D. J.; Leyland-Jones, B.; Shak, S.; Fuchs, H.; Paton, V.; Bajamonde, A.; Fleming, T.; Eiermann, W.; Wolter, J.; Pegram, M.; Baselga, J.; Norton, L., Use of chemotherapy plus a monoclonal antibody against HER2 for metastatic breast cancer that overexpresses HER2. *New Engl. J. Med.*, **2001**, *344*, 783-792.
- (7) Junutula, J. R.; Raab, H.; Clark, S.; Bhakta, S.; Leipold, D. D.; Weir, S.; Chen, Y.; Simpson, M.; Tsai, S. P.; Dennis, M. S.; Lu, Y.; Meng, Y. G.; Ng, C.; Yang, J.; Lee, C. C.; Duenas, E.; Gorrell, J.; Katta, V.; Kim, A.; McDorman, K.; Flagella, K.; Venook, R.; Ross, S.; Spencer, S. D.; Wong, W. L.; Lowman, H. B.; Vandlen, R.; Sliwkowski, M. X.; Scheller, R. H.; Polakis, P.; Mallet, W., Site-specific conjugation of a cytotoxic drug to an antibody improves the therapeutic index. *Nat. Biotechnol.*, **2008**, *26*, 925-932.
- (8) Shen, B.-Q.; Xu, K.; Liu, L.; Raab, H.; Bhakta, S.; Kenrick, M.; Parsons-Reponte, K. L.; Tien, J.; Yu, S.-F.; Mai, E.; Li, D.; Tibbitts, J.; Baudys, J.; Saadi, O. M.; Scales, S. J.; McDonald, P. J.; Hass, P. E.; Eigenbrot, C.; Trung, N.; Solis, W. A.; Fuji, R. N.; Flagella, K. M.; Patel, D.; Spencer, S. D.; Khawlil, L. A.; Ebens, A.; Wong, W. L.; Vandlen, R.; Kaur, S.; Sliwkowski, M. X.; Scheller, R. H.; Polakis, P.; Junutula, J. R., Conjugation site modulates the in vivo stability and therapeutic activity of antibody-drug conjugates. *Nat. Biotechnol.*, **2012**, *30*, 184-189.
- (9) Scott, A. M.; Wolchok, J. D.; Old, L. J., Antibody therapy of cancer. *Nat. Rev. Cancer.*, **2012**, *12*, 278-287.

- (10) Verma, S.; Miles, D.; Gianni, L.; Krop, I. E.; Welslau, M.; Baselga, J.; Pegram, M.; Oh, D.-Y.; Dieras, V.; Guardino, E.; Fang, L.; Lu, M. W.; Olsen, S.; Blackwell, K.; Grp, E. S., Trastuzumab emtansine for HER2-positive advanced breast cancer. *New Engl. J. Med.*, **2012**, *367*, 1783-1791.
- (11) Dudley, M. E.; Rosenberg, S. A., Adoptive-cell-transfer therapy for the treatment of patients with cancer. *Nat. Rev. Cancer*, **2003**, *3*, 666-675.
- (12) Rosenberg, S. A.; Restifo, N. P.; Yang, J. C.; Morgan, R. A.; Dudley, M. E., Adoptive cell transfer: a clinical path to effective cancer immunotherapy. *Nat. Rev. Cancer*, **2008**, *8*, 299-308.
- (13) Rosenberg, S. A.; Spiess, P.; Lafreniere, R., A new approach to the adoptive immunotherapy of cancer with tumor-infiltrating lymphocytes. *Science*, **1986**, *233*, 1318-1321.
- (14) Yron, I.; Wood, T. A.; Spiess, P. J.; Rosenberg, S. A., In vitro growth of murine T-cells .5. The isolation and growth of lymphoid-cells infiltrating syngeneic solid tumors. *J. Immunol.*, **1980**, *125*, 238-245.
- (15) Rosenberg, S. A.; Packard, B. S.; Aebersold, P. M.; Solomon, D.; Topalian, S. L.; Toy, S. T.; Simon, P.; Lotze, M. T.; Yang, J. C.; Seipp, C. A.; Simpson, C.; Carter, C.; Bock, S.; Schwartzentruber, D.; Wei, J. P.; White, D. E., Use of tumor-infiltrating lymphocytes and interleukin-2 in the immunotherapy of patients with metastatic melanoma a preliminary-report. *New Engl. J. Med.*, **1988**, *319*, 1676-1680.
- (16) Rosenberg, S. A.; Yannelli, J. R.; Yang, J. C.; Topalian, S. L.; Schwartzentruber, D. J.; Weber, J. S.; Parkinson, D. R.; Seipp, C. A.; Einhorn, J. N.; White, D. E., Treatment of patients with metastatic melanoma with autologous tumor-infiltrating lymphocytes and interleukin-2. *J Natl. Cancer. I.*, **1994**, *86*, 1159-1166.
- (17) Rosenberg, S. A.; Aebersold, P.; Cornetta, K.; Kasid, A.; Morgan, R. A.; Moen, R.; Karson, E. M.; Lotze, M. T.; Yang, J. C.; Topalian, S. L.; Merino, M. J.; Culver, K.; Miller, A. D.; Blaese, R. M.; Anderson, W. F., Gene-transfer into humans immunotherapy of patients with advanced melanoma, using tumor-infiltrating lymphocytes modified by retroviral gene transduction. *New Engl. J. Med.*, **1990**, *323*, 570-578.
- (18) Dudley, M. E.; Wunderlich, J. R.; Robbins, P. F.; Yang, J. C.; Hwu, P.; Schwartzentruber, D. J.; Topalian, S. L.; Sherry, R.; Restifo, N. P.; Hubicki, A. M.; Robinson, M. R.; Raffeld, M.; Duray, P.; Seipp, C. A.; Rogers-Freezer, L.; Morton, K. E.; Mavroukakis, S. A.; White, D. E.; Rosenberg, S. A., Cancer regression and autoimmunity in patients after clonal repopulation with antitumor lymphocytes. *Science*, **2002**, *298*, 850-854.
- (19) Yee, C.; Thompson, J. A.; Byrd, D.; Riddell, S. R.; Roche, P.; Celis, E.; Greenberg, P. D., Adoptive T cell therapy using antigen-specific CD8(+) T cell clones for the treatment of patients with metastatic melanoma: In vivo persistence, migration, and antitumor effect of transferred T cells. *Proc. Natl. Acad. Sci. USA*, **2002**, *99*, 16168-16173.

- (20) Dudley, M. E.; Wunderlich, J. R.; Yang, J. C.; Sherry, R. M.; Topalian, S. L.; Restifo, N. P.; Royal, R. E.; Kammula, U.; White, D. E.; Mavroukakis, S. A.; Rogers, L. J.; Gracia, G. J.; Jones, S. A.; Mangiameli, D. P.; Pelletier, M. M.; Gea-Banacloche, J.; Robinson, M. R.; Berman, D. M.; Filie, A. C.; Abati, A.; Rosenberg, S. A., Adoptive cell transfer therapy following non-myeloablative but lymphodepleting chemotherapy for the treatment of patients with refractory metastatic melanoma. *J. Clin. Oncol.*, **2005**, *23*, 2346-2357.
- (21) Morgan, R. A.; Dudley, M. E.; Wunderlich, J. R.; Hughes, M. S.; Yang, J. C.; Sherry, R. M.; Royal, R. E.; Topalian, S. L.; Kammula, U. S.; Restifo, N. P.; Zheng, Z.; Nahvi, A.; de Vries, C. R.; Rogers-Freezer, L. J.; Mavroukakis, S. A.; Rosenberg, S. A., Cancer regression in patients after transfer of genetically engineered lymphocytes. *Science*, **2006**, *314*, 126-129.
- (22) Prevost-Blondel, A.; Zimmermann, C.; Stemmer, C.; Kulmburg, P.; Rosenthal, F. M.; Pircher, H., Tumor-infiltrating lymphocytes exhibiting high ex vivo cytolytic activity fail to prevent murine melanoma tumor growth in vivo. *J. Immunol.*, **1998**, *161*, 2187-2194.
- (23) Ward, P. L.; Koeppen, H. K.; Hurteau, T.; Rowley, D. A.; Schreiber, H., Major histocompatibility complex class-I and unique antigen expression by murine tumors that escaped from CD8+ T-cell-dependent surveillance. *Cancer Res.*, **1990**, *50*, 3851-3858.
- (24) Schietinger, A.; Philip, M.; Liu, R. B.; Schreiber, K.; Schreiber, H., Bystander killing of cancer requires the cooperation of CD4(+) and CD8(+) T cells during the effector phase. *J. Exp. Med.*, **2010**, *207*, 2469-2477.
- (25) Tanaka, K.; Isselbacher, K. J.; Khoury, G.; Jay, G., Reversal of oncogenesis by the expression of a major histocompatibility complex class-I gene. *Science*, **1985**, *228*, 26-30.
- (26) Uyttenhove, C.; Maryanski, J.; Boon, T., Escape of mouse mastocytoma P815 after nearly complete rejection is due to antigen-loss variants rather than immunosuppression. *J. Exp. Med.*, **1983**, *157*, 1040-1052.
- (27) Spiotto, M. T.; Rowley, D. A.; Schreiber, H., Bystander elimination of antigen loss variants in established tumors. *Nat. Med.*, **2004**, *10*, 294-298.
- (28) Zhang, B.; Bowerman, N. A.; Salama, J. K.; Schmidt, H.; Spiotto, M. T.; Schietinger, A.; Yu, P.; Fu, Y.-X.; Weichselbaum, R. R.; Rowley, D. A.; Kranz, D. M.; Schreiber, H., Induced sensitization of tumor stroma leads to eradication of established cancer by T cells. *J. Exp. Med.*, **2007**, *204*, 49-55.
- (29) Bin, Z.; Karrison, T.; Rowley, D. A.; Schreiber, H., IFN-gamma- and TNF-dependent bystander eradication of antigen-loss variants in established mouse cancers. *J. Clin. Invest.*, **2008**, *118*, 1398-1404.
- (30) Spiotto, M. T.; Schreiber, H., Rapid destruction of the tumor microenvironment by CTLs recognizing cancer-specific antigens cross-presented by stromal cells. *Cancer immun.*, **2005,** *5*, 8-8.

- (31) Ge, Z.; Liu, S., Functional block copolymer assemblies responsive to tumor and intracellular microenvironments for site-specific drug delivery and enhanced imaging performance. *Chem. Soc. Rev.*, **2013**, *42*, 7289-7325.
- (32) Zhou, K.; Liu, H.; Zhang, S.; Huang, X.; Wang, Y.; Huang, G.; Sumer, B. D.; Gao, J., Multicolored pH-tunable and activatable fluorescence nanoplatform responsive to physiologic pH stimuli. *J. Am. Chem. Soc.*, **2012**, *134*, 7803-7811.
- (33) Webb, B. A.; Chimenti, M.; Jacobson, M. P.; Barber, D. L., Dysregulated pH: a perfect storm for cancer progression. *Nat. Rev. Cancer*, **2011**, *11*, 671-677.
- (34) Zhou, K.; Wang, Y.; Huang, X.; Luby-Phelps, K.; Sumer, B. D.; Gao, J., Tunable, ultrasensitive pH-responsive nanoparticles targeting specific endocytic organelles in living cells. *Angew. Chem. Int. Ed.*, **2011**, *50*, 6109-6114.
- (35) Volk, T.; Jahde, E.; Fortmeyer, H. P.; Glusenkamp, K. H.; Rajewsky, M. F., pH in human tumor xenografts effect of intravenous administration of glucose. *Brit J. Cancer.*, **1993**, *68*, 492-500.
- (36) Gerweck, L. E.; Seetharaman, K., Cellular pH gradient in tumor versus normal tissue: Potential exploitation for the treatment of cancer. *Cancer Res.*, **1996**, *56*, 1194-1198.
- (37) Wang, Y.; Zhou, K.; Huang, G.; Hensley, C.; Huang, X.; Ma, X.; Zhao, T.; Sumer, B. D.; DeBerardinis, R. J.; Gao, J., A nanoparticle-based strategy for the imaging of a broad range of tumours by nonlinear amplification of microenvironment signals. *Nat. Mater.*, **2014**, *13*, 204-212.
- (38) Iyer, A. K.; Khaled, G.; Fang, J.; Maeda, H., Exploiting the enhanced permeability and retention effect for tumor targeting. *Drug Discov. Today*, **2006**, *11*, 812-818.
- (39) Matsumura, Y.; Maeda, H., A new concept for macromolecular therapeutics in cancer-chemotherapy mechanism of tumoritropic accumulation of proteins and the antitumor agent SMANCS. *Cancer Res.*, **1986**, *46*, 6387-6392.
- (40) Maeda, H.; Wu, J.; Sawa, T.; Matsumura, Y.; Hori, K., Tumor vascular permeability and the EPR effect in macromolecular therapeutics: a review. *J. Control. Release*, **2000**, *65*, 271-284.
- (41) Lynn, D. M.; Amiji, M. M.; Langer, R., pH-responsive polymer microspheres: Rapid release of encapsulated material within the range of intracellular pH. *Angew. Chem. Int. Ed.*, **2001**, *40*, 1707-1710.
- (42) Bae, Y.; Fukushima, S.; Harada, A.; Kataoka, K., Design of environment-sensitive supramolecular assemblies for intracellular drug delivery: Polymeric micelles that are responsive to intracellular pH change. *Angew. Chem. Int. Ed.*, **2003**, *42*, 4640-4643.
- (43) Lee, E. S.; Na, K.; Bae, Y. H., Super pH-sensitive multifunctional polymeric micelle. *Nano Lett.*, **2005**, *5*, 325-329.

- (44) Paramonov, S. E.; Bachelder, E. M.; Beaudette, T. T.; Standley, S. M.; Lee, C. C.; Dashe, J.; Frechet, J. M. J., Fully acid-degradable biocompatible polyacetal microparticles for drug delivery. *Bioconjugate Chem.*, **2008**, *19*, 911-919.
- (45) Cohen, J. A.; Beaudette, T. T.; Tseng, W. W.; Bachelder, E. M.; Mende, I.; Engleman, E. G.; Frechet, J. M. J., T-cell activation by antigen-loaded pH-sensitive hydrogel particles in vivo: The effect of particle size. *Bioconjugate Chem.*, **2009**, *20*, 111-119.
- (46) Griset, A. P.; Walpole, J.; Liu, R.; Gaffey, A.; Colson, Y. L.; Grinstaff, M. W., Expansile nanoparticles: Synthesis, characterization, and in vivo efficacy of an acid-Responsive polymeric drug Delivery system. *J. Am. Chem. Soc.*, **2009**, *131*, 2469-+.
- (47) Beaudette, T. T.; Bachelder, E. M.; Cohen, J. A.; Obermeyer, A. C.; Broaders, K. E.; Frechet, J. M. J.; Kang, E.-S.; Mende, I.; Tseng, W. W.; Davidson, M. G.; Engleman, E. G., In vivo studies on the effect of co-encapsulation of CpG DNA and antigen in acid-degradable microparticle vaccines. *Mol. Pharm.*, **2009**, *6*, 1160-1169.
- (48) Tian, Y.; Su, F.; Weber, W.; Nandakumar, V.; Shumway, B. R.; Jin, Y.; Zhou, X.; Holl, M. R.; Johnson, R. H.; Meldrum, D. R., A series of naphthalimide derivatives as intra and extracellular pH sensors. *Biomaterials*, **2010**, *31*, 7411-7422.
- (49) Du, J.-Z.; Sun, T.-M.; Song, W.-J.; Wu, J.; Wang, J., A Tumor-acidity-activated charge-conversional nanogel as an intelligent vehicle for promoted tumoral-cell uptake and drug delivery. *Angew. Chem. Int. Ed.*, **2010**, *49*, 3621-3626.
- (50) Ko, J. Y.; Park, S.; Lee, H.; Koo, H.; Kim, M. S.; Choi, K.; Kwon, I. C.; Jeong, S. Y.; Kim, K.; Lee, D. S., pH-sensitive nanoflash for tumoral acidic pH imaging in live animals. *Small*, **2010**, *6*, 2539-2544.
- (51) Cheng, R.; Meng, F.; Deng, C.; Klok, H.-A.; Zhong, Z., Dual and multi-stimuli responsive polymeric nanoparticles for programmed site-specific drug delivery. *Biomaterials*, **2013**, *34*, 3647-3657.
- (52) Ling, D.; Park, W.; Park, S.-j.; Lu, Y.; Kim, K. S.; Hackett, M. J.; Kim, B. H.; Yim, H.; Jeon, Y. S.; Na, K.; Hyeon, T., Multifunctional tumor pH-sensitive self-assembled nanoparticles for bimodal imaging and treatment of resistant heterogeneous tumors. *J. Am. Chem. Soc.*, **2014**, *136*, 5647-5655.
- (53) Bachelder, E. M.; Beaudette, T. T.; Broaders, K. E.; Dashe, J.; Frechet, J. M. J., Acetal-derivatized dextran: An acid-responsive biodegradable material for therapeutic applications. *J. Am. Chem. Soc.*, **2008**, *130*, 10494-10495.
- (54) Broaders, K. E.; Cohen, J. A.; Beaudette, T. T.; Bachelder, E. M.; Frechet, J. M. J., Acetalated dextran is a chemically and biologically tunable material for particulate immunotherapy. *Proc. Natl. Acad. Sci. USA*, **2009**, *106*, 5497-5502.

- (55) Beaudette, T. T.; Cohen, J. A.; Bachelder, E. M.; Broaders, K. E.; Cohen, J. L.; Engleman, E. G.; Frechet, J. M. J., Chemoselective ligation in the functionalization of polysaccharide-based particles. *J. Am. Chem. Soc.*, **2009**, *131*, 10360-10361.
- (56) Cohen, J. A.; Beaudette, T. T.; Cohen, J. L.; Brooders, K. E.; Bachelder, E. M.; Frechet, J. M. J., Acetal-modified dextran microparticles with controlled degradation kinetics and surface functionality for gene delivery in phagocytic and non-phagocytic cells. *Adv Mater.*, **2010**, *22*, 3593-3597.
- (57) Cohen, J. L.; Schubert, S.; Wich, P. R.; Cui, L.; Cohen, J. A.; Mynar, J. L.; Frechet, J. M. J., Acid-degradable cationic dextran particles for the delivery of siRNA therapeutics. *Bioconjugate Chem.*, **2011**, *22*, 1056-1065.
- (58) Meenach, S. A.; Kim, Y. J.; Kauffman, K. J.; Kanthamneni, N.; Bachelder, E. M.; Ainslie, K. M., Synthesis, optimization, and characterization of camptothecin-loaded acetalated dextran porous microparticles for pulmonary delivery. *Mol. Pharm.*, **2012**, *9*, 290-298.
- (59) Kauffman, K. J.; Kanthamneni, N.; Meenach, S. A.; Pierson, B. C.; Bachelder, E. M.; Ainslie, K. M., Optimization of rapamycin-loaded acetalated dextran microparticles for immunosuppression. *Int. J. Pharm.*, **2012**, *422*, 356-363.
- (60) Duong, H. T. T.; Hughes, F.; Sagnella, S.; Kavallaris, M.; Macmillan, A.; Whan, R.; Hook, J.; Davis, T. P.; Boyer, C., Functionalizing biodegradable dextran scaffolds using living radical polymerization: New versatile nanoparticles for the delivery of therapeutic molecules. *Mol. Pharm.*, **2012**, *9*, 3046-3061.
- (61) Bachelder, E. M.; Beaudette, T. T.; Broaders, K. E.; Frechet, J. M. J.; Albrecht, M. T.; Mateczun, A. J.; Ainslie, K. M.; Pesce, J. T.; Keane-Myers, A. M., In vitro analysis of acetalated dextran microparticles as a potent delivery platform for vaccine adjuvants. *Mol. Pharm.*, **2010**, *7*, 826-835.
- (62) Peine, K. J.; Bachelder, E. M.; Vangundy, Z.; Papenfuss, T.; Brackman, D. J.; Gallovic, M. D.; Schully, K.; Pesce, J.; Keane-Myers, A.; Ainslie, K. M., Efficient delivery of the toll-like receptor agonists polyinosinic:Polycytidylic acid and CpG to macrophages by acetalated dextran microparticles. *Mol. Pharm.*, **2013**, *10*, 2849-2857.
- (63) Duong, A. D.; Sharma, S.; Peine, K. J.; Gupta, G.; Satoskar, A. R.; Bachelder, E. M.; Wyslouzil, B. E.; Ainsie, K. M., Electrospray encapsulation of toll-like receptor agonist resiquimed in polymer microparticles for the treatment of visceral leishmaniasis. *Mol. Pharm.*, **2013**, *10*, 1045-1055.
- (64) Schully, K. L.; Sharma, S.; Peine, K. J.; Pesce, J.; Elberson, M. A.; Fonseca, M. E.; Prouty, A. M.; Bell, M. G.; Borteh, H.; Gallovic, M.; Bachelder, E. M.; Keane-Myers, A.; Ainslie, K. M., Rapid vaccination using an acetalated dextran microparticulate subunit vaccine confers protection against triplicate challenge by bacillus anthracis. *Pharm. Res.*, **2013**, *30*, 1349-1361.

- (65) Suarez, S.; Grover, G. N.; Braden, R. L.; Christman, K. L.; Amutairi, A., Tunable protein release from acetalated dextran microparticles: A platform for delivery of protein therapeutics to the heart post-MI. *Biomacromolecules*, **2013**, *14*, 3927-3935.
- (66) Hoang, K. V.; Borteh, H. M.; Rajaram, M. V. S.; Peine, K. J.; Curry, H.; Collier, M. A.; Homsy, M. L.; Bachelder, E. M.; Gunn, J. S.; Schlesinger, L. S.; Ainslie, K. M., Acetalated dextran encapsulated AR-12 as a host-directed therapy to control Salmonella infection. *Int. J. Pharm.*, **2014**, *477*, 334-343.
- (67) Peine, K. J.; Guerau-de-Arellano, M.; Lee, P.; Kanthamneni, N.; Severin, M.; Probst, G. D.; Peng, H.; Yang, Y.; Vangundy, Z.; Papenfuss, T. L.; Lovett-Racke, A. E.; Bachelder, E. M.; Ainslie, K. M., Treatment of experimental autoimmune encephalomyelitis by codelivery of disease associated peptide and dexamethasone in acetalated dextran microparticles. *Mol. Pharm.*, **2014**, *11*, 828-835.
- (68) Lin, Z.; Li, J.; He, H.; Kuang, H.; Chen, X.; Xie, Z.; Jing, X.; Huang, Y., Acetalated-dextran as valves of mesoporous silica particles for pH responsive intracellular drug delivery. *Rsc Adv.*, **2015**, *5*, 9546-9555.
- (69) Zhang, Z.; Chen, X.; Chen, L.; Yu, S.; Cao, Y.; He, C.; Chen, X., Intracellular pH-sensitive PEG-block-acetalated-dextrans as efficient drug delivery platforms. *Acs Appl. Mater. Inter.*, **2013**, *5*, 10760-10766.
- (70) Khong, H. T.; Restifo, N. P., Natural selection of tumor variants in the generation of "tumor escape" phenotypes. *Nat. Immunol.*, **2002**, *3*, 999-1005.
- (71) Cafri, G.; Sharbi-Yunger, A.; Tzehoval, E.; Eisenbach, L., Production of LacZ inducible T Cell hybridoma specific for human and mouse gp100(25-33) peptides. *Plos One*, **2013**, *8*, e55583.
- (72) Clarke, S. R. M.; Barnden, M.; Kurts, C.; Carbone, F. R.; Miller, J. F.; Heath, W. R., Characterization of the ovalbumin-specific TCR transgenic line OT-I: MHC elements for positive and negative selection. *Immunol. Cell Biol.*, **2000**, *78*, 110-117.
- (73) Wright, K. O.; Murray, D. A.; Crispe, N. I.; Pierce, R. H., Quantitative PCR for detection of the OT-1 transgene. *BMC Immunol.*, **2005**, *6*, 20-20.
- (74) Ahmad, M.; Rees, R. C.; Ali, S. A., Escape from immunotherapy: possible mechanisms that influence tumor regression/progression. *Cancer Immunol. Immun.*, **2004**, *53*, 844-854.
- (75) Prabhakar, U.; Maeda, H.; Jain, R. K.; Sevick-Muraca, E. M.; Zamboni, W.; Farokhzad, O. C.; Barry, S. T.; Gabizon, A.; Grodzinski, P.; Blakey, D. C., Challenges and key considerations of the enhanced permeability and retention effect for nanomedicine drug delivery in oncology. *Cancer Res.*, **2013**, *73*, 2412-2417.
- (76) Maeda, H.; Bharate, G. Y.; Daruwalla, J., Polymeric drugs for efficient tumor-targeted drug delivery based on EPR-effect. *Eur. J. Pharm. Biopharm.*, **2009**, *71*, 409-419.

- (77) Taurin, S.; Nehoff, H.; Greish, K., Anticancer nanomedicine and tumor vascular permeability; Where is the missing link? *J. Control. Release*, **2012**, *164*, 265-275.
- (78) Azzopardi, E. A.; Ferguson, E. L.; Thomas, D. W., The enhanced permeability retention effect: a new paradigm for drug targeting in infection. *J. Antimicrob. Chemoth.*, **2013**, *68*, 257-274.
- (79) Danhier, F.; Feron, O.; Preat, V., To exploit the tumor microenvironment: Passive and active tumor targeting of nanocarriers for anti-cancer drug delivery. *J. Control. Release*, **2010**, *148*, 135-146.
- (80) Hennig, D.; Schubert, S.; Dargatz, H.; Kostenis, E.; Fahr, A.; Schubert, U. S.; Heinzel, T.; Imhof, D., Novel insights into appropriate encapsulation methods for bioactive compounds into polymers: A study with peptides and HDAC inhibitors. *Macromol. Biosci.*, **2014**, *14*, 69-80.
- (81) Gross, S.; Walden, P., Immunosuppressive mechanisms in human tumors: Why we still cannot cure cancer. *Immunol. Lett.*, **2008**, *116*, 7-14.
- (82) McGray, A. J. R.; Hallett, R.; Bernard, D.; Swift, S. L.; Zhu, Z.; Teoderascu, F.; VanSeggelen, H.; Hassell, J. A.; Hurwitz, A. A.; Wan, Y.; Bramson, J. L., Immunotherapy-induced CD8(+) T Cells Instigate Immune Suppression in the Tumor. *Mol. Ther.*, **2014**, *22*, 206-218.
- (83) Nagaraj, S.; Gupta, K.; Pisarev, V.; Kinarsky, L.; Sherman, S.; Kang, L.; Herber, D. L.; Schneck, J.; Gabrilovich, D. I., Altered recognition of antigen is a mechanism of CD8(+) T cell tolerance in cancer. *Nat. Med.*, **2007**, *13*, 828-835.
- (84) Ahmadzadeh, M.; Johnson, L. A.; Heemskerk, B.; Wunderlich, J. R.; Dudley, M. E.; White, D. E.; Rosenberg, S. A., Tumor antigen-specific CD8 T cells infiltrating the tumor express high levels of PD-1 and are functionally impaired. *Blood*, **2009**, *114*, 1537-1544.
- (85) Marincola, F. M.; Jaffee, E. M.; Hicklin, D. J.; Ferrone, S., Escape of human solid tumors from T-cell recognition: molecular mechanisms and functional significance. *Adv. Immunol.*, **2000**, *74*, 181-273.
- (86) Shrikant, P.; Mescher, M. F., Control of syngeneic tumor growth by activation of CD8(+) T cells: Efficacy is limited by migration away from the site and induction of nonresponsiveness. *J. Immunol.*, **1999**, *162*, 2858-2866.
- (87) Wick, M.; Dubey, P.; Koeppen, H.; Siegel, C. T.; Fields, P. E.; Chen, L. P.; Bluestone, J. A.; Schreiber, H., Antigenic cancer cells grow progressively in immune hosts without evidence for T cell exhaustion or systemic anergy. *J. Exp. Med.*, **1997**, *186*, 229-238.
- (88) Stephan, S. B.; Taber, A. M.; Jileaeva, I.; Pegues, E. P.; Sentman, C. L.; Stephan, M. T., Biopolymer implants enhance the efficacy of adoptive T-cell therapy. *Nat. Biotechnol.*, **2015**, *33*, 97-101.

- (89) Dubowchik, G. M.; Firestone, R. A.; Padilla, L.; Willner, D.; Hofstead, S. J.; Mosure, K.; Knipe, J. O.; Lasch, S. J.; Trail, P. A., Cathepsin B-labile dipeptide linkers for lysosomal release of doxorubicin from internalizing immunoconjugates: Model studies of enzymatic drug release and antigen-specific in vitro anticancer activity. *Bioconjugate Chem.*, **2002**, *13*, 855-869.
- (90) Dubowchik, G. M.; Firestone, R. A., Cathepsin B-sensitive dipeptide prodrugs. 1. A model study of structural requirements for efficient release of doxorubicin. *Bioorg. Med. Chem. Lett.*, **1998**, *8*, 3341-3346.
- (91) Dubowchik, G. M.; Mosure, K.; Knipe, J. O.; Firestone, R. A., Cathepsin B-sensitive dipeptide prodrugs. 2. Models of anticancer drugs paclitaxel (Taxol), mitomycin C and doxorubicin. *Bioorg. Med. Chem. Lett.*, **1998**, *8*, 3347-3352.
- (92) Doronina, S. O.; Toki, B. E.; Torgov, M. Y.; Mendelsohn, B. A.; Cerveny, C. G.; Chace, D. F.; DeBlanc, R. L.; Gearing, R. P.; Bovee, T. D.; Siegall, C. B.; Francisco, J. A.; Wahl, A. F.; Meyer, D. L.; Senter, P. D., Development of potent monoclonal antibody auristatin conjugates for cancer therapy. *Nat. Biotechnol.*, **2003**, *21*, 778-784.
- (93) Duffy, M. J., The role of proteolytic-enzymes in cancer invasion and metastasis. *Clin. Exp. Metastas.*, **1992**, *10*, 145-155.
- (94) Tomayko, M. M.; Reynolds, C. P., Determination of subcutaneous tumor size in athymic (nude) mice. *Cancer Chemoth. Pharm.*, **1989**, *24*, 148-154.